

# A new p-y Approach to Pile Foundations with Arbitrary Dimensions under Monotonic Load in Cohesive Soils

Von der

**Fakultät für Bauingenieurwesen und Geodäsie  
der  
Gottfried Wilhelm Leibniz Universität Hannover**

zur Erlangung des akademischen Grades

**DOKTOR-INGENIEUR  
Dr.-Ing.**

genehmigte Dissertation  
von

M. Sc. Mauricio Marcelo Terceros Almanza

**2021**

Die vorliegende Arbeit wurde als Dissertation im Rahmen des Promotionsverfahrens an der Fakultät für Bauingenieurwesen und Geodäsie der Leibniz Universität Hannover eingereicht und angenommen.

Referent:	Prof. Dr.-Ing. Martin Achmus
Korreferentin:	Prof. Dr.-Ing. habil. Kerstin Lesny
Kommissionsmitglied:	Prof. Dr.-Ing. Peter Schaumann
Vorsitz:	Prof. Dr.-Ing. Udo Nackenhorst
Tag der Promotion:	22.07.2021

To my dear father whom I miss so much.





## Vorwort des Herausgebers

Die im Zusammenhang mit der Energiewende beschlossene Installation von Windenergieanlagen auf dem Meer bzw. Offshore hat neue Herausforderungen für die Geotechnik gebracht. Aufgrund der speziellen Belastungsbedingungen von Offshore-Windenergieanlagen (große Wind- und Wellenlasten auf Strukturen mit relativ geringem Eigengewicht) treten neue Fragestellungen hinsichtlich der Bemessung der Gründungselemente in den Fokus.

Zumeist wurden und werden Offshore-Windenergieanlagen bislang auf Monopiles, d. h. einzelnen Stahlrohrpfählen mit sehr großen Durchmessern, gegründet. Für solche Pfähle bestehen offene Fragen hinsichtlich des geeigneten Berechnungsverfahrens. Üblicherweise kommt in der Praxis die p-y-Methode zum Einsatz, welche ein Bettungsmodulverfahren mit nichtlinearen Federkennlinien ist. Die Federkennlinien („p-y-Kurven“) sind von den Eigenschaften des Bodens abhängig und im Allgemeinen auch tiefenabhängig.

Bestehende p-y-Ansätze für bindige Böden sind nicht ohne Weiteres auf die speziellen Belastungsrandbedingungen von Offshore-Windenergieanlagen und auf die großen Durchmesser der eingesetzten Monopiles übertragbar. Herr Terceros hat sich der Aufgabe gewidmet, eine neue p-y-Methode für Monopiles in bindigen Böden zu entwickeln, welche für beliebige Rand- und Lastbedingungen eine realistische Prognose des Tragverhaltens gewährleistet. Als Methode zur Problemlösung hat er die numerische Simulation mittels der Finite Elemente-Methode gewählt. Durch die Nachrechnung verschiedener in der Literatur dokumentierter Feldversuche mit dem von ihm entwickelten numerischen Modell weist er nach, dass das Simulationsmodell das Verhalten von Pfählen in bindigen Böden sehr zutreffend beschreiben kann.

Im Anschluss wird das Simulationsmodell zur systematischen Analyse bereits vorhandener p-y-Ansätze eingesetzt. In umfassenden Parameterstudien werden Belastungsbedingungen, Pfahlgeometrie und Baugrundbedingungen variiert und die Ergebnisse von p-y-Ansätzen mit denen der numerischen Simulation verglichen. Damit kann deutlich gezeigt werden, dass keiner der bestehenden p-y-Ansätze geeignet ist, um das Systemverhalten für beliebige Parameter hinreichend genau zu erfassen. Konsequenterweise entwickelt Herr Terceros schließlich einen neuen p-y-Ansatz und weist nach, dass mit diesem im gesamten von ihm untersuchten Parameterraum gute Übereinstimmung mit den Ergebnissen der numerischen Simulation erzielt wird. Der Ansatz besteht aus einer Basis- p-y-Kurve, die über einen „y-multiplier“ iterativ an die ermittelte Biegelinie des Pfahls angepasst wird. Hierdurch wird indirekt die gegenseitige Beeinflussung der Federn des Modells sowie auch der Einfluss einer Scherkraft am Pfahlfuß berücksichtigt.

Der entwickelte p-y-Ansatz bedarf natürlich noch der experimentellen Validierung. Er stellt aber in jedem Fall eine wichtige Weiterentwicklung von p-y-Methoden für Pfähle in bindigen Böden dar.

M. Achmus

## **Author's Preface**

The present thesis was written during my work as a research assistant at the Institute of Geotechnical Engineering (IGtH) of the Leibniz University Hannover. The efficient design of foundation structures for offshore wind turbines is one of the central topics of research at the IGtH, which stands in close thematic connection to this research project. Based on a theoretical and numerical analysis together with experiences from practical projects, the primary goal was to create the basis for a new reliable design methodology for laterally loaded pile foundations.

The new modelling approach that has emerged from this work can not only be used for the design of monopile foundations, but also for the general design of laterally loaded piles from different application fields. It can be effortlessly implemented in pile design programmes such as that developed in this thesis.

My special thanks go to my doctoral adviser and main examiner Prof. Dr.-Ing. M. Achmus, who enabled me to write this thesis through the awarded freedom as well as the ideal framework conditions. Furthermore, I would like to thank him for the valuable advice throughout this thesis, for the extraordinarily intensive support and willingness to discuss, always concluding with a solution-based approach.

Additionally, I would like to convey my thanks to Prof. Dr.-Ing. K. Lesny for assuming the co-examination, and for his interest and critical assessment of the thesis. Further thanks to Prof. Dr.-Ing. Peter Schaumann for presiding over the doctoral committee and Prof. Dr.-Ing. Udo Nackenhorst for participating in the doctoral procedure as a member of the doctoral committee.

I also would like to thank my dear colleagues of the Institute for the support and pleasant atmosphere during the many hours of work to ensure the success of this thesis. In particular, special thanks go to Dr.-Ing. Klaus Thieken for all the support that he has given me on this work through his broad experience in offshore projects. Furthermore, I would like to extend my thanks to Mr. Rinke for creating the high-quality drawings.

Finally, yet most importantly, I am most grateful for my beloved wife's extraordinary understanding and patience, particularly in the final phase of my thesis that coincided with the arrival of our precious daughter.

M. Terceros

## Abstract

Offshore wind technology offers great potential to provide clean and renewable energy, representing a potential alternative to the use of fossil fuels. The main obstacle associated with its implementation is the high capital cost. An efficient foundation design consequently means a reduction in cost that ensures the economic feasibility of future wind farms. This thesis makes a contribution to the optimisation of monopile foundation design subjected to lateral loading conditions in cohesive soils.

For the geotechnical design of laterally loaded piles, the p-y approaches according to offshore guidelines such as API (2014) and DNVGL (2016) are extensively used due to their simplicity and versatility. An assessment of the horizontal load-bearing behaviour of piles embedded in cohesive soil is carried out to account for a comprehensive analysis of soil resistance. Indeed, pile foundations can be completely founded on cohesive soil despite its low resistance. The layered soils are in any case frequently composed at least partially of cohesive soils.

For piles embedded in cohesive soils, a differentiation of the p-y methods is established by means of the soil consistency, i.e. the p-y methods proposed by Matlock (1970) for soft clay and Reese et al. (1975) for stiff clay differ considerably in their complexity from each other. However, the p-y curves specified in the guidelines are based solely on the exponential function proposed by Matlock, whereby different linearisations are recommended by API (2014) and DNVGL (2016) for its general application.

Various experimental and numerical investigations demonstrate, however, considerable inadequacies of the stated basic function to accurately model the behaviour of the pile-soil interaction for large-diameter piles. In this sense, several alternative p-y approaches, which explicitly intend to account for the effect of large-diameter piles, are assessed. An extensive comparative study of static p-y approaches with respect to soft and stiff clays as well as unified p-y methods is conducted based on more than 900 three-dimensional simulations using the finite element method. A conclusive validation of the numerical model is accomplished by five field tests introduced in the literature with various pile geometries and soil conditions.

Taking into consideration that the results of the p-y approach according to Matlock, the linear approximation according to the API (2014), and the DNVGL (2016) guidelines as well as further alternative approaches are not generally valid for arbitrary pile geometries and soil conditions, a new, generally applicable p-y approach for cohesive soils is developed in a consistent manner, based on the findings from the numerical comparative study.

**KEYWORDS:** offshore wind turbine, p-y method, clay, monopile, diameter effect

## **Abstract in German (Kurzfassung)**

Die Offshore-Windtechnologie bietet ein großes Potenzial für die Versorgung mit erneuerbaren und sauberen Energien und ist daher eine potenzielle Alternative zur Nutzung fossiler Brennstoffe. Das Haupthindernis bei ihrer Umsetzung liegt in den hohen Investitionskosten. Eine effiziente Bemessung von Gründungen führt daher zu einer Kostenreduzierung, welche die wirtschaftliche Realisierbarkeit der Errichtung zukünftiger Windparks sicherstellt. Die vorliegende Arbeit soll dazu beitragen, die Bemessungsaspekte für Monopile-Gründungen unter lateraler Belastung in bindigen Böden zu optimieren.

Für die geotechnische Bemessung lateral belasteter Pfähle werden die in den Offshore-Richtlinien wie API (2014) und DNVGL (2016) empfohlenen p-y-Ansätze aufgrund ihrer Einfachheit und Vielseitigkeit weitgehend angewendet. Eine Auswertung des horizontalen Tragverhaltens der in einen bindigen Boden eingebetteten Pfähle erfolgt, um eine umfassende Analyse des Bodenwiderstandes zu ermöglichen. In der Tat können Pfahlgründungen trotz des geringen Bodenwiderstandes vollständig in bindige Böden gegründet werden. Dennoch sind bei geschichteten Böden häufig auch bindige Bodenschichten anzutreffen.

Für in bindigen Böden eingebettete Pfähle wird eine Differenzierung der p-y-Methoden anhand der Konsistenz vorgenommen, d. h. die von Matlock (1970) für weichen Ton und Reese et al. (1975) für steifen Ton vorgeschlagenen p-y-Methoden unterscheiden sich in ihrer Komplexität deutlich voneinander. Dennoch basieren die in den Richtlinien angegebenen p-y-Kurven lediglich auf dem exponentiellen Ansatz nach Matlock, wobei jeweils unterschiedliche Linearisierungen nach API (2014) und DNVGL (2016) zur allgemeinen Anwendung empfohlen werden.

Diverse experimentelle und numerische Untersuchungen zeigen jedoch relevante Unzulänglichkeiten der beschriebenen Grundfunktion, um die Boden-Pfahl-Interaktion für Pfähle mit großem Durchmesser genau zu modellieren. In diesem Zusammenhang werden mehrere alternative p-y-Ansätze, die explizit den Effekt großer Durchmesser berücksichtigen sollen, bewertet. Eine umfangreiche Vergleichsstudie von statischen p-y-Ansätzen für weiche und steife Tone wird auf der Grundlage von mehr als 900 dreidimensionalen Simulationen mit der Finite-Elemente-Methode durchgeführt. Eine eindeutige Validierung des numerischen Modells wird mittels fünf in der Literatur eingeführter Feldversuche mit diversen Pfahldimensionen und Bodenbedingungen verwirklicht.

In dem Wissen, dass sowohl die Ergebnisse des Ansatzes nach Matlock, die linearen Approximationen gemäß der API (2014) und der DNVGL (2016) Richtlinien als auch weitere alternative Ansätze für beliebige Pfahlgeometrie und Bodenbedingungen nicht generell gültig sind, ist ein neuer, allgemein anwendbarer p-y-Ansatz für bindigen Böden, basierend auf den Ergebnissen der numerischen Vergleichsstudie, in konsistenter Form entwickelt worden.

**SCHLAGWORTE:** Offshore-Windenergieanlage, p-y-Ansatz, Ton, Monopile, Durchmesser-Effekt

## CONTENT

<b>1</b>	<b>INTRODUCTION.....</b>	<b>1</b>
1.1	Motivation .....	1
1.2	Problem .....	2
1.3	Objectives.....	2
1.4	Solution .....	2
<b>2</b>	<b>FOUNDATION STRUCTURES FOR OFFSHORE WIND TURBINES .....</b>	<b>5</b>
2.1	General .....	5
2.2	Typical offshore substructures .....	6
2.3	Monopile foundation .....	9
2.4	Geotechnical design of monopiles .....	9
2.4.1	General .....	9
2.4.2	p-y method.....	11
2.4.3	Distinction of p-y approaches for different load conditions .....	12
2.4.4	GEO-2 design proof for ULS .....	13
2.4.5	GEO-3 design proof for ULS .....	14
2.4.6	SLS verification.....	16
<b>3</b>	<b>THEORETICAL BASIS FOR LATERALLY LOADED PILES.....</b>	<b>17</b>
3.1	General .....	17
3.2	Analysis methods of laterally loaded piles.....	17
3.3	The p-y method analysis .....	19
3.4	Components of p-y curves.....	22
3.5	Initial stiffness $K_i$ .....	23
3.6	Ultimate bedding resistance $p_u$ .....	24
3.6.1	Wedge failure mechanism.....	25
3.6.2	Flow-around failure mechanism.....	29
3.7	Response of rigid, flexible, and semi-flexible pile-soil systems.....	30
3.8	Limitations of p-y curves .....	33
3.9	Influence of the diameter on p-y approaches .....	35
<b>4</b>	<b>THE STATE OF KNOWLEDGE OF SEMI-EMPIRICAL P-Y CURVES .....</b>	<b>37</b>
4.1	General .....	37
4.2	Subgrade reaction method according to DIN 1054: 2010-12 .....	37
4.3	Non-linear p-y curves for soft clay .....	38
4.3.1	Matlock (1970).....	38
4.3.2	API (2014).....	40
4.3.3	DNVGL (2016) .....	42
4.3.4	Stevens & Audibert (1979) .....	43

4.3.5	Kim et al. (2009) .....	45
4.3.6	Kirsch et al. (2014).....	46
4.3.7	Jeanjean et al. (2017).....	48
4.4	Non-linear p-y curves for stiff clay .....	49
4.4.1	Reese & Cox (1975).....	50
4.4.2	Dunnavant & O'Neill (1989) .....	52
4.4.3	Pisa design model (2016) .....	54
4.5	Non-linear p-y curves for the unified method.....	58
4.5.1	Sullivan et al. (1980) .....	59
4.5.2	Gazioglu & O'Neill (1984) .....	62
4.6	Pile design programme (IGtHPile).....	64
<b>5</b>	<b>NUMERICAL MODEL FOR SHORT-TERM LOADING.....</b>	<b>67</b>
5.1	General .....	67
5.2	Constitutive model .....	68
5.3	Undrained Analysis .....	71
5.4	Back-calculation of field tests .....	73
5.4.1	Lake Austin field test .....	74
5.4.2	Sabine field test .....	75
5.4.3	Incheon Bridge field test (driven steel pile) .....	76
5.4.4	Incheon Bridge field test (drilled shaft) .....	77
5.4.5	Manor field test .....	78
<b>6</b>	<b>EVALUATION OF EXISTING P-Y APPROACHES .....</b>	<b>81</b>
6.1	General .....	81
6.2	Results for a reference system.....	81
6.3	Parametric study with undrained shear strength $s_u$ constant over depth .....	84
6.3.1	Variation of pile dimensions .....	84
6.3.2	Variation of load eccentricity $h$ .....	89
6.3.3	Variation of wall thickness $t$ .....	91
6.3.4	Variation of clay consistency .....	91
6.3.5	Variation of the plasticity index $PI$ .....	93
6.3.6	Variation of the over-consolidation ratio $OCR$ .....	94
6.3.7	Variation of individual soil parameters .....	96
6.4	Parametric study with linearly increasing undrained shear strength $s_u$ over depth.....	98
6.4.1	Results for a reference system.....	99
6.5	Requirements for a new, generally applicable p-y approach .....	104
6.6	Interim conclusion.....	104
<b>7</b>	<b>DEVELOPMENT OF A NEW MODELLING APPROACH.....</b>	<b>107</b>
7.1	General .....	107
7.2	Limitations of common p-y approaches .....	107
7.3	Conception of the new modelling approach.....	110

---

7.4	Determination of ultimate bedding resistance $p_u$ .....	111
7.5	Derivation of the initial stiffness $K_i$ .....	115
7.6	Derivation of “basic p-y curves” .....	117
7.7	Consideration of the pile tip effect and pile deflection line .....	124
7.8	Summarised calculation procedure .....	127
<b>8</b>	<b>EVALUATION OF THE NEW MODELLING APPROACH .....</b>	<b>129</b>
8.1	General .....	129
8.2	Comparison between numerical and analytical solutions .....	129
8.2.1	Parametric study for evaluating the new modelling approach .....	133
8.2.2	Undrained shear strength $s_u$ linearly increasing over depth .....	140
<b>9</b>	<b>DISCUSSION .....</b>	<b>147</b>
<b>10</b>	<b>CONCLUSION AND PERSPECTIVE .....</b>	<b>149</b>
	<b>REFERENCE .....</b>	<b>153</b>
	<b>APPENDIX A .....</b>	<b>161</b>
	<b>APPENDIX B.....</b>	<b>167</b>
	<b>APPENDIX C .....</b>	<b>173</b>

## List of Figures

2-1: Main components of an OWT with a monopile foundation .....	5
2-2: Typical foundation concepts depending on the water depth.....	7
2-3: Schematic representation of p-y relationships for static, cyclic and reloading conditions.....	13
2-4: GEO-2 for ULS design proof according to German standard DIN 1054:2010-12 (after Thieken et al. 2013).....	14
2-5: GEO-3 for ULS design proof according to DNVGL (2018) guideline.....	15
2-6: Graphical estimation of elastic and plastic rotations .....	16
3-1: Assumed model of the subgrade reaction method (left) and set of p-y curves (centre) as well as the soil pressure around the pile (right) .....	20
3-2: Iterative process to adjust the secant stiffness of p-y curves .....	22
3-3: Typical non-linear p-y curve (left) and resulting subgrade reaction modulus (right) .....	22
3-4: Three-dimensional failure mechanisms of laterally loaded piles for gapping (left) and no-gapping conditions (right).....	25
3-5: Schematic three-dimensional diagrams of the passive wedge failure (left) and its respective simplified model (right) for clay soils (after Reese et al. 1958).....	26
3-6: Forces acting on the soil wedge failure for gap (left) and non-gap (right) conditions (after Reese et al. 1958) .....	28
3-7: The flow-around mechanism for deep lateral resistance in cohesive soil for square pile (left) after Reese (1958) and upper bound solutions (right) after Randolph et al. (2011) .....	29
3-8: Schematic variation of the failure mechanisms of laterally loaded piles for rigid (left) and flexible (right) pile after Broms (1964).....	32
4-1: Subgrade reaction method for pile foundations subjected to monotonic loading conditions.....	37
4-2: Exemplary p-y curves according to Matlock (1970), the variation of the stiffness parameter $\epsilon_{50}$ (left) as well as the ultimate bedding resistance parameters $s_u$ and $J$ (right) .....	40
4-3: Exemplary p-y curves (left) and secant bedding stiffness (right) according to Matlock (1970), API (2014) and DNVGL (2016) .....	41
4-4: Related initial stiffness from the p-y curve linearisation .....	43
4-5: Exemplary p-y curves by alternative approaches for small and large diameter pile.....	44
4-6: Bedding stiffness $E_{py} = p / y$ for soil parameter related to 4-5 with normalised displacement $y / D = 0.0005$ .....	47
4-7: Exemplary p-y curves (left) and secant bedding stiffness (right) according to Jeanjean et al. (2017) under no-gap and gap conditions .....	49
4-8: Characteristic shape of p-y curves according to Reese & Cox (1975) for stiff clay subjected to static loading conditions .....	50
4-9: Exemplary p-y curves according to Reese & Cox (1975), variation of the stiffness parameter $\epsilon_{50}$ (left) as well as the undrained shear strength $s_u$ (right) .....	52
4-10: Bedding stiffness $E_{py} = p / y$ for soil parameter according to Fig. 4-14 with normalised head displacement $y / D = 0.0005$ .....	54
4-11: Comparison of the key features of the proposed analysis models: traditional p-y analysis (left), assumed soil reactions (centre) and analysis model (right) according to PISA (2016).....	55



4-12: Influence of the various components of soil reactions according to PISA (2016) on the computed response of pile-soil system for  $h / D = 5$  and  $D / t = 90$  ..... 58

4-13: Characteristic shape of p-y curves according to Sullivan et al. (1980) for the unified method subjected to static loading conditions ..... 59

4-14: Exemplary p-y curves for stiff clay and unified approaches for small and large diameter piles ..... 61

4-15: Characteristic shape of p-y curves according to Gazizoglu & O’Neill (1984) for a unified method subjected to static loading conditions ..... 63

5-1: Finite element mesh of the pile-soil system used for simulations ..... 67

5-2: Approximation of the soil stiffness in Plaxis 3D for the consideration of the stiffness exponent  $m$ ,  $\lambda_{ES}$  and  $\lambda_{G0}$  (reference system of the FEM study) ..... 70

5-3: Stress paths depending on the respective undrained analysis with HSsmall constitutive model ..... 71

5-4: Comparison of the depth-lateral deflection (left) and bending moment (right) for the “Lake Austin” field test ..... 75

5-5: Comparison of the depth-lateral deflection (left) and bending moment (right) for the “Sabine River” field test ..... 76

5-6: Comparison of the depth-lateral deflection (left) and bending moment (right) in the “Incheon Bridge” field test (driven steel pile) ..... 77

5-7: Comparison of the depth-lateral deflection (left) and bending moment (right) for the “Incheon Bridge” field test (drilled shaft)..... 78

5-8: Comparison of the load-deflection (left) and bending moment (right) for the “Manor” field test..... 79

6-1: Load-displacement curves (top) and moment-rotation curves (bottom) for the reference system..... 82

6-2: Pile deflection lines (left) and secant bedding stiffness (right) of the reference system ..... 83

6-3: Quotient of lateral stiffness  $K_{p-y} / K_{FEM}$  based on the approaches by Matlock (1970) and FEM ..... 85

6-4: Quotient of lateral stiffness  $K_{p-y} / K_{FEM}$  based on the approaches by API (2014) and FEM..... 86

6-5: Quotient of lateral stiffness  $K_{p-y} / K_{FEM}$  based on the approaches by DNVGL (2016) and FEM ..... 86

6-6: Quotient of lateral stiffness  $K_{p-y} / K_{FEM}$  based on the approaches by Stevens et al. (1979) and FEM ..... 87

6-7: Quotient of lateral stiffness  $K_{p-y} / K_{FEM}$  based on the approaches by Kim et al. (2009) and FEM ..... 88

6-8: Quotient of lateral stiffness  $K_{p-y} / K_{FEM}$  based on the approaches by Kirsch et al. (2014) and FEM..... 88

6-9: Quotient of lateral stiffness  $K_{p-y} / K_{FEM}$  for varied load eccentricity based on the reference system of the FEM study ..... 90

6-10: Quotient of lateral stiffness  $K_{p-y} / K_{FEM}$  for varied wall thickness based on the reference system of the FEM study..... 91

6-11: Quotient of lateral stiffness  $K_{p-y} / K_{FEM}$  for a varied clay consistency based on the reference system of the FEM study ..... 92

6-12: Quotient of lateral stiffness  $K_{p-y} / K_{FEM}$  for a varied plasticity index PI based on the reference system of the FEM study ..... 94

6-13: Quotient of lateral stiffness  $K_{p-y} / K_{FEM}$  for a varied over-consolidation ratio based on the reference system of the FEM study..... 95

6-14: Secant bedding stiffness for separately varied soil parameters based on the reference system of the FEM study..... 97

6-15: Load-displacement curves (top) and moment-rotation curves (bottom) for the reference system ( $D = 6$  m,  $L = 36$  m) with linearly increasing parameters over depth ..... 99

6-16: Pile deflection lines (left) and secant bedding stiffness (right) for the reference system ( $D = 6$  m,  $L = 36$  m) with linearly increasing parameters over depth ..... 100

6-17: Quotient of lateral stiffness  $K_{p-y} / K_{FEM}$  for varied parameter with linearly increasing parameters over depth ... ..... 101

7-1: Impact of pile bending on bedding soil resistance (D = 6 m, L = 36 m, soft clay).....	108
7-2: Influence of the pile bending on the p-y curves (D = 6 m, L = 36 m, soft clay).....	109
7-3: Course of the load-bearing capacity factor $N_p$ resulting from the FEM analysis and p-y approach recommended by OGLs, as well as the new modelling approach.....	113
7-4: Comparison of the load-bearing capacity factor $N_p$ depending on the soil consistency and pile diameters for two reference depths .....	114
7-5: Initial stiffness ratios for the pile foundations embedded in different cohesive soils with varying diameters for two reference depths .....	116
7-6: Derivation of the empirical factor $F_{ac}$ by varying the ratio of the dynamic shear modulus $G_0^{ref}$ to static soil stiffness modulus $E_{oed}^{ref}$ .....	119
7-7: Comparison of the p-y curves obtained from FEM and new modelling approach for a pile with constant horizontal displacement (D = 1 m, soft clay).....	120
7-8: Comparison of the p-y curves obtained from FEM and the new modelling approach for a pile with constant horizontal displacement (D = 6 m, soft clay).....	122
7-9: Influence of undrained behaviour on the p-y curves obtained from the HSsmall constitutive material model by applying the “undrained analysis B” .....	123
7-10: Comparison of secant bedding stiffness obtained from FEM and new modelling approach based on $Mult_y = 1.0$ (D = 6 m, L= 36 m, soft clay) .....	125
7-11: Definition and equations for the new modelling approach .....	128
8-1: Evaluation of the results obtained from the FEM, API (2014) and the new modelling approach for a slender pile foundation (D = 1 m, L= 12 m, medium soft clay).....	130
8-2: Evaluation of the results obtained from the FEM, API (2014) and the new modelling approach for a monopile foundation (D = 6 m, L= 36 m, medium soft clay) .....	132
8-3: Quotient of lateral stiffness $K_{p-y} / K_{FEM}$ based on the new modelling approach and FEM without applying y-multipliers .....	134
8-4: Quotient of lateral stiffness $K_{p-y} / K_{FEM}$ based on the new modelling approach and FEM applying y-multipliers .....	135
8-5: Parameter study for the evaluation of the new modelling approach based on the variation of the remaining geometrical pile parameters .....	137
8-6: Parameter study for the evaluation of the new modelling approach based on the variation of the remaining soil condition parameters .....	138
8-7: Parameter study for the evaluation of the new modelling approach based on the variation of coupled soil condition parameters.....	139
8-8: Evaluation of the results obtained from the FEM, API (2014) and the new modelling approach for the reference system with linearly increasing undrained shear strength $s_u$ (D = 6 m, L = 36 m).....	141
8-9: Quotient of lateral stiffness $K_{p-y} / K_{FEM}$ based on the new modelling approach and FEM for varied parameters with linearly increasing undrained shear strength $s_u$ .....	143
8-10: Parameter study for the evaluation of the new modelling approach based on the variation of coupled soil condition parameters with linearly increasing undrained shear strength $s_u$ .....	144

## List of Tables

3-1: Recommendations for the lateral bearing capacity factor $N_p$ at deep depth .....	30
3-2: Relationship of the coefficient of the subgrade reaction $K_p$ to undrained shear strength of stiff over-consolidated clay .....	31
4-1: Initial stiffness values of $K_s$ for static loading conditions according to Reese & Cox (1975) .....	51
4-2: Representative values of $\varepsilon_{50}$ according to Reese & Cox (1975) .....	51
4-3: Normalisation of pile reaction components according to PISA (2016) .....	56
4-4: Method parameters for monopiles in stiff clay at Cowden site PISA (2016) .....	57
4-5: Typical values for $K_s$ according to Sullivan et al. (1980) .....	60
4-6: Typical values for $\varepsilon_{50}$ according to Sullivan et al. (1980) .....	60
4-7: Typical calibration factors according to Sullivan et al. (1980) .....	60
4-8: Soil degradability factor $F$ according to Gazioglu & O'Neill (1984) for static loading .....	63
5-1: Soil parameters used for back-analysis of the field tests .....	74
6-1: Clay parameters used for reference systems and parametric study .....	81
6-2: Clay parameters used for the parametric study regarding the clay consistency .....	92
6-3: Clay parameters used for the parametric study regarding the over-consolidation ratio .....	95
6-4: Clay parameters used for simulations with linearly increasing parameters over depth .....	98

## List of Symbols

### Latin alphabet symbols

<i>Symbol</i>	<i>Dimension / Unit</i>	<i>Description</i>
$A_s$	[-]	Non-dimensional coefficient (stiff clay)
$B$	[-]	Skempton coefficient
$B_k$	[F]	Characteristic effect of action
$s'_k$	[F·L <sup>-2</sup> ]	Characteristic effective cohesion
$s_{u,k}$	[F·L <sup>-2</sup> ]	Characteristic undrained shear strength
$s_{u,a}$	[F·L <sup>-2</sup> ]	Average undrained shear strength
$D$	[L]	Pile diameter
$D_{ref}$	[L]	Reference diameter
$EI$	[F·L <sup>2</sup> ]	Flexural stiffness
$e$	[-]	Void ratio
$E_{ph,k}$	[F]	Resultant passive horizontal earth pressure force
$E_{50}$	[F·L <sup>-2</sup> ]	Secant stiffness in a standard drained triaxial test
$E_{oed}$	[F·L <sup>-2</sup> ]	Tangent stiffness for primary oedometer loading
$E_p$	[F·L <sup>-2</sup> ]	Modulus of elasticity of steel
$E_s$	[F·L <sup>-2</sup> ]	Static oedometric soil stiffness
$E_{sd}$	[F·L <sup>-2</sup> ]	Dynamic oedometric soil stiffness
$E_u$	[F·L <sup>-2</sup> ]	Undrained oedometric soil stiffness
$E_{ur}$	[F·L <sup>-2</sup> ]	Un- and reloading stiffness from a drained triaxial test
$F$	[-]	Soil degradability factor
$F_{ac}$	[-]	Empirical factor
$G_0$	[F·L <sup>-2</sup> ]	Dynamic shear modulus
$G_{ur}$	[F·L <sup>-2</sup> ]	Unloading shear modulus
$h$	[L]	Load eccentricity
$H_B$	[F]	Based shear force
$H_k$	[F]	Characteristic lateral load
$H_{d,ult}$	[F]	Ultimate load-bearing capacity
$J$	[-]	Empirical coefficient
$k$	[-]	Exponent of the OCR

$k_0$	[F·L <sup>-2</sup> ]	Coefficient of horizontal earth pressure at rest
$K'$	[F·L <sup>-2</sup> ]	Effective bulk modulus of the soil skeleton
$K_i$	[F·L <sup>-2</sup> ]	Initial stiffness
$K_s$	[F·L <sup>-3</sup> ]	Initial stiffness (used for stiff clay)
$K$	[F·L <sup>-2</sup> ]	Subgrade reaction modulus
$K_u$	[F·L <sup>-2</sup> ]	Undrained bulk modulus
$K_w$	[F·L <sup>-2</sup> ]	Bulk modulus of pore water
$L$	[L]	Embedded pile length
$M_k$	[F·L]	Characteristic moment load
$M_B$	[F·L]	Base Moment
$Multy$	[-]	y-multipliers
$N_p$	[-]	Load-bearing capacity factor
OCR	[1]	Over consolidation ratio
$p_u$	[F·L <sup>-2</sup> ]	Ultimate bedding resistance
$p_{res}$	[F·L <sup>-2</sup> ]	Residual bedding resistance
$p_{ref}$	[F·L <sup>-2</sup> ]	Reference stress
$p_{steady}$	[F·L <sup>-2</sup> ]	Steady state pore stress
$p_{exc}$	[F·L <sup>-2</sup> ]	Excess pore water pressure
$p_w$	[F·L <sup>-2</sup> ]	Pore water pressure
PI	[-]	Plasticity index
$Q_K$	[1]	Quotient of lateral stiffness
$t$	[L]	Wall thickness
$W$	[F]	Weight of the soil
$y$	[L]	Lateral displacement
$y_{50}$	[L]	Reference displacement
$z$	[L]	Depth below surface
$z_0$	[L]	Depth of rotation point (also termed as zero-deflection point)
$z_{cr}$	[L]	Critical depth

## Greek alphabet symbols or symbols including Greek alphabet symbols

<i>Symbol</i>	<i>Dimension / Unit</i>	<i>Description</i>
$\alpha$	[-]	Pile-soil adhesion factor
$\varepsilon_v$	[-]	Volume expansion
$\gamma_{0.7}$	[-]	Reference shear strain at 72.2%
$\gamma$	[F·L <sup>-3</sup> ]	Unit weight of soil
$\gamma'$	[F·L <sup>-3</sup> ]	Buoyant unit weight of soil
$\gamma_{s'}$	[-]	Partial safety factor for effective cohesion
$\gamma_{su}$	[-]	Partial safety factor for undrained shear strength
$\gamma_{\phi'}$	[-]	Partial safety factor for effective soil friction angle
$\gamma_E$	[-]	Partial safety factor for effect of action
$\gamma_R$	[-]	Partial safety factor for resistance
$\gamma_s$	[F·L <sup>-3</sup> ]	Unit weight of steel
$\gamma_w$	[F·L <sup>-3</sup> ]	Unit weight of water
$\varepsilon_{50}$	[-]	Strain at 50 % of maximum stress
$\Theta_{\text{elastic}}$	[°]	Elastic head rotation
$\Theta_{\text{perm}}$	[°]	permanent (plastic) head rotation
$\Theta_{\text{perm,max}}$	[°]	Maximal accumulated permanent head rotation
$\Theta_{\text{total}}$	[°]	Total head rotation
$\lambda_{E_{oed}}$	[-]	Stress exponent of $E_{oed}$
$\lambda_{G_0}$	[-]	Stress exponent of $G_0$
$\nu$	[-]	Poisson's ratio
$\nu_u$	[-]	Undrained Poisson's ratio
$\sigma$	[F·L <sup>-2</sup> ]	Total stress
$\sigma'$	[F·L <sup>-2</sup> ]	Effective stress
$\sigma'_m$	[F·L <sup>-2</sup> ]	Main effective principal stress
$\sigma'_v$	[F·L <sup>-2</sup> ]	Overburden pressure
$\xi$	[-]	Empirical coefficient related to the degree of clay consolidation
$\phi'_k$	[°]	Characteristic effective soil friction angle
$\phi_u$	[°]	Friction angle of the undrained soil
$\psi$	[°]	Soil dilatancy

### Legend:

[Dimension]:	L : Length	M : Mass	T : Time	F = M·L·T <sup>-2</sup> : Force
[Unit]:	° : Degree	rad : Radian		

**Abbreviations:**

<i>Abbreviation</i>	<i>Description</i>
ALS	Accidental limit state
API	American Petroleum Institute
BSH	Federal Maritime and Hydrographic Agency
BMWi	Federal Ministry for Economic Affairs and Energy
BS-P	Persistent design situation
EEZ	Exclusive economic zone
ESP	Effective stress path
FE	Finite element
FEM	Finite element method
FLS	Fatigue limit state
GBS	Gravity-based foundations
GW	Gigawatt
HSsmall	Hardening soil model with small-strain stiffness
NFA	Natural frequency analysis
OGL	Offshore guidelines
OWT	Offshore wind turbine
SDM	Stiffness degradation method
SLS	Serviceability limit state
TSP	Total stress path
ULS	Ultimate limit state





# 1 Introduction

## 1.1 Motivation

In the last decades, the effects of global warming mainly due to the greenhouse gas emissions released by the burning of fossil fuels, have given rise to environmental awareness. Energy politics have clearly turned towards renewable energy sources such as wind power, solar energy and hydropower. The energy transition conducted by Germany has well established targets over time, e.g. an increase of renewable energy from 55 to 60 percent of the gross electricity consumption in Germany until 2035 as stated by EEG (2017). For this purpose, the amount of offshore wind turbines (OWTs) has to be increased considerably through the construction of offshore wind farms along the North and Baltic seas. The installed capacity of offshore wind energy is expected to expand from 6.5 GW in 2020 to up to 15 GW in 2030 in order to achieve the requested targets set by the EEG.

The geotechnical design of OWTs is mainly based on the experiences of the offshore industry regarding oil and gas platforms. Nevertheless, these design methods and recommendations suggested by this sector are not fully transferable to the OWT foundations, mainly due to the discrepancy in the loading conditions, i.e. the vertical loads are considerably smaller than those of typical offshore platforms, resulting in horizontal loads of similar magnitude to the vertical loads.

The foundation structure for OWTs is an essential component for the appropriate performance of the turbine during its life span. The monopile is currently the preferred foundation concept for the OWTs at water depths less than 40 meters due to the cost-effectiveness in terms of mass production and installation process. The large-diameter monopile consists of a single steel tube driven into the seabed. The discontinuous lateral loads and overturning moments generated by the extremely cyclic nature of wind and waves acting on the superstructure are transferred into the subsoil across the complete pile length of the shaft surface as well as at the tip of the monopile foundations.

For the geotechnical design of OWTs, the requirements such as the foundation stiffness and the cost-effectiveness play a significantly greater role compared to the previous application of the offshore foundation in the petroleum industry. The cost of the offshore foundation structure, e.g. the construction and installation process, constitutes around 25 percent of the total cost of an offshore wind farm project according to RAB & DTI (2007).

An optimisation of foundation structures in terms of geotechnical design aspects is highly desirable to ensure economic feasibility. Therefore, the development of new calculation methodologies for analysing the pile-soil interaction is definitely required. The feasibility of carrying out comprehensive parameter studies is currently a reality due to the growing capability of numerical modelling. Consequently, it is possible to have an accurate comprehension of the behaviour of a pile-soil system (cf. Achmus et al. 2014, 2016 and 2017a).

## 1.2 Problem

For the design of monopile foundations, the p-y method is traditionally employed to describe the relationship between the bedding resistance  $p$ , acting against the pile wall, and the lateral deflection  $y$  of the pile. The large diameter piles ( $D = 6 - 10$  m) used for the monopile foundation provide an approximately rigid behaviour with a quite small slenderness ratio ( $L/D \leq 5$ ), which is located outside of the original range of its usual application. The traditional p-y methods which were adopted for the offshore oil and gas industry, are invariably calibrated for flexible piles with small diameters, i.e. slender piles ( $D < 1$  m). Numerous experimental and numerical investigations have already demonstrated relevant shortcomings of existing p-y curves for piles with large diameters (such as monopile foundations) embedded in cohesive soils (e.g. Stevens et al. 1979, Kim et al. 2009, Haiderali & Madabhushi 2013 and Kirsch et al. 2014). Reliable calculation methods for the design analysis are therefore required to overcome this lack of knowledge.

## 1.3 Objectives

The present thesis contributes to the efforts to fulfil the requirement for research with regard to the description of the load-bearing behaviour of laterally loaded, large-diameter pile foundations embedded in cohesive soil.

The main task is to develop a new, generally valid p-y approach for the design of laterally loaded pile foundations embedded in cohesive soil used for arbitrary pile dimensions, as well as different load levels. In this regard, the lateral bearing capacity obtained from the pile-soil interaction has to be predicted quite realistically. It is noteworthy that the proposed p-y approach is limited to the exclusive treatment of short-term monotonic loading conditions. However, its referential character has a direct influence on all geotechnical aspects of the monopile foundation design.

## 1.4 Solution

The following steps are required to achieve the objective described above:

- Establishment of a theoretical basis to the analysis of pile foundation behaviour subjected to lateral loading conditions
- Suitability analysis of the p-y approaches used for the design of single laterally loaded piles embedded in cohesive soil according to the API (2014) and DNVGL (2016) guidelines, as well as further alternative p-y approaches introduced in the literature
- Development of reliable three-dimensional numerical models from its validation by several field tests for predicting the load-bearing behaviour of piles with a large diameter subjected to short-term lateral loading conditions
- Evaluation of the impact of pile dimensions, as well as soil conditions on the pile-soil system to identify the crucial parameters by using comprehensive parameter studies

- 
- Proposing a new analytical method based on validated three-dimensional numerical models to obtain an optimal correlation between soil reactions and the lateral deflection of the pile foundation
  - Verification of the proposed p-y approach used for arbitrary pile dimensions, soil conditions and diverse load levels

Note that all p-y approaches used for the analysis of laterally loaded piles embedded in soft clay and stiff clay, as well as the new p-y method proposed in this thesis, have been successfully implemented in the in-house code IGtHPile design programme (cf. Terceros et al. 2015), which is based on object-oriented programming techniques.



## 2 Foundation structures for offshore wind turbines

### 2.1 General

From a general point of view, OWTs are complex systems formed by structural and mechanical elements exposed to extreme boundary conditions on the seas. Extremely salty air, salt water, powerful wind forces, strong currents, and the waves are some of the main conditions that offshore wind energy turbines must be designed to withstand.

Fig. 2-1 shows the main components of an OWT with a monopile foundation. A wind energy turbine basically consists of the substructure, the tower, the nacelle, and the rotor, which is composed of three blades and a central hub. The largest component of a wind turbine is the tower, generally built with tubular steel sections, providing structural support to the nacelle which is coupled to rotor blades. The main components required for the operation of a wind power plant are located in the nacelle. The substructure refers to the transition piece, the foundation and the scour protection. It is noted that modern OWTs with a capacity of 8 to 14 megawatts are very large structures. The tower can reach heights of over 100 meters. In Germany, currently used rotors have a diameter between 107 and 126 meters, although the most recent turbines have rotor diameters of about 150 meters, as stated by BMWi (2015a, 2015b).

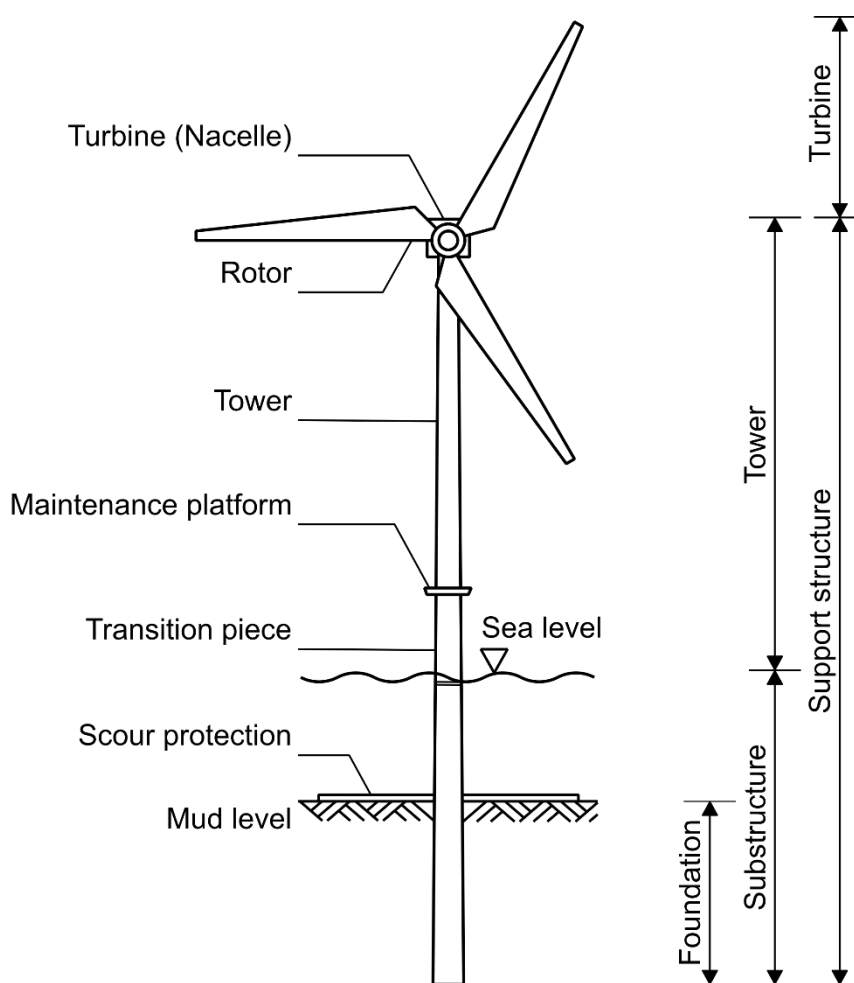


Fig. 2-1: Main components of an OWT with a monopile foundation

## 2.2 Typical offshore substructures

The substructure is an essential component that must ensure the optimal functionality of OWTs. Its design mainly obeys site-specific conditions. Critical factors such as water depth, geotechnical site characteristics, the load conditions, as well as the potential impact on the marine environment must be taken into account when selecting an appropriate foundation concept (cf. Lesny 2010). Obviously, the foundation design has a strong influence on the technical feasibility of offshore wind energy turbines.

The different loading conditions acting on the OWT structure (i.e. the vertical and the horizontal load under dynamic conditions) are transferred to the surrounding soil. The selection of the type of foundation concept mainly depends on water depth. The fixed bottom foundations are used for shallow water and transition, whereas the floating foundation concepts correspond to deep water. Bottom fixed foundation concepts have a part of the substructure submerged in the water and directly transfer the loading conditions in general to the subsoil. Monopile, gravity-based foundations (GBS), tripod, jacket and suction bucket belong to this group. Floating foundation concepts are only suitable if fixed foundations are not feasible mainly due to the limitation of water depth. A floating wind energy turbine is commonly anchored to the seabed. Fig. 2-2 shows the previously listed substructure foundation concepts. In the following, the aforementioned concepts of substructures for offshore wind turbines will be briefly described to obtain a clear overview.

### *Gravity-based foundations (GBS)*

Gravity-based foundations were initially developed as an alternative to deep pile substructures where pile foundations are not feasible due to the site's soil conditions. Gravity-based foundations are basically large reinforced concrete shell structures that rest on the surface of seabed characterised by a high load bearing capacity. Environmental lateral loading condition and overturning moment are transferred via distribution of contact pressures on the base. The self-weight and also the corresponding foot-area are thus of great significance for this foundation type. In order to avoid pumping effects, skirts are usually provided around the foundation. Interior skirts could also be provided under the base if the foundation area is very large. The installation method is performed with the construction of the concrete structure on a dry dock. Afterwards, the structure is floated out and towed to the final place, where it is filled with additional ballast, causing the foundation to sink and to become embedded in the seabed. Sub-base grouting is carried out around the foundation to maintain the platform level to obtain uniform stresses across the foundation. Grouting also becomes important whenever the seabed is uneven or sloping.

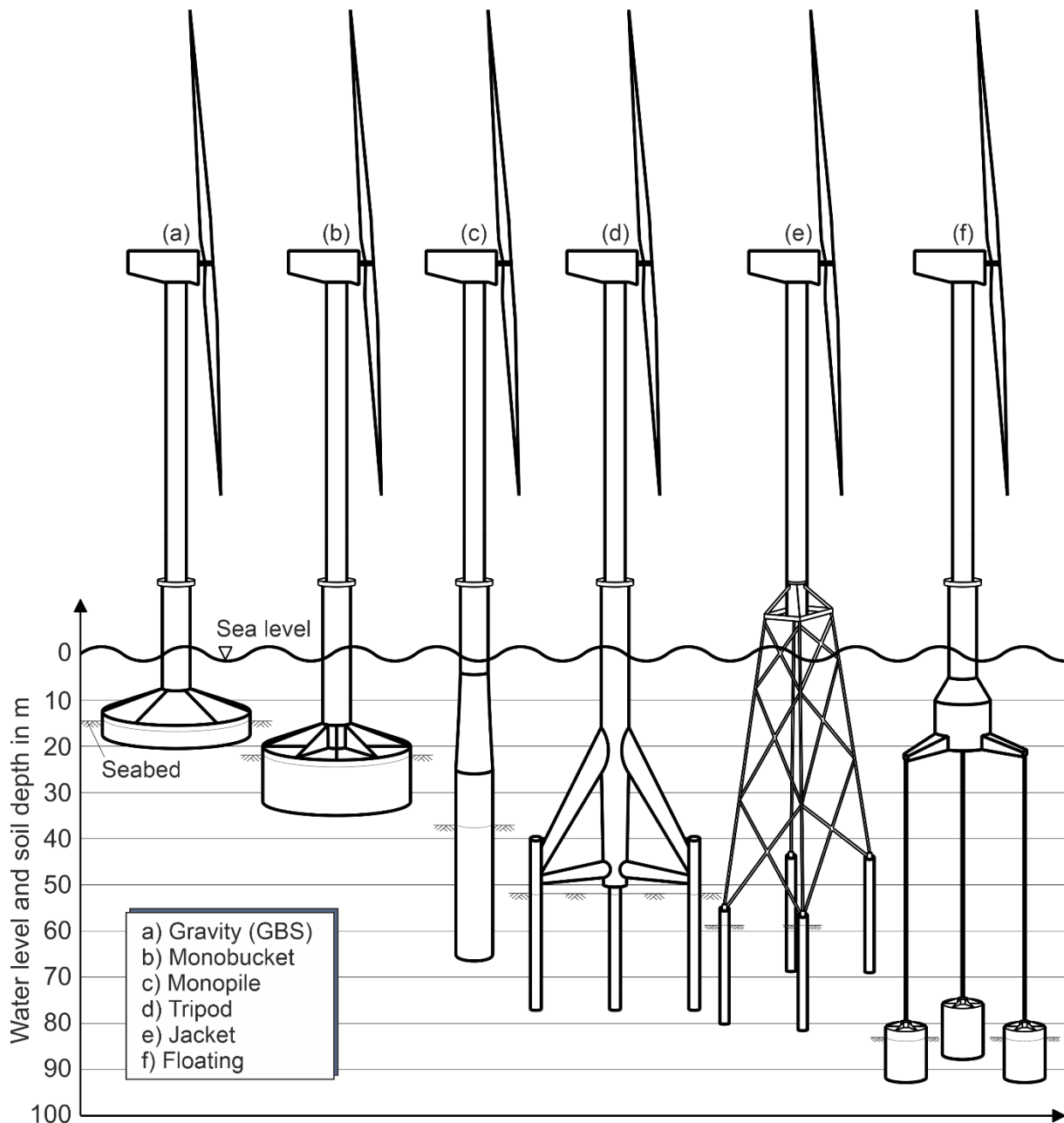


Fig. 2-2: Typical foundation concepts depending on the water depth

### *Monobucket foundation*

Monobucket is also known as monopod foundation or suction caisson. This concept consists of a steel cylindrical bucket closed at the top by means of a sealed lid and opened at the bottom. Large diameters and shallow penetration depths characterise a bucket foundation. Along with side friction on the skirt and suction pressure, the soil's weight encompassed within the bucket helps the foundation to withstand tension loads. Compression loads are transmitted to the soil through side friction and end bearing. The stability of the structure under wave loading is ensured due to the low period of a wave, whose short-time duration is not enough for the bucket to be pulled out from the soil, resulting in the so-called boot effect, for further details see Nielsen et al. (2017). The installation of a suction bucket foundation

consists of two phases. The self-weight installation phase occurs when the substructure sinks into the seabed. The suction installation phase occurs by reaching the required penetration depth by pumping the water enclosed within the bucket using a submersible pump. Pumping of the water generates a differential pressure through the sealed lid, which develops a suction, i.e. negative hydrostatic pressure. Suction inside the bucket leads to seepage whereby the effective stresses on the outer soil increase whilst the effective stresses inside the skirt decrease; the end bearing of a skirt tip also decreases, facilitating the skirt penetration. Advantages of monopods are the low level of noise and vibration during the installation as well as the possibility to easily remove the steel bucket from the seabed once the wind turbine life ends.

### ***Tripod foundation***

Tripod foundations consist of a triangular frame fixed to the seabed by steel pipe piles of smaller diameter. Each corner is also diagonally and horizontally braced to a transition piece located in the centre of the structure. The tripod-braced frame provides the foundation with large structural rigidity and a small, exposed surface. Loading is transmitted to each pile through the lattice structure. Compression loads are transferred to the subsoil by skin friction along the pile shaft and end bearing. Depending on the water depth, the piles are driven through sleeves attached to the base of the structure legs by either above-water hydraulic hammers or underwater hammers. Once the required penetration depth is reached, the piles are grouted to the sleeves.

### ***Jacket foundation***

Jacket foundation also known as lattice tower structure, consists of a space-braced frame fixed to the subsoil by four steel pipe piles. This type of foundation has been extensively used by the oil and gas industry. Load transfer and installation method are identical to the tripod foundation, being also the axial load crucial for the design analysis. There are adaptations of substructure concepts from either tripod or jacket foundations that are fixed by suction buckets. This innovative concept is known as multipod foundation and combines the advantages of the suction bucket with the structural rigidity of the braced frame.

### ***Floating foundation***

Floating foundations have been adapted from the oil and gas industry and developed as a solution for higher quality wind resources in locations with large water depths, where fixed foundation concepts are not feasible. The substructure consists of a floating wind energy turbine spliced through tensioned anchor legs to the selected foundation concept at the seabed. The floating structure is partially submerged to keep the legs in tension. For this purpose, either ballast tanks or tension systems are used, as seen in Fig. 2-2 (f). GBS, driven or drilled piles and suction buckets are commonly used as anchors. The most common



floating foundation concepts are the spar buoy, the tension-legged platform, the stabilised buoyancy and the semi-submersible.

## 2.3 Monopile foundation

The monopile foundation, which is the focus of the present research, currently represents the most common foundation concept for the OWT structure in German sea regions. For offshore wind energy turbines with monopile foundation, the wind tower is supported by a large diameter, thick-walled steel pipe pile through a transition piece (cf. Fig. 2-2 c). Monopile diameters are usually up to  $D = 6$  m with small ratio of embedded length to diameter  $L / D \leq 5$ , however diameters of up to  $D = 10$  m are already being manufactured to be used in deeper waters. Environment lateral loading and overturning moment are transferred into the surrounding subsoil by bedding pressures over the shaft surface along the pile foundation and shear stresses acting at the pile toe. Bedding resistances lead to distributed stress along the pile length, which also vary around the circumference. In addition, tensile and compression loads are transmitted to the soil through interface shear stresses and end bearing. Monopile foundations are characterised by a relatively stiff pile behaviour that ensures almost fully mobilization of the soil.

Monopiles are usually driven into the seabed by either large impact or vibration hammers. Although the installation time is relatively short, the impact-driven pile foundation yields high noise emissions that may affect marine life during the installation phase. As a mitigation measure, the bubble curtain is one of the most commonly used methods for reducing the noise related to impact pile driving underwater; for more details see Bohne et al. (2019).

The embedment of a monopile foundation in a marine environment modifies the flow pattern, resulting in increasing local sediment transport. This leads to scour of the seabed around the monopile foundation. A significant reduction of the lateral stiffness and ultimate capacity can be yielded by the effect of scour on monopile foundation (cf. Bayton et al. 2019). Consequently, scour protections are commonly installed around monopile foundations to prevent the long-term impact of scour on the bedding resistance of the pile foundations of OWTs.

## 2.4 Geotechnical design of monopiles

### 2.4.1 General

The responsible authority in Germany for verification and approval requirements of offshore installations within the exclusive economic zone (EEZ) is the Federal Maritime and Hydrographic Agency (BSH). Therein, special regulations are developed by BSH to define the minimal design requirements and thus enable the approval of offshore wind farms. The BSH “Minimum requirements concerning the constructive design of offshore structures within the EEZ” (2015) is particularly relevant for the geotechnical design of OWT foundations. In addition, the BSH “Standard Ground Investigations” (2014) refers to geological and geotechnical site investigations for planning and construction of offshore wind farms.

The BSH standards recommend the application of German standards (DIN 1054:2010-12), Eurocode 7 (DIN EN 1997-1:2009-09), and (DIN EN 1997-1/NA:2010-12) as the basis for the calculation and the geotechnical design of OWTs. Additional regulations as “Recommendations on Piling” (EA-Pfähle 2012) and “American Petroleum Institute Recommendations” (API 2014) are permissible to accomplish certain specific conditions for the geotechnical design analysis. The DNVGL (2018) guideline provides an accredited independent certification, but requires some additional controls. It is remarkable that the consideration of the cyclic load effects represents a basic criterion for all design aspects as stated by BSH (2015).

For the geotechnical design of monopile foundations used for OWTs, the Ultimate Limit State (ULS) and the Serviceability Limit State (SLS) design analysis have to be fulfilled similarly to common pile foundations. The structural integrity of the installation of OWTs, which is subjected to extreme events typically occurring during a storm event, has to be ensured by the geotechnical ULS design proof. According to Eurocode 7 (DIN EN 1997-1:2009-09) the ULS design proof can be carried out by using either the GEO-2 or GEO-3 design procedure to verify a sufficient soil strength, i.e. preventing to trigger the failure mechanism of the pile-soil system. The German standard (DIN 1054: 2010-12 and EA-Pfähle 2012) explicitly stipulates the application of the GEO-2 proof for the design of laterally loaded piles. In offshore engineering applications, particularly in an international context, the GEO-3 design proof is commonly applied for analysing laterally loaded piles, according to DNVGL 2018 (cf. section 2.4.2).

For the SLS design proof, the foundation stiffness and the accumulation of deformations due to long-term cyclic loading have to be taken into account to ensure the minimal required stiffness of the foundation structure, and also that the displacements and rotations remain within tolerable limits to ensure the turbine functionality. Usually, the maximum allowed rotation at the monopile head must not exceed  $0.5^\circ$ , as exemplified by DNVGL (2018), i.e. the maximum rotation for the installation process is set at  $0.25^\circ$  and the remaining rotation can be utilised by long-term cyclic loading condition.

The Accidental Limit State (ALS) design proof may also be required to ensure the structural integrity of the installation of OWTs when its resistance has been reduced by structural damage caused by a short-impact accident. In concordance with BSH (2015), the ALS design proof shall be carried out as far as such conditions are probable (e.g. ship collisions).

In addition, the oscillation behaviour of the overall structure and therewith the foundation stiffness under periodic loads is also relevant to the geotechnical design analysis. The foundation stiffness due to operational loads, which also determines the structural dynamic behaviour, is often a driving aspect that influences the design in terms of monopile diameter and wall thickness. Herein, the permissible bandwidth of eigenfrequency (NFA), as well as the structural fatigue of the steel construction are decisive for the design, resulting from the foundation stiffness yielded by small strains. The Fatigue Limit State (FLS) design proof is commonly carried out by using the approach “soft-stiff” such that the natural frequency of the overall structure is located within 1P and 3P of the excitation frequency to avoid resonance effects that could cause an impact on overall structural load at fatigue loading levels. Therefore,

an exact prediction of the foundation stiffness for the complete load-deformation ranges becomes crucially significant. For offshore wind turbine foundations, the SLS and FLS design proofs are often regarded as the most relevant for the geotechnical design analysis, as outlined in Sørensen (2012).

For the geotechnical design practice of laterally loaded piles, the influence of cyclic loads on soil resistance is generally taken into account by appropriate reduction of the strength parameters of static p-y curves. The verification of ULS and SLS design proof can be carried out by using cyclic p-y approaches whose p-y formulation is exposed in the offshore guidelines such as API (2014) and DNVGL (2016).

In addition to the usual geotechnical verification (ULS) and (SLS), the influence of the stiffness of the pile foundations on the vibration behaviour of the overall facilities is coming into focus. The permissible natural frequencies (NFA) in the range of small horizontal displacements are decisive. This requires an accurate prediction of the pile foundation stiffness to avoid resonance effects and the associated high fatigue loads. In current design practice, high foundation stiffness is considered for predicting the un- and reloading behaviour utilizing the application of static p-y curves (cf. Achmus et al. 2019).

For the geotechnical design of pile foundations of OWTs, the so-called pile length criteria are commonly applied for calculating the required embedded pile length. Four different pile length criteria are frequently used, which are directly related to the p-y curves, (cf. Achmus et al. 2017b).

The present thesis focuses on the examination of static p-y curves which have a direct influence on all geotechnical aspects of foundation design due to its referential character. The innovative static p-y approach introduced in section 7 can be taken as a basis for the development of a new cyclic p-y approach whereby the degradation mechanisms of soil capacity must be considered due to the effect of long-term cyclic loading conditions.

### **2.4.2 p-y method**

For the geotechnical analysis of monopile foundations, the p-y methods are widely applied to predict the load-bearing behaviour of laterally loaded single piles. To this effect, the non-linear, depth-dependent load-deformation p-y characteristic of the soil springs (also termed p-y curves) are utilized for determining the relationship of the lateral soil resistance against the lateral pile deflection. In other words, a p-y curve is only one of a set of p-y curves, which describe the lateral-load transfer along the pile length depending on the depth and lateral deflection.

The construction of the p-y curves presented by offshore regulations such as API (2014) and DNVGL (2016) is a function of the soil type. These have been shown to be reliable and applicable to the small pile diameters that were commonly used for jacket structures in the offshore industry. However, the validity of these semi-empirical p-y methods for large-diameter piles has been questioned on several occasions (cf. section 3.9). However, the p-y curves proposed by Matlock (1970) are still predominantly recommended in OGLs for cohesive soils.

To predict the bedding resistance for the analysis of pile foundations supporting the offshore structures, the p-y curves must be applied taking into account the effects of cyclic degradation on lateral strength and stiffness. However, according to DNVGL (2018), the application of p-y methods for piles with diameters more than 1.0 m is subject to validation by using FE analysis. In practice, such calibration of the p-y curves is occasionally conducted by applying the p-y multipliers for adjusting both the stiffness and the strength based on the results of the numerical models.

### **2.4.3 Distinction of p-y approaches for different load conditions**

Small vertical loads, large dynamic horizontal loads and overturning moments usually characterise the loading conditions on a substructure of offshore wind turbines, as stated by Malhotra (2011). An OWT structure is a highly dynamic system with significant non-linear behaviour and dynamic responses that has to withstand static, cyclic, stochastic and transient loading conditions.

For the application of p-y approaches, three types of loading condition situations can be certainly identified (i.e. static, cyclic and reloading conditions). Static p-y curves describe the foundation response caused by monotonic loading conditions. Due to the reference character of static p-y curves, this represents a reliable basis for defining other types of p-y approaches related to the design of laterally loaded piles.

Similarly, the long-term cyclic effects on the response of the pile-soil system can be represented by using cyclic p-y curves. The degradation of ultimate bedding resistance and the accumulation of deformations resulting from cyclic loading usually comes into consideration by modifying static p-y curves.

Finally, reloading p-y curves intend to predict the foundation stiffness caused by repeated un- and reloading. In other words, they describe the foundation stiffness due to passing through an un- and reloading hysteresis. Numerical investigations in non-cohesive soils conducted by Achmus et al. (2019) already demonstrated that the reloading stiffness could be described by using the initial slope of static p-y curves. Obviously, this presupposes that degradation effects for the reloading stiffness are not to be expected.

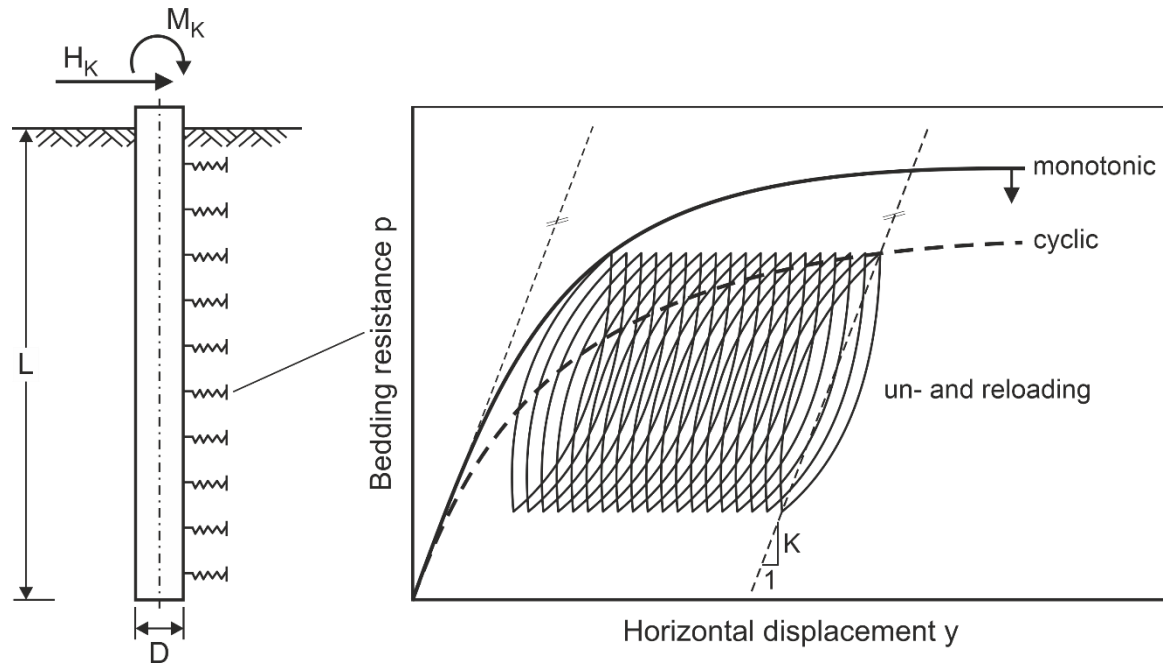


**Fig. 2-3: Schematic representation of p-y relationships for static, cyclic and reloading conditions**

The three types of p-y approaches (static, cyclic and reloading) illustrated in Fig. 2-3 are considered in distinct key aspects for the design of OWT pile foundations. The applications of p-y approaches can be categorised into two groups when it comes to the design of laterally loaded piles.

- Ultimate Limit State (ULS) and Serviceability Limit State (SLS): The cyclic horizontal load-bearing behaviour of the pile-soil system is determined by using cyclic p-y approaches. Consequently, the degradation of ultimate bedding resistance and accumulation of deformations during the whole lifetime of the OWT is theoretically included.
- Natural Frequency Analysis (NFA) and Fatigue Limit State (FLS): The reloading p-y approaches are applied to characterise the horizontal load-bearing behaviour of the pile foundation due to un- and reloading conditions. It is remarkable that reloading p-y curves for clay soil do not currently exist and are quite limited for sand. The application of the initial slope of static p-y approaches is basically feasible and often conducted in practice. However, this could be considered a poor concept since the foundation stiffness is implicitly underpredicted. Note that when it comes to the Fatigue Limit State FLS design proof of OWT structures, neither an overestimation nor an underestimation of the foundation stiffness is conservative in general.

#### 2.4.4 GEO-2 design proof for ULS

The geotechnical ULS design proof is conducted to ensure the structural integrity of the OWTs, thereby the GEO-2 limit state must be fulfilled for the design of laterally loaded piles described by the DIN 1054:2010-12 guideline and EA-Pfähle (2012) recommendations. By doing so, the partial safety factors  $\gamma_E = 1.4$  and  $\gamma_R = 1.35$  are usually selected (for persistent design situation

BS-P) according to the DIN 1054: 2010 -12 guideline that is applied to the characteristic effect force  $B_k$  and the resultant passive earth pressure force  $E_{ph,k}$ , respectively.

$$B_k \cdot \gamma_E \leq \frac{E_{ph,k}}{\gamma_R} \quad (2-1)$$

$$B_d \leq E_{ph,d} \quad (2-2)$$

The GEO-2 design proof essentially verifies that the design value of the effect force  $B_d$  must be smaller than or equal to the design value of the soil resistance  $E_{ph,d}$ , as seen in Eq. 2-2.

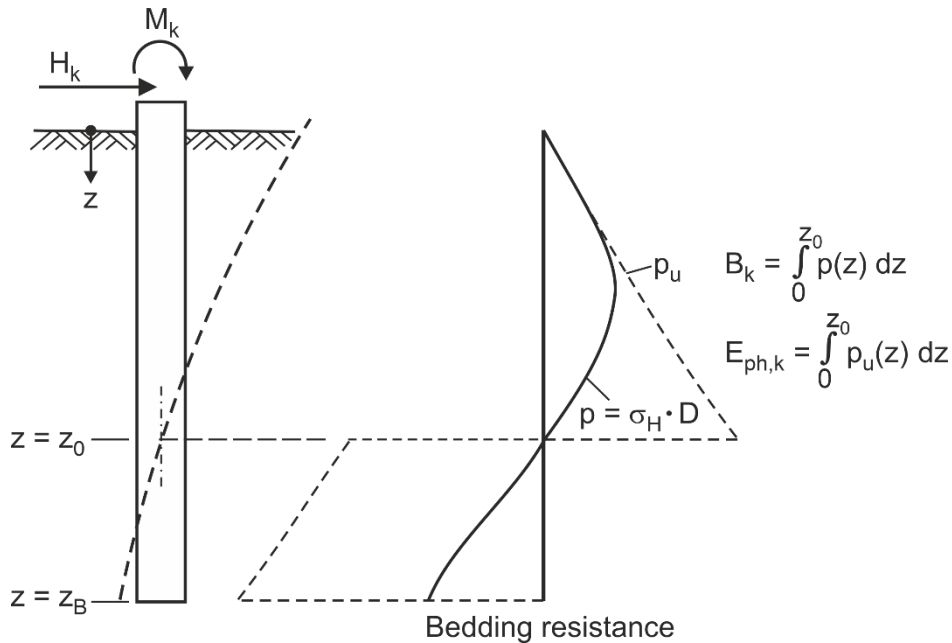


**Fig. 2-4: GEO-2 for ULS design proof according to German standard DIN 1054:2010-12 (after Thieken et al. 2013)**

Fig. 2-4 shows a pile-soil system loaded by a characteristic lateral force  $H_k$  and its respective overturning moment  $M_k$  at the pile head. For calculating the characteristic effect force  $B_k$ , the stress reaction  $p$  must be integrated from the free surface to the pile pivot (also termed as zero-deflection point  $z_0$  of the pile foundation). Similarly, the soil resistance  $E_{ph,k}$  must be calculated, considering the integration of the ultimate bedding resistance  $p_u$ , e.g. by assuming the  $p_u$  of the respective  $p$ - $y$  curves. Note that for calculating both cases (i.e. effect force  $B_k$  and also soil resistance  $E_{ph,k}$ ) the application of suitable  $p$ - $y$  curves becomes crucial for carrying out a reliable design proof.

#### 2.4.5 GEO-3 design proof for ULS

According to DNVGL (2018), the GEO-3 limit state corresponds to the geotechnical ULS design proof for laterally loaded pile. In contrast to GEO-2, the results of the GEO-3 proof are independent of the pile stiffness, as stated by Achmus (2012a).

In this instance, the partial safety factors  $\gamma_{\phi'}$ ,  $\gamma_{s'} = 1.15$  and  $\gamma_{su} = 1.25$  recommended by DNVGL (2018) are applied to the characteristic shear parameters, such as the friction angle  $\phi'_k$ ,

the effective cohesion  $s'_k$ , and the undrained cohesion  $s_{u,k}$ , respectively. The required p-y curves for calculating the soil resistance are derived by using the decreased design shear parameters given in Eq. 2-3, 2-4 and 2-5.

$$\varphi'_d = \tan^{-1} \frac{\tan \varphi'_k}{\gamma_\varphi} \quad (2-3)$$

$$s'_{d} = \frac{s'_k}{\gamma_c}; \quad s_{u,d} = \frac{s_{u,k}}{\gamma_{su}} \quad (2-4, 2-5)$$

For the design of laterally loaded piles, the applied load is increased until the equilibrium of the pile-soil system is no longer possible, thus obtaining the design value for ultimate load-bearing capacity  $H_{d,ult}$  which results from the failure state. The design pile head load  $H_d$  is determined by applying the partial safety factor  $\gamma_E = 1.35$  to the characteristic lateral load  $H_k$ .

$$H_k \cdot \gamma_E \leq H_{d,ult} (\varphi'_d; s'_d; s_{u,d}) \quad (2-6)$$

$$H_d \leq H_{d,ult} (\varphi'_d; s'_d; s_{u,d}) \quad (2-7)$$

GEO-3 design procedure leads to the comparison of the design pile head load  $H_d$  with the ultimate load-bearing capacity  $H_{d,ult}$ . For that, the Eq. 2-7 gives the governing condition.

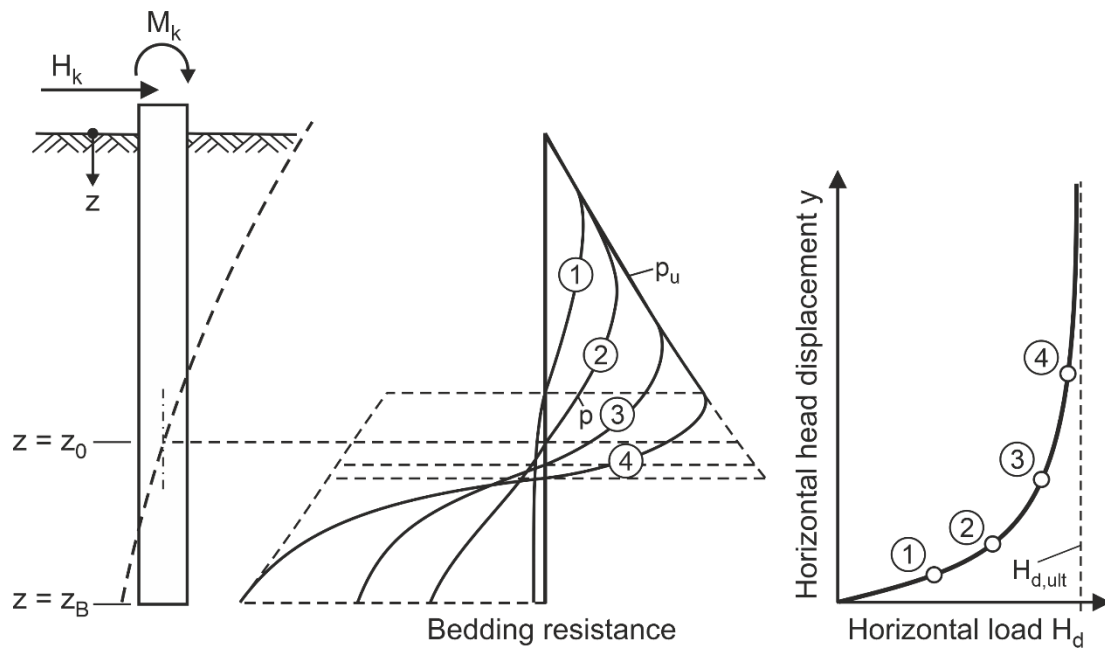


Fig. 2-5: GEO-3 for ULS design proof according to DNVGL (2018) guideline

Fig. 2-5 shows the horizontal load-bearing behaviour of the pile-soil system with a further load increase until the ultimate load-bearing capacity  $H_{d,ult}$  is reached (as seen in ④). The latter is evidently asymptotic to the load-displacement curve. For almost rigid piles, the zero-deflection point of pile moves downwards, while the soil resistance is entirely mobilised with increasing lateral loading condition.

### 2.4.6 SLS verification

The SLS design analysis verifies the permanent rotation of the pile head under characteristic extreme load cases that have to remain within tolerable limits for the functionality of the turbine. In this respect, the extreme load level of the characteristic ULS loads is taken into account for design storms as required by the BSH (2015). In addition, the accumulated deformation due to cyclic loading must be calculated over the entire structural lifetime, according to the DNVGL (2018). The typical specific limit of the accumulated permanent head rotation is normally set to  $\Theta_{\text{perm,max}} = 0.25^\circ$  at the seabed (i.e. maximum tilting of the pile at the head). According to common practice, the permanent (plastic) head rotation  $\Theta_{\text{perm}}$  is calculated by subtracting the elastic portion  $\Theta_{\text{elastic}}$  of this rotation from the total head rotation  $\Theta_{\text{total}}$  after the applied number of cycles, as given by Eq. 2-8.

$$\Theta_{\text{perm}} = \Theta_{\text{total}} - \Theta_{\text{elastic}} \leq \Theta_{\text{perm,max}} \quad (2-8)$$

Fig. 2-6 shows qualitatively the elastic and plastic parts of the pile head rotations, which are represented graphically by applying a tangent line to the first part of the moment-rotation curve at the seabed level. Evidently, the initial slope of the non-linear p-y curve becomes decisive for calculating the permanent head rotation  $\Theta_{\text{perm}}$ .

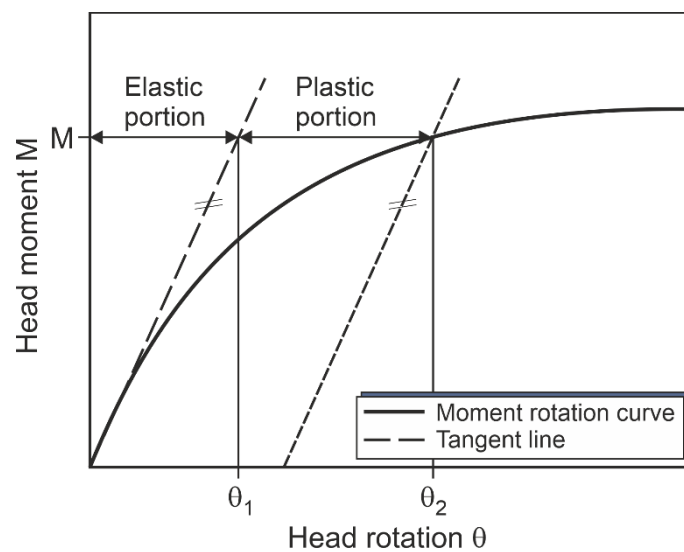


**Fig. 2-6: Graphical estimation of elastic and plastic rotations**

In fact, the accumulated deformations yielded by cyclic laterally loaded piles can be determined by applying the cyclic p-y curves according to DNVGL (2016), but the results have to be verified by using numerical models. Note that the static p-y curves introduced in section 7 could be adequate to consider the long-term cyclic lateral loading conditions by reducing both the stiffness and soil strength, certainly leading to an increase of the permanent head rotation  $\Theta_{\text{perm}}$ .



## 3 Theoretical basis for laterally loaded piles

### 3.1 General

The analysis of laterally loaded piles essentially requires three-dimensional models to realistically reproduce the pile-soil interaction. The horizontal load-bearing behaviour of the pile-soil system is highly non-linear, mainly due to the variation of soil stiffness and strength over depth. The pile-soil interaction mechanism is influenced by many complexities such as strength non-homogeneity, pile-soil adhesion, and suction (in the following also termed “gapping”) at the active side of the pile embedded in cohesive soils according to Murff & Hamilton (1994).

The laterally loaded pile foundations can be categorised into active and passive piles, depending on the location of the applied lateral loading. The active piles are subjected to external lateral load applied at the pile head, such as the OWT foundations and retaining walls. Passive piles however primarily support loads along the pile length due to earth pressure and are commonly used for containing instabilities, e.g. piles for slope stabilisation, bored pile walls to support deep excavation or embankment.

The framework of this thesis is limited to monotonic lateral loading conditions for piles embedded in a cohesive soil, i.e. active piles loaded laterally. The relevance of static loading conditions for analysing the horizontal load-bearing behaviour of a pile is quite remarkable since it is taken as the essential basis to develop future analytical procedures for other types of loading. In the case of non-cohesive soils, for instance, the un- and reloading stiffness of the monopile-soil system, which is decisive for the eigenfrequency of the overall structure, can be approximated by the initial stiffness (slope) of the static load-deflection and moment-rotation curves as described by Achmus et al. (2019). A further application of the method analysis for static loading conditions results in the degradation of its shear strength properties to capture a realistic horizontal load-bearing behaviour of pile foundations subjected to cyclic lateral loading, similar to all traditional p-y methods recommended by API (2014) and DNVGL (2016).

This chapter deals with the most relevant aspects of the mechanical behaviour of piles subjected to static lateral loading. This theoretical basis is mainly focused on the analysis of the laterally loaded pile foundation embedded in cohesive soils.

### 3.2 Analysis methods of laterally loaded piles

Despite technological advances, the analysis of pile foundations, in particular of laterally loaded piles, remains a challenging task for geotechnical engineers. In this section, a general description of the most significant analysis methods proposed in the literature will be introduced for providing an overall overview. The methods for analysing laterally loaded piles can normally be divided into the following categories.

### *The elasticity method*

Based on the theory of elasticity, Poulos & Davis (1980) proposed the elasticity method for analysing piles subjected to lateral loading and overturning moment embedded in an ideal elastic mass. The elastic solution can be used for calculating the displacement and rotation at the pile head for both free and fixed headed conditions. The theory of elasticity considers the soil mass as continuous but adopting a linear-elastic behaviour, which is considered unrealistic since all types of soil behave non-linear elastic-plastic. Therefore, this method could only be valid for very small strains of the pile, assuming an ideal elastic behaviour of the soil in this deformation range.

### *The limit state method*

The simplest procedure that currently exists is the limit state method, based mainly on the determination of the ultimate bedding resistance such as that proposed by Broms (1964a, 1964b) for calculating the lateral displacements at the pile head and the corresponding maximum bending moment of single laterally loaded piles embedded in the soil. The application of such methods is basically conducted by manual calculations and tables or graphics. However, the proposed methods should be applied with caution since the mobilised soil reactions are generally assumed to be linear elastic-perfectly plastic. There are limit state methods that only provide the ultimate bedding resistance, such as that proposed by Randolph & Houlsby (1984) and Martin & Randolph (2006), for instance.

### *The strain wedge method*

Norris (1986) first introduced the strain wedge method to predict the horizontal load-bearing behaviour of flexible piles, based on the model of a passive wedge forming at the front of the pile. The response of a three-dimensional pile-soil interaction using the passive wedge is correlated with the parameters of traditional p-y curves to simplify one-dimensional beam model. The free-body diagram with the respective forces of the passive wedge used for the development of this method is quite similar to that used by Reese et al. (1974) for describing the load-bearing behaviour of the pile-soil system (cf. section 3.6.1). Note that the strength parameters used to define the behaviour of mobilised soil reactions are derived from triaxial tests. Furthermore, as stated by Ashour et al. (2002), layered soils can be taken into account for analysing pile-soil interactions.

### *The subgrade reaction method*

The concept of the subgrade reaction method was originally introduced by Winkler (1867) for describing the load-bearing behaviour of an elastic foundation based on an Euler-Bernoulli beam model supported on a set of uncoupled linear elastic spring characteristics (using Hooke's law). The soil reaction  $p$  and the horizontal displacement  $y$  are linearly related through the application of a subgrade reaction modulus  $K_{py} = p / y$  at any point of the soil-foundation system. The linear dependency between the soil reaction  $p$  and the pile

deflection  $y$ , which leads to highly inaccurate analysis, does not allow to predict the ultimate bedding resistance, for instance. The Winkler modelling approach cannot fully capture the three-dimensional behaviour patterns of the pile-soil system due to the constant stiffness against the depth for analysing laterally loaded piles. Subsequently, the p-y method was first proposed by McClelland and Focht (1958) and later more thoroughly developed by Reese and Matlock with regard to cohesive soils. The load-bearing behaviour of pile foundations subjected to lateral loading conditions is calculated, based on the Winkler foundation analysis with certain adaptations. The pile foundation is modeled as a beam element supported by non-linear, soil- and depth-dependent characteristics of soil springs acting orthogonally to the pile axis. The p-y method is merely a non-linear correlation between the mobilised soil reaction force per unit length  $p$  and lateral deflection  $y$  along the pile shaft. However, the independence between adjacent springs has not yet been overcome, considering soil as theoretically non-continuous (cf. section 3.8).

### *The finite element method*

For analysing the pile-soil interaction, the application of finite element methods allows the soil to be treated as a continuum (cf. Abdel-Rahman et al. 2005, Achmus et al. 2014). Furthermore, the non-linear behaviour of soil in terms of deformations and bearing capacity can be realistically reproduced by using numerical simulations for complicated loading conditions (e.g. either dynamic loading or arbitrary combinations of axial, lateral, and torsion loading). Achmus et al. (2016) developed three-dimensional numerical models for capturing the load-bearing behaviour of laterally loaded monopile foundations embedded in soft clay, demonstrating that it is feasible to carry out comprehensive parametric studies with the existing computational capacity. However, the numerical models highly depend on the application of suitable constitutive material models to correctly reflect the horizontal load-bearing behaviour of the pile-soil system. The numerical simulations can be used to conduct extrapolations in terms of either soil conditions and pile dimensions. Its respective calibration which is based on the comparison with the results obtained from data of field tests with diverse properties is essential to obtain reliable results.

## **3.3 The p-y method analysis**

The p-y curves (also known as p-y spring characteristics) are most commonly used in practice when it comes to the general design of laterally loaded pile foundations. The p-y methods correspond to the classification of semi-empirical correlations since the relationship of the mobilised soil reaction  $p$  against the lateral deflection  $y$  of the pile is based on the measurements from lateral load tests.

For the derivation of p-y curves, the application of electrical resistance strain gauges on the instrumented pile foundations and the data from soil testing laboratory is quite common, as stated by Gazioglu & O'Neill (1984).

The p-y method for cohesive soils generally recommended in the OGLs such as API (2014) and DNVGL (2016), and extensively used in practice is based on the finding of Matlock, even though the p-y method proposed was exclusively developed for soft clay, mainly derived from the lateral load test of Sabine River, as stated by Matlock (1962). Additionally, the construction of p-y curves for stiff clay proposed by Reese & Cox (1975) was merely appointed by API (2007) without any further details.

The laterally loaded pile foundation is modelled as one-dimensional beam finite elements which are formulated on the assumption of either Euler-Bernoulli or Timoshenko beam theory. The shear stresses in the cross section of the beam are neglected by the Euler-Bernoulli beam theory. In contrast, the Timoshenko beam theory considers the contribution of shear stresses around the pile, leading to a redistributed moment. Besides that, the soil around the pile is idealised as a set of non-linear, depth-dependent spring characteristics at discrete points along the embedded length of the pile. The idealisation of the laterally loaded pile model, which is applied in several finite element programmes such as that developed in this thesis to carry out the comparative study introduced in section 6 and 8, is provided in Fig. 3-1 (left).

The mobilised soil reaction  $p$  is described as a non-linear function of the lateral deflection  $y$  of the pile as can be seen in the set of p-y curves illustrated in Fig. 3-1 (centre). The pile displacements are specified at nodal points over the depths at which the p-y curves are applied, denoting the influence of the high non-linearity of soil behaviour. Anyhow, the red line represents the pile deflection line. The increase of soil resistance per unit of length against the depths is likewise captured to describe the non-linear response of the soil. It is remarkable that traditional p-y curves exhibit a symmetry between positive and negative displacements in all depths of the model, including the lower section of the pile, disregarding the high shear strength at the pile tip produced particularly for rigid piles.

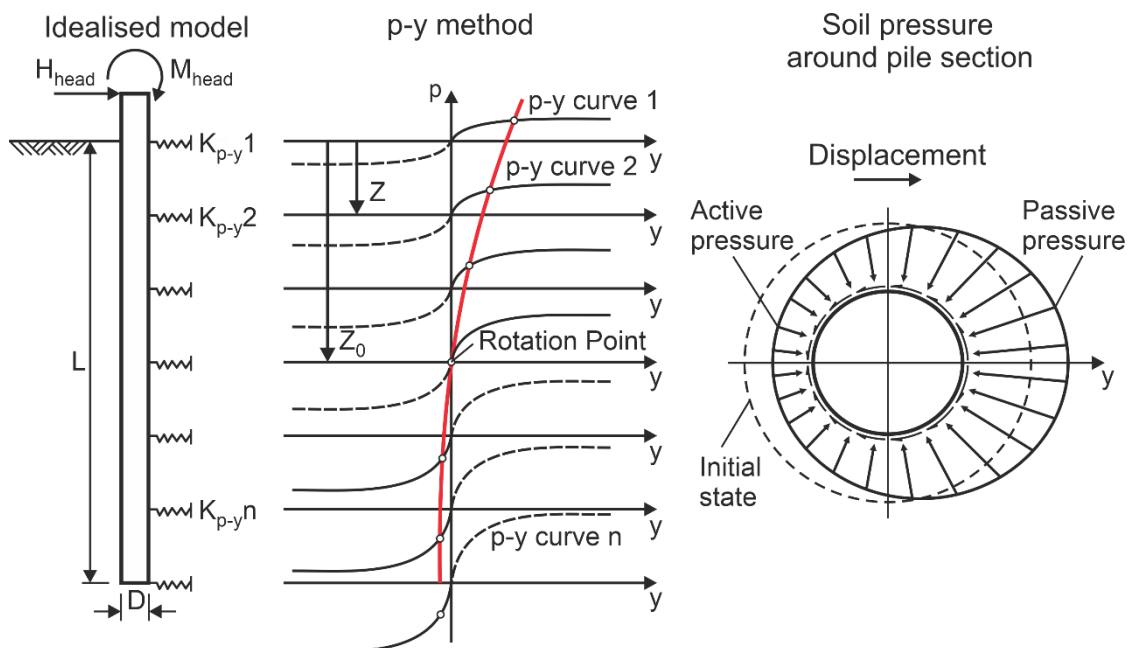


**Fig. 3-1: Assumed model of the subgrade reaction method (left) and set of p-y curves (centre) as well as the soil pressure around the pile (right)**

Fig. 3-1 (right) shows the initial state of a pile installed in upright position and without bending stress, describing a uniform distribution of radial stresses, normally applied to the wall of the pile, but when the pile is pushed laterally through the soil producing a bending moment. Thereby a region of high stress in front of the pile and low stress at the active side of the pile is yielded due to a redistribution of stress to obtain the equilibrium of the pile-soil system, which is subjected to lateral load at the pile head. The net soil resistance calculated for the corresponding cross section which is opposite to the existing lateral displacement of the pile, is obtained by the integration of normal and shear (tangent) stresses around the respective circular cross section of the pile.

Hetenyi (1946) introduced the derivation of a non-linear, fourth-order differential equation applied to beam-column elements, representing the idealised model of an elastic pile foundation subjected not only to lateral and moment loads but also to axial loads. In general, the axial load on a laterally loaded pile foundation has a relatively small or negligible influence on the bending moment. However, it is sometimes required to find the buckling load for a pile, and therefore the axial load is also considered in the derivation. The conventional form of the differential equation, which is denoted by DNVGL (2016), is taken as a basis for solving the relationship between the displacement and the stress of the pile at any point along the embedded length of the pile for arbitrary load conditions applied at the pile head.

$$E \cdot I \cdot \frac{d^4 \cdot y}{d \cdot x^4} + Q_A \cdot \frac{d^2 \cdot y}{d \cdot x^2} + p(y) + q = 0 \quad (3-1)$$

$$\text{with } E \cdot I \cdot \frac{d^3 \cdot y}{d \cdot x^3} + Q_A \cdot \frac{d \cdot y}{d \cdot x} = Q_L \quad \text{and} \quad E \cdot I \cdot \frac{d^2 \cdot y}{d \cdot x^2} = M \quad (3-2)$$

where  $E \cdot I$  is the bending stiffness of the pile,  $y$  is the lateral deflection of the pile,  $Q_A$  is the axial load on the pile head,  $Q_L$  is the lateral force at the pile head,  $p(y)$  is the lateral soil reaction derived from non-linear  $p$ - $y$  curves,  $q$  is the distributed load along the pile, and  $M$  is the bending moment in the pile,  $x$  denotes the position along the pile's axis. The solution of the differential equation provides all required design information such as pile deflection, bending moment and shear force along the beam span (as idealisation of the pile foundation).

The laterally loaded pile foundation is basically a problem of the pile-soil interaction whereby the mobilised soil reaction is a non-linear function of the pile deflection, and similarly the pile deflection depends on the mobilised soil reaction. The solution must satisfy the aforementioned non-linear differential equation and compatibility conditions with respect to the  $p$ - $y$  curves to obtain the equilibrium of the pile-soil system. The solution normally requires numerical methods that are solved by using iterative procedures, e.g. Newton-Raphson method. For solving the non-linear differential equation of elastic beam model supported by non-linear springs, the initial stiffness  $K_1$  of  $p$ - $y$  curves can be applied as starting value for calculating the displacements  $y_1$  at the nodal points along the embedded length of the pile. The soil resistance  $p_1$ , which must be compared with the existing resistance of known non-linear  $p$ - $y$  curves, corresponds to the calculated displacement  $y_1$  using the assumed secant stiffness  $K_1$ . The deviation obtained from the soil resistance that is calculated with the existing resistance is used

for adapting the respective secant stiffness  $K_2$  for the next iteration, so that the calculation process is repeated to reach the convergence, as illustrated in Fig. 3-2.

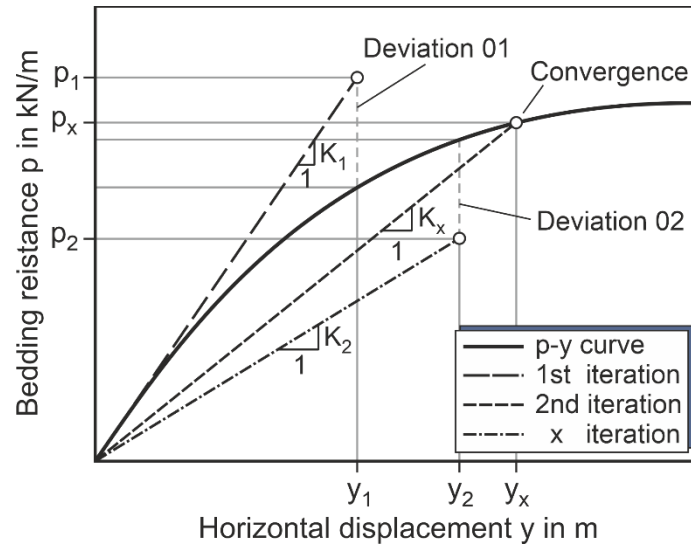


Fig. 3-2: Iterative process to adjust the secant stiffness of p-y curves

### 3.4 Components of p-y curves

The typical p-y curve can be characterised by three components that define its attributes at various load levels. The initial stiffness of p-y curves (also known as initial slope) describes the highest stiffness that can be assumed as a suitable approximation of the un- and reloading stiffness for monopile foundations embedded in sand, as stated by Achmus et al. (2019). The ultimate bedding resistance  $p_u$  implies that the soil behaves perfectly plastic. In cohesive soils, a degradation of the soil resistance may be produced after the peak of the curves, particularly for cyclic loading conditions. The shape of the p-y curves which is decisive for the stiffness response of the soil represents the transition part between the initial stiffness and the ultimate bedding resistance  $p_u$ . Note that all traditional p-y methods for cohesive soils were invariably derived from field load tests under undrained soil conditions.

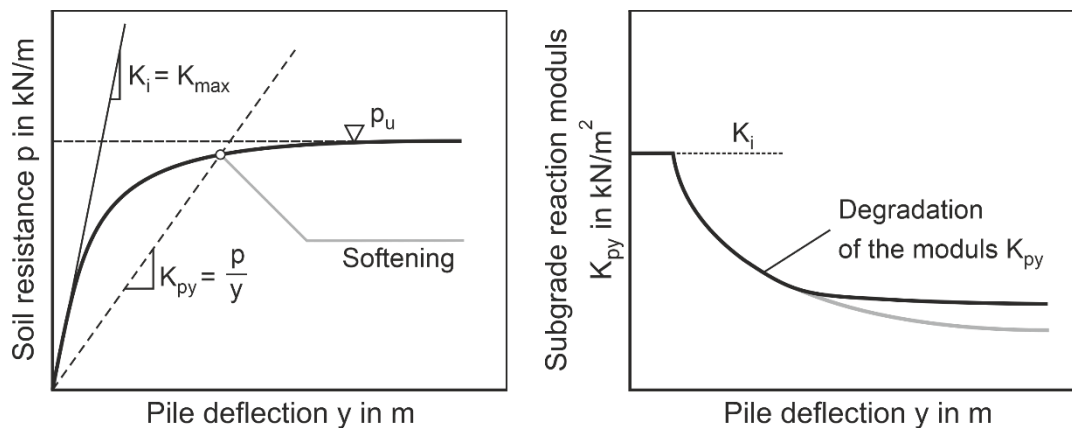


Fig. 3-3: Typical non-linear p-y curve (left) and resulting subgrade reaction modulus (right)

The typical qualitative shape of a p-y curve for cohesive soil that belongs to a set of p-y curves for a short-term monotonic loading is represented in Fig. 3-3 (left). The initial slope of the p-y curve, which represents the highest stiffness, is defined by the constant value  $K_i$  for very small deflections of the pile. The gradual reduction of the lateral resistance that increases the pile deflection until it reaches the ultimate bedding resistance, defines the shape of the p-y curve. The latter is empirically determined, based on the results of the lateral load field test, as stated by Isenhower et al. (2015). The p-y curves are limited by the ultimate bedding resistance  $p_u$ . The perfectly ideal non-linear behaviour of soil is described by  $p_u$  as an asymptotic behaviour, meaning no more gain of shear strength with increasing pile deflections.

The subgrade reaction modulus  $K_{py}$  is defined as the secant modulus  $p / y$  and varies as a non-linear function of the lateral deflection  $y$ , the soil properties, pile stiffness, the type of load, and the depth  $z$  below the free soil surface. The pile-soil behaviour in terms of displacements and subgrade reaction modulus  $K_{py}$  is characterised, which decays with increasing pile deflection as seen in Fig. 3-3 (right).

The p-y curves for stiff clay proposed by Reese & Cox (1975) describe the degradation of the bedding resistance after the peak by either static or cyclic loading conditions, where the fully plastic range begins. The grey lines in Fig. 3-3 represent the degradation (also known as softening behaviour) of the soil. The level of degradation for stiff clay depends on the number of load cycles. It is noteworthy that the degradation for stiff clay also exists under static load but is less pronounced in that case. According to Reese et al. (2001), the degradation takes place mainly from erosion, as water is pumped out through the gap that is formed around the pile. Another possible cause of degradation is the removal of clay that surrounds the pile.

### 3.5 Initial stiffness $K_i$

The initial stiffness that is defined by the initial slope of the p-y curve (i.e. modulus of subgrade reaction) can be used to approximately calculate the un- and reloading stiffness of the pile foundation for the overall dynamic simulations of the whole OWT structure, assuming that the horizontal load-bearing behaviour of the pile-soil system is linear for very small strains. By doing so, the estimation of the initial stiffness is relevant when it comes to the NFA and FLS proofs for the design of offshore wind turbines (cf. Thieken et al. 2018b).

The initial stiffness of p-y curves did not receive great attention for defining the traditional p-y approaches since they were mainly used to verify the ULS design proof of the pile supported offshore oil and gas platforms. Reese et al. (1975) first introduced the definition of the initial slope of the p-y curves for stiff clay using an initial straight-line portion as a function of the average undrained shear strength  $s_{u,a}$  (cf. section 4.4.1).

The parabolic function proposed by Matlock (1970) for soft clay (cf. section 4.3.1) provides infinite initial stiffness, thereby not allowing its application for very small strains. The linearisations of the p-y approach developed by Matlock, recommended in the offshore guidelines such as API (2014) and DNVGL (2016) are generally used to determine the shape of spring characteristics for cohesive soils. By doing so, the linearisations shall counteract the

infinite initial stiffness of the p-y curve formulation which is associated with the overestimation of the bedding resistances for small strains (cf. section 6.3).

Based on the numerical analysis of field and laboratory tests, Kim et al. (2009) developed an entirely new p-y approach that considered a hyperbolic function to enable the definition of initial stiffness which is a function of the soil properties and also pile dimensions. It is also remarkable that Jeanjean (2009) proposed a hyperbolic tangent p-y formulation for soft clay, based on the results from centrifuge tests and finite element modeling. The dynamic shear modulus  $G_0$  is included in the basic p-y formulation for defining the initial stiffness.

In the framework of the Pisa Project (2016), an innovative approach has been developed that differs from the conventional p-y approaches, considering also rotational springs characteristics (also termed as m- $\psi$  curves) along the pile length. For modelling the soil reaction resulting from shear strength at the pile tip, two additional springs characteristics are also incorporated, which define the base shear force and the base moment of the pile toe. Interestingly, all of the aforementioned spring characteristics have a specific definition of the initial stiffness derived by the calibration function obtained from the numerical analysis validated by the stiff glacial clay till at Cowden (Byrne et al. 2020). The initial slope of the spring characteristics located along the pile length are characterised by using a simple depth variation function together with the respective pile diameter (cf. section 4.4.3).

### 3.6 Ultimate bedding resistance $p_u$

The ultimate bedding resistance  $p_u$  (also termed ultimate lateral bearing capacity) can be defined as the maximum mobilised soil reaction force per unit length that the pile-soil system is able to withstand before triggering the failure mechanism of the soil. The lateral collapse mode of a single pile was described in detail by Murff & Hamilton (1994) for cohesive soils, proposing the distinction between two failure mechanisms that develop near the free soil surface in one case and at deep depth in the other case.

Due to the influence of free soil surface on the soil failure mechanism, only a (conical) passive wedge failure mechanism is placed in front of the pile at shallow depths, provided that a gap condition occurs at the active side of the pile as represented in Fig. 3-4 (left). Instead, the mechanism of active and passive wedge failure would take place in case a no-gap formation occurs as seen in Fig. 3-4 (right). In isotropic soils, both wedges are identical but at opposite sides of the pile and counteract each other according to Jeanjean et al. (2017).

At a certain depth, the influence of the free soil surface on the mode of failure no longer exists and yields a flow failure mechanism of the soil around the pile in a horizontal plane at deep depths as specified by Randolph & Houlsby (1984). This mode of failure is depicted in Fig. 3-4 at the bottom of the pile-soil systems. In this failure mechanism, the non-gap formation between pile and soil is inherent.



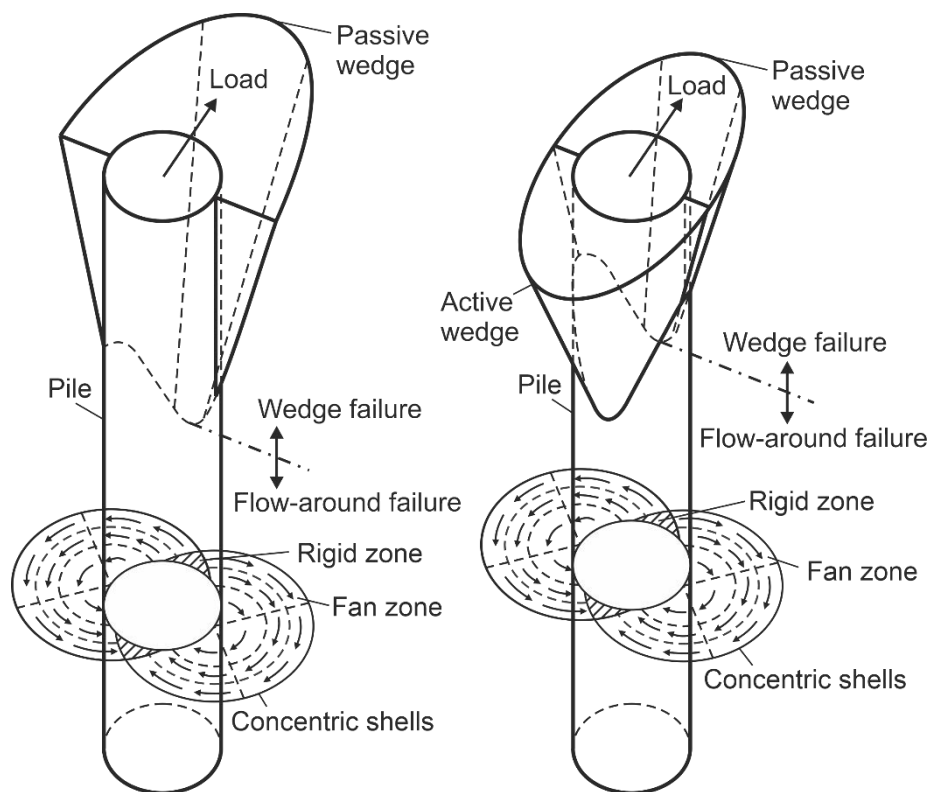


**Fig. 3-4: Three-dimensional failure mechanisms of laterally loaded piles for gapping (left) and no-gapping conditions (right)**

The transition depth (also termed critical depth) between both failure mechanisms of soil takes place at a certain depth in which the ultimate bedding resistance is identical for both failure modes. When the passive wedge failure mechanism only occurs, the transition depth is usually deeper than for both active and passive wedge failure mechanisms as reported by Senanayake (2016), based on the analysis of lateral load tests.

### 3.6.1 Wedge failure mechanism

A three-dimensional free-body diagram with respective applied forces was proposed by Reese et al. (1958) to analyse the lateral strength provided by a passive wedge failure generated from the forward movement of a pile-soil system. The strength properties of strongly over-consolidated clay used in a full-scale lateral load test of steel-pipes was considered to define the boundary condition of the analytical model, e.g. an average undrained shear strength  $s_{u,a}$  over the height  $z$ , and also a gap formation (resulting in passive wedge failure only). The free-body diagram illustrated in Fig. 3.5 presents an overview of all existing forces that impact on the soil wedge failure.

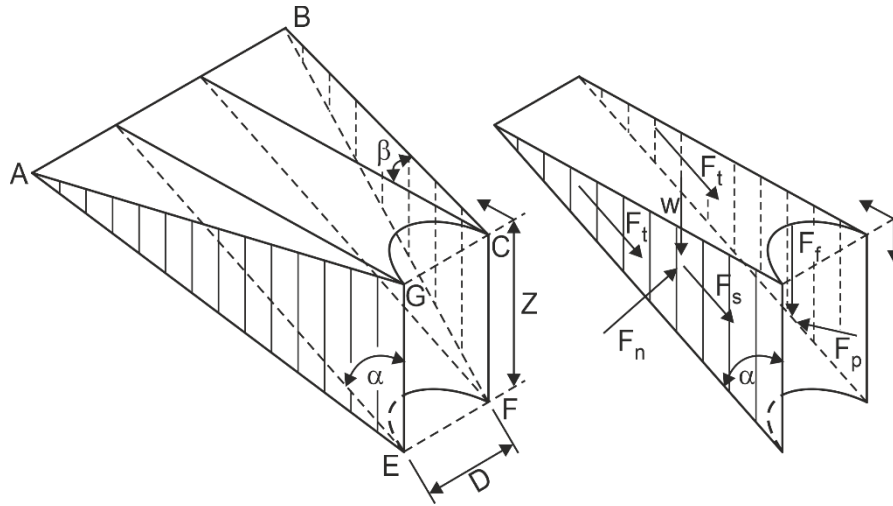


**Fig. 3-5: Schematic three-dimensional diagrams of the passive wedge failure (left) and its respective simplified model (right) for clay soils (after Reese et al. 1958)**

Based on the assumption that the width of the wedge is identical to the pile diameter  $D$ , the horizontal angle  $\beta$  is set to zero as seen in Fig. 3.5 (right). The equilibrium of forces (Newton's first law) along the inclined plane at the bottom of the wedge failure defined by the four vertices AEFB leads to the equation.

$$F_p \cdot \sin \alpha = F_s + F_f \cdot \cos \alpha + 2 \cdot F_t + W \cdot \cos \alpha \quad (3-3)$$

The angle  $\alpha$  results from the vertical pile with respect to the inclined failure plane for which the force  $F_n$  lies orthogonal and is thus not taken into account for the equilibrium of forces, but the friction force  $F_s$  acting parallel at the bottom failure plane of the wedge is defined as:

$$F_s = s_{u,a} \cdot D \cdot z \cdot \sec \alpha = s_{u,a} \cdot D \cdot z \cdot \frac{1}{\cos \alpha} \quad (3-4)$$

The friction force  $F_f$ , acting on the vertical face of the pile defined by the vertices GEFC, counts on a reduction factor  $\kappa$  for the shear resistance along the pile-soil interface surface.

$$F_f = \kappa \cdot s_{u,a} \cdot D \cdot z \quad (3-5)$$

The friction forces  $F_t$  acting on both triangular surfaces at the sides of the wedge failure defined by the vertices AGE and BCF result from:

$$F_t = \frac{s_{u,a} \cdot z^2}{2} \cdot \tan \alpha \quad (3-6)$$

The weight  $W$  of the soil wedge failure is obviously a function of the soil weight  $\gamma$ .

$$W = \frac{\gamma \cdot D \cdot z^2}{2} \cdot \tan \alpha \quad (3-7)$$

Resolving the above equations, the following expression is obtained for calculating the force  $F_p$  on the sliding surface of the pile.

$$F_p = \frac{s_{u,a} \cdot D \cdot z}{\sin \alpha \cdot \cos \alpha} + \kappa \cdot s_{u,a} \cdot D \cdot z \cdot \cot \alpha + s_{u,a} \cdot z^2 \cdot \frac{1}{\cos \alpha} + \frac{\gamma \cdot z^2 \cdot D}{2} \quad (3-8)$$

The force  $F_p$  is differentiated with respect to the height  $z$  of the wedge failure to find the soil resistance  $p$  per unit length of the pile.

$$\frac{\partial F_p}{\partial z} = p = \frac{s_{u,a} \cdot D}{\sin \alpha \cdot \cos \alpha} + \kappa \cdot s_{u,a} \cdot D \cdot \cot \alpha + 2 \cdot s_{u,a} \cdot z \cdot \frac{1}{\cos \alpha} + \gamma \cdot z \cdot D \quad (3-9)$$

The ultimate bedding resistance  $p_u$  is commonly normalised by the undrained shear strength  $s_{u,a}$  and the pile diameter  $D$  to obtain the dimensionless factor  $N_p$  for the bearing capacity factor at shallow depths, which is characteristic for cohesive soil.

$$N_p = \frac{p}{s_{u,a} \cdot D} \quad (3-10)$$

$$\frac{p}{s_{u,a} \cdot D} = \frac{1}{\sin \alpha \cdot \cos \alpha} + \kappa \cdot \cot \alpha + \frac{2 \cdot z}{D \cdot \cos \alpha} + \frac{\gamma \cdot z}{s_{u,a}} \quad (3-11)$$

Factoring the Eq. 3.11, the bearing capacity factor  $N_p$  proposed by Reese et al. (1958) for stiff clays in the presence of water assumes the inclination angle  $\alpha = 45^\circ$  of the failure plane and the reduction factor  $\kappa = 0$ , thus considering a smooth condition.

$$N_p = \left( \frac{1}{\sin \alpha \cdot \cos \alpha} + \kappa \cdot \cot \alpha \right) + \frac{2 \cdot z}{D \cdot \cos \alpha} + \frac{\gamma \cdot z}{s_{u,a}} \quad (3-12)$$

$$N_p = 2 + 2 \cdot \sqrt{2} \cdot \frac{z}{D} + \frac{\gamma \cdot z}{s_{u,a}} \quad (3-13)$$

Matlock (1970) considered a comparable formulation for soft clays, except that a fully rough pile was implicated, i.e. reduction factor  $\kappa$  was set to one for rough conditions, thus increasing the bearing capacity factor from 2 to 3 on the free soil surface. Additionally, instead of the theoretical constant of  $2 \cdot \sqrt{2} = 2.83$ , an empirical coefficient  $J$  was assumed between 0.5 to 0.25, based on the calibration from Sabine River and Lake Austin field tests, respectively (cf. section 5.4). The effect of an active wedge failure was also neglected due to the presumption of a gap formation at the active side of the pile.

$$N_p = 3 + J \cdot \frac{z}{D} + \frac{\gamma \cdot z}{s_{u,a}} \quad (3-14)$$

The total bearing capacity factor  $N_p$  in isotropic soils used for the determination of the wedge failure mechanism at shallow depths is indicated in Eq. 3-14 that comes from the equilibrium of the passive wedge failure that is taken as an essential basis by most of the models exposed in this thesis.

In the event of no-gap formations, the soil resistance resulting from an active wedge would also have to be considered in the equilibrium of forces to realistically capture the failure mechanism of the soil. The forces acting on the passive and active wedge resulting from the failure mechanism of soil at shallow depths are represented in detail in Fig. 3-6.

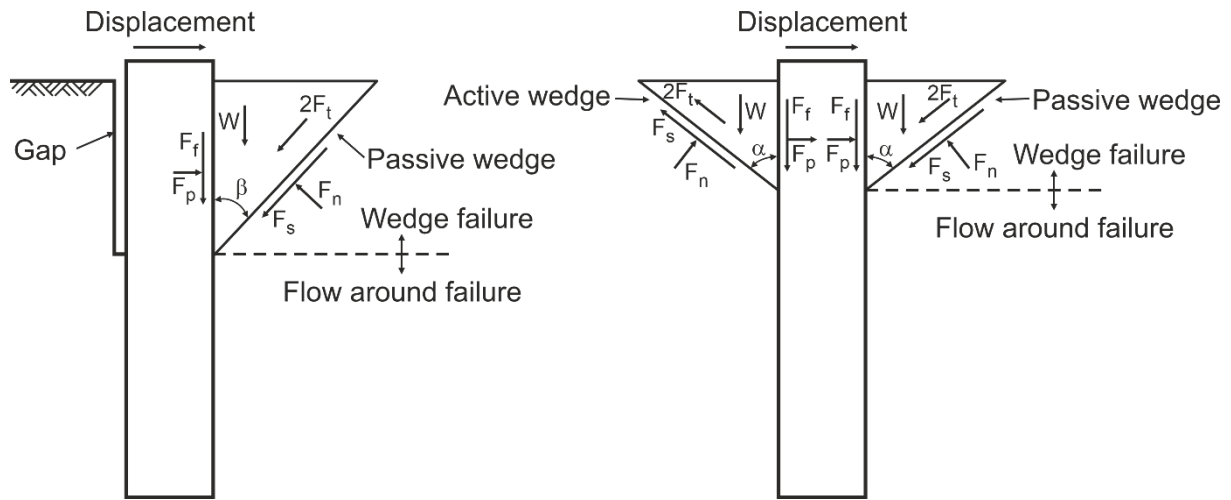


Fig. 3-6: Forces acting on the soil wedge failure for gap (left) and non-gap (right) conditions (after Reese et al. 1958)

The distinction between active and passive wedge failures is basically that the friction force  $F_s$  acting at the bottom failure plane and the friction forces  $F_t$  acting on the sides of wedge failure is applied upwards due to the active wedge pulling down in contrast to the friction forces of the passive wedge pushing upwards. By resolving the equilibrium of forces on the inclined plane at the bottom of the active wedge failure, the following equation is derived.

$$F_p \cdot \sin \alpha = F_s - F_f \cdot \cos \alpha + 2 \cdot F_t - W \cdot \cos \alpha \quad (3-15)$$

Similar to the passive wedge, the force  $F_p$  on the sliding surface of the pile is obtained by differentiating the Eq. 3-16 with respect to the height  $z$ .

$$\frac{\partial F_p}{\partial z} = p = \frac{s_{u,a} \cdot D}{\sin \alpha \cdot \cos \alpha} - \kappa \cdot s_{u,a} \cdot D \cdot \cot \alpha + 2 \cdot s_{u,a} \cdot z \frac{1}{\cos \alpha} - \gamma \cdot z \cdot D \quad (3-16)$$

Assuming also the inclination angle  $\alpha = 45^\circ$  and the reduction factor  $\kappa = 0$ , a formulation similar to the passive wedge failure is obtained, except for the weight component (the negative sign) which could considerably reduce the bearing capacity factor  $N_p$ .

$$N_p = \left( \frac{1}{\sin \alpha \cdot \cos \alpha} - \kappa \cdot \cot \alpha \right) + \frac{2 \cdot z}{D \cdot \cos \alpha} - \frac{\gamma \cdot z}{s_{u,a}} \quad (3-17)$$

$$N_p = 2 + 2 \cdot \sqrt{2} \cdot \frac{z}{D} - \frac{\gamma \cdot z}{s_{u,a}} \quad (3-18)$$

It becomes apparent that the average undrained shear strength  $s_{u,a}$  has a decisive role to contribute to the resistance of the pile-soil system in this instance. Meaning that if  $s_{u,a}$  is not high enough to maintain the stability of the sloping active wedge, this could have a negative effect on the result of the equilibrium of forces.

The mobilisation of both active and passive wedges due to a no-gap formation yields a combined effect that is obtained by adding the equations 3-13 and 3-18, resulting in the simplification of the weight components due to the opposite direction and the duplication of

shear strength by having the same direction of shear forces. The application of the next equation is limited to isotropic soils.

$$N_p = 2 \cdot \left( 2 + 2 \cdot \sqrt{2} \cdot \frac{z}{D} \right) \quad (3-19)$$

Similar to the aforementioned analytical development, Senanayake (2016) introduces a limit equilibrium of forces for calculating the bearing capacity factor  $N_p$  but considers a linear increase of the undrained shear strength  $s_u$  over depth. Despite this, a description of such calculation procedure will not be undertaken as it does not apply to the examined p-y approaches of the present study.

### 3.6.2 Flow-around failure mechanism

The ultimate bedding resistance due to the flow-around failure mechanism at the horizontal plane was firstly investigated by Reese (1958) and based on the limit equilibrium analysis, i.e. the impact on eight soil elements which deform around a square pile, was the object of study to identify some behavioural patterns, as seen in Fig. 3-7 (left). Subsequently, a plastic limit analysis (based on the theory of plasticity) was introduced by Randolph & Houlsby (1984) and revisited by Martin & Randolph (2006) that assumed a homogeneous, isotropic, and perfectly plastic cohesive material with undrained shear strength  $s_u$ . The bearing capacity factor  $N_p$  was determined in the context of lower and upper bound plasticity solutions (i.e. for fully smooth and fully rough interface conditions) which ranges from  $6 + \pi$  to  $4 \cdot \sqrt{2} + 2 \cdot \pi$  (i.e. approximately from 9.14 to 11.94). However, a linear relationship  $N_p = 9 + 3 \cdot \alpha$  was proposed for most engineering purposes, thereby the adhesion factor  $\alpha$  at the pile-soil interface surface lies between 0 and 1 for a fully smooth and rough pile, respectively.

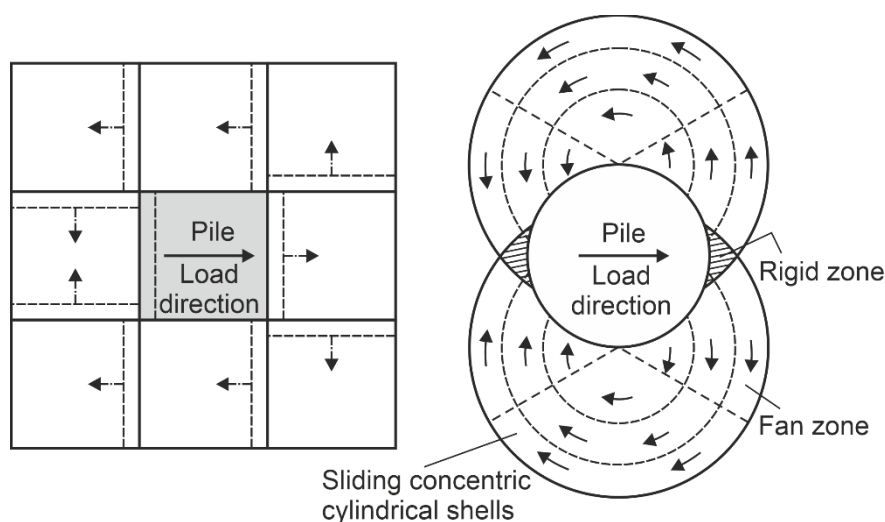


**Fig. 3-7: The flow-around mechanism for deep lateral resistance in cohesive soil for square pile (left) after Reese (1958) and upper bound solutions (right) after Randolph et al. (2011)**

The flow-around mechanism described by Randolph & Gourvenec (2011) for rough conditions (i.e. upper bound solution) of an advancing pile consists of the circular sliding of the soil around the pile by forming a rigid zone at the front and backside of the pile, fan zones adjacent to the

pile, as well as concentric sliding lines. The orientation of the arrows represents the motion of soil around the pile as can be seen in Fig. 3-7. A similar behaviour is produced by smooth conditions (i.e. lower bound solution) but with the exception that no rigid region exists, and in contrast to the rough conditions, a lower resistance to slip of the soil is yielded.

A summary in chronological order of the dimensionless factor  $N_p$  of the bearing capacity in the flow-around failure mechanism is provided in Table 3-1.

**Table 3-1: Recommendations for the lateral bearing capacity factor  $N_p$  at deep depth**

Reference	Pile-soil adhesion	$N_p$	Range	Description
Units	-	-	-	-
Matlock (1962)	Smooth pile	9		Assumed by industry consense
Broms (1964)	Smooth pile	9	8.28 to 12.56	Below a 1.5 diameter
Reese et al. (1975)	Rough pile	11		
Stevens & Audibert (1979)	Rough pile	12		Empirical recommendation
Sullivan (1980)	Smooth pile	9		
Randolph & Houlsby (1984)		10.5	9.14 to 11.94	Theoretical justification
Dunnivant et al. (1989)	Smooth pile	9		Empirical recommendation
Murff & Hamilton (1994)	Smooth pile	9		
Zhang et al. (2016)	Rough pile	11.94		Finite element analysis
Jeanjean et al. (2017)	Rough smooth	12		

It should be noted that the offshore guidelines as the API (2014) and the DNVGL (2016) implicitly assumed a smooth pile conditions due to the recommendations of Matlock (1962) for laterally loaded piles embedded in soft clays when it comes to the flow-around mechanism failure.

### 3.7 Response of rigid, flexible, and semi-flexible pile-soil systems

The load transfer mechanism into the soil, as well as the deflection characteristics of the pile foundation subjected to lateral loading conditions, mainly depends on the flexibility of the pile foundation, as stated by Briaud et al. (1984). In case of rigid and flexible piles, behavioural patterns can be clearly identified for laterally loaded piles, as described below.

The almost rigid pile (also termed short pile) provides a nearly linear deflection with a unique zero-deflection point  $z_0$ . Along the entire embedded length of the pile, the bedding soil resistance is mobilised, generating a considerable displacement at the pile tip that comparatively represents a significant portion of the lateral displacement at the pile head. An increase in the bending stiffness for rigid piles provides no additional resistance reflected in the foundation

stiffness at the pile head, but a change of the embedded pile length increases or decreases the pile head stiffness significantly.

The flexible pile (also termed long pile) is characterised by a curved deflection line with at least two zero-deflection points  $z_0$ . A plastic hinge (also known as fracture) which governs the lateral bearing capacity is generated at the depth of the maximum positive moment of the pile. Above the plastic hinge, the soil reaction is significantly mobilised but in the lower part of the pile no displacements occur for an ideal flexible pile, resulting in the pile tip at a fixed position. In contrast to rigid piles, the bending stiffness of the pile is decisive to define the bearing capacity, but an increment of the embedded length has no effect on the pile head stiffness.

By a semi-flexible pile foundation, both the bending stiffness and the embedded pile length affect the stiffness of the pile head. Displacement at the pile toe and moment bending will be simultaneously generated under lateral loading conditions.

Broms (1964b) developed a simplified method to calculate the displacements and moments of piles in cohesive soils using the concept of a coefficient of subgrade reaction. By applying this method, it is possible to analyse single piles of arbitrary length (i.e. both rigid and flexible piles), with a free or a fixed head pile. The method is limited to lateral loading conditions that are less than one-third of the ultimate bedding resistance  $p_u$ , assuming that up to that level of soil resistance its mechanical behaviour is entirely linear elastic.

According to Broms (1964b) the numerical value of the coefficient of the subgrade reaction  $K$  for piles driven in cohesive soils depends on the diameter of the pile, the load distribution as well as the depth of a particular loaded area of soil that will be considered. In the analysis from Broms, it is assumed that in case of stiff over-consolidated clays the coefficient of the subgrade reaction may be approximately constant over depth. For this case, the coefficient of the subgrade reaction proposed by Terzaghi (1955) shall be used that is based on load-deflection measurements by using a 30 inch diameter plate. The subgrade reaction values  $K_p$  from Terzaghi related to the undrained shear strength  $s_u$  of the clay are shown in Table 3-2.

**Table 3-2: Relationship of the coefficient of the subgrade reaction  $K$  to undrained shear strength of stiff over-consolidated clay**

Consistency	Firm to stiff	Stiff to very stiff	Hard
Undrained shear strength $s_u$ kN/m <sup>2</sup>	50 - 100	100 - 200	> 200
Range of $K$ MN/m <sup>3</sup>	15 - 30	30 - 60	> 60

For normally consolidated clays and silts, it can be expected that the coefficient of the subgrade reaction increases linearly with depth. In this case, the coefficient  $K$  depends on the coefficient of the modulus variation  $n_h$  which has been obtained directly from lateral loading tests on instrumented piles for cohesive soils.

The lateral deflections, bending moments, and soil reactions depend merely on the dimensionless length  $\beta \cdot L$  for which  $\beta$  is determined, as follows:

$$\beta = \sqrt[4]{\frac{K \cdot D}{4 \cdot E \cdot I}} \quad (3-20)$$

Where it depends on the stiffness of the pile section  $E \cdot I$ , the coefficient of subgrade reaction  $K$  and the pile diameter  $D$ . It is assumed that a free headed pile behaves like a rigid pile when the dimensionless length  $\beta \cdot L$  is smaller than 1.5. The pile behaves as a flexible pile when the length  $\beta \cdot L$  is greater than 2.5. Values in between can be expected to belong to semi-flexible piles.

The simplified distribution of the ultimate bedding resistance and the bending moments suggested by Broms (1964b) are represented in Fig. 3-8, for both rigid and flexible piles. The bedding resistance, which is approximated by a rectangular distribution, shall be assumed to be zero from the free soil surface to the depth of  $1.5 \cdot D$ , since it is considered that the upper soil layer does not offer resistance, while the ultimate bedding resistance per meter of the pile reaches a threshold value of  $9 \cdot s_u \cdot D$  in both cases.

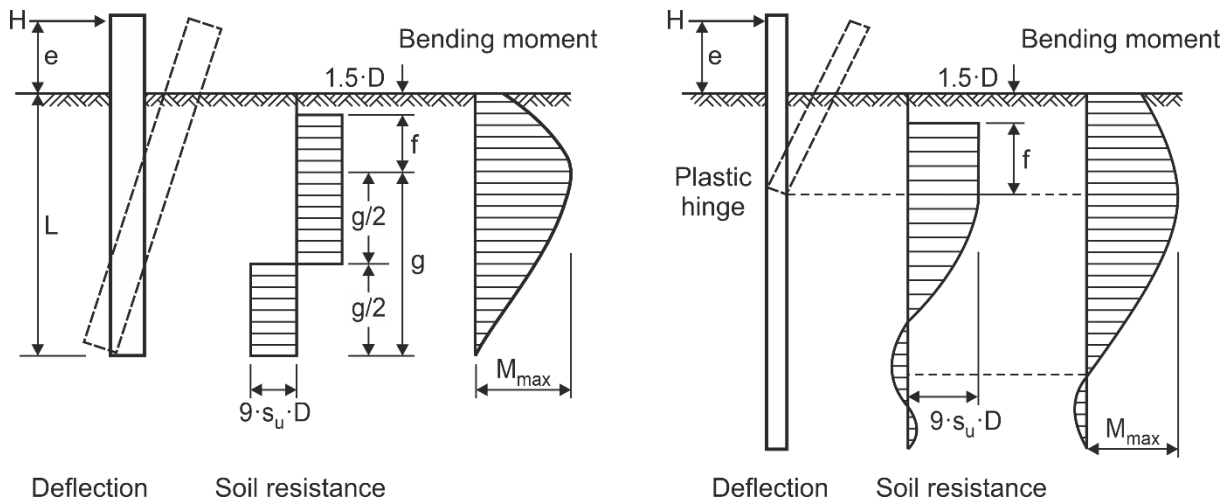


**Fig. 3-8: Schematic variation of the failure mechanisms of laterally loaded piles for rigid (left) and flexible (right) pile after Broms (1964)**

Fig. 3-8 (left) shows the failure mechanical for a perfectly rigid pile embedded in cohesive soil. A unique one zero-deflection point  $z_0$  exists around which the entire pile body rotates, mobilising the bedding resistance along the embedded pile length, which leads to the bearing capacity being defined predominantly by the soil resistance. The location of the maximum bending moment  $M_{max}$  is set at  $f + 1.5 \cdot D$ .

Similarly, the lateral collapse mode (i.e. failure mechanism) for the flexible pile is depicted in Fig. 3-8 (right). At least three zero-deflection points  $z_0$  can be identified by the course of soil resistance, which is typically for flexible piles. The formation of a plastic hinge is evident and located at the depth where the maximum positive moment is yielded. Above the plastic hinge, the displacements of the pile are quite large, while at its lower part of the pile they are relatively small. It can be confirmed that the bedding soil resistance in the lower part is not fully mobilised.



### 3.8 Limitations of p-y curves

The commonly used p-y approaches are taken as a basis for the analytical calculation methodology for the analysis of piles subjected to lateral loading conditions. However, the derivation of such a p-y correlation between the soil resistance  $p$  and the pile deformation  $y$  is essentially empirical which results in certain limitations to appropriately describe the pile-soil interaction. Such limitations of p-y curves are listed here after:

#### *Diameter effect*

All traditional p-y methods are generally calibrated on flexible, small diameter piles (i.e. sand:  $D \leq 0.61$  m, soft clay:  $D \leq 0.32$  m, and stiff clay:  $D \leq 0.61$ ) with a focus on the load-bearing behaviour of the pile-soil system under extreme loads for the ULS design proof, as stated by DNVGL (2016). Therefore, the validation basis of the p-y approaches recommended by OGLs such as API (2014) and DNVGL (2016) differs significantly from the required conditions of large-diameter monopiles ( $D \approx 6 - 10$  m,  $L/D \approx 3 - 5$ ), whereby the usual characteristic of slender piles becomes questionable at least for such conditions. The stiff behaviour of the monopile foundations results in the complete mobilisation of soil reactions along the embedded length of the pile, which does not occur in slender piles. Experience with monopile foundations with such large dimensions is essentially lacking. Numerous experimental and numerical investigations have already demonstrated significant shortcomings of the traditional p-y curves, which are frequently applied for monopile foundations in sand or clay (cf. section 3.9).

#### *Shearing force at the pile-toe*

The shearing force at the pile-toe is particularly relevant for rigid piles according to Reese & Van Impe (2011), i.e. when a unique zero-deflection point usually exists. The bedding resistance along the pile shaft is not adequately captured by the traditional p-y methods due to the lack of the shearing force. Thielen et al. (2015a) proposed a new innovative p-y method for piles with arbitrary dimensions in non-cohesive soils that considers the effect of shearing forces at the pile-toe as a function of pile dimensions by using the tip stretching factor  $S_{F_{py,tip}}$  to realistically reproduce the horizontal load-bearing behaviour of the pile-soil system. Likewise, Byrne et al. (2017) introduce an additional non-linear p-y curve at the pile toe to capture base shear effects (cf. section 4.4.3).

#### *Soil considering as non-continuum*

The soil generally behaves like a continuum, i.e. the deformation of the soil resulting from an applied loading affects the soil behaviour at other points. The p-y method analysis does not treat the soil as a continuum due to the use of a series of uncoupled non-linear spring characteristics. The bedding resistance derived from the p-y curves to achieve the system equilibrium subjected to lateral loading conditions are independent of each other. The assumption of a non-continuum of soil could lead to unexpected results, particularly in

layered soil stratification when the difference of shear forces of the surrounding layers is substantial. The overlay approach, which considers the interaction effects of soil layering through the adaptation of p-y curves, was introduced by Georgiadis (1983). Note that the validation of the aforementioned overlay approach was conducted by using a field load test on instrumented flexible piles foundations. The overlay approach should also be experimentally validated for rigid pile foundations.

Thieken et al. (2018a) carried out comprehensive parameter studies in layered, non-cohesive soil by using three-dimensional numerical simulations to evaluate the suitability of Georgiadis overlay procedure and concluded that it is generally not an adequate manner to treat the interaction effects of adjacent soil layers.

### ***Interaction of axial and lateral loading***

The influence of axial load on the bedding soil resistance is not generally taken into account for the design of foundation piles. The lateral and axial bearing behaviour of the pile-soil system is separately determined by subgrade reaction methods since the p-y and t-z curves are not coupled at all. Numerical investigations as carried out by Thieken & Achmus (2012) indicate that the interaction effects resulting from the simultaneous application of both loads (i.e. axial and lateral directions) for piles in clay under undrained conditions are however insignificant.

### ***Long-term cyclic loading***

The loads usually applied to the OWT structures are typically cyclic in nature due to changing wind and wave forces. The impact that load cycles may have on the long-term performance of a monopile foundation is a critical point for geotechnical design. The procedure adopted in OGLs or the EA-Pfähle (2012) modifies the static p-y curves using suitable empirical factors to reduce the mechanical soil properties such as stiffness and strength, but this degradation of static p-y curves was obtained from field tests with a rather limited number of cycles (e.g. sand: 100 cycles, soft clay: 200, stiff clay: 100). The resulting p-y approaches are not a function of the number of load cycles, which is quite questionable for analysing the cyclic behaviour of pile foundations subjected to long-term loading conditions. Note that Welch & Reese (1972) were the only ones who introduced a cyclic p-y approach for stiff clay with no free water depending on the number of load cycles, which results in an increase of lateral displacements with a growing number of cycles (i.e. the bearing behaviour becomes softer during cyclic loading).

### 3.9 Influence of the diameter on p-y approaches

The typical p-y curves developed from the results of long slender piles with diameters of up to 1 m have evidently not been calibrated for large pile diameters such as monopile foundations for analysing their pile's load-bearing behaviour. In this respect, DNVGL (2018) recommends that the results must be consequentially validated, e.g. by FE analysis, in order to recognise this shortcoming, which is also known as the "diameter effect".

The suitability of p-y approaches for sand under static loading conditions was thoroughly evaluated in a comprehensive numerical study by Achmus et al. (2014) and Thieken et al. (2015b, 2015c). Based on these numerical investigations, it could be demonstrated that the foundation stiffness of large diameter piles is overestimated for extreme loads (as decisive for ULS as for SLS proofs), but underestimated for small loads (as decisive for NFA as for FLS proofs). Based on these findings, a new p-y approach subsequently introduced by Thieken et al. (2015a) was developed which is able to reproduce validated numerical simulation results for arbitrary pile dimensions and load levels.

Investigation about the suitability of the p-y approach proposed by Matlock (1970) for soft clay is quite common. Stevens & Audibert (1979) concluded, based on seven laterally loaded piles with pile diameters in the range of  $D = 0.28 - 1.50$  m, that the foundation stiffness is considerably underestimated by Matlock (1970) approach for large pile diameters. Using the results of field tests, Stevens & Audibert proposed a modification of Matlock approach to account for the influence of piles with large diameters more accurately. Kim et al. (2009) reported the results of two field tests with the diameters  $D = 1.02$  m and  $D = 2.4$  m, which were carried out in anticipation of the construction of the Incheon Bridge, South Korea. Based on the theoretical considerations and field test results, Kim et al. (2009) developed a completely new p-y approach for arbitrary pile dimensions embedded in cohesive soils. Haiderali & Madabhushi (2013) confirm that the foundation stiffness which resulted from Matlock approach by using numerical simulations was underestimated. Kirsch et al. (2014) propose a modification of Matlock's approach which results in an increase of the foundation stiffness for all pile diameters. However, neither an experimental nor a numerical verification of the proposed approach was introduced by the authors.

Based on experimental evaluations of laterally loaded piles with diameters of 0.27 m, 1.22 m, and 1.83 m in over-consolidated clay, O'Neill & Dunnavant (1984) reported that the soil response can most effectively be defined by non-linear correlation with the pile diameter. Gazioglu & O'Neill (1984) state that the distinction between soft clay and rigid clay is virtually artificial. A new p-y approach is introduced as an integrated clay method, based on a theoretical analysis and the load test results used for soft and stiff p-y approaches. In contrast to the threshold displacement which is linearly dependent on the diameter as proposed by Matlock, the new p-y formulation includes a non-linear relationship with the pile diameter.

Achmus et al. (2016) reported the first results of a comprehensive comparative study to evaluate six static p-y approaches in soft, normally consolidated clay subjected to static loading conditions by means of 250 three-dimensional numerical simulations validated by pile load

tests also used for Matlock (1970) and Kim et al. (2009) to calibrate their respective p-y approaches. Herein, the suitability of p-y approaches regarding varied pile dimensions was verified. The results of the comparative study demonstrated that the deviations between numerical simulations and analytical results strongly depend on the pile diameter by which the approaches for larger diameters basically become more conservative. It is also found that the infinite initial stiffness introduced by Matlock's p-y formulation yields an overprediction of the foundation stiffness in case of small lateral loading conditions when compared to the validated numerical results.

Concluding, none of the existing p-y approaches was found to be generally valid for arbitrary pile dimensions. Based on the knowledge obtained, the requirements for a new p-y method, which is valid for arbitrary soil conditions, pile dimensions as well as diverse load levels can be defined.

## 4 The state of knowledge of semi-empirical p-y curves

### 4.1 General

For the analysis of laterally loaded piles, the p-y method has been successfully applied due to its relatively simple implementation as one-dimensional finite element model. Regarding offshore applications, the shapes of non-linear spring characteristics applied in the p-y methods have been determined by conducting field load tests on instrumented piles.

API (2014) and DNVGL (2016) guidelines describe the construction of p-y curves depending on the soil's type. The OGLs take as a basis the p-y approach proposed by Matlock (1970) for cohesive soil. However, several proposals of p-y approaches for either soft or stiff clay have been introduced that attempt to overcome the shortcomings of traditional p-y methods (cf. section 3.8). A comprehensive evaluation of the most representative p-y methods introduced in the OGLs and also literature will be conducted. The deviations for predicting the horizontal load-bearing behaviour of pile-soil systems shall be identified by using comparative analysis.

### 4.2 Subgrade reaction method according to DIN 1054: 2010-12

The German standard DIN 1054:2010-12 particularly recommends that the analysis of laterally loaded piles be conducted by using lateral load tests. The reaction modulus of subgrade  $K$  can be established from the results of such field tests. It is noted that the application of the subgrade reaction method, i.e. the bilinear function, is only suitable for a rough estimation of pile deformations, due to its very strong dependency on the modulus of the subgrade reaction  $K$ . As a result, the application is limited to the estimation of bending moments and shear forces as well as horizontal bearing capacity. The ULS design proof may also be carried out for laterally loaded pile foundations.

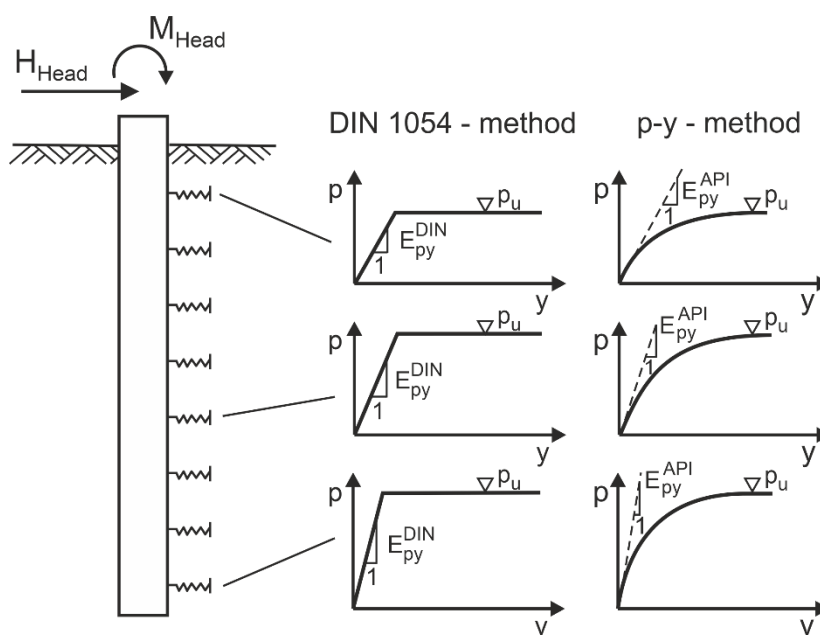


Fig. 4-1: Subgrade reaction method for pile foundations subjected to monotonic loading conditions

A comparison of the subgrade reaction method proposed by DIN 1054: 2010-12 with the traditional p-y methods regarding the shape of spring characteristics is depicted in Fig. 4-1. The bilinear course of the spring characteristics is merely defined by the subgrade reaction modulus  $K$  and the ultimate bedding resistance  $p_u$ .

The subgrade reaction modulus  $K$ , which presumes arbitrary distribution over the depth, can be obtained from the ratio between the oedometric stiffness modulus  $E_s$  and the outer pile diameter  $D$ .

$$K = \frac{E_s}{D} \quad (4-1)$$

The bedding soil resistance  $p$  must not be greater than the passive earth pressure  $e_{ph}$  along the embedded pile length. The German standard DIN 4085:2011-05 can be considered for calculating the parameter  $e_{ph}$ .

$$p = K_s \cdot y \leq e_{ph} \quad (4-2)$$

The validity of the method according to DIN 1054:2010-12 requires that the calculated displacement at the pile head does not exceed 3 percent of the pile diameter or 2 centimeters, whichever is less.

### 4.3 Non-linear p-y curves for soft clay

Monopile foundations can be completely founded in cohesive soils despite its comparatively low resistance. Anyhow, the presence of cohesive layers into the soil profile is quite common, partially at least. To obtain an integrated analysis of laterally loaded piles concerning bearing capacity for layered soil, the load-bearing behaviour of cohesive soils must be thoroughly examined.

The present chapter is concerned with descriptions of the six most known p-y methods for soft clay that have been introduced in the literature. The evaluation of the p-y approach is conducted by comparative studies.

#### 4.3.1 Matlock (1970)

Presumably for cohesive soils, the most commonly used p-y approach was proposed by Matlock (1970) that is defined by an exponential course of the bedding resistance against the horizontal displacement, culminating in a threshold displacement  $y = 8 \cdot y_{50}$  wherein the ultimate bedding resistance  $p_u$  lies.

$$p = 0.5 \cdot p_u \cdot \left( \frac{y}{y_{50}} \right)^{\frac{1}{3}} \leq p_u \quad (4-3)$$

Here,  $y_{50}$  represents the horizontal displacement on reaching half of the ultimate bedding resistance  $p_u$  that is calculated as a function of the outer pile diameter  $D$  and the strain  $\epsilon_{50}$ . The latter is the strain at one half the maximum principal stress  $\epsilon_{50}$  obtained from laboratory of undrained compression triaxial tests of undisturbed soil samples. The definition of the reference

displacement  $y_{50}$  is based on the concepts of Skempton (1954) that combine elasticity theory, ultimate strength methods, and laboratory soil properties to predict the load-settlement curves subjected to short-term loading conditions for strip footing in clay. Note that the linear dependency of the displacement  $y_{50}$  on the pile diameter  $D$  remains in permanent discussion by researchers (cf. section 3.9).

$$y_{50} = 2.5 \cdot \varepsilon_{50} \cdot D \quad (4-4)$$

The ultimate bedding resistance  $p_u$  is calculated in dependence of the undrained shear strength  $s_u$ , the submerged unit soil weight  $\gamma'$ , the depth below soil surface  $z$ , the outer pile diameter  $D$ , and the empirical constant  $J$ . The latter depends on the clay consistency, usually defined in the range from 0.5 to 0.25 for soft clay  $s_u \leq 50$  kPa to stiff clay  $s_u \geq 96$  kPa and linearly interpolated in between. The load-bearing capacity factor  $N_p$  is commonly used for calculating the ultimate bedding resistance  $p_u$  through a distinction between the wedge failure mechanism at shallow depths and the flow-around failure mechanism at deep depths, whereby the minimum factor  $N_p$  becomes decisive (cf. section 3.6). Note that the formulation developed by Matlock takes on a rough interface surface and a gap formation at the active side of the pile for the calculation of the ultimate bedding resistance  $p_u$  for the wedge failure mechanism, while a smooth interface surface is considered for the flow-around failure mechanism.

$$N_p = \min \left\{ 3 + J \cdot \frac{z}{D} + \frac{\gamma' \cdot z}{s_u} \right. \quad (4-5)$$

$$p_u = N_p \cdot D \cdot s_u \quad (4-6)$$

Matlock conducted a series of field tests, first at “Lake Austin” and subsequently at “Sabine River”. The p-y method proposed for soft clay has been developed mainly from the results of the “Sabine River” field test and confirmed later with the results of the field test “Lake Austin”, as stated by Matlock (1962). Note that both field tests are used for the validation of the numerical model introduced in section 5.4.

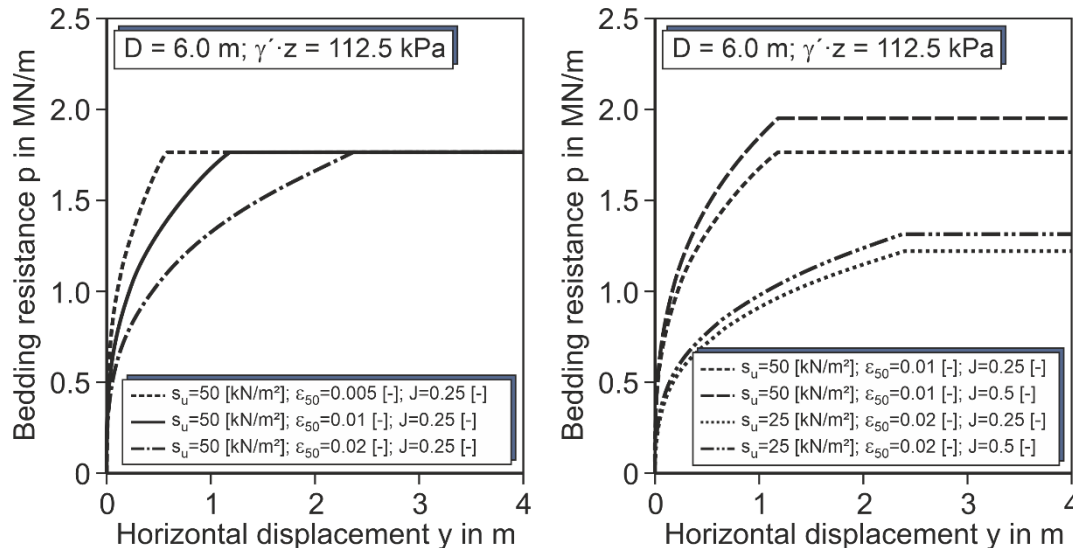


**Fig. 4-2: Exemplary p-y curves according to Matlock (1970), the variation of the stiffness parameter  $\epsilon_{50}$  (left) as well as the ultimate bedding resistance parameters  $s_u$  and  $J$  (right)**

The course of the p-y curves according to Matlock is exemplarily illustrated in Fig. 4-2 for a six meters diameter monopile foundation embedded in soft clay. The linear dependence of the p-y curve (see Eq. 4-4) results in a duplication of the bedding stiffness when the strain  $\epsilon_{50}$  (Fig. 4-2, left) is halved, while an increment of the undrained shear strength  $s_u$  or the empirical parameter  $J$  leads to an increase of both the ultimate bedding resistance  $p_u$  and the bedding stiffness. In other words, while the parameters for the ultimate bedding resistance ( $z$ ,  $\gamma'$ ,  $s_u$ ,  $J$ ) influence the stiffness and the ultimate bedding resistance, the strain  $\epsilon_{50}$  only affects the bedding stiffness of the soil.

#### 4.3.2 API (2014)

The p-y curves characterised by API (2014) describe an approximation of the Matlock curve by four (API 2002) or six (API 2014) predefined points on the p-y curve which are linearly connected. The two additional points defined by API (2014) are emphasised in bold font in Fig. 4-3 (left). Obviously, the bedding stiffness in the initial part of the curve is considerably reduced by both linearisation, especially by API (2002), compared to the original curves developed by Matlock.

Fig. 4-3 (right) shows the relationship of the secant bedding stiffness against the lateral displacement, clearly confirming the influence of linear approximation, especially for design aspects that take into account small load levels (i.e. NFA, FLS). Although the correction of the initial stiffness would only require linearisation of the initial part of the curve, API (2014) establishes the complete curve characterisation using the predefined curve points. This depends on the ratio of bedding resistance to ultimate bedding resistance  $p / p_u$  as well as the ratio of lateral displacement to reference displacement  $y / y_{50}$  denoted in Fig. 4-3 (left). It is remarkable that the displacement value of the first point of the curve is already set in the centimeter range for monopile foundations (i.e. large-diameter pile foundations).



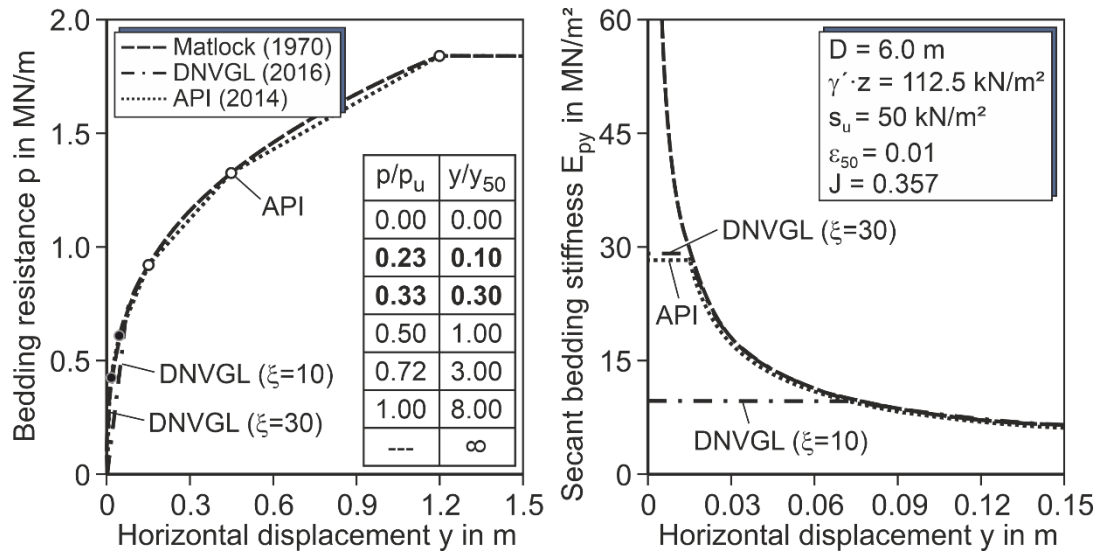


Fig. 4-3: Exemplary p-y curves (left) and secant bedding stiffness (right) according to Matlock (1970), API (2014) and DNVGL (2016)

The p-y curve proposed by Matlock (1970) and corresponding linearisation according to API (2014) and DNVGL (2016) and its respective secant bedding stiffness  $E_{py} = p / y$  for a pile diameter  $D = 6 \text{ m}$  and a depth  $z = 15 \text{ m}$  are separately shown in Fig. 4-3. It is remarkable that the infinite initial stiffness of Matlock's curve resulting from the parabolic function is clearly highlighted. A strong difference in the initial stiffness becomes obvious between the curves proposed by Matlock and the curves defined by API (2014) and DNVGL (2016). This effect, almost unknown in the design practice, will severely influence the outcome of the OWT structure design for the small load range. Geotechnical engineers dealing with the design of OWT foundations should therefore strongly discern between the p-y curves according to the API (2014) and the original approach proposed by Matlock.

When comparing this to Matlock's approach, the linearisation of API (2014) results in a constant reduction ratio  $E_{py,API}/E_{py,Matlock} = 0.34$  due to the predefined curve points for the normalised displacement  $y/D = 0.0005$  (i.e. very small strains), considering the boundary conditions exposed in Fig. 4-5. In other words, the linearisation leads to an approximate third of the secant bedding stiffness  $E_{py}$  proposed by Matlock. The same normalised displacement is considered by DNVGL (2016) resulting in a reduction factor  $E_{py,API}/E_{py,DNVGL,10} = 0.12$  for normally consolidated clay and  $E_{py,API}/E_{py,DNVGL,30} = 0.35$  for over-consolidated clay. Therefore, this represents a considerably conservative treatment compared to the API (2014) for very small strains. For the approaches according to Stevens & Audibert, Kim et al. and Kirsch et al., no linearisations are considered since they are not addressed in any of the original documents.

### 4.3.3 DNVGL (2016)

Alternatively, DNVGL (2016) recommends the exclusive linearisation of the initial part of the original p-y curve developed by Matlock, which are essential for FLS and NFA design proofs, by applying the initial stiffness  $K_i$  given by Eq. 4-7. Herein, the empirical coefficient is recommended to  $\xi = 10$  for normal consolidated clay  $OCR = 1$  and to  $\xi = 30$  for over-consolidated clay independently of the magnitude of over-consolidation ratio  $OCR > 1$ . Note that no guidance is given regarding the transition between both values.

$$K_i = \xi \cdot \frac{P_u}{D \cdot (\varepsilon_{50})^{0.25}} \quad (4-7)$$

A comparison of the linearisations reveals that the described procedure of DNVGL (2016) yields lower initial stiffnesses compared to the approach of API (2014). This applies particularly in the case that a normally consolidated clay ( $\xi = 10$ ) is assumed. It has to be emphasised that the linearisation of the example in Fig. 4-3 reaches up to a displacement of 70 mm, i.e. the whole normally relevant range of typical monopile design. Obviously, the first point of the linearisation of the p-y curves is of crucial importance.

The definition of the initial stiffness is after all comparable to API (2014) approach since again a fixed point of the curve is applied for the respective linearisation according to DNVGL (2016). By equating the exponential approach of Matlock (Eq. 4.3) with the initial stiffness  $K_i$  (Eq. 4.7), this curve point can be defined with respect to the  $p / p_u$  and  $y / y_{50}$  ratios and compared to API (2014). The location of the curve point according to DNVGL (2016) is obtained from Eq. 4-8 and 4-9.

$$\frac{y}{y_c} = (5 \cdot \xi \cdot \varepsilon_{50}^{0.75})^{-1.5} \quad (4-8)$$

$$\frac{p}{p_u} = (20 \cdot \xi \cdot \varepsilon_{50}^{0.75})^{-0.5} \quad (4-9)$$

The differences of initial stiffness resulting from the linearisations are demonstrated in Fig. 4-4, where the dependency between the related initial stiffness ( $(p / p_u) / (y / y_{50})$ ) and the  $\varepsilon_{50}$ -value is provided. Due to the pre-defined curve points by API (2014), the related initial stiffness is independent of the  $\varepsilon_{50}$ -value. In contrast, the initial stiffness of DNVGL (2016) linearisation depends on the  $\varepsilon_{50}$ -value. Fig. 4-4 demonstrates that DNVGL (2016) approach for normally consolidated clay ( $\xi = 10$ ) always results in smaller initial stiffness compared to the approach proposed by API (2014), but an intersection of both approaches approximately takes place at  $\varepsilon_{50} \approx 1.0$  % when taking into account over-consolidated clay. However, it is questionable whether the combination of  $\varepsilon_{50} > 1.0$  % and  $OCR > 1$  is practically relevant. Hence, DNVGL (2016) linearisation is seen as basically more conservative than the approach introduced by API (2014) for very small strains.

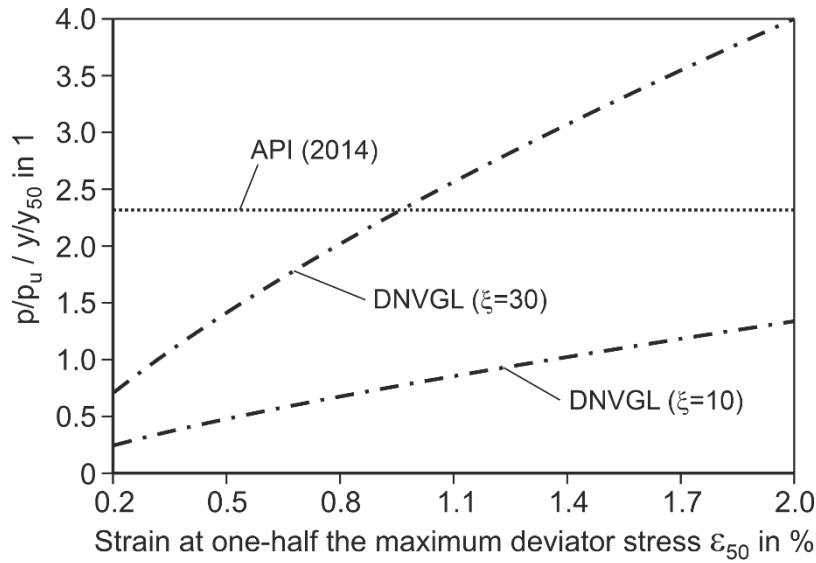


**Fig. 4-4: Related initial stiffness from the p-y curve linearisation**

The different linearisations of the original p-y approach proposed by Matlock have a decisive influence on the applied bedding resistance, particularly for very small strains. Due to these large differences, the approaches proposed by Matlock (1970), API (2014), and DNVGL (2016) are considered separately within the comparative studies (cf. section 6).

#### 4.3.4 Stevens & Audibert (1979)

Stevens & Audibert (1979) recommend a modification of the original p-y approach proposed by Matlock, accounting for a non-linear decrease of the reference displacement  $y_{50}$  or a non-linear increase of the bedding stiffness with a pile diameter  $D$ , respectively (see Eq. 4-10).

$$y_{50} = 2.5 \cdot \varepsilon_{50} \cdot D_{\text{ref}} \cdot \left( \frac{D}{D_{\text{ref}}} \right)^{0.5} \quad (4-10)$$

This formulation increases the bedding stiffness for diameters larger than the reference diameter  $D_{\text{ref}} = 0.32$  m equivalent to the pile diameter of the “Lake Austin” and the “Sabine River” field tests used for the calibration of p-y curves developed by Matlock.

In addition to the adjustment of the  $y_{50}$  formulation, Stevens & Audibert recommend an increase of ultimate bedding resistance  $p_u$  compared to Matlock’s approach. The minimal load-bearing capacity factor  $N_p$  from Eq. 4-11 is considered as the decisive value for calculating the maximal bedding resistance  $p_u$ .

$$N_p = \min \left\{ 5 + J \cdot \frac{z}{D} + \frac{\gamma^2 \cdot z}{s_u} \right. \quad (4-11)$$

$$p_u = N_p \cdot D \cdot s_u \quad (4-12)$$

In contrast to Matlock’s original approach, a rough interface surface is considered to determine the bearing capacity factor  $N_p$  for both mechanical failure mechanisms.

Fig. 4-5 shows exemplary p-y curves of Stevens & Audibert, Kim et al., and Kirsch et al. approaches compared with the respective p-y curves defined by Matlock for small and large diameter piles at shallow and deep depths. The corresponding soil parameters used for the comparison are completely stated in Table 6-1.

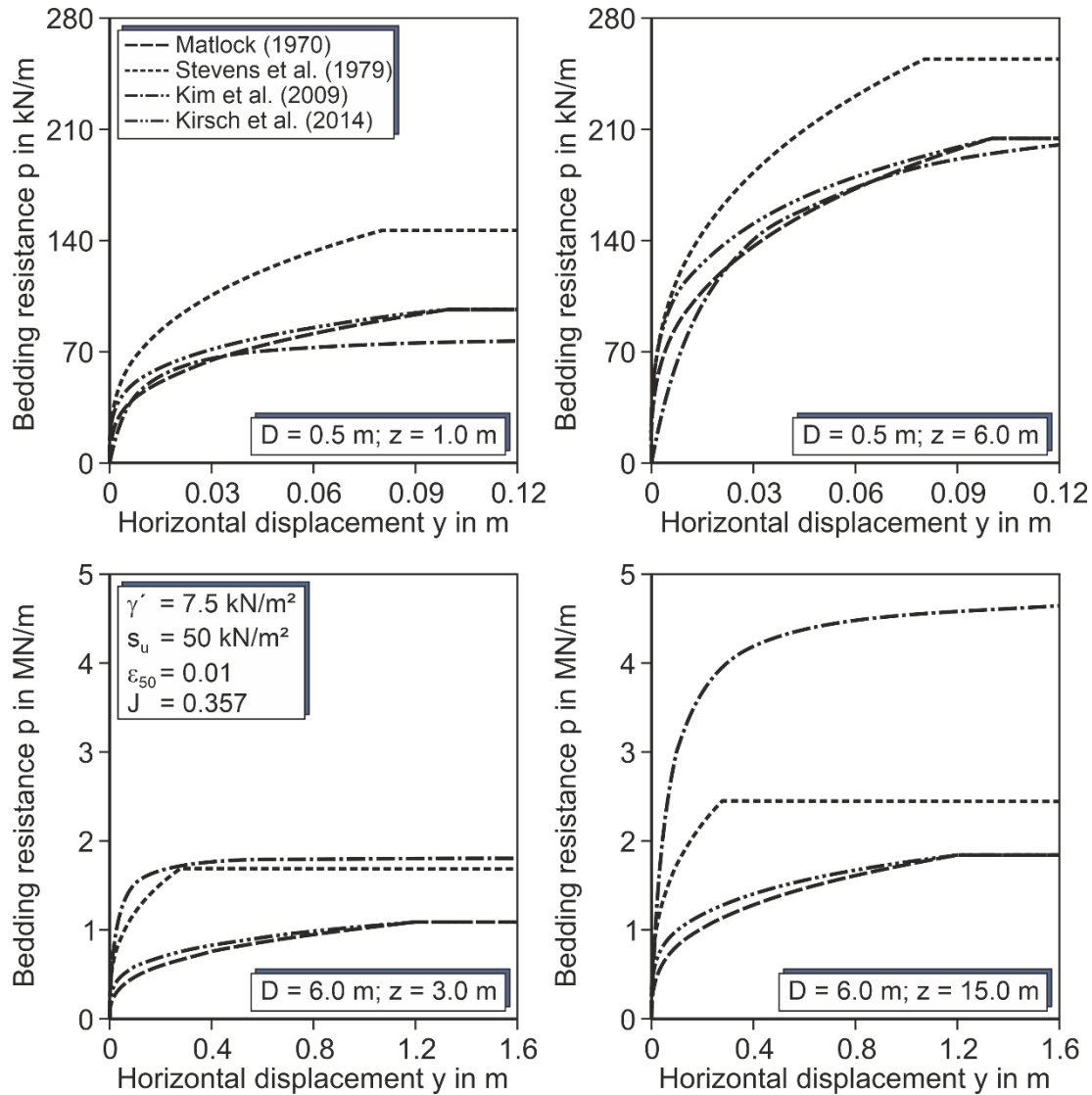


**Fig. 4-5: Exemplary p-y curves by alternative approaches for small and large diameter pile**

Obviously, Stevens & Audibert's approach results in a significantly larger bedding stiffness and ultimate bedding resistance  $p_u$  than Matlock's approach for both the diameters and the reference depths considered. However, when it comes to deeper depths, Kim et al.'s approach result in the largest bedding resistance. The comparison of the p-y curves proposed by Kirsch et al. with the one proposed by Matlock shows that the threshold displacement to reach the ultimate bedding resistance  $p_u$  and likewise  $p_u$  remains unaffected, in contrast to the initial stiffness and the bedding stiffness.

### 4.3.5 Kim et al. (2009)

An entirely new p-y curve formulation was proposed by Kim et al. (2009). The approach is based on the theoretical analysis and the results of two field tests with pile diameters  $D = 1$  m and  $D = 2.4$  m. Both field tests are used for the validation of the numerical model proposed in this thesis (cf. section 5.4).

Supported by a rigid and flexible analysis of laterally loaded piles, Kim et al. indicated that the introduced approach is valid for arbitrary pile dimensions. A hyperbolic function given by Eq. 4-13 is taken into account to define the shape of p-y curves. It is noteworthy that the initial stiffness is described by using a finite initial bedding stiffness coefficient  $K_i$ , contrary to Matlock's original approach which defined it as infinite.

$$p = \frac{y}{\frac{1}{K_i} + \frac{y}{p_u}} \quad (4-13)$$

Here, the initial bedding stiffness coefficient  $K_i$  is calculated as a function of the undrained shear strength  $s_u$ , the stiffness factor  $k_c$ , the Poisson's ratio  $\nu$ , the reference diameter  $D_{ref} = 1$  m, the outer pile diameter  $D$ , and the piles' flexural rigidity  $E \cdot I$  (see Eq. 4-14). The stiffness factor  $k_c$  depends on the plasticity index  $PI$  and the over-consolidation ratio  $OCR$ . Hereinafter,  $k_c$  is set to 300 representing a normally consolidated soft clay with  $OCR = 1$  and the plasticity index  $PI = 50$ . For further details on the definition of  $k_c$ , see Kim et al. (2008).

$$K_i = 17.4 \cdot \frac{k_c \cdot s_u}{(1 - \nu^2)} \cdot \sqrt{\frac{D}{D_{ref}}} \cdot \left( \frac{k_c \cdot s_u \cdot D^4}{E \cdot I} \right)^{0.66} \quad (4-14)$$

The ultimate bedding resistance  $p_u$  results as a function of the undrained shear strength  $s_u$ , the pile diameter  $D$ , the depth below soil surface  $z$ , and the reference depth  $z_{ref} = 1$  m. The distinction between the two failure mechanisms proposed by Murff & Hamilton (1994) are not considered by Kim et al. for calculating the ultimate bedding resistance  $p_u$ , as confirmed in Eq. 4-15.

$$p_u = 3.25 \cdot s_u \cdot D \cdot \left( \frac{z}{z_{ref}} \right)^{0.59} \quad (4-15)$$

An exemplary comparison of p-y curves proposed by Kim et al. with the other p-y approaches is also shown in Fig. 4-5. The wall thicknesses, which influence the initial stiffness of the p-y curves proposed by Kim et al., are set to  $t = 8.85$  mm ( $D = 0.5$  m) and  $t = 36.35$  mm ( $D = 6$  m), being consistent with the parameters of the subsequent comparative study. For small pile diameters, Kim et al.'s approach basically yields a smaller bedding stiffness than the outcome of Matlock's approach. This stands in contrast to typical monopile dimensions in which a considerably larger bedding resistance is obtained. A significantly large ultimate bedding resistance  $p_u$  is yielded, particularly for large pile diameters at deep depths. In this respect, it is noted that the ultimate bedding resistance  $p_u$  is calculated using Eq. 4-15, thus at deep depths resulting in larger bedding resistance than calculated by Matlock's approach limited by  $p_u = \leq 9 \cdot s_u \cdot D$ . In the latter, the ultimate resistance  $p_u$  results from a full-flow failure

mechanism due to plastic flow-around the pile shaft that is absorbed mainly by the lateral bearing capacity of the soil at deep depths for the flow-around condition according to Randolph & Houlsby (1984).

#### 4.3.6 Kirsch et al. (2014)

Kirsch et al. (2014) suggest a modification of Matlock's approach by adjusting the strain value  $\varepsilon_{50}$  using Eq. 4-16. The adaption leads to an increase of the bedding resistance especially in the range of small horizontal displacement, resulting from the ratio of bedding resistance to ultimate bedding resistance  $p / p_u$ , as well as the ratio of static stiffness modulus to the dynamic stiffness modulus  $E_s / E_{s,d}$ . The latter is derived from the dynamic shear modulus  $G_0$ , which is fundamental for very small shear strains. It is noted that the determination of the threshold displacement and the ultimate bedding resistance  $p_u$  remains unchanged.

$$\varepsilon_{50,mod} = \varepsilon_{50} \cdot \left[ 1 + \left( 1 - \frac{p}{p_u} \right) \cdot \left( \frac{E_s}{E_{s,d}} - 1 \right) \right] \quad (4-16)$$

To conduct a comparative analysis, a numerical characterisation of the different p-y approaches is carried out with regard to the secant bedding stiffness  $E_{py} = p / y$  for a normalised displacement  $y / D = 0.0005$ , corresponding to  $y = 3$  mm and pile diameter  $D = 6$  m. It should be noted that Kirsch's approach also assumes the infinite initial stiffness proposed by Matlock, being decisive for very small strains.

Fig. 4-6 shows the quotient of the secant bedding stiffness resulting from the aforementioned p-y approaches which refer to Matlock's approach in terms of contour plots for a wide range of pile diameters  $D = 0.5 - 8$  m and relative depths  $z / D = 0 - 5$ . Consequently, a value  $> 1$  means that the evaluated approach yields a stiffer behaviour than that predicted by Matlock's approach. Additionally, the secant bedding stiffness  $E_{py}$  of Matlock's approach is depicted in Fig. 4-6 (upper, right), showing its increment with increasing depths and diameters.

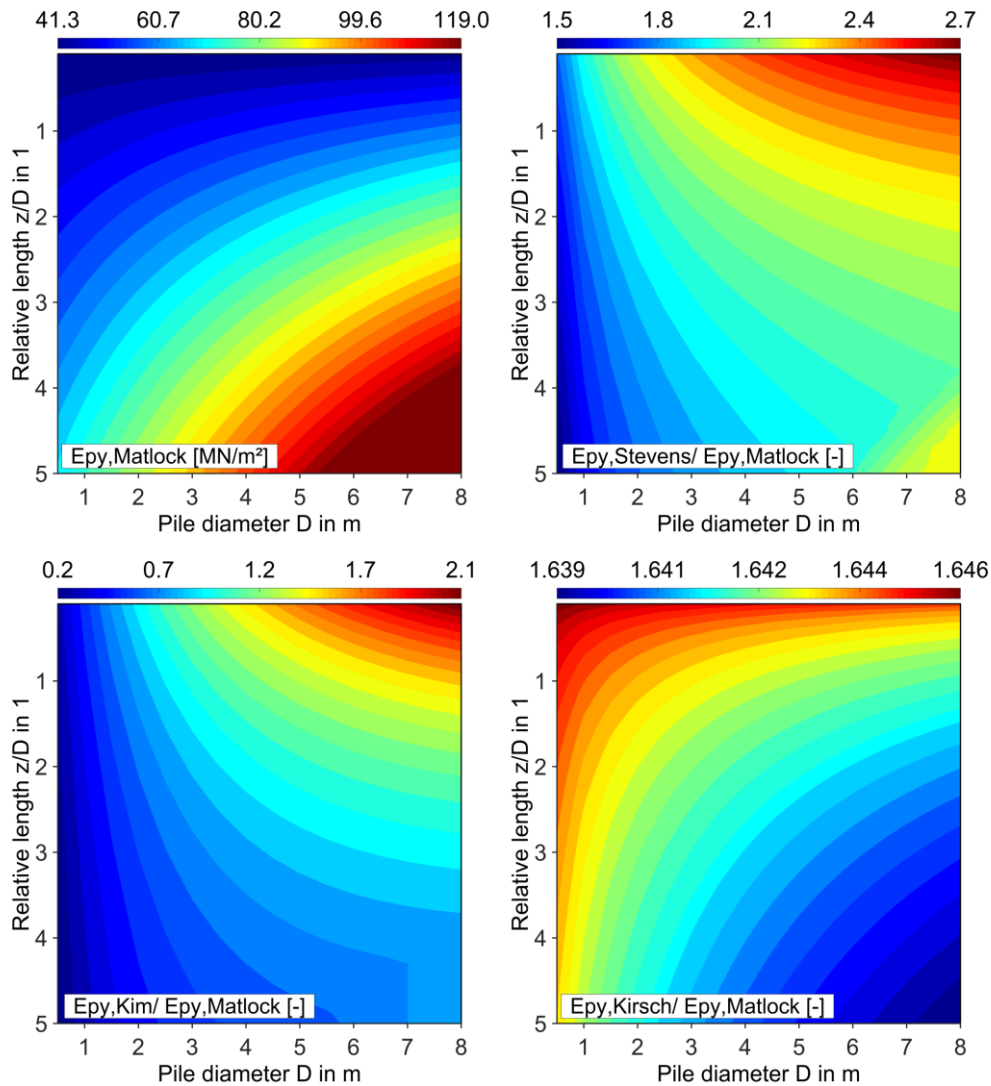


**Fig. 4-6: Bedding stiffness  $E_{py} = p / y$  for soil parameter related to Fig. 4-5 with normalised displacement  $y / D = 0.0005$**

The alternative approach proposed by Kirsch et al. indicates a higher bedding stiffness compared to Matlock's approach, as shown in Fig. 4-6 (bottom, right). Various dependencies of diameter  $D$  and reference depth  $z / D$  are visible. However, the approach by Kirsch et al. exhibits an almost constant ratio in comparison to the Matlock approach, although strongly varying ratios  $E_s / E_{s,d}$  at different depths were considered. In fact, the mathematical analysis of Eq. 4-16 indicated that the marginal influence of the term  $E_s / E_{s,d}$  on the results of this approach produces an actual ratio much smaller than 0.1 for soft clay ( $E_s / E_{s,d} \ll 0.1$ ). Consequently, the increment results predominantly from the term  $p / p_u$  in which an approximately constant increase factor is given for related arbitrary displacements. The p-y curves resulting from the Kim et al. approach are likewise compared to Matlock's approach in Fig. 4-6 (bottom, left). As mentioned, the wall thickness which influences the initial stiffness of the p-y curves was set identical to the values used for the coming parameter study (see Eq. 6-1). For small pile diameters, the bedding stiffness is smaller compared to the outcome of Matlock's approach. In contrast, the stiffness is significantly large for typical monopile diameters.

Fig. 4-6 (upper, right) highlights the larger foundation stiffness by the Stevens & Audibert approach compared to Matlock's approach for pile diameters and all depths. For typical monopile diameters in the range  $D = 6 - 8$  m, bedding stiffness is increased by a factor of 2.1 - 2.7, demonstrating that the foundation stiffness is more than double the value resulting from Matlock's approach.

#### 4.3.7 Jeanjean et al. (2017)

Jeanjean et al. (2017) introduced a new static p-y approach, which can be used for predicting the horizontal load-bearing behaviour of steel pipe piles embedded in either very soft or stiff clay. For deriving the proposed p-y curves, the results of 1-g and centrifuge lateral pile load tests were used for improving the prediction of the pile response concerning traditional p-y curves recommended by offshore guidelines (e.g. API 2014 and DNVGL 2016).

The load-bearing capacity factor  $N_p$  results from the basis of the limit analysis and the finite element analysis (FEA). The assumption of gapping or no-gapping formation at the active side of pile foundation becomes decisive for calculating  $N_p$ . The pile-soil interaction is likewise controlled using the pile-soil adhesion factor  $\alpha$  (i.e.  $\alpha = 0$  for smooth conditions and  $\alpha = 1$  for fully rough conditions).

$$N_p = \min \begin{cases} N_{p0} + \frac{\gamma' \cdot z}{s_{u,0} + s_{u,1}} & \rightarrow \text{gapping conditions} \\ \frac{2 \cdot N_{p0}}{9 + 3 \cdot \alpha} & \rightarrow \text{no-gapping conditions} \end{cases} \quad (4-17)$$

The lateral bearing capacity factor  $N_{p0}$  due to the passive wedge failure mechanism is a function of the model parameters  $N_1 = 12$  and  $N_2 = 3.22$  (for more details see Yu et al. 2015).

$$N_{p0} = \min \left\{ \frac{N_1 - (1 - \alpha) - (N_1 - N_2) \cdot \left[ 1 - \left( \frac{z}{d \cdot D} \right)^{0.6} \right]^{1.35}}{9 + 3 \cdot \alpha} \right\} \quad (4-18)$$

$$d = 16.8 - 2.3 \cdot \log \lambda \geq 14.5 \quad (4-19)$$

$$\lambda = \frac{s_{u,0}}{s_{u,1} \cdot D} \quad (4-20)$$

For moderately non-linear soil profiles,  $s_u$  obtained from Eq. 4-21 depends on the shear strength at the soil surface  $s_{u,0}$  and the rate of increase of the shear strength  $s_{u,1}$  over depth  $z$ .

$$s_u = s_{u,0} + s_{u,1} \cdot z \quad (4-21)$$

The ultimate bedding resistance  $p_u$  is eventually calculated, as follows:

$$p_u = N_p \cdot D \cdot s_u \quad (4-22)$$

The shape of the normalised p-y curves was determined from an extensive database of direct simple shear tests DSS (around 537 marine clay samples) and finite element analysis. Eleven



predefined points, which are linearly connected, define the shape of p-y curves proposed by Jeanjean et al. (2017). These predefined points which depend on the ratio of bedding soil resistance to ultimate bedding resistance  $p / p_u$  and the ratio of lateral displacement to the pile diameter  $y / D$  are separately introduced by Jeanjean et al. for soft clay  $s_u \leq 100$  kPa and stiff clay  $s_u > 100$  kPa. The table presented in Fig. 4-7 corresponds to predefined points for soft clay.

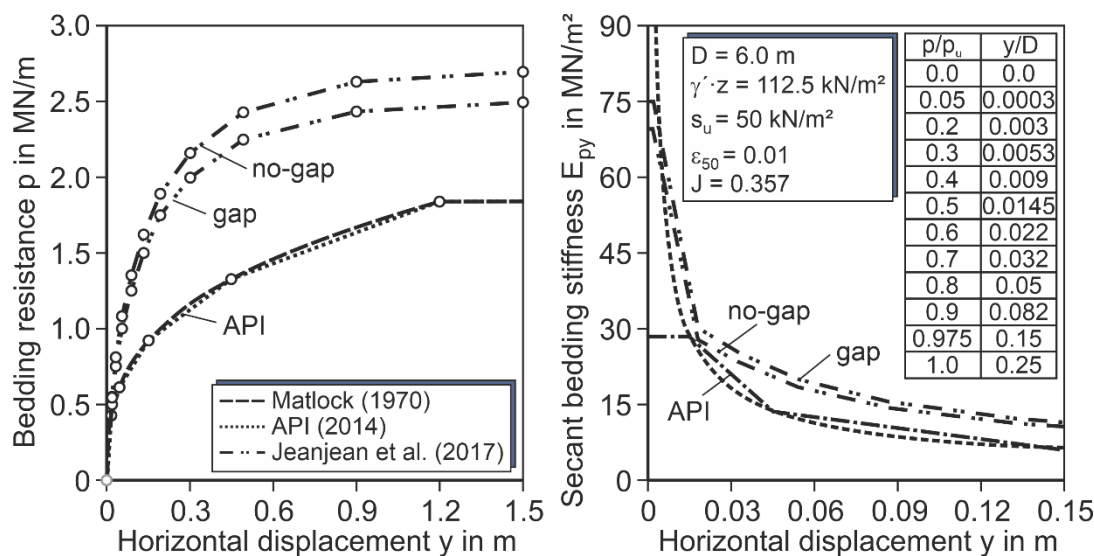


**Fig. 4-7: Exemplary p-y curves (left) and secant bedding stiffness (right) according to Jeanjean et al. (2017) under no-gap and gap conditions**

The bedding stiffness and the ultimate bedding resistance  $p_u$  of the p-y curves provided by API (2014) are significantly smaller than the ones resulting from Jeanjean et al.'s approach for both no-gap and gap conditions, as seen in Fig. 4-7 (left).

Similar to API (2014) recommendations, the first predefined point specifies the initial slope of p-y curves which is concretely associated with the initial stiffness of the pile-soil system. The initial stiffness introduced by Jeanjean et al. yields a significant increment compared to that recommended by API (2014), but it turns out to be smaller than that provided by Matlock's p-y approach due to the infinite initial stiffness (see Fig. 4-7 right). It is noted that the p-y curves proposed by Jeanjean et al., even though a gap formation at the active side of the laterally loaded pile is also considered, do not exhibit a strain-softening soil response for large displacements.

#### 4.4 Non-linear p-y curves for stiff clay

The p-y approaches derived from a lateral load test on piles embedded in soft clay are improperly used in practice to also predict the load-bearing behaviour of laterally loaded piles in stiff clay. API (2014) explicitly remarks that a softening soil response has a greater impact on stiff clay than soft clay, particularly for cyclic loading conditions. However, a specified p-y approach for stiff clay is not recommended in almost all offshore guidelines, except to API (2007) that just refers to the construction of p-y curves for stiff clay by using the p-y approach proposed by Reese & Cox (1975) without giving more details.

This section deals with the description of three p-y methods for stiff clay that have been introduced in the literature. The comprehensive evaluation of the following p-y methods is also based on comparative studies.

#### 4.4.1 Reese & Cox (1975)

Reese & Cox (1975) proposed a complex p-y correlation for describing the response of a pile-soil system in stiff clay with free water for short-term loading, exclusively based on results of a field test at a site near Manor, Texas (cf. section 5.4.5). Note that a softening soil response for large displacement takes place in the static p-y curves, indicating that the degradation of the soil strength would result due to a gap formation at the active side of the laterally loaded pile.

The ultimate bedding resistance  $p_u$  is calculated by applying the minimum value  $N_p$  resulting from Eq. 4-23, which is obviously derived from the mechanical failure mechanisms. The wedge failure mechanism was characterised based on the equilibrium of a three-dimensional body (cf. section 3.6). Note that the average undrained shear strength  $s_{u,a}$  over the depth  $z$  is required for its application.

$$p_u = \min \left\{ \left( 2 + 2.83 \cdot \frac{z}{D} + \frac{\gamma' \cdot z}{s_{u,a}} \right) \cdot D \cdot s_{u,a} \right. \\ \left. 11 \cdot D \cdot s_u \right. \quad (4-23)$$

The characteristic shape of p-y curves consists of four specific sections represented in Fig. 4-8 (i.e. for two parabolic functions and three straight lines).

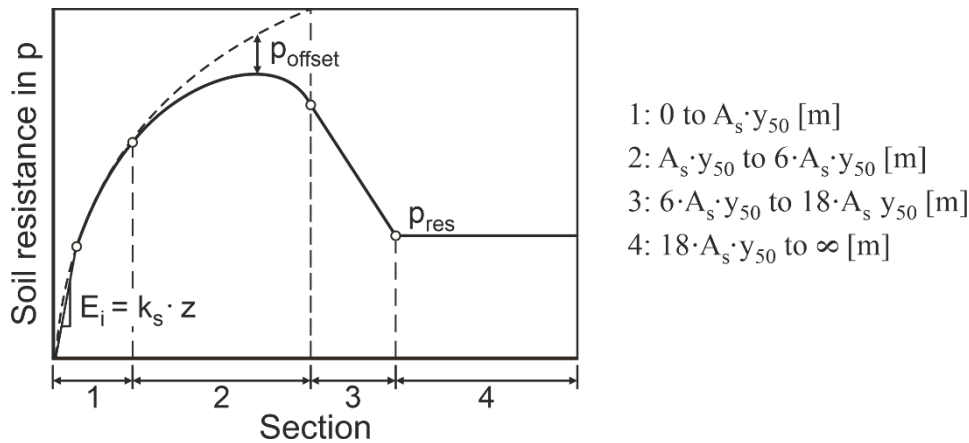


**Fig. 4-8: Characteristic shape of p-y curves according to Reese & Cox (1975) for stiff clay subjected to static loading conditions**

The smaller secant stiffness between the initial straight line Eq. 4-24 and the power function Eq. 4-25 defines the beginning of a static p-y curve characteristic for section 1. The initial straight line is a function of the initial stiffness  $K_s$  obtained from Table 4-1 which depends on the average undrained shear strength  $s_{u,a}$ .

$$p = K_s \cdot z \cdot y \quad (4-24)$$

**Table 4-1: Initial stiffness values of  $K_s$  for static loading conditions according to Reese & Cox (1975)**

* $s_{u,a}$ ; kPa	50 - 100	100 - 200	200 - 400
$K_s$ (static) MN/m <sup>3</sup>	135	270	540

\* Using the average undrained shear strength  $s_{u,a}$

The static p-y curve characteristic for section 1 derives from the following equations.

$$p = 0.5 \cdot p_u \cdot \left( \frac{y}{y_{50}} \right)^{0.5} \quad (4-25)$$

$$A_s = 0.2 + 0.4 \cdot \tanh(0.62 \cdot z/D) \quad (4-26)$$

$$y_{50} = \varepsilon_{50} \cdot D \quad (4-27)$$

Here, the non-dimensional coefficient  $A_s$  resulting from Eq. 4-26 was introduced to reconcile the differences in the results between the theoretical formulation and that obtained from experimental results. The reference displacement  $y_{50}$  is a linear function that depends on the pile diameter  $D$ , as also proposed by Matlock. The representative values of strain at one half of the maximum principal stress  $\varepsilon_{50}$  are listed as follows:

**Table 4-2: Representative values of  $\varepsilon_{50}$  according to Reese & Cox (1975)**

* $s_{u,a}$ ; kPa	50 - 100	100 - 200	200 - 400
$\varepsilon_{50}$	0.007	0.005	0.004

\* Using the average of undrained shear strength  $s_{u,a}$

The static p-y curve characteristic for section 2 results from Eq. 4-28. The ultimate bedding resistance  $p_u$  is located in this section followed by the post-peak softening soil response. The threshold displacement corresponding to  $p_u$  is not required for the construction of p-y curves.

$$p = 0.5 \cdot p_u \cdot \left( \frac{y}{y_{50}} \right)^{0.5} - 0.055 \cdot p_u \cdot \left( \frac{y - A_s \cdot y_{50}}{A_s \cdot y_{50}} \right)^{1.25} \quad (4-28)$$

The static p-y curve characteristic for section 3 specified from Eq. 4-29 results in a connection of the last parabolic function with the residual bedding resistance  $p_{res}$ .

$$p = 0.5 \cdot p_u \cdot \sqrt{6 \cdot A_s} - 0.411 \cdot p_u - \frac{0.0625}{y_{50}} \cdot p_u \cdot (y - 6 \cdot A_s \cdot y_{50}) \quad (4-29)$$

The static p-y curve characteristic for section 4 represents the residual bedding resistance  $p_{res}$ , which is characterised by a horizontal straight line.

$$p_{res} = 0.5 \cdot p_u \cdot \sqrt{6 \cdot A_s} - 0.411 \cdot p_u - 0.75 \cdot p_u \cdot A_s \quad (4-30)$$

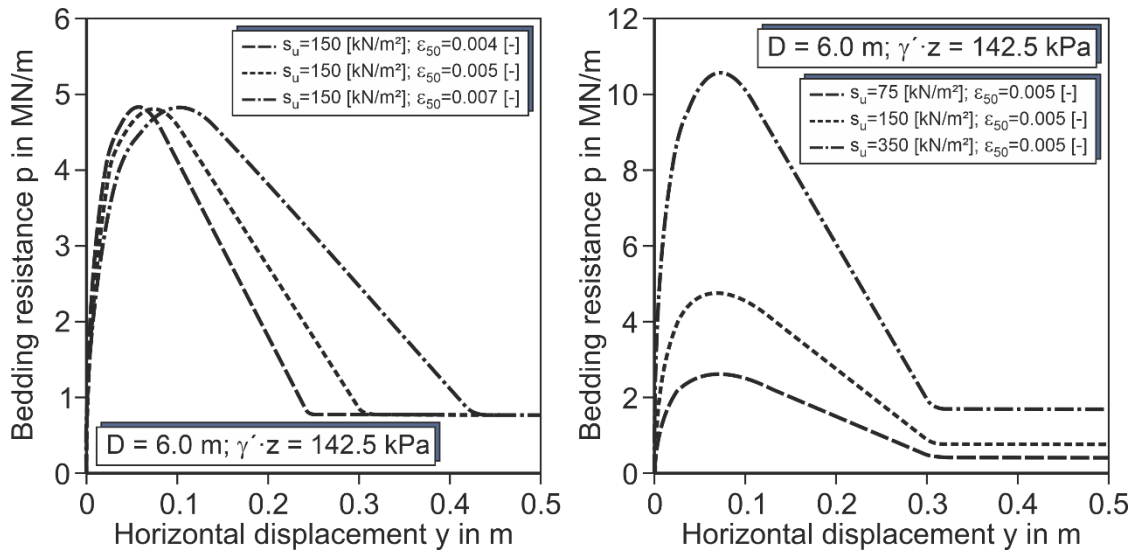


Fig. 4-9: Exemplary p-y curves according to Reese & Cox (1975), variation of the stiffness parameter  $\varepsilon_{50}$  (left) as well as the undrained shear strength  $s_u$  (right)

Fig. 4-9 shows the course of the p-y curves as proposed by Reese & Cox (1975) for six-meter diameter monopile foundations embedded in stiff clay with the variation of soil properties. The linear dependence of  $y_{50}$  obtained from Eq. 4-27 results in a duplication of the bedding stiffness when the strain  $\varepsilon_{50}$  is halved, while an increment of the undrained shear strength  $s_u$  leads to an increase of bedding stiffness, ultimate bedding resistance  $p_u$  and residual bedding resistance  $p_{res}$ . This means that the strain  $\varepsilon_{50}$  only affects the bedding stiffness while the parameters for the ultimate bedding resistance ( $z$ ,  $\gamma'$ ,  $s_u$ ) also influence the ultimate bedding resistance  $p_u$  and residual bedding resistance  $p_{res}$ . It is remarkable that identical behavioural patterns occur in Matlock's p-y curves.

#### 4.4.2 Dunnavant & O'Neill (1989)

A practical p-y relationship for submerged, over-consolidated stiff clay is proposed by Dunnavant & O'Neill based on a series of full-scale lateral load tests on instrumented piles. The p-y derivation was conducted for adequately predicting the effect of the pile diameter on the bedding soil resistance, being particularly well suited to large-diameter piles. It becomes evident that static p-y curves do not exhibit degradation of soil strength (i.e. no-softening soil response) after the threshold deflection  $y = 8 \cdot y_{50}$ . However, it was remarked in the original documents that this could take place when a gap formation at the active side of the pile occurs, as usual for cyclic laterally loaded piles.

Similar to the previous p-y criteria, a distinction is made between the previously described mechanical failure mechanisms of a pile-soil system for calculating the load-bearing capacity factor  $N_p$ . Note that the average undrained shear strength  $s_{u,a}$  is also required to calculate  $N_p$  for shallow depths.

$$N_p = \min \left\{ 2 + \frac{\sigma'_v}{s_{u,a}} + 0.4 \cdot \frac{z}{D} \right. \quad (4-31)$$

The ultimate bedding resistance  $p_u$  is likewise given by:

$$p_u = N_p \cdot D \cdot s_u \quad (4-32)$$

The reference deflection  $y_{50}$ , which corresponds to one half to the ultimate bedding resistance  $p_u$ , depends on the strain at one half of the maximum principal stress  $\varepsilon_{50}$ , the pile diameter  $D$  and the relative stiffness  $K_R$  of pile-soil stiffness. Unquestionably, a linear dependence on the pile diameter  $D$  does exist, but not on  $K_R$ .

$$y_{50} = 0.0063 \cdot \varepsilon_{50} \cdot D \cdot K_R^{-0.875} \quad (4-33)$$

Where  $K_R$  is a function of the flexural stiffness  $E \cdot I$  of the pile, strength-correlated soil modulus  $E_s$  and the pile length  $L$ .

$$K_R = \frac{E \cdot I}{E_s \cdot L^4} \quad (4-34)$$

A hyperbolic function in contrast to the power function adopted by Reese & Cox defines the shape of the introduced p-y curves, as follows.

$$p = 1.02 \cdot \tanh \left[ 0.537 \cdot \left( \frac{y}{y_{50}} \right)^{0.7} \right] \quad (4-35)$$

Dunnavant et al.'s approach does not provide a clear definition of the initial slope of p-y curves. For a very small strain, the secant bedding stiffness  $E_{py} = p / y$  resulting from p-y curves are shown in Fig. 4-10 (left). Contour plots are used for a wide range of pile diameters  $D = 0.5 - 8$  m and relative depths  $z / D = 0 - 5$ , for a normalised head displacement  $y / D = 0.0005$  (i.e. for very small head displacements). The soil parameters and pile dimension correspond to that presented in Fig. 4-14 (bottom). It should also be noted that Dunnavant et al.'s p-y curves apply the relative stiffness  $K_R$  which directly depends on the pile length  $L$ ; as a result contour plots are exclusively valid for the corresponding pile length (in this case  $L = 36$  m).

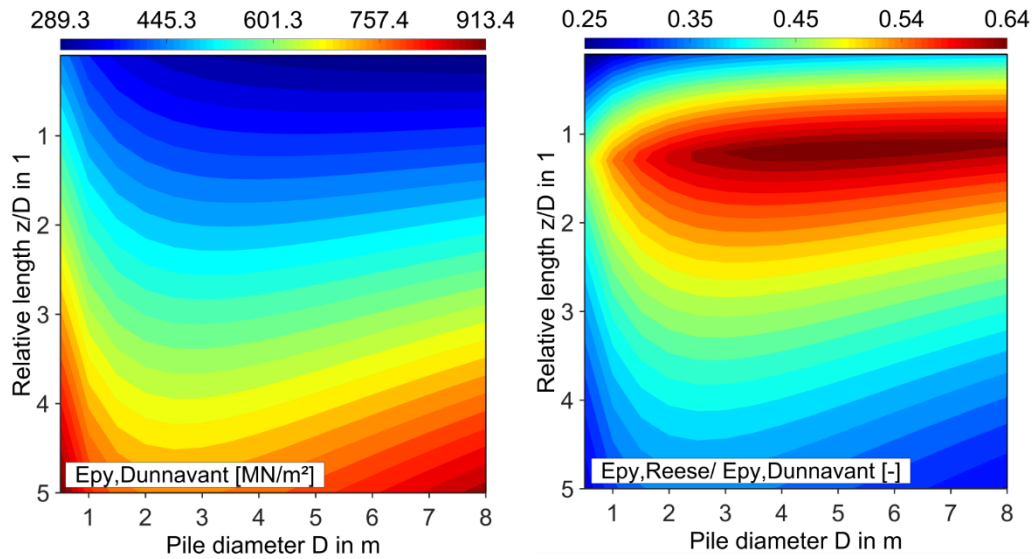


**Fig. 4-10: Bedding stiffness  $E_{py} = p / y$  for soil parameter according to Fig. 4-14 with normalised head displacement  $y / D = 0.0005$**

The quotient of the secant bedding stiffness resulting from the aforementioned p-y approaches are depicted in Fig. 4-10 (right). Unquestionably, for very small head displacements the secant stiffness of p-y curves proposed by Dunnavant et al. is overpredicted when compared to that resulting from Reese & Cox's approach for all pile diameters analysed. However, this distribution of deviations changes depending on the applied pile length, due to the introduction of the relative stiffness  $K_R$  by Dunnavant et al. in the p-y formulation. Note that the secant stiffness resulting from the p-y curves introduced by Reese & Cox are identical for deep depths due to the imposition of an initial stiffness  $K_s$  associated with Table 4-1, which impacts the secant stiffness for very small strain.

#### 4.4.3 Pisa design model (2016)

The joint industry PISA project focused on the development of an innovative approach to the design of laterally loaded piles, specifically adjusted to the offshore wind energy industry. The main characteristic of this new approach is the integration of additional spring characteristics to represent the pile-soil interaction. In addition to the lateral soil reactions that are generally taken into account for conventional p-y approaches, the PISA design model also includes distributed moments acting along the embedded length of the pile as well as the contributions of a shear force and moment applied at the pile base.

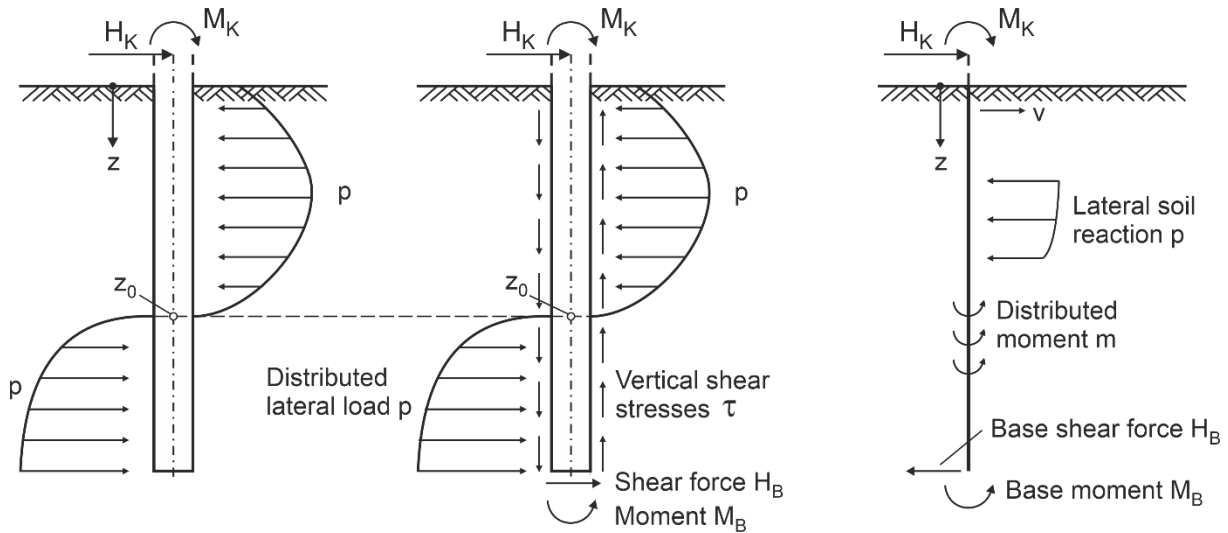


**Fig. 4-11: Comparison of the key features of the proposed analysis models: traditional p-y analysis (left), assumed soil reactions (centre) and analysis model (right) according to PISA (2016)**

Fig. 4-11 (left) depicts the lateral soil reactions commonly applied for the traditional p-y analysis. Besides that, to enable the comparison between the analysis methods, the additional soil reactions proposed by PISA project are also depicted. The four individual components resulting from the soil reactions involved in the improved analysis model (see free body diagram in Fig. 4-11 right) are listed below.

- Distributed load curves (p-y curves) represent the relationship between the distributed lateral load p (i.e. applied along the embedded pile length) and lateral displacement y, usually applied to traditional p-y approaches.
- Distributed moment curves (m-ψ curves) represent the relationship between the distributed moment m (i.e. applied along the embedded pile length) and the pile cross-section rotation θ, and associate with the vertical shear stresses τ developed on the pile shaft.
- Base shear curve ( $H_B$ -y curve) represents the relationship between the shear force  $H_B$ , (i.e. applied at pile base) and the lateral displacement of the pile toe y.
- Base moment curve ( $M_B$ - ψ curve) represents the relationship between the base moment  $M_B$  (i.e. applied at the pile base) and the rotation θ of the pile toe.

All soil reaction curves are defined by applying a conical function with the following general form Eq. 4-36, in which x represents normalised displacement variables detailed in Table 4-3 and y is the respective loading variable. The four main variables (i.e. the limit displacement  $x_u$ , the ultimate reaction  $y_u$ , the curvature factor n and the initial stiffness k) define the general shape of the conical function. These parameters can be independently predetermined which is quite practical compared to the existing p-y functions proposed by conventional p-y methods.

$$-n \cdot \left( \frac{y}{y_u} - \frac{x}{x_u} \right)^2 + (1 - n) \cdot \left( \frac{y}{y_u} - \frac{x \cdot k}{y_u} \right) \cdot \left( \frac{y}{y_u} - 1 \right) = 0 \quad (4-36)$$

For which the real positive roots of y are given by:

$$y = y_u \cdot \frac{2 \cdot c}{-b + \sqrt{b^2 - 4 \cdot a \cdot c}} \quad x \leq x_u \quad (4-37)$$

$$y = y_u \quad x > x_u \quad (4-38)$$

Where:

$$a = 1 - 2 \cdot n \quad (4-39)$$

$$b = 2 \cdot n \cdot \frac{x}{x_u} - (1 - n) \cdot \left( 1 + \frac{x \cdot k}{y_u} \right) \quad (4-40)$$

$$c = \frac{x \cdot k}{y_u} \cdot (1 - n) - n \cdot \frac{x^2}{x_u^2} \quad (4-41)$$

The parameters (i.e.  $x_u$ ,  $y_u$ ,  $k$  and  $n$ ) have to fulfil the following conditions:  $0 \leq n \leq 1$  and  $x_u > y_u / k$  to properly apply Eq. 4-36.

In contrast to traditional p-y approaches, the application of soil reaction curves in the analytical model (subsequently also denoted as 1D model) requires to be expressed in an appropriate set of normalised variables listed in Table 4-3. The 1D model represented by a line of beam finite elements is based on Timoshenko's beam theory, due to the inclusion of the pile cross-section rotations.

**Table 4-3: Normalisation of pile reaction components according to PISA (2016)**

Component	Clay Normalisation
Distributed load, p	$p / (s_u \cdot D)$
Lateral displacement, v	$v \cdot I_R / D$
Distributed moment, m	$m / (s_u \cdot D^2)$
Pile rotation, $\psi$	$\psi \cdot I_R$
Base shear load, $H_B$	$H_B / (s_u \cdot D^2)$
Base moment, $M_B$	$M_B / (s_u \cdot D^3)$

Note that all components or normalised soil reactions remain independent from each other for stiff clay, but when it comes to sand, the distributed load p and moment m are coupled (for more details see PISA project 2016), causing the soil reaction curves to become variable along the iterative process required to reach the equilibrium of the pile-soil system.

The concept for building the soil reaction curves using PISA design model significantly differs from traditional p-y approaches. The layer-specific soil parameters (i.e. strength and stiffness properties) are used to derive traditional p-y curves, while PISA curves have to be determined on the basis of a calibration study by using 3D finite element simulations on comparable pile dimensions and loading conditions. Consequently, the parameters of the PISA procedure are



not directly obtained from soil parameters. However, instead of that system-dependent method parameters without any strict physical meaning are applied.

In the PISA final report, a precise description does not exist for deriving the previously mentioned system-dependent method parameters from a set of 3D numerical models, but it gives a unique example of method parameters for stiff clay calibrated by piles located at the testing sites at Cowden. Depth-dependent functions are applied for obtaining the soil reaction curve parameters, which are summarised in Table 4-4. For defining the four individual soil reaction curves a total of 16 depth-dependent functions are required, which are a function of both the pile diameter  $D$  and the depth  $z$ .

**Table 4-4: Method parameters for monopiles in stiff clay at Cowden site PISA (2016)**

Soil reaction component	Parameter	Air-filled gap expression	Water-filled gap expression
Distributed lateral load, $p$	Ultimate strain, $v_{pu}$	200	200
	Initial stiffness, $k_p$	$-1.11 \cdot z/D + 8.17$	$-1.11 \cdot z/D + 8.13$
	Curvature, $n_p$	$-0.07 \cdot z/D + 0.92$	$-0.06 \cdot z/D + 0.93$
	Ultimate reaction, $p_u$	$11.66 - 8.64 \cdot e^{(-0.37 \cdot z/D)}$	$9.78 - 6.73 \cdot e^{(-0.36 \cdot z/D)}$
Distributed moment, $m$	Ultimate rotation, $\psi_{mu}$	10	
	Initial stiffness, $k_m$	$-0.12 \cdot z/D + 0.98$	
	Curvature, $n_m$	0	
	Ultimate moment, $m_u$	$-0.05 \cdot z/D + 0.38$	
Base shear, $H_B$	Ultimate strain, $v_{Hu}$	300	
	Initial stiffness, $k_H$	$-0.32 \cdot z/D + 2.58$	
	Curvature, $n_H$	$-0.04 \cdot z/D + 0.76$	
	Ultimate reaction, $H_{Bu}$	$-0.07 \cdot z/D + 0.59$	
Base moment, $M_B$	Ultimate rotation, $\psi_{Mu}$	200	
	Initial stiffness, $k_M$	$-0.002 \cdot z/D + 0.19$	
	Curvature, $n_M$	$-0.15 \cdot z/D + 0.99$	
	Ultimate reaction, $M_{Bu}$	$-0.07 \cdot z/D + 0.65$	

\* The system-dependent method parameters are valid for the following conditions:  $2 < L/D < 6$ ,  $5 < D < 10$ ,  $5 < h/D < 15$ ,  $60 < D/t < 110$  and  $0 < z/D < 6$ .

The PISA design model assumes a gap formation at the active side of the pile for stiff clay. However, a distinction is made between air-filled gap and water-filled gap conditions for

predicting the pile's load-bearing behaviour, indicating that the inclusion of water instead of air into the gap slightly reduces the ultimate bedding resistance (i.e. for the distributed lateral load,  $p$ ). Note that the remaining soil reaction components are identical between both gapping conditions.

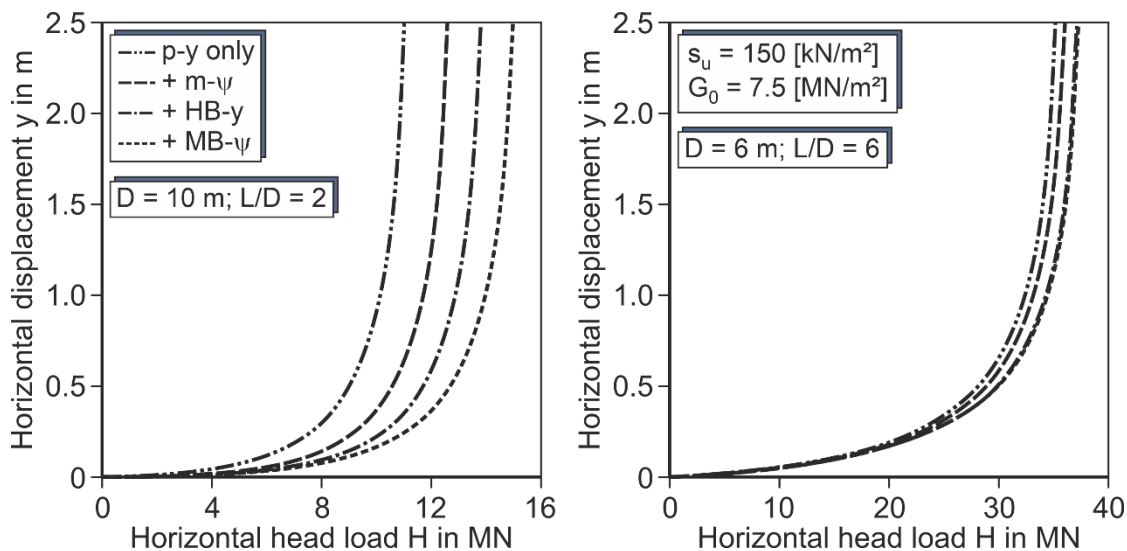


**Fig. 4-12: Influence of the various components of soil reactions according to PISA (2016) on the computed response of pile-soil system for  $h/D = 5$  and  $D/t = 90$**

Fig. 4-12 shows the lateral load-deflection curves for stiff clay computed using the PISA design model, which was successfully implemented in the pile design programme IGtHPile. Two ratios of embedded pile length  $L$  to diameter  $D$  (i.e.  $L/D = 2$  and  $L/D = 6$ ) are selected to reflect the effect of soil reaction components on the load-bearing behaviour resulting from the laterally loaded pile. The system-dependent method parameters come from the calibration of the testing sites at Cowden (see Table 4-4 in water-filled gap expression). The contribution of each soil reaction component in the 1D model results in increasing soil resistance at whole load levels. The overall pile behaviour becomes significantly stiffer by using all four components compared to the unique soil reaction component proposed by the traditional p-y approach. Evidently, the contribution of each soil reaction component mainly depends on the flexibility of the pile foundation having more effects on rigid than flexible piles. This is particularly identified in the soil reaction of the base moment  $M_B-\psi$ , as seen in Fig. 4-12 (right).

#### 4.5 Non-linear p-y curves for the unified method

As stated by Gazioglu & O'Neill (1984), the differentiation of p-y methods into soft and stiff clay categories for predicting the load-bearing behaviour of laterally loaded piles is an artificial classification. The best-known lateral field load tests on instrumented piles conducted for soft and stiff clay (cf. section 5.4) are simultaneously reanalysed to develop a unified p-y method that would be applicable without the distinction of the soil's consistency. The most representative unified p-y approaches will now also be discussed.

### 4.5.1 Sullivan et al. (1980)

Sullivan et al. (1980) mainly based his study on the field load tests reported by Matlock and Reese et al. and introduced an alternative p-y approach either for soft or stiff clay. Nonetheless, additional field load tests for submerged clay were highly recommended by Sullivan et al., particularly for the appropriate recalibration of the parameters F and A.

The smallest ultimate bedding resistance  $p_u$  resulting from Eq. 4-42 is assumed decisive. The first two equations for calculating  $p_u$  refer to shallow depths, having a distinction between the average undrained shear strength  $s_{u,a}$  and the undrained shear strength  $s_u$ . The third equation for calculating  $p_u$  corresponds to deep depths, considering a smooth interface for the pile-soil interaction.

$$p_u = \min \begin{cases} (2 \cdot s_{u,a} + \gamma') \cdot D + 0.833 \cdot s_{u,a} \cdot z \\ (3 \cdot D + 0.5 \cdot z) \cdot s_u \\ 9 \cdot s_u \cdot D \end{cases} \quad (4-42)$$

Three schematic sections represented in Fig. 4-13 define the shape of the proposed p-y curve (i.e. one power function and three straight lines). Note that the so-called unified p-y method also considers the softening soil response limited by the residual bedding resistance  $p_{res}$ .

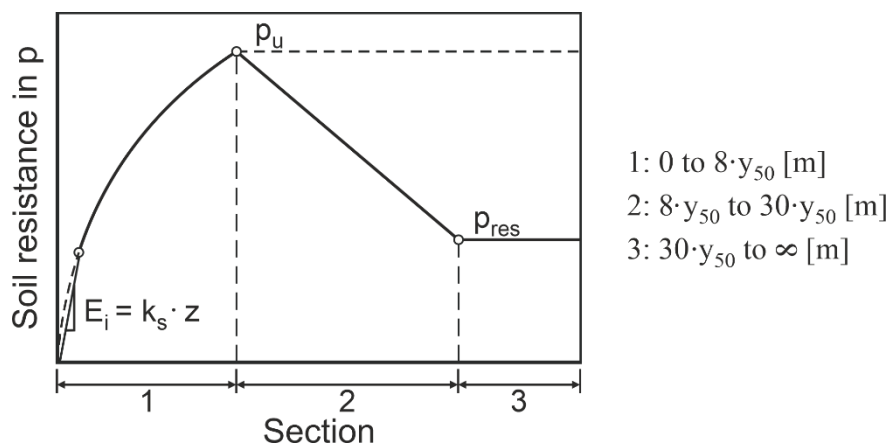


**Fig. 4-13: Characteristic shape of p-y curves according to Sullivan et al. (1980) for the unified method subjected to static loading conditions**

Similar to Reese et al., the initial portion of the p-y curve is a straight line given by Eq. 4-43. The interception with the parabolic functions Eq. 4-44 corresponds to its limit. The Table 4-5 indicated the reference values for the initial stiffness  $K_s$ .

$$p = K_s \cdot z \cdot y \quad (4-43)$$

**Table 4-5: Typical values for  $K_s$  according to Sullivan et al. (1980)**

$s_u$ , kPa	$K_s$ , MN/m <sup>3</sup>
12 – 25	8
25 – 50	27
50 – 100	80
100 – 200	270
200 – 400	800

The static p-y curve characteristic for section 1 derived from Eq. 4-44 contains the ultimate bedding resistance  $p_u$ , which is reached at the threshold displacement  $8 \cdot y_{50}$ . Thereafter, the softening soil response takes places up to the residual bedding resistance  $p_{res}$ , see section 2.

$$p = 0.5 \cdot p_u \cdot \left( \frac{y}{y_{50}} \right)^{\frac{1}{3}} \quad (4-44)$$

The reference displacement  $y_{50}$  has a similar treatment to that given by Matlock (i.e. the linear dependency of the  $y_{50}$  on the pile diameter  $D$ ) but including the parameter  $A$ . The reference values of the strain at one half of the maximum principal stress  $\epsilon_{50}$  are listed in Table 4-6.

$$y_{50} = A \cdot \epsilon_{50} \cdot D \quad (4-45)$$

**Table 4-6: Typical values for  $\epsilon_{50}$  according to Sullivan et al. (1980)**

$s_u$ , kPa	$\epsilon_{50}$
12 – 25	0.02
25 – 50	0.01
50 – 100	0.007
100 – 200	0.005
200 – 400	0.004

The parameters  $A$  and  $F$  have to be defined through comparison with soil properties of Sabine and Manor clay field load tests (cf. section 5.4). Table 4-7 indicates the representative values for the parameters  $A$  and  $F$  used in such cases.

**Table 4-7: Typical calibration factors according to Sullivan et al. (1980)**

Site	Sabine River	Manor
A	2.5	0.35
F	1.0	0.5

The static p-y curve characteristic for section 3 comes from Eq. 4-46, selecting the smaller residual bedding resistance  $p_{res}$  of both equations. Note that  $12 \cdot D$  represents the depth after which the ultimate bedding resistance  $p_u$  does not suffer any degradation of soil strength.

$$p_{res} = \begin{cases} p_u \cdot \left[ F + (1 - F) \cdot \frac{z}{12 \cdot D} \right] & z < 12 \cdot D \\ p_u & z \geq 12 \cdot D \end{cases} \quad (4-46)$$

Fig. 4-14 shows exemplary p-y curves from the unified method according to Sullivan et al., and Gazioglu & O'Neill compared to the p-y curves specifically used for stiff clay proposed by Dunnavant et al. and Reese & Cox for small and large diameter piles at shallow and deep depths. The corresponding clay parameter used for the comparison is also provided in Fig. 4-14. In addition, the strength-correlated soil modulus  $E_s$  introduced by Dunnavant et al. and Gazioglu & O'Neill is set at  $10000 \text{ kN/m}^2$ . Regarding the pile dimension, the wall thickness  $t$  used for both pile diameters comes from Eq. 6-1.

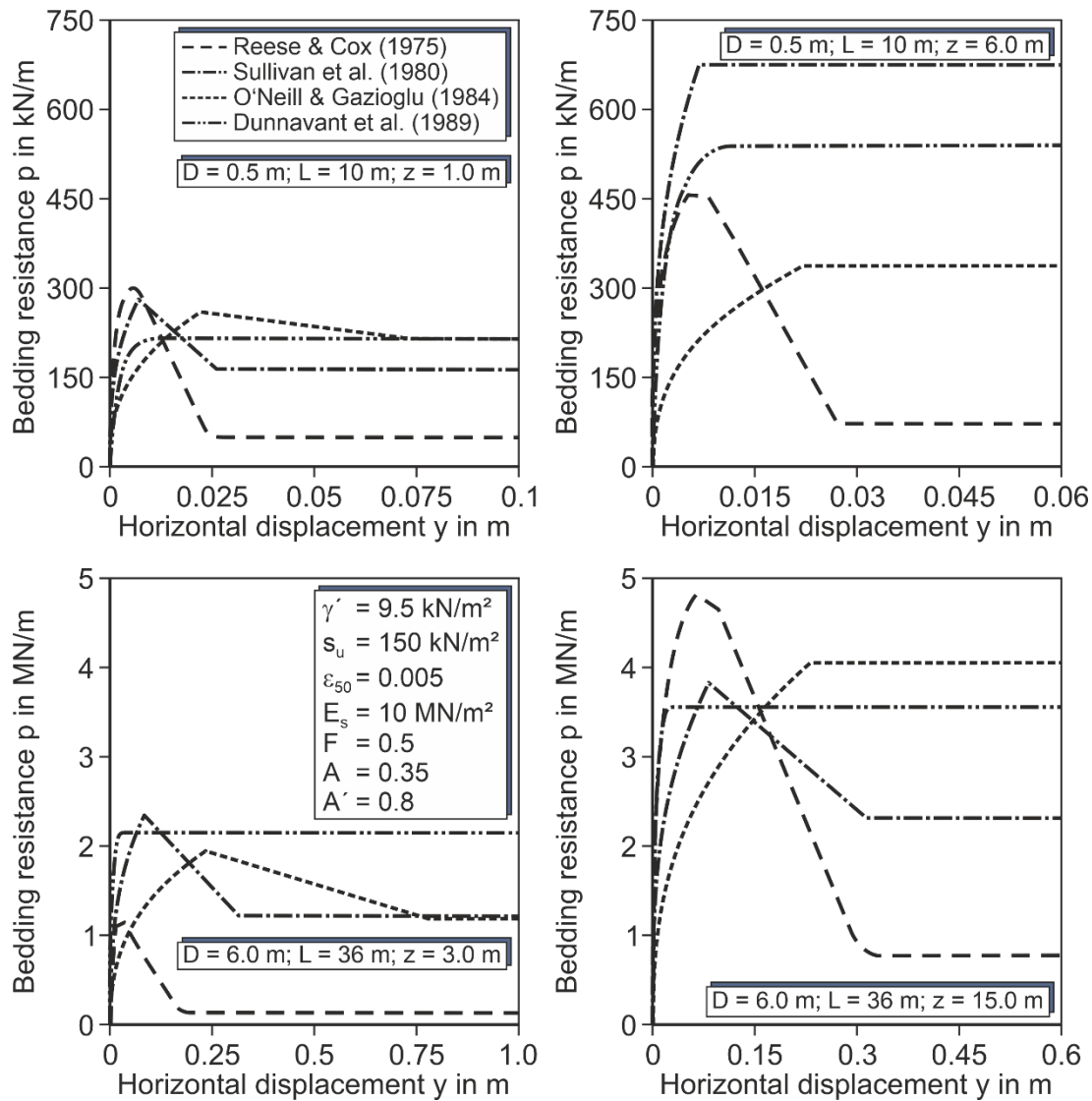


Fig. 4-14: Exemplary p-y curves for stiff clay and unified approaches for small and large diameter piles

Gazioglu & O'Neill's approach result in smaller bedding stiffness compared to other p-y approaches, but the ultimate bedding resistance  $p_u$  presents different trends. Reese & Cox's p-y curves describe identical behaviour at the beginning of the p-y curve with respect to the unified p-y curves proposed by Sullivan et al. due to the inclusion of an identical straight line that defines the initial stiffness of the p-y curve. The bedding stiffness resulting from Dunnivant et al. changes depending on the flexibility of the pile, being stiffer for large diameter piles  $D = 6$  m and softer for smaller diameter piles  $D = 0.5$  m compared to the remaining p-y approaches. Please remember that the Dunnivant et al. approach considers the relative stiffness  $K_R$  of the pile-soil system that has a great effect on the pile's load-bearing behaviour. It is remarkable that a wide range of residual bedding resistances  $p_{res}$  exists exclusively depending on the p-y approach applied.

#### 4.5.2 Gazioglu & O'Neill (1984)

Gazioglu & O'Neill developed a semi-empirical p-y method valid for different consistencies of clay, based on the results of 21-field load tests at 11 different locations, representing a significantly wide range of soil conditions. This p-y method was called the "Integrated Clay Method" and contains empirical terms reflecting the ductility of soil, the relative pile-soil stiffness and the degradability of soil.

Similar to the aforementioned p-y approaches for calculating the load-bearing capacity factor  $N_p$ , both mechanical failure mechanisms are included in Eq 4-47, remarking a critical depth  $z_{cr}$  below soil surface which depends on relative pile-soil stiffness.

$$N_p = \min \left\{ 3 + 6 \cdot \frac{z}{z_{cr}} \right. \quad (4-47)$$

$$z_{cr} = L_c/4 \quad (4-48)$$

Based on the finite element studies developed by Randolph (1981), the critical pile length  $L_c$  of a quasi-elastic soil in which the pile-soil response is essentially unaffected by further penetrations. This can be calculated as a function of the flexural stiffness  $E \cdot I$  of the pile, the soil modulus  $E_s$  related to the undrained shear strength  $s_u$  and the pile diameter  $D$ .

$$L_c = 3 \cdot \left( \frac{E \cdot I}{E_s \cdot D^{0.5}} \right)^{0.286} \quad (4-49)$$

In contrast to previous p-y methods, for deriving the ultimate bedding resistance  $p_u$  the reduction factor  $F$  given in Table 4-8 is applied based on the soil ductility and type of loading condition situations.

$$p_u = F \cdot N_p \cdot D \cdot c_u \quad (4-50)$$

**Table 4-8: Soil degradability factor F according to Gazioglu & O'Neill (1984) for static loading**

* UU triaxial compression failure strain	< 0.02	0.02 < $\epsilon_f$ < 0.06	$\epsilon_f > 0.06$
Factor F	0.5	0.75	1.0

\* Using the failure strain from a UU triaxial compression test  $\epsilon_f$

Fig. 4-15 schematically shows the construction of static p-y curves, which are made up of three well-defined sections.

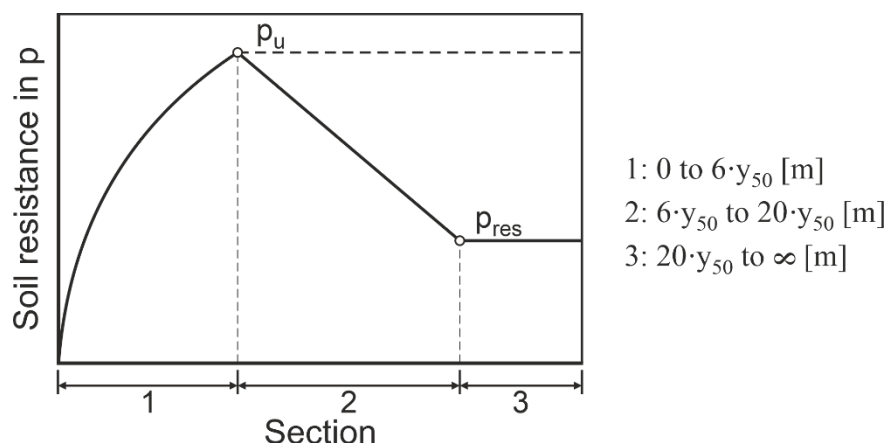


**Fig. 4-15: Characteristic shape of p-y curves according to Gazioglu & O'Neill (1984) for a unified method subjected to static loading conditions**

For calculating the reference displacement  $y_{50}$ , a non-linear dependence on the pile diameter  $D$  is defined, resulting in a dimensionally consistent equation in contrast to the one proposed by Stevens and Audibert (1979). The authors presented seven well-documented, full-scale static and cyclic load tests to define the factor  $A' = 0.8$  as reference value.

$$y_{50} = A' \cdot \epsilon_{50} \cdot D^{0.5} \cdot \left( \frac{E \cdot I}{E_s} \right)^{0.125} \quad (4-51)$$

The static p-y curve characteristic for section 1 defined from Eq. 4-52 provides an initially infinite soil stiffness due to the application of a power function as follows:

$$p = 0.5 \cdot p_u \cdot \left( \frac{y}{y_{50}} \right)^{0.387} \quad (4-52)$$

The static p-y curve characteristic for section 2 describes the softening soil response which is characterised by a straight line joining the other two segments of the curve. The residual segment of static p-y curves derived from Eq. 4-53 introduces the critical depth  $z_{cr}$  given by Eq. 4-48, meaning the depth limit at which the softening soil response takes place.

$$p_R = \begin{cases} p_u \cdot \left[ F + (1 - F) \cdot \frac{z}{z_{cr}} \right] & z < z_{cr} \\ p_u & z \geq z_{cr} \end{cases} \quad (4-53)$$

## 4.6 Pile design programme (IGtHPile)

Currently, different commercial programmes are available for the design of pile foundations. The analysis of pile foundations using these programmes is generally based on the solution of a differential equation, which describes the behaviour of a beam-column supported by non-linear spring characteristics. However, the results obtained from the pile design programmes disagree significantly with each other in several respects. The reason for such discrepancies is unclear since the technical manuals provided for the programmes usually do not include detailed information on the implemented calculation procedures. Besides that another limitation of the use of commercial programmes is that their source codes are generally closed, preventing further implementations or improvements as well as updates that could be made by the user. Therefore, the pile design programme IGtHPile has been developed at the Institute for Geotechnical Engineering (IGtH) since 2014, which allows the analysis and the design of single piles subjected to axial or lateral loading conditions uncoupled (cf. Terceros et al. 2015). It has to be mentioned that the programme is only being developed for research and academic purposes.

In contrast to other programmes, the pile design programme IGtHPile offers the capability for calculating pile foundations subjected to cyclic axial loading conditions according to Achmus (2012b). Likewise, the implementation of other calculation procedures is feasible, e.g. the design of pile foundations supporting offshore structures subject to cyclic lateral loading conditions.

Numerical techniques such as the Finite Element Method (FEM) have been implemented for analysing pile foundations, which are idealized as a one-dimensional beam element that is supported by nonlinear spring characteristics. This beam analysis can be applied using different theories such as Timoshenko and Euler-Bernoulli in the programme. For solving the model an iterative procedure is applied that is carried out to achieve equilibrium of the forces and compatibility of pile deformation.

The pile design programme IGtHPile has a modular design and is implemented under the concept of the object-oriented programming technique. Consequently, an efficient organization of the source code is achieved. As a programming language, Visual Basic .Net has been selected for the development of the programme.

Both input and output of data can be controlled through a Windows-based Graphical User Interface (GUI) that provides a bilingual programme whereby the user can select the language between German and English, thus ensuring user-friendliness. To properly evaluate the results, they are displayed graphs together with their respective tables. The results can be exported to Microsoft Office Excel to enable further the post-processing of the data output. The analysis options are found in the main panel, which is divided into sub-topics like axial and lateral loading conditions since the respective analysis is carried out separately.



All p-y methods used for analysing and evaluating laterally loaded pile foundations embedded in cohesive soil (cf. appendix B) have been implemented in the freely accessible IGtHPile design programme, which enables the following capabilities to be calculated:

- Calculation of the pile deflection line, the distribution of bending moment and shear force as well as the ultimate bedding resistance  $p_u$  along the pile length
- Determination of the load-displacement curves and the moment-rotation curves at the pile head for evaluating the stiffness of the soil-pile system
- Generation of p-y curves for cohesive and non-cohesive soils subjected to static or cyclic loading conditions according to offshore guidelines such as API (2014) and DNVGL (2016) as well as further alternative approaches proposed in the literature
- Estimation of the critical embedded pile length to reach the minimum pile head deflection according to EA-Pfähle (2012)
- Calculation of the capacity proof for laterally loaded pile foundations for GEO-2 and GEO-3 limit states
- Determination of the nonlinear Stiffness Matrix for single pile according to Terceros et al. (2015)
- Consideration of the general and local scour depths and the limit depth according to API (2014)

In addition, the implementation of a third module in the pile design programme IGtHPile was required for the calibration of the new modelling approach introduced in section 7. Thus, the post-processing of the data output of the Plaxis 3D is carried out to obtain the p-y curves resulting from the numerical analysis. For the post-processing of the data output, Plaxis 3D provides the bedding resistance only in terms of contact stresses in the normal and orthogonal direction at the stress points. The stresses must be transformed into a global coordinate system and integrated for the pile section under consideration. In this respect, the weight factors of the stress points described by Dunavant (1985) are required. This is a challenging task (performed in the third module) since the elements are usually of different sizes and the values are given in table form more or less randomly. For the generation of the p-y curves, several load steps have to be analysed. Besides that, the pile deflection lines must be extracted from the nodal points also found in the table form. The third module of the pile design programme IGtHPile also offers the facility to compare the p-y curves obtained from the numerical models with the p-y methods introduced in section 4, which is decisive for the development and the calibration of the new modelling approach proposed in the presented thesis.

In conclusion, the capabilities of the pile design programme IGtHPile are briefly described in this section for the analysis and design of single piles under different load conditions (axially or laterally loaded pile foundations). Based on the concept of the object-oriented programming technique, several methods of calculation are implemented in the programme, recommended by API (2014) and DNVGL (2016) as well as further alternative approaches proposed in the literature. The employment of a GUI allows the presentation of the results in graphics together with tables. The implementation of new calculation methods in the pile design programme is feasible.



## 5 Numerical model for short-term loading

### 5.1 General

The finite element method (FEM) is used for the numerical simulation of horizontal load-bearing behaviour of a pile subjected to lateral loading conditions. The three-dimensional numerical simulation of the pile-soil interactions is carried out using the Finite Element (FE) programme Plaxis 3D. Due to the existing symmetry of both geometrical and loading condition situations, only half of the pile-soil system is modeled in order to reduce the computational effort. The mesh fineness and model dimensions were optimised by a previous sensitivity study to avoid an impact of the boundary conditions on the pile-soil interaction, so that sufficiently accurate results are obtained for a minimum number of elements. The normalised model dimension used for the simulations is illustrated in Fig. 5-1. The reference system of the FEM study ( $D = 6$  m;  $L = 36$  m) was discretised by an average of roughly 200000 tetrahedron elements (10 node elements), in which a mesh refinement was conducted in the surroundings of the pile.

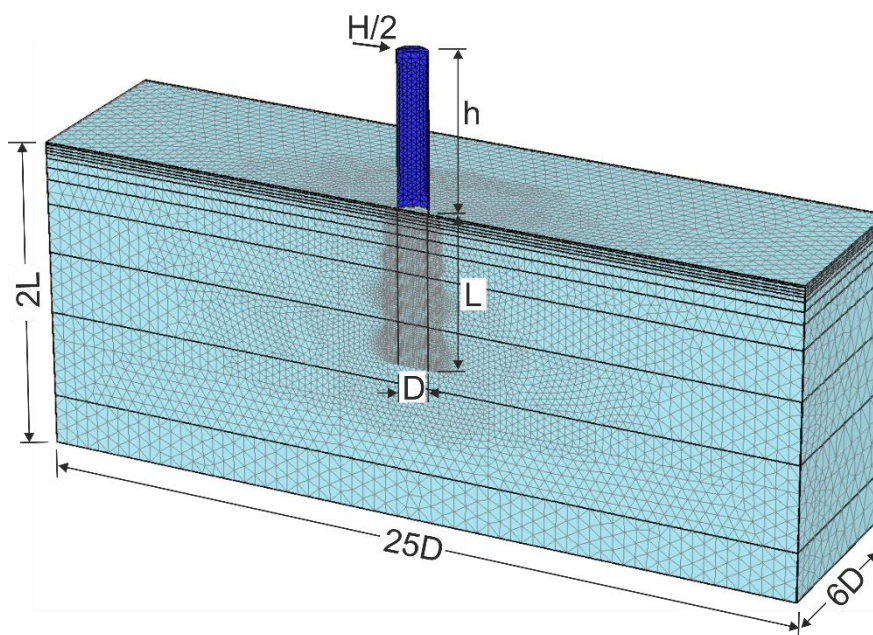


**Fig. 5-1: Finite element mesh of the pile-soil system used for simulations**

The open tubular pile with a wall thickness  $t$  was assigned to the properties of steel material with the modulus of elasticity  $E_p = 2.1 \cdot 10^8$  kN/m<sup>2</sup>, the Poisson's ratio  $\nu = 0.27$  and the buoyant unit weight  $\gamma_s = 68$  kN/m<sup>3</sup>. For the application of the lateral load and its respective overturning moment, the pile was extended with a load eccentricity  $h$  above the free soil surface with a nearly rigid behaviour ( $E_p = 1 \cdot 10^6$  GPa,  $\gamma_s = 0.1$  kN/m<sup>3</sup>,  $\nu = 0.27$ ). An elastoplastic contact was considered between the pile and the surrounding soil with maximum shear stress set to 50 % of the soil shear strength (parameter of the FE programme Plaxis 3D:  $R_{inter} = 0.5$ ). Note that the virtual interface thickness, which influences the normal and tangential stiffness of the contact element was selected in accordance with the default settings of the programme Plaxis 3D. This results at least in numerical stability to the change of stiffness.

The simulations consist of a three-step procedure: in the first step the initial stress state is generated by exclusive consideration of soil elements. The horizontal stress  $\sigma_H$  is related to the coefficient of horizontal earth pressure at rest which is set to  $k_0 = 1$  for undrained soil conditions ( $\varphi_u = 0$ ). In the second step, the examined pile foundation was installed in a “wished-in-place” procedure by the activation of the elements representing the foundation structure, as well as the contact between the pile elements and the surrounding soil. A very slight settlement of the pile results from the self-weight of the pile. Finally, the lateral load  $H$  with its respective overturning moment is applied at the centre of a rigid top plate corresponding to the eccentricity height  $h$  (see Fig. 5-1).

The effects of the foundation installation on the stiffness and soil strength around the foundation are not considered, but such effects might be captured in the design practice by empirical correlations, for instance. However, the required simplification seems to be justified by the good agreement of the results from the FEM-calculations with the ones considered in the field tests (cf. section 5.4).

## 5.2 Constitutive model

The mechanical behaviour of the soil is reproduced using the material model Hardening Soil small (HSsmall) according to Benz (2007), which is an extension of the Hardening Soil (HS) model proposed by Schanz (1998). The HSsmall constitutive model considers fundamental properties of soil behaviour such as stress- and strain-dependent stiffness, as well as hyperbolic stress-strain relation for deviatoric stress variations which appears to be suitable for the current problem, whereby the short-term monotonic loading conditions is exclusively investigated for the present study.

The soil stiffness for very small shear strains ( $\gamma < 10^{-6}$ ) is described by the dynamic shear modulus  $G_0$  in the model. For the determination of the dynamic shear modulus  $G_0$ , the Kim et al. (1981) approach, which is based on a large number of resonant column experiments on different types of cohesive soil, will be used hereafter. According to Kim et al., the dynamic shear modulus  $G_0$  depends on the void ratio  $e$ , the mean effective principal stress  $\sigma_m$ , the over-consolidation ratio OCR, the stress exponent  $\lambda_{G0}$  and the exponent  $k$  of the over-consolidation ratio OCR. The relationship between the exponent  $k$  and the plasticity index PI corresponds to EAD (2002). The mean effective principal stress  $\sigma_m$  in kPa is used to obtain the dynamic shear modulus  $G_0$  in kPa as given by Eq. 5-1.

$$G_0 = 1576 \cdot \frac{(2.973 - e)^2}{1 + e} \cdot \text{OCR}^k \cdot \sigma_m^{\lambda_{G0}} \quad (5-1)$$

The stiffness degradation is described as a non-linear function of the shear strain  $\gamma$  according to Dos Santos & Correia (2001). The reference shear strain  $\gamma_{0.7}$  corresponds to the shear strain at which the soil stiffness is reduced to 72.2 % of the initial value. The reference shear strain  $\gamma_{0.7}$  applied hereafter results as a function of the plasticity index PI according to the correlation proposed by Stokoe et al. (2004), i.e. a linear increment for  $\gamma_{0.7}$  from  $\gamma_{0.7} = 0.0001$  for PI = 0 up to  $\gamma_{0.7} = 0.0006$  for PI = 100.

$$\frac{G}{G_0} = \frac{1}{1 + 0.385 \cdot \gamma/\gamma_{0.7}} \quad (5-2)$$

For large shear strain, the degradation is limited by the static soil stiffness. The HSsmall constitutive model distinguishes three types of soil stiffness: the tangent stiffness for primary oedometer loading  $E_{\text{oed}}$ , the secant stiffness in a standard drained triaxial test  $E_{50}$ , and the unloading and reloading stiffness from a drained triaxial test  $E_{\text{ur}}$ .

In general, the three stiffness moduli are defined as stress dependent. However, in the undrained analysis B applied in this study (cf. section 5.3), the stress dependence is eliminated according to Brinkgreve et al. (2013). In order to consider a depth-dependent soil stiffness, the homogeneous clay was divided into several layers, for which the stiffness parameters are determined depending on the initial stress state, such that the required depth-dependence according to Eq. 5-3 to 5-6 is shaped using the Plaxis 3D formulation (see Fig. 5-2).

$$E_{\text{oed}} = E_{\text{oed}}^{\text{ref}} \cdot \left( \frac{c \cdot \cos \varphi' + \sigma'_1 \cdot \sin \varphi'}{c \cdot \cos \varphi' + p_{\text{ref}} \cdot \sin \varphi'} \right)^m \quad (5-3)$$

$$E_{50} = E_{50}^{\text{ref}} \cdot \left( \frac{c \cdot \cos \varphi' + \sigma'_3 \cdot \sin \varphi'}{c \cdot \cos \varphi' + p_{\text{ref}} \cdot \sin \varphi'} \right)^m \quad (5-4)$$

$$E_{\text{ur}} = E_{\text{ur}}^{\text{ref}} \cdot \left( \frac{c \cdot \cos \varphi' + \sigma'_3 \cdot \sin \varphi'}{c \cdot \cos \varphi' + p_{\text{ref}} \cdot \sin \varphi'} \right)^m \quad (5-5)$$

$$G_0 = G_0^{\text{ref}} \cdot \left( \frac{c \cdot \cos \varphi' + \sigma'_3 \cdot \sin \varphi'}{c \cdot \cos \varphi' + p_{\text{ref}} \cdot \sin \varphi'} \right)^m \quad (5-6)$$

Whereas the dynamic shear modulus  $G_0$  is adapted according to Eq. 5-1, the oedometer modulus  $E_{\text{oed}}$  is fitted to the stress-dependent oedometric stiffness formulations given in Eq. 5-7. The reference stress for the stiffness formulation is usually (and also in this study) set to  $p_{\text{ref}} = 100 \text{ kN/m}^2$ .

For the presented investigations, the following equation introduced by Ohde (1939) is applied to describe the shape of oedometric stiffness over depth.

$$E_{\text{oed}} = E_{\text{oed}}^{\text{ref}} \cdot \left( \frac{\sigma_m}{\sigma_{\text{at}}} \right)^{\lambda_{E_{\text{oed}}}} \quad (5-7)$$

The reference oedometric stiffness parameter  $E_{\text{oed}}^{\text{ref}}$  defines the soil stiffness at the reference stress  $\sigma_{\text{at}} = 100 \text{ kN/m}^2$  whereas the exponent  $\lambda_{E_{\text{oed}}}$  rules the stress dependency with respect to the mean principal stress  $\sigma_m$ .

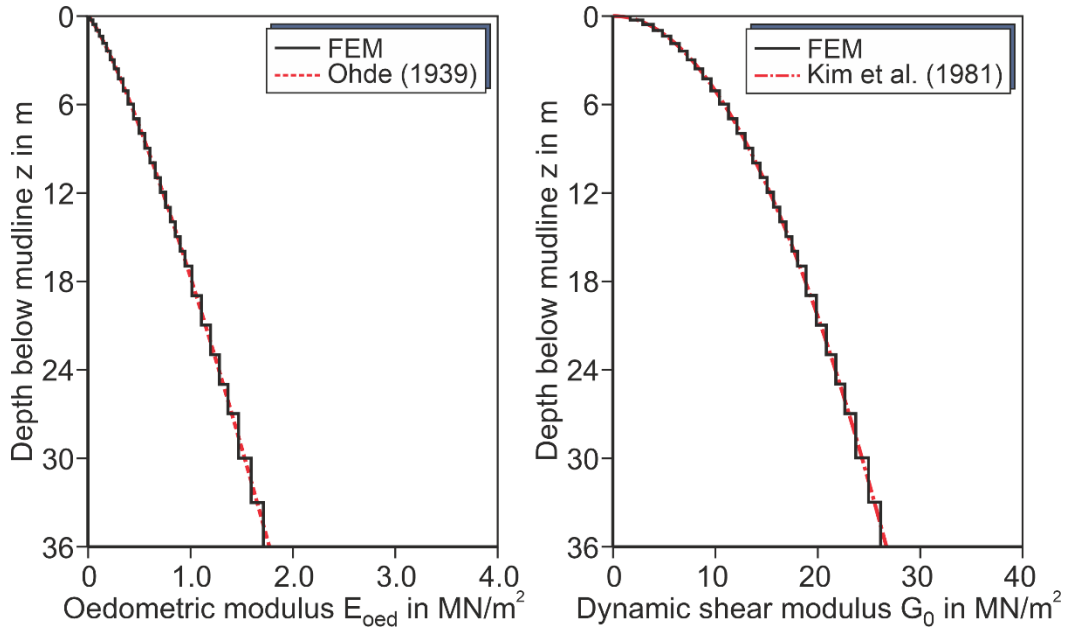


**Fig. 5-2: Approximation of the soil stiffness in Plaxis 3D for the consideration of the stiffness exponent  $m$ ,  $\lambda_{Es}$  and  $\lambda_{G0}$  (reference system of the FEM study)**

Fig. 5-2 shows the required course adaptation of  $E_{0ed}$  or  $G_0$ , which was fairly well approximated using various layers with different parameters. The selected procedure also allows the consideration of different stress exponents for  $G_0$ , and  $E_{0ed}$ , whereas the original formulation of the HSsmall constitutive model in Plaxis 3D has not differentiated between them.

The reference values of the oedometric stiffness  $E_{0ed}$  and the stiffness exponent  $m = 1$  are based on the EAU (2012) bandwidth. The values used in the back-calculation of the field tests “Lake Austin” and “Sabine River” are defined on the basis of the available information (cf. section 5.4). In accordance with Benz (2007), the values for  $E_{50}^{ref}$  and  $E_{ur}^{ref}$  are selected in dependence on the magnitude  $E_{0ed}^{ref}$ . It applies  $E_{50}^{ref} = 2 \cdot E_{0ed}^{ref}$  and  $E_{ur}^{ref} = 5 \cdot E_{50}^{ref}$  according to Terceros et al. (2019).

In this thesis, however, a recalibration of the numerical model is conducted to enable the inclusion of stiff clay through the “Manor” field test used for numerical validation, resulting in  $E_{50}^{ref} = 3 \cdot E_{0ed}^{ref}$  and  $E_{ur}^{ref} = 6 \cdot E_{50}^{ref}$ . The remaining parameters for the recalibration are presented in Table 5.1.

It is also noteworthy that for the HSsmall material, the upper limit ratio between the dynamic shear modulus  $G_0$  and the unloading shear modulus  $G_{ur}$  is limited by Plaxis 3D to  $G_0 / G_{ur}$  to 20 without a physical justification. Note that  $G_{ur}$  is related to  $E_{ur}$ , as seen in Eq. 5-8.

$$G_{ur} = \frac{E_{ur}}{2 \cdot (1 + \nu)} \quad (5-8)$$

The selected exponent  $m = 0.8$  that corresponds to the recalibration, provides a smaller ratio  $G_0 / G_{ur}$ , especially near the soil surfaces, thus leading to numerical stability.

### 5.3 Undrained Analysis

For an undrained analysis of the pile-soil system behaviour, isotropic soil conditions are assumed, in which the soil is fully saturated (consequently, the assumption to  $\phi_u = 0$  is valid, as stated by Wehnert 2006), besides that “no-flow” condition in the pore water is likewise accepted.

The FE-calculation is generally conducted by using the total stress  $\sigma$ . In this respect, the relationship between the total stress  $\sigma$ , the effective stress  $\sigma'$  and the pore water pressure  $p_w$  is expressed by using the basic concept of soil mechanics proposed by Terzaghi (1925).

$$\sigma = \sigma' + p_w \quad (5-9)$$

An additional distinction is made between the steady state pore stress  $p_{\text{steady}}$ , and the excess pore stress  $p_{\text{exc}}$  to describe the pore water pressure  $p_w$ . The programme Plaxis 3D offers two variants or alternatives for calculating the built-up of excess pore water pressures  $p_{\text{exc}}$  during the plastic calculations and the consolidation process analysis.

Fig. 5-3 shows a qualitative overview of the total and effective stress paths (i.e. the deviatoric stress  $q$  versus the mean stress  $p$ ) generated from the respective undrained analysis, currently implemented in the Plaxis 3D programme. The undrained soil behaviour can be defined using three different analyses, detailed below.

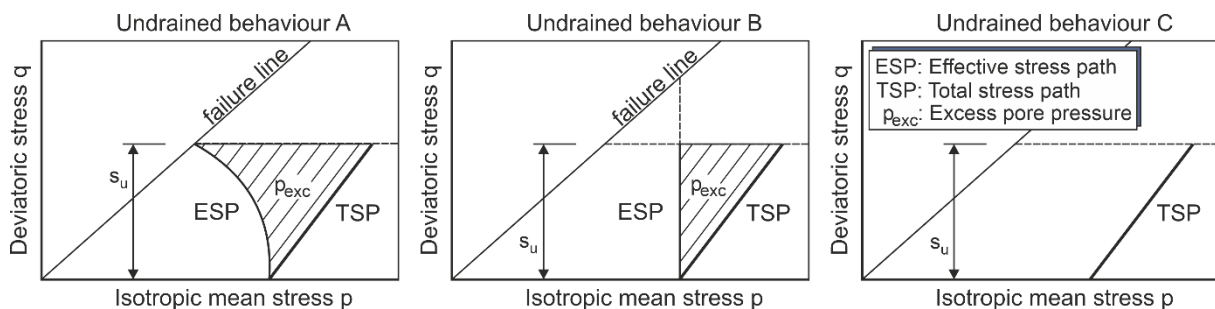


Fig. 5-3: Stress paths depending on the respective undrained analysis with HSsmall constitutive model

#### Undrained behaviour A

The undrained analysis A comes from using the effective strength parameters ( $\phi'$ ,  $s'$  and  $\psi$ ) as well as the effective stiffness parameters ( $E'$  and  $\nu'$ ). By applying the undrained analysis A, the undrained shear strength  $s_u$ , contrary to the other undrained analysis represents a result that mainly depends on the selected constitutive material law (i.e.  $s_u$  is a consequence of model, and thus not an input parameter). Fig. 5-3 (left) shows a plausible effective stress path (ESP), resulting in the failure at a realistic value of undrained shear strength  $s_u$ . This realistic prediction of excess pore pressure  $p_{\text{exc}}$  ensures that the undrained consolidation analysis can be correctly conducted. Note that the dilatancy parameter  $\psi$  other than zero may result in infinite strength of the soil (i.e. unrealistically large shear strength).

### Undrained behaviour B

The undrained analysis B is carried out in terms of the undrained shear strength ( $s_u$ ,  $\phi_u = 0^\circ$  and  $\psi = 0^\circ$ ) as well as the effective stiffness parameters ( $E'$  and  $\nu'$ ). This method also distinguishes between effective and total stresses, which would enable it to undertake a consolidation analysis, even though the ESP compared to results of triaxial tests is generally not plausible, leading to unrealistic predictions of excess pore pressure  $p_{exc}$  as seen in Fig. 5-3 (centre). Despite this, the application of the undrained analysis B can be considered appropriate for short-term undrained loading conditions since it merely requires the total stresses for its treatment, as is the case for offshore pile foundations loaded laterally in cohesive soils due to its permanent non-drained condition. Note that the features of the HSsmall constitutive model are strongly degenerated (i.e. neither cap nor stress dependency, as described in Brinkgreve et al. 2013).

### Undrained behaviour C

The undrained analysis C is based on the conventional total stresses with the undrained shear strength parameters ( $s_u$ ,  $\phi_u = 0^\circ$  and  $\psi = 0^\circ$ ) as well as undrained stiffness parameters ( $E_u$  and  $\nu_u = 0.495$ ). There is no distinction between effective stresses and excess pore pressures  $p_{exc}$  due to the exclusive application of total stresses. Fig. 5-3 (right) illustrates the total stress path (TSP) resulting from the present undrained analysis. The acceptance of this undrained analysis is mainly due to the possibility of using undrained shear strength parameters that can be measured directly in situ (e.g.  $s_u$  is treated as input parameter). The main disadvantage is that its application for consolidation analysis is not possible due to the lack of the prediction of the distribution of excess pore pressures  $p_{exc}$ . Note that this type of analysis is not available in the advanced constitutive model as HSsmall.

The numerical models proposed in this thesis for studying the lateral load-bearing behaviour of the pile-soil system are carried out by using the undrained analysis B. As stated above, this variant considers an effective stress analysis using undrained shear parameters. Here the increments of the excess pore water pressure  $\Delta p_{exc}$  are determined, based on the application of the bulk modulus of pore water  $K_w$ , the porosity  $n$ , and the increment of volume expansion  $\Delta \epsilon_v$ .

$$\Delta p_{exc} = \frac{K_w}{n} \cdot \Delta \epsilon_v \quad (5-10)$$

The bulk modulus of the pore fluid  $K_{w,ref} / n$  referred to a certain depth can be derived from the difference of the undrained bulk modulus  $K_u$  and the (effective) bulk modulus of the soil skeleton  $K'$ .

$$\frac{K_{w,ref}}{n} = K_u - K' \quad (5-11)$$

A fully incompressible behaviour of the soil can be induced, when the undrained Poisson's ratio is set at  $\nu_u = 0.5$ , but this results in the non-convergence of the finite element model due to the singularity of the global stiffness matrix (i.e. the determinant of the matrix becomes zero).



Consequently, the standard setting of the Plaxis 3D programme is applied, i.e.  $v_u = 0.495$ , for calculating the undrained bulk modulus  $K_u$ .

$$K_u = \frac{2 \cdot G \cdot (1 + v_u)}{3 \cdot (1 - 2 \cdot v_u)} \quad (5-12)$$

The shear modulus  $G$  and the bulk modulus of the soil skeleton  $K'$  results as a function of the un- and reloading stiffness  $E_{ur}$  and (effective) Poisson's ratio  $v'$ , as seen below.

$$G = \frac{E_{ur}}{2 \cdot (1 + v')} \quad (5-13)$$

$$K' = \frac{E_{ur}}{3 \cdot (1 - 2 \cdot v')} \quad (5-14)$$

The pore pressure parameter  $B$  according to Skempton (1954) can be determined from the relation of the increments existing between the excess pore water pressure  $\Delta p_{exc}$  and the total stress  $\Delta p$ , as seen in Eq. 5-15. Skempton's  $B$ -parameter used to define the partially water-saturated soils always assumes values within a range from 0 to 1, and described a fully unsaturated and saturated soil, respectively.

$$B = \frac{\Delta p_{excess}}{\Delta p} = \frac{1}{1 + \frac{n \cdot K'}{K_w}} \quad (5-15)$$

Note that Skempton's  $B$ -parameter indirectly depends on an undrained Poisson's ratio  $v_u$  defined in Eq. 5-12. For the proposed numerical model in this thesis, the standard value proposed by Plaxis 3D concerning the undrained Poisson's ratio  $v_u = 0.495$  is essentially applied, which is considered as the reference parameter, resulting in an almost fully water-saturated soil (i.e. Skempton's  $B$ -parameter becomes almost one).

## 5.4 Back-calculation of field tests

Pile load tests with very large diameters are not financially feasible and also unusual. The author is not aware of the existence of large diameter piles entirely embedded in cohesive soil. Therefore, the validation of the proposed numerical model has to be carried out on field test results from small pile dimensions. The larger pile diameters can then be examined by FEM procedures to obtain a clear overview of the mechanical behaviour of the soil under such conditions. It has to be stressed that this merely refers to a computational extrapolation, though.

For a conclusive validation of the numerical model, a total of five field tests are considered such, as the pile load tests originally used for the calibration of the  $p$ - $y$  approaches proposed by Matlock 1970 ( $D = 0.32$  m), Kim et al. 2009 ( $D = 1.02$  m;  $D = 2.40$  m), and Reese et al. 1975 ( $D = 0.610$  m). Evidently, the validation is supported by a set of the database on a comparatively wide range of pile dimensions. In addition, various soil consistencies are also included that range from soft to medium soft clay. The stiff clay is also considered by using the "Manor" field test to calibrate the proposed numerical model. The introduced numerical model is

therefore considered as suitable for the extrapolation of soil conditions, as well as pile dimensions, notably including the diameter effect.

**Table 5-1: Soil parameters used for back-analysis of the field tests**

Parameter	$\gamma'$	$s_u$	$E_{oed}^{ref}$	$e$	OCR	$k$	PI	$\gamma_{0.7}$	$\epsilon_{50}$	J	$K_s$
Units	kN/m <sup>3</sup>	kPa	kPa	-	1	-	%	-	-	-	kN/m <sup>3</sup>
<b>Lake Austin</b>	10.0	38.3	650	1.45	4.0	0.3	41	$2.0 \cdot 10^{-4}$	0.012	0.25	
<b>Sabine River</b>	5.5	14.4	650	1.45	1.0	0.42	68	$4.0 \cdot 10^{-4}$	0.020	0.50	
<b>Manor</b>											
0.0 – 0.9	8.1	25-70	4200-4400	1.1-1.05	10	0.4	60	$3.0 \cdot 10^{-4}$	0.007		135000
0.9 – 1.52	9.4	70-163	4400-4800	1.05-1.0	10	0.4	60	$3.0 \cdot 10^{-4}$	0.007		270000
1.52 – 4.11	10.3	163-333	4800-12000	1.0-0.55	10	0.4	60	$3.0 \cdot 10^{-4}$	0.005		540000
4.11 – 6.55	10.3	333	12000	0.55	10	0.4	60	$3.0 \cdot 10^{-4}$	0.004		540000
6.55 – 9.14	10.8	333-1100	12000-30000	0.55-0.5	10	0.4	60	$3.0 \cdot 10^{-4}$	0.004		540000
9.14 – 20.0	10.8	1100	30000	0.5	10	0.4	60	$3.0 \cdot 10^{-4}$	0.004		540000
<b>Incheon Bridge</b>											
Upper clay	7.5	15-30	600	1.5	1.5	0.3	25-30	$2.5 \cdot 10^{-4}$	0.02	0.5	
Lower clay	7.5	30-50	700	1.4	1.5	0.3	30-35	$2.5 \cdot 10^{-4}$	0.01	0.5	
Silty clay	7.8	70	900	1.3	1.5	0.3	35-40	$2.5 \cdot 10^{-4}$	0.005	0.25	

\* The parameters  $\lambda_{Eoed} = 0.8$ ,  $\lambda_{G0} = 0.5$ ,  $\nu = 0.45$  and  $\nu_{ur} = 0.495$  are valid for all field tests

The clay parameters used for the numerical simulations to reproduce the field tests are listed in detail in Table 5-1. The parameters of the “Lake Austin” and “Sabine River” field tests were derived from Matlock’s report. Likewise, the papers presented by Reese et al. (1975) used for the derivation of the p-y curves in stiff clay provide the required information of the “Manor” field test. Finally, Kim et al. (2009) report the soil parameters used for the “Incheon Bridge” field test with relatively large pile diameters. Subsequently, the pile load tests taken into account by the author will be extensively presented in the following. For further details, refer to the original documentation.

#### 5.4.1 Lake Austin field test

Matlock (1970) reported a field test conducted near “Lake Austin” (USA). The driven steel pipe pile used ( $L = 12.8$  m;  $D = 0.32$  m;  $t = 12.7$  mm) was embedded in soft clay and laterally loaded with an eccentricity  $h = 0.064$  m. Free water was existent above the soil surface during the pile load tests. The soil conditions were classified as inorganic clay of high plasticity, i.e. CH according to the unified soil classification. The slightly over-consolidated clay was described

having an undrained shear strength (reported average  $s_u = 38.3 \text{ kN/m}^2$ ) being fairly constant over the depths. The soil parameters indicated in the original reports (such as soil weight  $\gamma'$ , undrained shear strength  $s_u$ ) but also the available information on the basis of experience, were used to derive parameters required for the numerical simulations. As such, the reference values of the oedometric stiffness and the respective stress exponent were applied according to the recommendations of the EAU (2012). The soil parameters selected are summarised in Table 5-1.

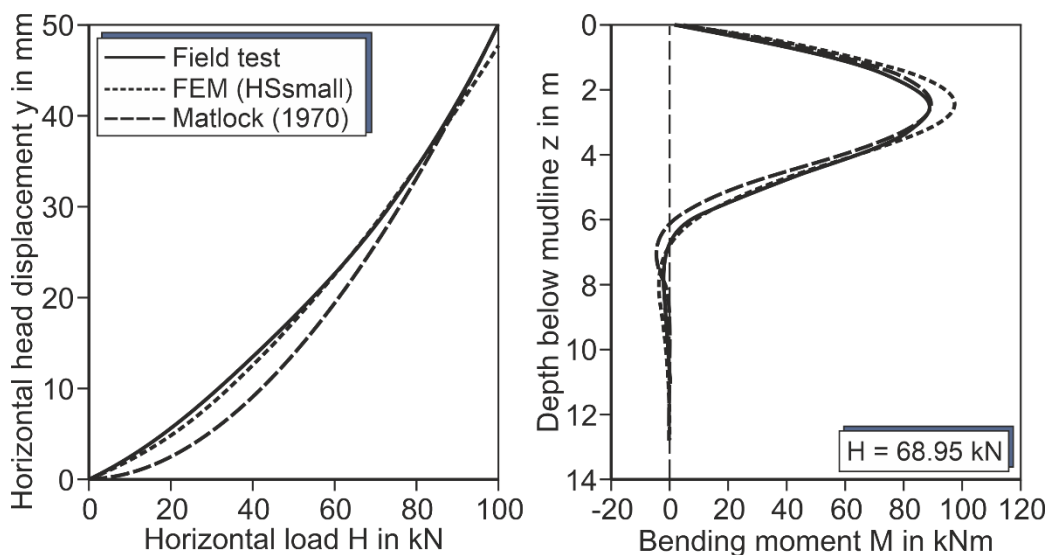


**Fig. 5-4: Comparison of the depth-lateral deflection (left) and bending moment (right) for the “Lake Austin” field test**

The results of the field test and the FE simulation, as well as the approach by Matlock, are represented in Fig. 5-4 in terms of the load-displacement curves and the distribution of bending moment along the pile length obtained from electrical-resistance strain gauges for a lateral load  $H = 68.95 \text{ kN}$ . A poor agreement can be appreciated based on these results as the p-y approach by Matlock deviates significantly from the experimental values, especially for small and middle displacements. Even though Matlock includes the “Lake Austin” field test in the report of the p-y approach for soft clay, large differences are evident for the initial part of the load-displacement curve. The large initial stiffness of the approach is probably associated with the infinite initial stiffness of the p-y curves proposed by Matlock. In contrast, good agreement is reached by numerical back-calculation, despite the fact that at the specified load level a slight overestimation of the bending moment in the upper part of the pile is recognised.

#### 5.4.2 Sabine field test

A second field test was conducted near “Sabine River” (USA) with the same test pile that had already been used in “Lake Austin”. The clay with very soft consistency was also described as predominantly homogeneous with an almost constant undrained shear strength (reported average:  $s_u = 14.4 \text{ kN/m}^2$ ). The soil parameters, which are the basis of the numerical investigations, can be identified in Table 5-1. The results of the field test and the corresponding numerical calculation for the validation are depicted in Fig. 5-5. There is again a good

agreement between the experimental and the FE simulation results, which conclusively confirms the suitability of the numerical model proposed.

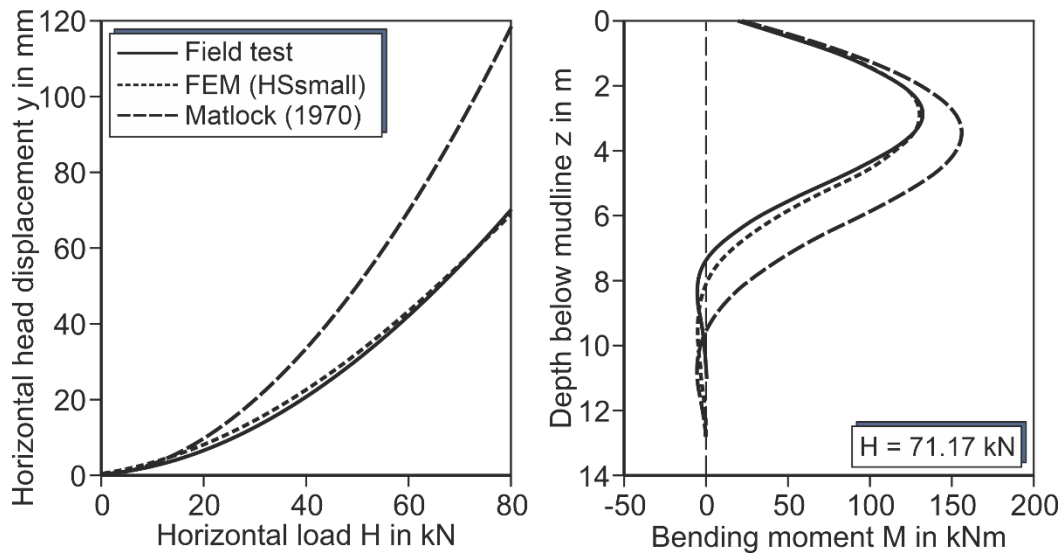


**Fig. 5-5: Comparison of the depth-lateral deflection (left) and bending moment (right) for the “Sabine River” field test**

A relatively strong deviation can also be observed between the experimental results and Matlock’s approach for large displacements, whereby a considerable underestimation of the measured resistances is evident in this instance. Likewise, the underprediction of the pile stiffness results in a strong overestimation of the distribution of the bending moment. For such reasons, the general applicability of Matlock’s approach to arbitrary soil conditions appears to be at least questionable. It should also be noted that Matlock took the “Sabine River” field test as the main basis to develop the  $p$ - $y$  curve formulation for soft clay.

### 5.4.3 Incheon Bridge field test (driven steel pile)

Kim et al. (2009) introduced the result of two field tests conducted before the construction of the “Incheon Bridge” (South Korea). The driven steel pile had an embedded length  $L = 26.6$  m, a diameter  $D = 1.02$  m and wall thickness  $t = 16$  mm (see Fig. 5-6). The test pile was laterally loaded with an eccentricity  $h = 0.5$  m. At the relevant depths, the soil profile consists of low plasticity silts (ML) and slightly over consolidated clays (CL). The soil parameters used for the simulation are summarised in Table 5-1.

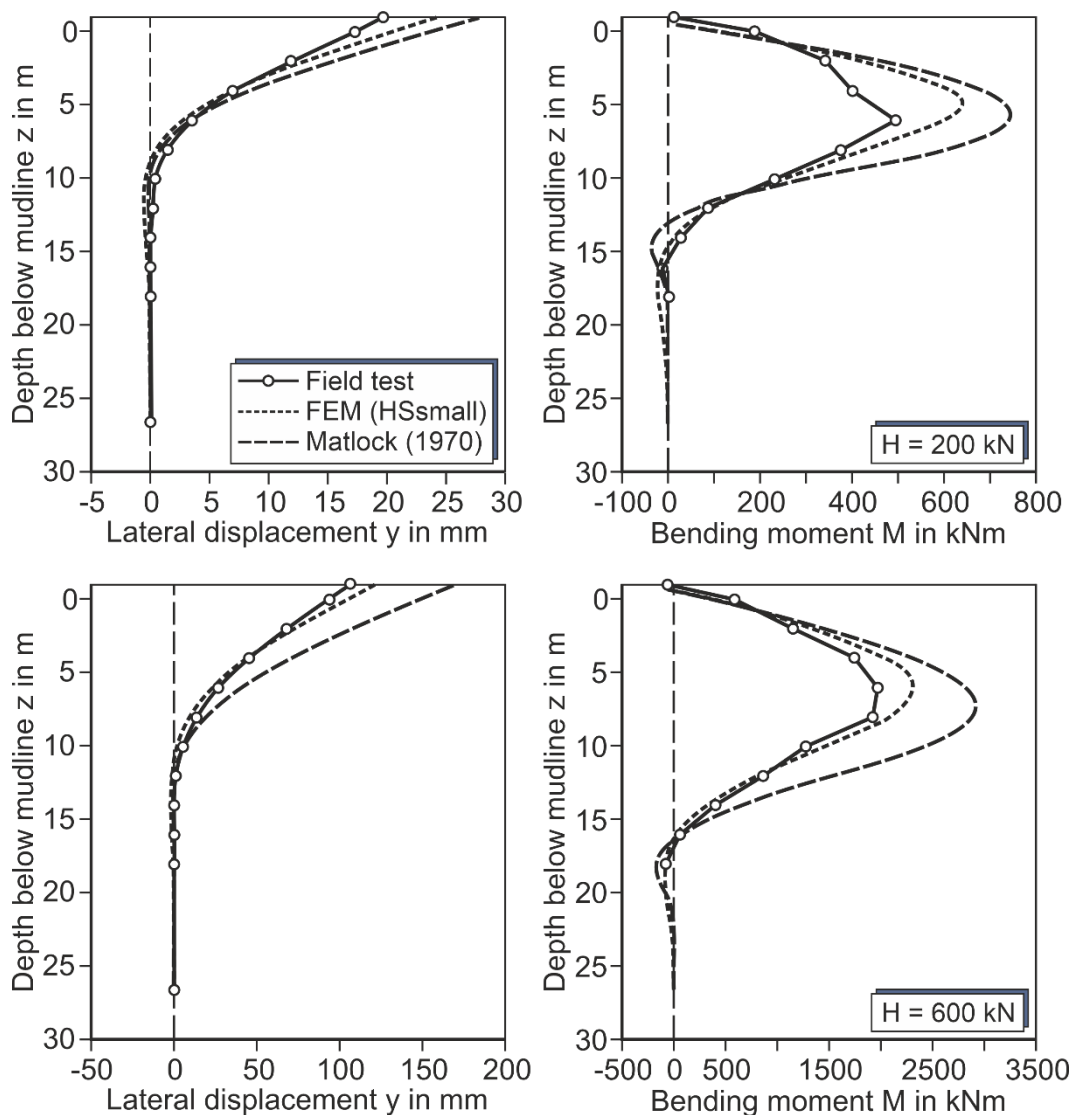


**Fig. 5-6: Comparison of the depth-lateral deflection (left) and bending moment (right) in the “Incheon Bridge” field test (driven steel pile)**

As results of the “Incheon Bridge” field test, the deflection along the pile and the corresponding distribution of the bending moment are given for two load levels (e.g. 200 kN and 600 kN). The pile deflections and in particular the distribution of bending moments are found to be overestimated by Matlock’s approach. The numerical results agree satisfactorily with the results of the field test, despite the maximum bending moments is slightly overestimated.

#### 5.4.4 Incheon Bridge field test (drilled shaft)

In the same study, Kim et al. (2009) introduce results of field test on drilled pile with embedded length  $L = 45$  m and diameter  $D = 2.4$  m installed close to the driven steel pile (identical soil parameters, Table 5-1). The elastic modulus of the reinforced concrete pile is specified to  $E = 36400$  MPa. The lateral load  $H$  was applied directly in height of free soil surface  $h = 1$  m. Note that the rough surface of the bored pile is accounted for in the contact surface (0.8 times the shear strength of the soil).

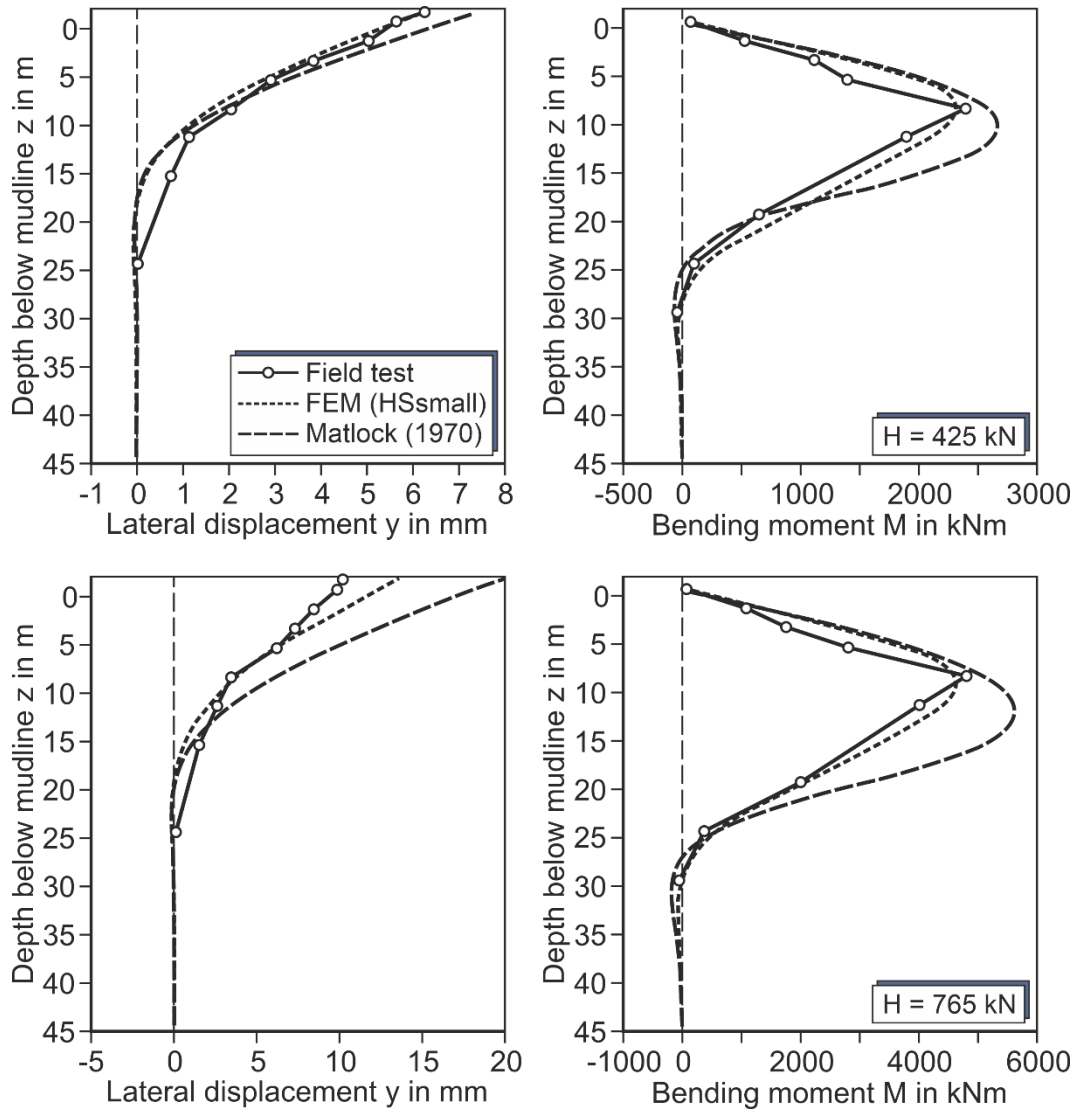


**Fig. 5-7: Comparison of the depth-lateral deflection (left) and bending moment (right) for the “Incheon Bridge” field test (drilled shaft)**

The results of the “Incheon Bridge” field test are depicted in Fig. 5-7 in terms of the deflection lines and the distribution of bending moments along the pile length. Once again, the p-y approach proposed by Matlock overestimates the pile deflection, particularly for large loads. This underestimation of the bedding resistance likewise results in an overestimation of the distribution of the pile’s bending moment. On the contrary, the numerical model again reasonably describes the field test results for both load levels considered.

#### 5.4.5 Manor field test

Reese et al. (1975) reported the results from pile load tests conducted at a site near “Manor” (USA) that is taken as the essential basis in the derivation of the p-y curve formulation for stiff clay. The pile with diameter  $D = 0.610$  m, which had been already used in the test of laterally loaded piles in sand for the “Mustang Island” field test, was once again driven into fissured inorganic stiff clay, strongly over-consolidated. The total length of the embedded pile length was  $L = 15.2$  m long with a wall thickness  $t = 9.525$  mm, reinforced by the addition of

15.875 mm thick wrappers to the upper part of the pile, i.e.  $L = 7.01$  m. The water table was above the soil surface during the whole pile load test. Short-term static load with an eccentricity  $h = 0.305$  m was applied, among others. For the measuring of the distribution of the bending moment, electrical-resistance strain gauges were applied only to the upper part  $L = 9.75$  m. The soil parameters used in this field test are briefly listed in Table 5-1.

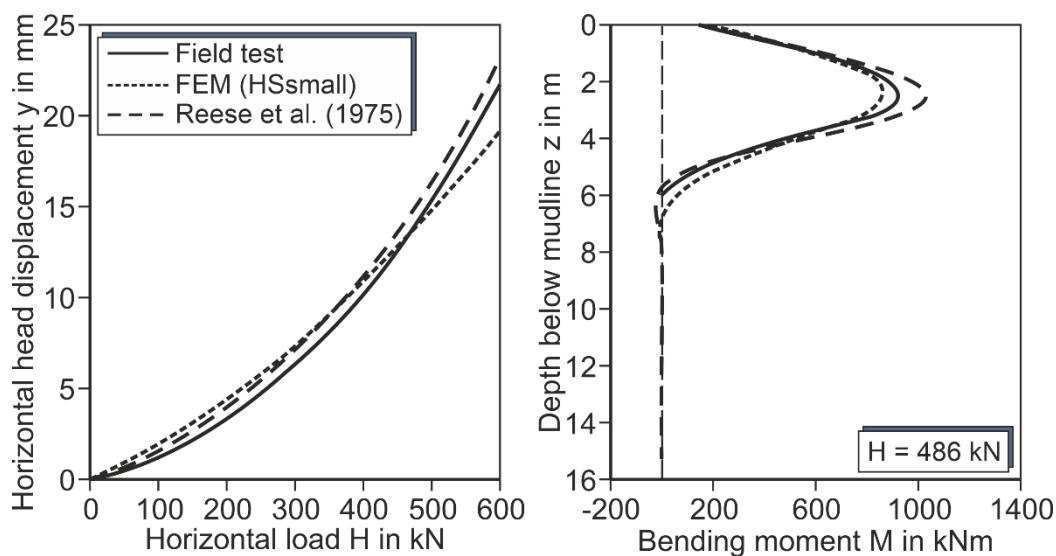


**Fig. 5-8: Comparison of the load-deflection (left) and bending moment (right) for the “Manor” field test**

Fig. 5-8 (left) depicts the results of the load-displacement curve, whereby the bedding resistance is moderately underestimated by Reese et al. (1975), resulting in larger displacements for all load levels. The numerical results of the three-dimensional simulations indicate a slight underestimation of the foundation stiffness in the initial part of the load-displacement curve, but there is an overestimation for large load levels. Fig. 5-8 (right) shows the distribution of the bending moments along the pile length for a lateral load  $H = 486$  kN. Here it becomes evident that the result of the numerical simulation is more suitable for the experimental values of the field test than those yielded by the analytical method according to Reese et al.





## 6 Evaluation of existing p-y approaches

### 6.1 General

The validity of the p-y approaches commonly used for the design of laterally loaded piles embedded in soft clay is analysed by comparing them with the results obtained from FE simulations. Even though the results of FE simulations cannot necessarily be taken into account as “correct” due to the model idealisations and particularly its extrapolation character, field tests with large diameter piles are unavailable for an explicit validation. The proposed numerical model (cf. section 5) is taken as basis and as the best possible option for evaluating the p-y approaches introduced.

A similar study can be found in Terceros et al. (2019), where “medium soft clay” is regarded as reference soil parameter. Besides, the calibration of the numerical model was carried out regardless of the “Manor” field test for stiff clays, but the results obtained confirm the trends of the present study.

### 6.2 Results for a reference system

The reference parameters of soil used for the subsequent comparative study are summarised in Table 6-1. Three types of clays with diverse consistencies are taken into account to evaluate the load-bearing behaviour of the pile under lateral loading conditions. The soil parameters selected for the FEM study are based on the experience of typical properties of clay.

**Table 6-1: Clay parameters used for reference systems and parametric study**

Parameter	$\gamma'$	$s_u$	$E_{oed}^{ref}$	$e$	OCR	$k$	PI	$\gamma_{0.7}$	$\epsilon_{50}$	J
Units	kN/m <sup>3</sup>	kPa	kPa	-	1	-	%	-	-	-
Very soft clay	6.5	20	600	1.5	1.0	0.35	50	$3.0 \cdot 10^{-4}$	0.02	0.5
Soft clay	7.5	50	800	1.4	1.0	0.35	50	$3.0 \cdot 10^{-4}$	0.01	0.357
Medium soft clay	8.5	90	1000	1.3	1.0	0.35	50	$3.0 \cdot 10^{-4}$	0.0075	0.25

\* The parameters  $\lambda_{Eoed} = 0.8$ ,  $\lambda_{G0} = 0.5$ ,  $\nu = 0.45$  and  $\nu_{ur} = 0.495$  are valid for all reference parameters

Initially, the results for a reference system are presented and discussed separately. The reference system considered is a typical monopile foundation ( $D = 6$  m,  $L = 36$  m,  $t = 36.35$  mm) which is laterally loaded with a load eccentricity  $h = 30$  m above the embedded point at the free soil surface. A relatively small wall thickness  $t$  is selected to achieve a similar load-bearing behaviour as the full-size monopiles, in most cases embedded in strongly load-bearing layers at certain depths. The soil type used for the reference system corresponds to “soft clay” at this instance, whose parameters are listed in Table 6-1.

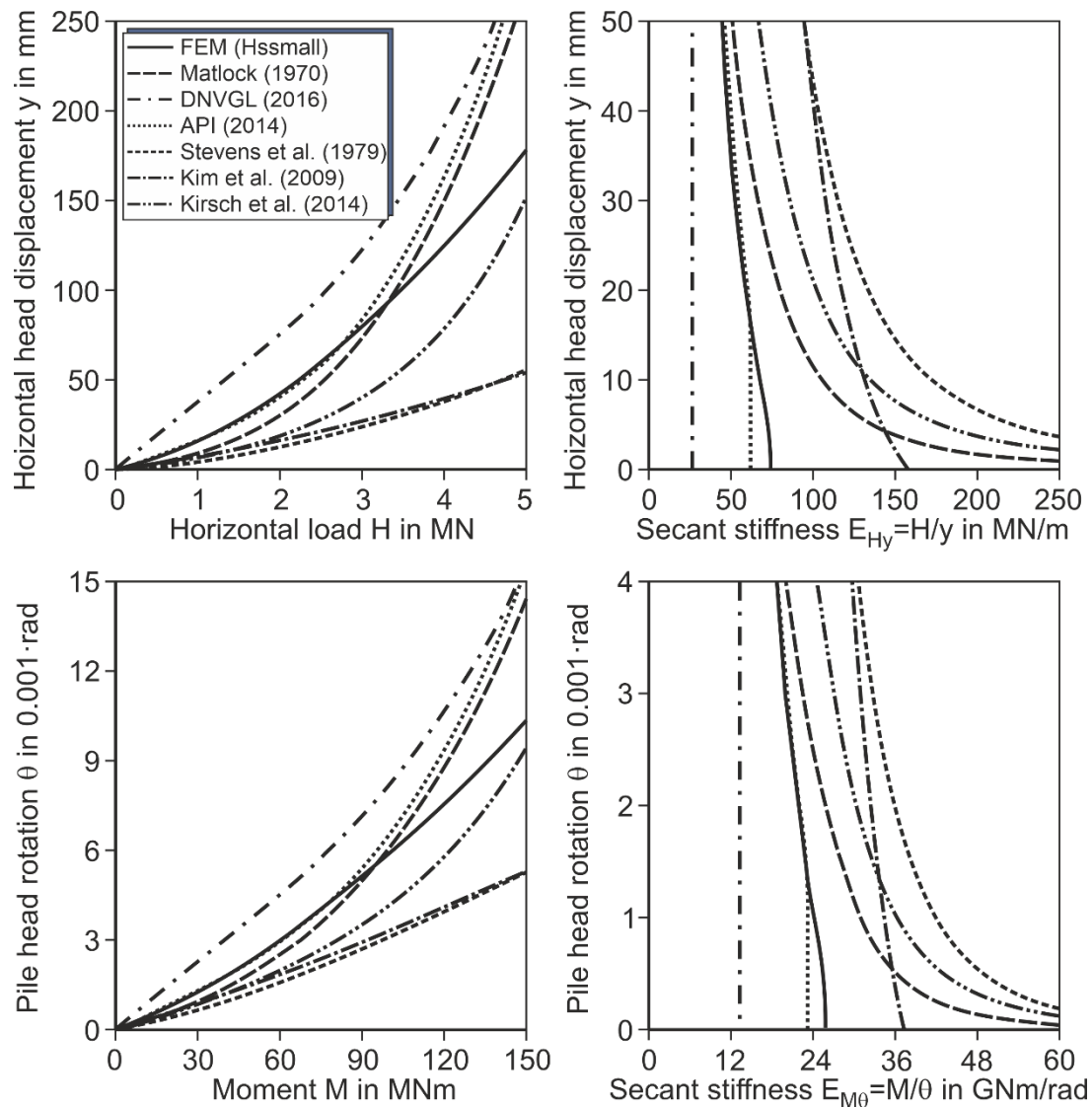


**Fig. 6-1: Load-displacement curves (top) and moment-rotation curves (bottom) for the reference system**

The load-displacement curves and their corresponding moment-rotation curves by comparing the FEM results to the six p-y approaches examined are shown in Fig. 6-1 (i.e. loads and deformations at the free soil surface). Additionally, the secant stiffness-deformation curves against the pile deformations are represented (cf. Fig. 6-1, right) to highlight the horizontal load-bearing behaviour for small loading conditions, demonstrating that the initial part of the examined p-y curves is quite diverse for the design of a monopile foundation (related to SLS, FLS). The current presentation enables an evaluation of diverse ranges of horizontal displacements and rotations. Note that the FEM results are identified with solid lines to distinguish them from the proposed p-y approaches, while the results of Matlock's approach represented by dashed lines are particularly relevant.

It can be stated that the comparison of load-displacement curves with the moment-rotation curves leads to approximately identical conclusions. Therefore, the results of the load-displacement dependencies are exclusively discussed in the following. Matlock's approach results in a significantly larger foundation stiffness than that of the FEM simulation for small load levels, but the deviations compared to the FEM results decrease with increasing loads. In

the initial part of the curves, the linearisations according to API (2014) and DNVGL (2016) coincide considerably better with the FEM results than the other p-y approaches, whereby both p-y approaches lead to a smaller foundation stiffness than the FEM results. DNVGL (2016) yields the smallest resistance, causing large deviations from the FEM results. By increasing the bedding stiffness according to Kim et al. and Kirsch et al., greater deviations can be observed than with Matlock's approach. Stevens & Audibert's approach yields the largest foundation stiffness at least in the specific load level considered. This latter p-y approach even considers an infinite initial stiffness, as proposed by Matlock's original approach.

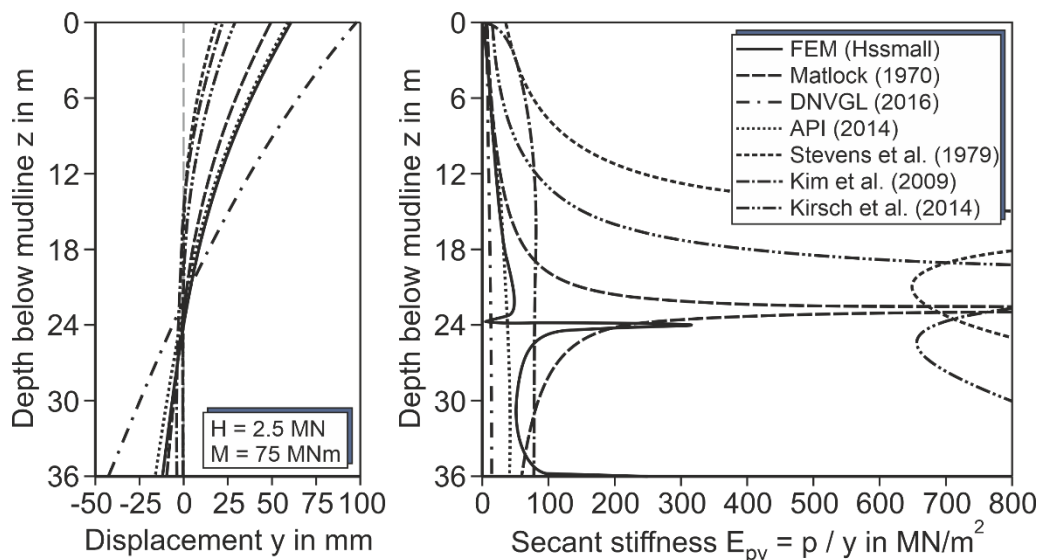


**Fig. 6-2: Pile deflection lines (left) and secant bedding stiffness (right) of the reference system**

Similarly to the foundation stiffness referred to, the loads and deformations at the pile head can also be contrasted by using the secant bedding stiffness  $E_{py} = p / y$  along the pile shaft and the pile deflection line for a specific load level, as can be seen in Fig. 6-2. The secant bedding stiffness resulting from the respective p-y approach is compared to the numerically achieved result for one horizontal head displacement. The large discrepancies in the predicted displacements resulting in a bandwidth of displacement courses for semi-flexible (Stevens & Audibert, Kim et al., and Kirsch et al.) to almost rigid (DNVGL 2016) pile-soil systems are evident here when it comes to the pile deflection lines. Anyhow, the most significant agreement regarding the prognosis of pile deformations is obtained from API (2014) approach for the reference system in the specific load level. However, none of the investigated analytical p-y approaches result in a good agreement on the distribution of the secant stiffness  $E_{py}$  across the embedded pile with the results of the FEM calculations used here for the comparison study. The predictions of the zero-deflection point  $z_0$ , which can be derived from the peak in the secant stiffness, also do not match with the FE results. Additionally, none of the existing p-y approaches are able to account for the larger resistance near to the pile toe (also termed as pile toe shearing) which strongly contributes to the resistance of the pile-soil system, particularly for large diameter piles.

### 6.3 Parametric study with undrained shear strength $s_u$ constant over depth

In order to obtain a basic knowledge of the applicability of the examined p-y approaches under diverse boundary conditions, a comprehensive parameter study is carried out by modifying the pile dimensions and soil properties, as well as the application of diverse load levels acting on the pile head. In the following section, a constant undrained shear strength  $s_u$  over the depth is assumed to evaluate the horizontal load-bearing behaviour of the pile, while the stiffness parameters are considered depth-dependent to properly capture the non-linear behaviour of the soil (cf. section 5.2).

#### 6.3.1 Variation of pile dimensions

Large bandwidth of pile dimensions is investigated using FE simulations considering the variation of pile diameters ( $D = 0.5 - 8$  m), as well as the pile lengths related to the pile diameters ( $L/D = 4 - 12$ ). The bandwidth covers a large part of the laterally loaded piles currently erected in the wind farm projects. The numerical models are extrapolated to around 400 pile-soil systems for each type of soil parameters considered. The load eccentricity  $h$  and the wall thicknesses  $t$  of the piles are normalised with the pile diameter  $D$  to enable a meaningful presentation of the pile dimension effect on the discrepancies between the results of the examined p-y approaches and the FE simulations. Hence, the load eccentricity is adjusted to 5 times the pile diameter  $D$ , as well as the wall thickness  $t$  that is defined by Eq. 6-1 in form of a pile driving criterion introduced by API (2014). However, a reduced factor of 0.005 instead of 0.0125 is applied by this equation, mainly to consider the low bedding resistance of soft clay.

$$t \text{ [mm]} = 0.005 \cdot D \text{ [mm]} + 6.35 \text{ [mm]} \quad (6-1)$$

The most representative results of the parametric study are given in terms of contour plots in Fig. 6-3 to 6-8 for the remaining findings, see Appendix C. It is noted that the black dots in the figures indicate the supporting points of the plots, where each point represents a calculation result. The plots represent the quotient of the lateral stiffnesses resulting from the examined p-y approaches and numerical simulations ( $Q_K = K_{p-y} / K_{FEM}$ ) for the corresponding normalised head displacements  $y / D$ . Therefore, values larger than one indicate that the p-y approach overestimates the numerical results whereas a value smaller than one suggests an underestimation of the foundation stiffness. For a comparative analysis of the FE simulation results, three normalised displacements are taken into account to evaluate the load-bearing behaviours of the pile subjected to lateral loading conditions. The displacements  $y = 0.0005 \cdot D$ ,  $y = 0.01 \cdot D$  and  $y = 0.03 \cdot D$  at the pile head are selected to give the best possible overview of the discrepancies in diverse load levels, as well as the respective dependencies on the pile dimensions. Due to the non-linearities of the p-y approaches, varying deviations from the results of the FEM calculations are obtained in dependence on the corresponding normalised displacements considered. Note that based on the results exposed in Fig. 6-1, it is acknowledged that particularly for small displacements, the quantitative deviations strongly depend on the lateral head displacement. However, this type of presentation enables the characterisation of the examined p-y approaches with regard to the validity for piles of arbitrary dimensions.

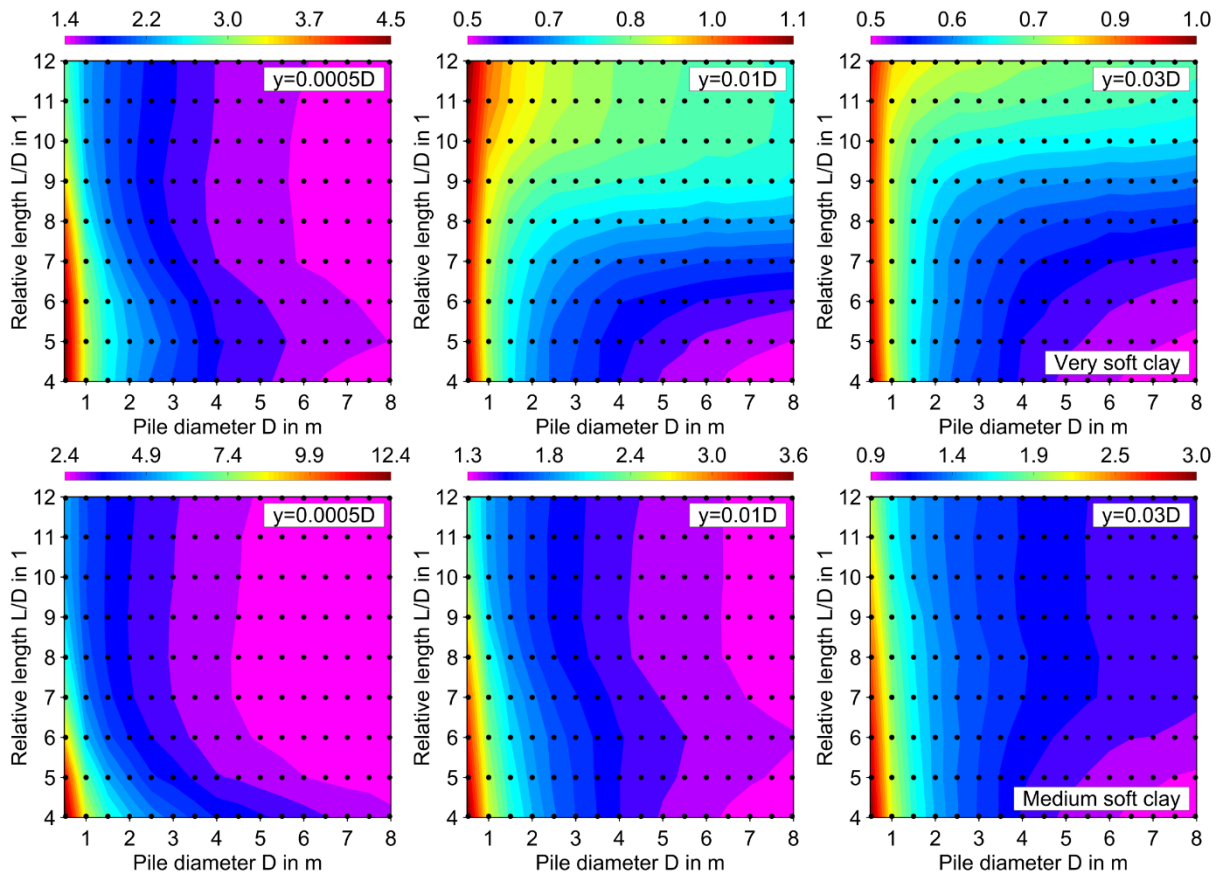


**Fig. 6-3: Quotient of lateral stiffness  $K_{p-y} / K_{FEM}$  based on the approaches by Matlock (1970) and FEM**

The results obtained from Matlock's approach in terms of quotients  $Q_K$  yield diverse deviations from the FEM results for the three normalised displacements. Relevant differences are detected for pile diameters smaller than  $D < 1.5$  m. For the smallest normalised head displacement  $y = 0.0005 \cdot D$ , a strong overestimation of foundation stiffness arises which becomes a maximal value for small pile diameters in combination with small relative length. The discrepancy becomes smaller for larger head displacements, partially obtaining a good agreement with the predicted resistance of the FE simulations for very soft clay (i.e. for a normalised head displacement  $y = 0.03 \cdot D$ ), but still an overestimation for medium soft clay, although it is considerably reduced.

The deviations from the FEM results are therefore high for small pile diameters, which is initially unexpected, considering that the method is calibrated on such small pile diameters. Nevertheless, comparison of the results of the "Lake Austin" field test with the p-y approach already exhibited an overestimation of the foundation stiffness, in particular for small loads (cf. section 5.4.1). In fact, Matlock's approach yields a better agreement with FEM results applied to large pile diameters than the typical pile diameters used for its calibrations. It is also noted that the discrepancy to the FEM results is even larger with increasing clay consistency. These obtained outcomes tend to be qualitatively produced in all approaches based on the (original) standard function proposed by Matlock.

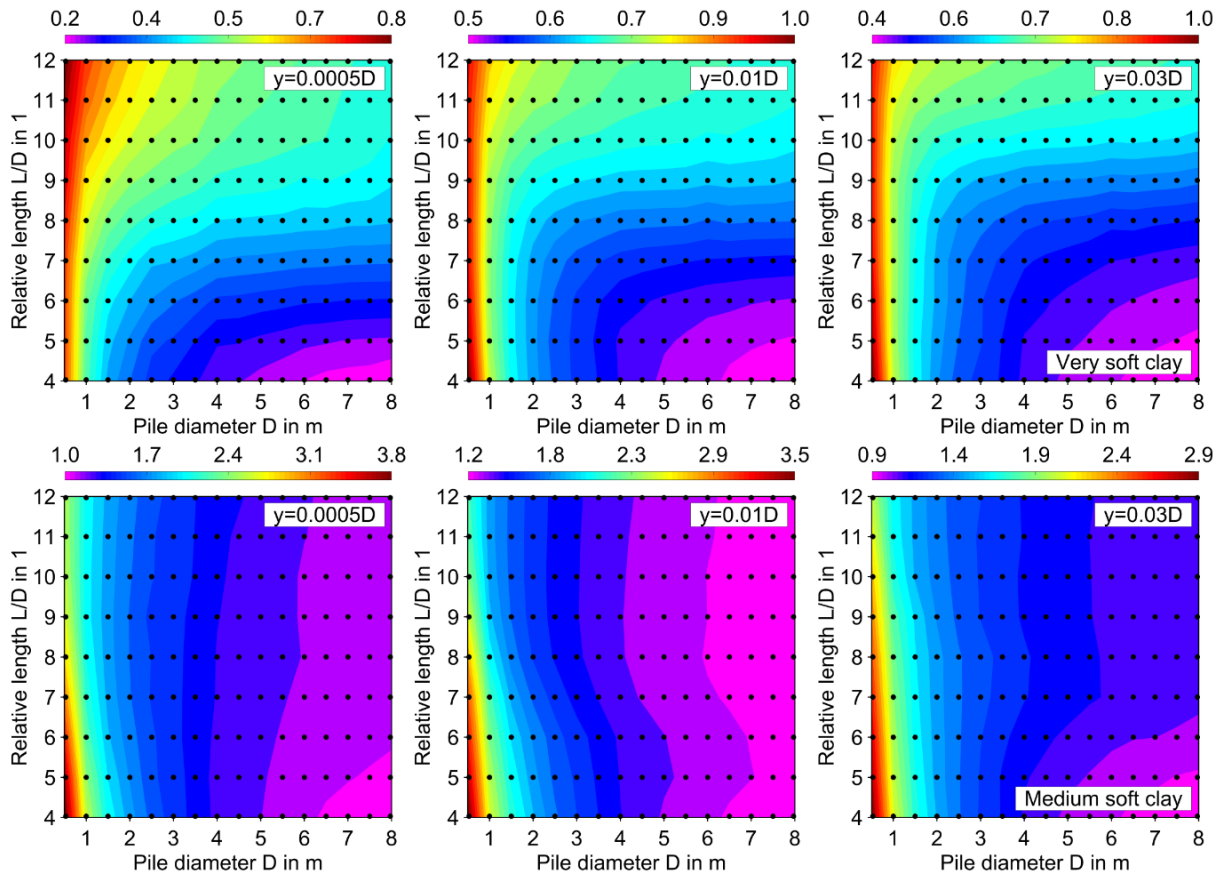


Fig. 6-4: Quotient of lateral stiffness  $K_{p-y} / K_{FEM}$  based on the approaches by API (2014) and FEM

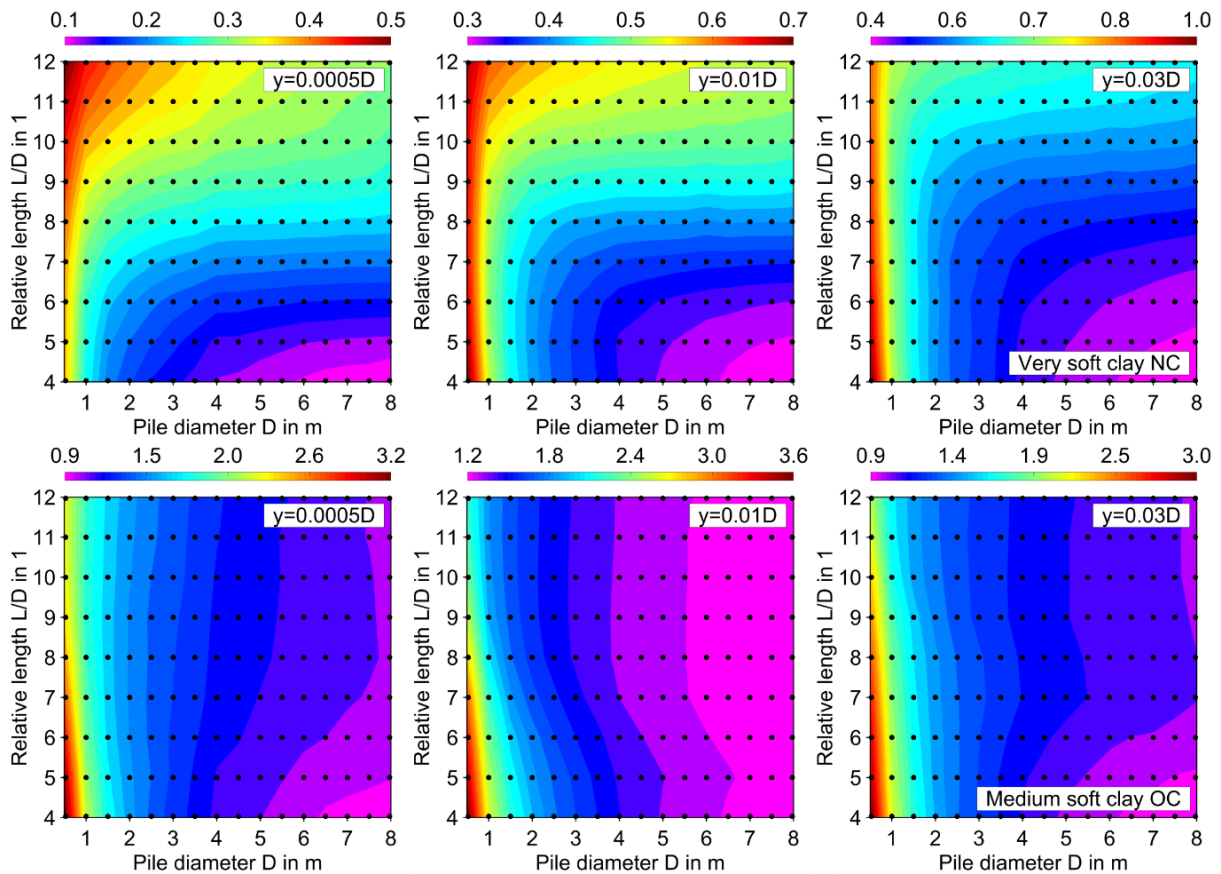


Fig. 6-5: Quotient of lateral stiffness  $K_{p-y} / K_{FEM}$  based on the approaches by DNVGL (2016) and FEM



Except for the smallest head displacement, the resulting distribution of discrepancies obtained from the approach by API (2014) are almost identical to that yielded by Matlock's approach, demonstrating that the impact of the approximation of Matlock's curve by specified discretisation points to the fact that the foundation stiffness is significantly smaller for large head displacements. Evidently, the linearisation proposed by API (2014) leads to a marked effect notably for the small displacement range, even yielding an underestimation of the foundation stiffness in very soft clay. A good agreement between the results of FEM and the approach by API (2014) can be found in small diameters for the pile installed in very soft clay, as well as for large-diameter piles embedded in medium soft clay.

The approach by DNVGL (2016) for normally consolidated clay (i.e. by using  $\xi = 10$ ) underestimates the numerical results calculated by the pile embedded in very soft clay, even more so than the results yielded by API (2014) approach, particularly for the smallest head displacement. Here, the minimum quotient  $Q_K = 0.1$  becomes very evident, which turns out to be the greatest underestimation of the foundation stiffness for all examined p-y approaches. In contrast, whether over-consolidated clay (i.e. by using  $\xi = 30$ ) is taken into account, the approach unquestionably results in higher resistances compared to that yielded for normally consolidated clay. Assuming that the calculation results from the FEM reproduce the horizontal load-bearing behaviour of the pile foundations more accurately, then the results of the approaches from the offshore guidelines and recommendations are significantly improved by applying a finite initial stiffness in contrast to Matlock's original approach.

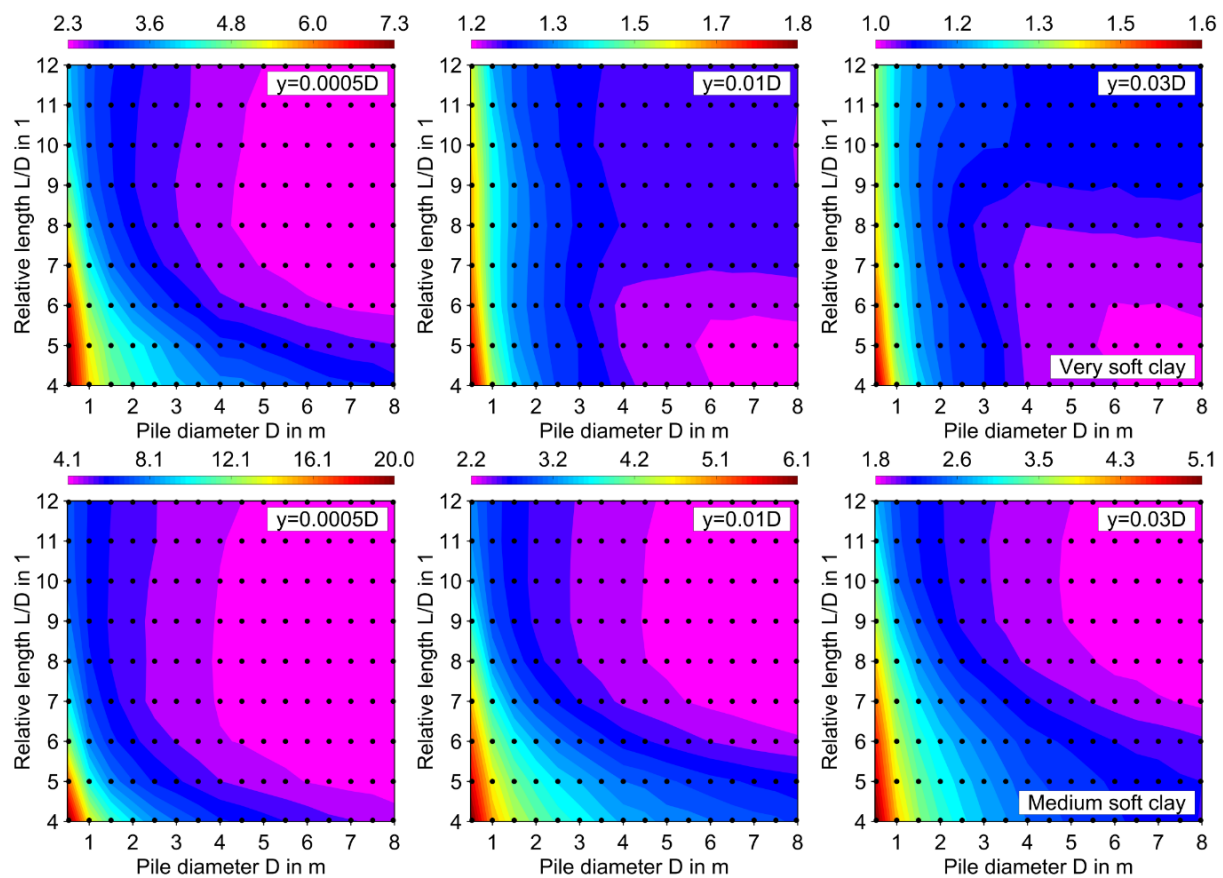


Fig. 6-6: Quotient of lateral stiffness  $K_{p-y} / K_{FEM}$  based on the approaches by Stevens et al. (1979) and FEM

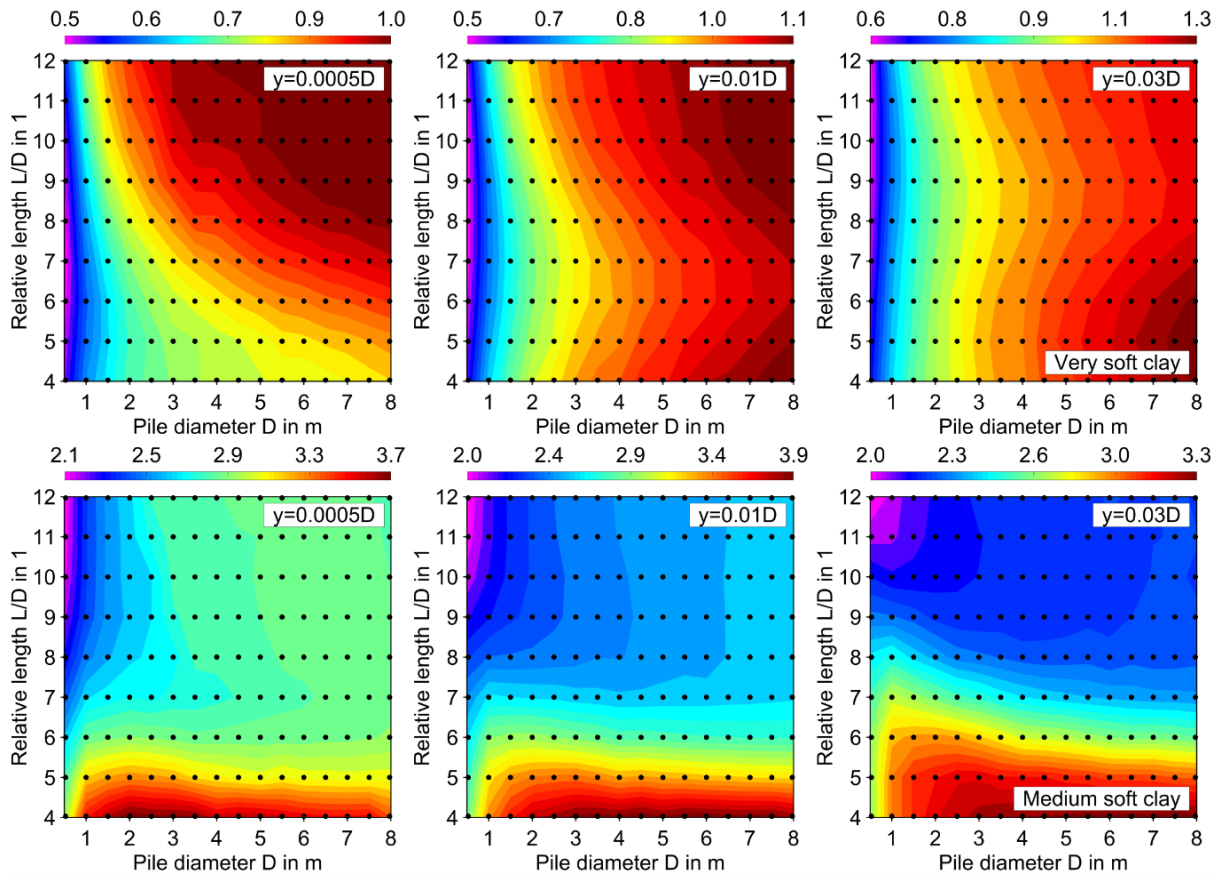


Fig. 6-7: Quotient of lateral stiffness  $K_{p-y} / K_{FEM}$  based on the approaches by Kim et al. (2009) and FEM

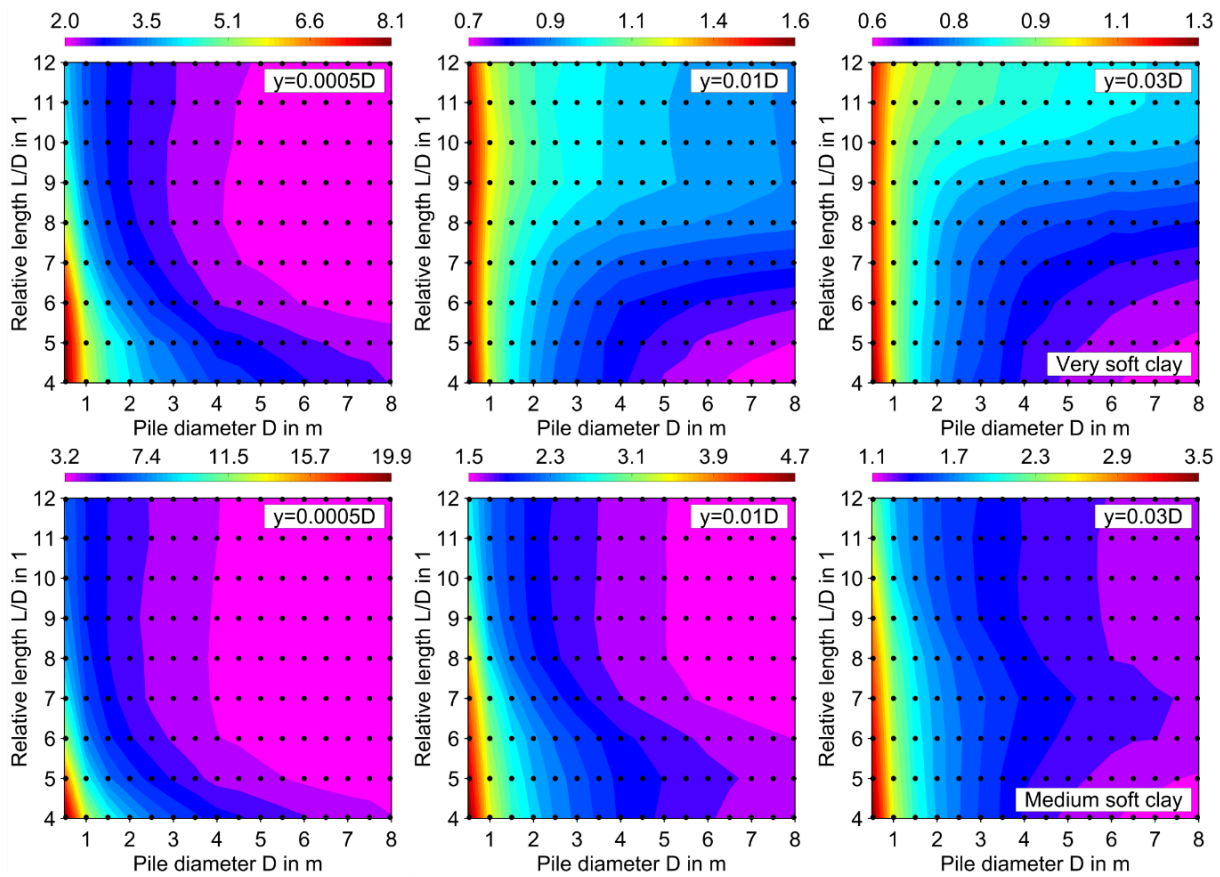


Fig. 6-8: Quotient of lateral stiffness  $K_{p-y} / K_{FEM}$  based on the approaches by Kirsch et al. (2014) and FEM



The contour plots based on the results of Stevens & Audibert's approach and FE simulations depict the same qualitative deviations obtained from Matlock's approach, which is caused by the applications of the same underlying basic p-y relationship. However, the approach results in a stiffer behaviour which causes overestimation of the foundation resistances for all pile dimensions, head displacements and clay consistencies, except for the large head displacement ( $y = 0.03 \cdot D$ ) of large-diameter piles installed in very soft clay. It becomes evident that the overestimation of foundation resistances reaches the highest quotient  $Q_K$ , i.e. 20 times the numerical results for small diameter piles combined with small pile lengths embedded in medium soft clay.

The approach by Kim et al. (2009) results in completely different dependencies with regards to the pile dimensions due to the application of a completely different basic function on the p-y curves with finite initial stiffness (cf. section 4.3.5). The predictions of the approach by Kim et al. yield considerably higher soil resistance compared to the FEM results at a relatively small pile length embedded in medium soft clay for all head displacements. The deviations to the numerical results are much more associated with the pile diameters than the relative pile length, when it comes to laterally loaded piles embedded in very soft clay, particularly for large head displacements ( $y = 0.01 \cdot D$  and  $y = 0.03 \cdot D$ ).

The modified p-y approach by Kirsch et al. (2014) results in almost the same dependencies with regards to the pile diameter, which is essentially caused by Matlock's underlying curves. However, the increased foundation stiffness, which takes place particularly for small head displacements, results in an increase of the overestimation already identified for the p-y approach by Matlock. For the smallest head displacements ( $y = 0.0005 \cdot D$ ), the underestimation of the pile head deflection is increasing, especially for relative pile lengths  $L / D$  in a range of about 5 - 6. The existence of individual cases with a good agreement is evident at certain combinations of pile head displacements and clay consistencies, but any pattern can be recognised in the contour plots. Anyhow, the Kirsch et al. approach results in larger resistances for the whole range of displacements, becoming maximal at small displacements.

### 6.3.2 Variation of load eccentricity h

To obtain a precise overview of the geometrical parameters about the effect on the foundation stiffness, the load eccentricity  $h$  is independently varied while the remaining parameters are unaffected. The results produced by the reference system (cf. section 6.2) are also highlighted by filled symbols in the present study. The secant stiffness resulting from the numerical simulations  $K_{FEM}$  is related to different p-y approaches by using the aforementioned relationship, i.e. the quotient  $Q_K = K_{p-y} / K_{FEM}$  of the secant stiffness. Similar to the previous parametric study, values equal to one mean an exact coincidence between the results of the numerical simulation and the p-y approaches in terms of foundation stiffness.

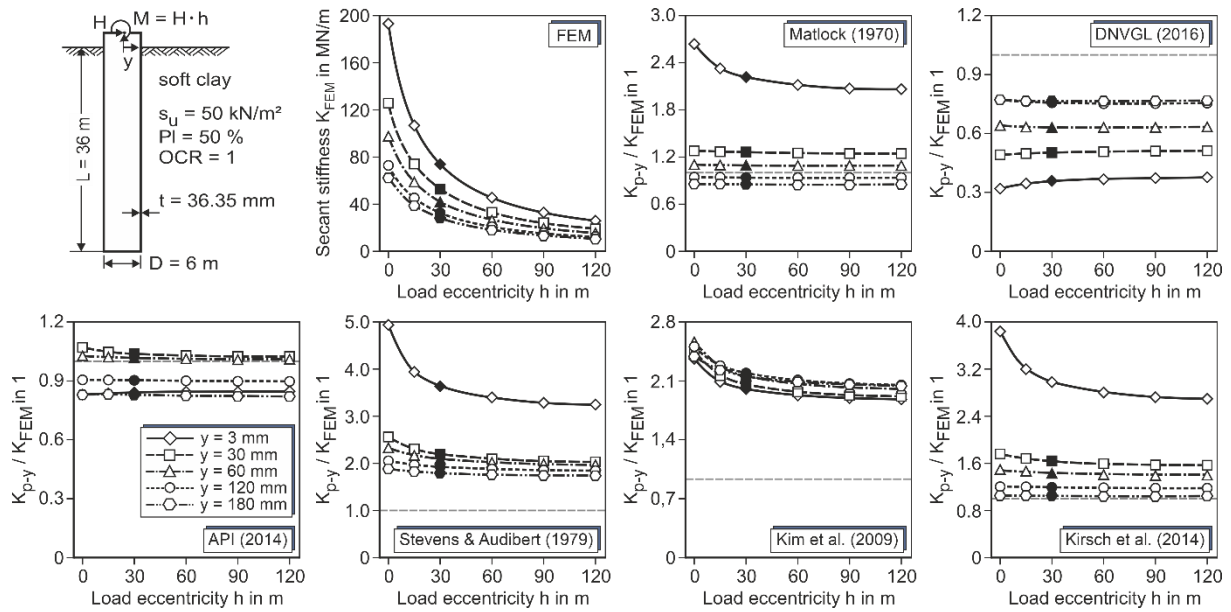


**Fig. 6-9: Quotient of lateral stiffness  $K_{p-y} / K_{FEM}$  for varied load eccentricity based on the reference system of the FEM study**

The effect of the load eccentricity  $h$  on the suitability of the p-y approaches is depicted in Fig. 6-9. As to be expected, the numerically achieved foundation stiffness decreases considerably with increasing load eccentricity  $h$ . It is remarkable that the deviations between the numerical and analytical results are nearly identical for load eccentricities  $h > 30\text{ m}$ , regardless of the applied p-y approach. For smaller load eccentricities, significant differences can be observed, i.e. an increase of the quotient  $Q_K$  occurs most frequently. The discrepancies are presumably associated with the poorly fitted bedding resistances along the pile shaft, as well as with the incorrect prediction of the zero-deflection point  $z_0$ , which depends significantly on the load eccentricity  $h$ .

### 6.3.3 Variation of wall thickness t

Fig. 6-10 shows the variation of the pile stiffness as a function of the wall thickness  $t$  of the reference system. Due to the rather large bandwidth of the wall thickness  $t$  considered, almost the whole range from completely flexible to completely rigid pile behaviour is covered.

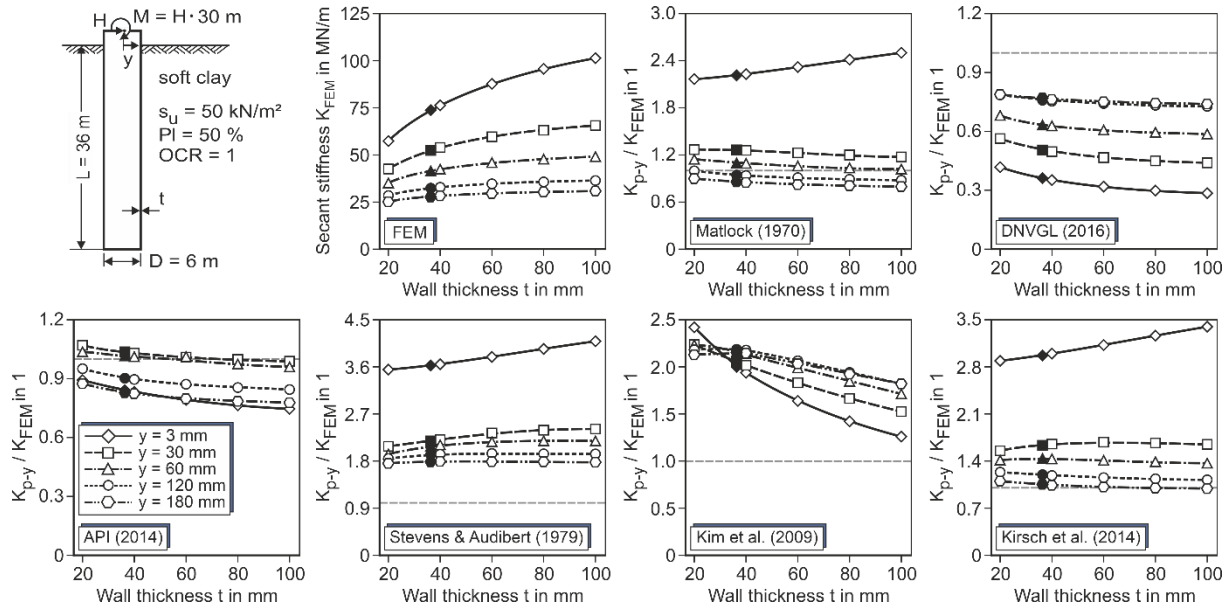


**Fig. 6-10: Quotient of lateral stiffness  $K_{p-y} / K_{FEM}$  for varied wall thickness based on the reference system of the FEM study**

The foundation stiffness increases with the pile stiffness due to a stronger mobilisation of the bedding resistance in large depths. Herein, the largest effect of increased pile stiffness is recognised for small loads. It is noteworthy that the discrepancies of the analytical results are nearly independent of the pile stiffness, considering the significant mismatch of the bedding resistances along the pile shaft. Only the approach proposed by Kim et al. (2009), which implies a p-y curve formulation dependent on the pile stiffness (represented by the wall thickness  $t$ ) yields a noteworthy difference in the deviations for the smallest head displacement. However, the p-y curve formulation depending on the pile stiffness does not improve the accuracy of the p-y approach regarding varied pile stiffness.

### 6.3.4 Variation of clay consistency

The clay consistency is used for the following parametric study as a measure of stiffness and shear strength. The requirements to describe soft soils using the consistency index are discussed by Burland (1990) and Kiekbusch (1999), among others. In addition, investigations were carried out by Vogt (2017) regarding the geotechnical boundary problem of laterally loaded piles embedded in soft soils, which explain the structural and time influence on the determination of p-y curves. This assignment of soil parameters for clay consistencies, shown in Table 6-2, is therefore only to be considered as indicative. The soil parameters that do not appear in Table 6-2, correspond to the reference system of the FEM study according to Table 6-1.

Table 6-2: Clay parameters used for the parametric study regarding the clay consistency

Parameter	$\gamma'$	$s_u$	$E_{oed}^{ref}$	$e$	$n$	$\epsilon_{50}$	$J$
Units	kN/m <sup>3</sup>	kN/m <sup>2</sup>	kN/m <sup>2</sup>	-	-	-	-
Reference System	8.5	90.0	1000	1.30	0.56	0.0075	0.25
Soft	8.0	70.0	900	1.35	0.57	0.00875	0.3035
↓	7.5	50.0	800	1.40	0.58	0.010	0.375
↓	7.0	35.0	700	1.45	0.59	0.015	0.4285
Very soft	6.5	20.0	600	1.50	0.6	0.020	0.5

\* The soil parameters  $\lambda_{E_{oed}} = 0.8$ ,  $\lambda_{G_0} = 0.5$ ,  $\nu_u = 0.495$ , and  $B = 0.903$  are valid for the respective study.

The results of the comparative study between the FEM and p-y approaches with regards to the clay consistency are depicted in Fig. 6-11. The secant stiffness resulting from the FE calculations  $K_{FEM} = H / y$  are given as a function of the undrained shear strength  $s_u$ . The achieved numerical foundation stiffness  $K_{FEM}$  becomes higher with increasing consistency, due to larger undrained shear strength  $s_u$  and soil stiffness applied. The comparative calculations according to the p-y methods indicate a stronger influence of the consistency or shear strength and stiffness of clay on the foundation stiffness for all p-y methods. A good agreement with the FEM results can only be obtained with a certain combination of shear strength and pile head displacement, whereby different deviations are noticeable for each p-y approach.

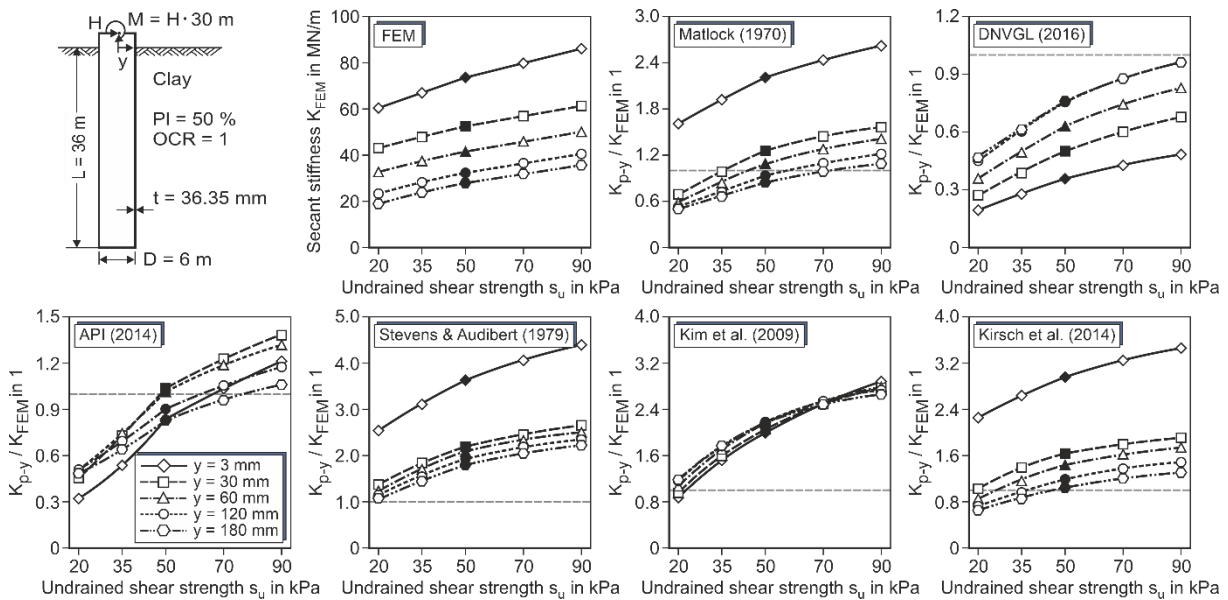


Fig. 6-11: Quotient of lateral stiffness  $K_{p-y} / K_{FEM}$  for a varied clay consistency based on the reference system of the FEM study

A comparison of the results between FEM and Matlock’s approach reveals a poor correlation of the clay consistencies. The same trend can be seen in the back calculation analysis of the “Lake Austin” and “Sabine River” pile load tests when using Matlock’s approach (cf.

section 5.4). Even though both tests represent the whole calibration basis of the underlining p-y approach, significant deviations between the experimental and analytical results are evident. Herein, the foundation stiffness obtained from the “Lake Austin” field test ( $s_u = 38.3$  kPa) is overestimated while the foundation stiffness from the “Sabine River” field test ( $s_u = 14.4$  kPa) is underestimated. Moreover, the successful back-calculations of both pile load tests through the numerical model presented in section 5.4 also demonstrate the suitability of the applied numerical model and give confidence regarding the identified trend in soil consistency. Fig. 6-11 shows the best fit of Matlock’s approach to the numerical results for  $s_u = 50$  kN/m<sup>2</sup>, although a considerable overestimation of the foundation stiffness takes place for the initial stiffness. For all normalised head displacements, the approximation of Matlock’s curve introduced by DNVGL (2016) produces a substantial underestimation of the foundation stiffness, particularly for low values of  $s_u$  (i.e. for very soft clay). The p-y approach proposed by API (2014) recommendations yields similar outcomes to the approach developed by Matlock, except for the smallest head displacement ( $y = 3$  mm) due to the application of finite initial stiffness. The alternative p-y approaches according to Stevens & Audibert, Kim et al., and Kirsch et al. produce a larger foundation stiffness compared to Matlock’s approach and thus the undrained shear strength  $s_u$ , for which the best fit is obtained, is shifted. A significant overestimation of the initial stiffness is recognised in the alternative p-y approaches that take into account an infinite initial stiffness as proposed by Matlock.

### 6.3.5 Variation of the plasticity index PI

In contrast to the aforementioned study, the results in Fig. 6-12 are valid for an exclusive variation of the plasticity index PI, i.e. all remaining soil parameters are set identically to the parameters of the aforementioned reference system (cf. section 6.1). The effect of different plasticity of the soil is modelled by varying the reference shear strain  $\gamma_{0.7}$ .

The influence of the plasticity index PI on the foundation stiffness becomes obvious in Fig. 6-12. Here, a strong increase of the foundation stiffness by increasing the plasticity index PI is obtained except for the initial stiffness reflected in the head displacement  $y = 3$  mm. This behaviour is associated with the strain-dependent stiffness degradation being regulated by the reference shear strain  $\gamma_{0.7}$ . It is remarkable that this frequently denoted “small strain stiffness” significantly affects the monopile behaviour for the design-relevant deformation range (SLS, ULS). This stands in contrast to piles embedded in sand where the combination of a smaller ratio  $G/G_0$ , and a smaller reference shear strain ( $PI = 0$ ;  $\gamma_{0.7} = 1 \cdot 10^{-4}$ ) reduce the relevant range of the strain-dependent soil stiffness.

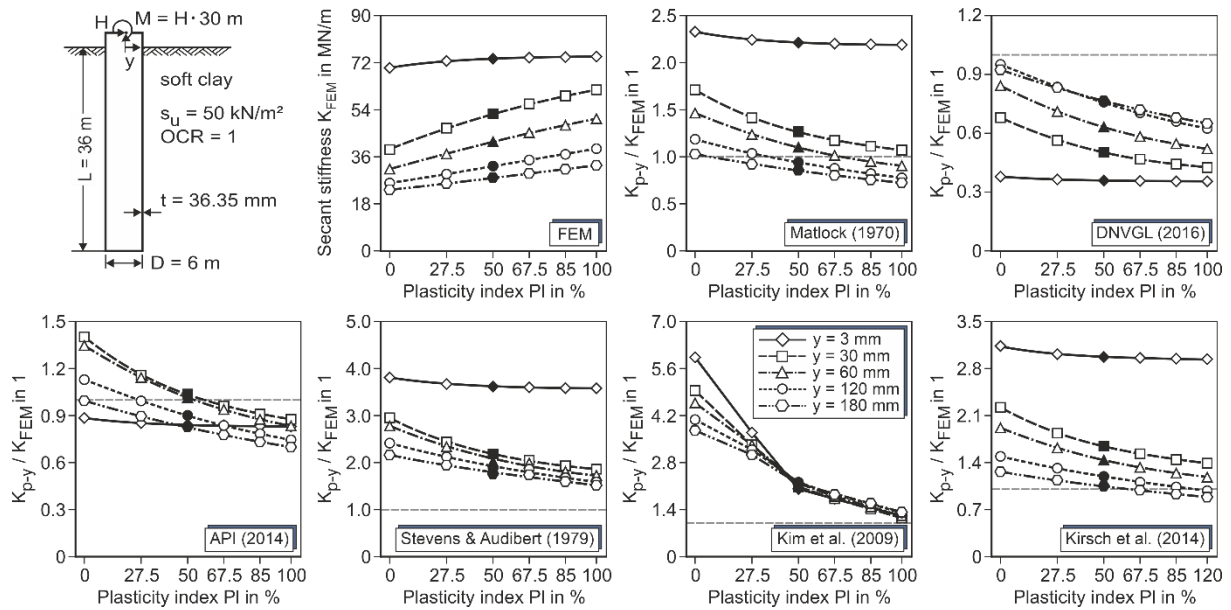


**Fig. 6-12: Quotient of lateral stiffness  $K_{p-y} / K_{FEM}$  for a varied plasticity index PI based on the reference system of the FEM study**

Note that except for the approach by Kim et al. (2009), the plasticity is not considered as an input parameter for the p-y curve formulation and thus the effect of plasticity is not adequately captured. Even though the plasticity index PI is accounted for by Kim et al., the considerable impact obtained from the numerical results is not reflected, particularly showing substantial deviations for  $\text{PI} = 0$ .

### 6.3.6 Variation of the over-consolidation ratio OCR

The previous parametric studies are based on parameters for normally consolidated clay, that were derived from field tests and recommendations of the committee for EAU (2012). However, for the German North and Baltic Seas, where monopile foundations are often used for OWT structures, over-consolidated clays with considerably higher stiffness are frequently observed. The p-y approaches examined in this study are also frequently adopted in design practice for cohesive soils, which are actually proposed for soft clays and therefore a slightly over-consolidated state. Subsequently, the comparative study has been extended to soil with an over-consolidation ratio  $\text{OCR} > 1$ . The assumption of a constant shear strength  $s_u$  over the depth is hereby maintained, although it is unrealistic for larger OCR values. Therefore, the results can be considered as an approximate orientation with respect to the influence of the over-consolidation ratio OCR. The exponent  $k$  that directly influences OCR is determined as a function of the plasticity index PI, (cf. EAD 2002). The soil parameters considered as a basis (insofar they deviate from the parameters of the reference system of the FEM study) are summarised in Table 6-3. For further parameters, refer to Table 6-1 once again.

Table 6-3: Clay parameters used for the parametric study regarding the over-consolidation ratio

Parameters	OCR	k	PI	$\gamma_{0.7}$	$v_u$	B	$\epsilon_{50}$	$f_{ES}$	$f_{G0}$
Units	1	-	-	-	-	-	-	1	1
Reference System (normally consolidated)	1	0.357	50	0.0003	0.495	0.903	0.01	1.0	1.0
Slightly over-consolidated	2	0.327	44	0.00027	0.49	0.8	0.0095	2.0	1.5
	4	0.291	37.5	0.00024	0.48	0.6	0.009	4.0	2.5
	6	0.244	30	0.00021	0.47	0.4	0.0085	6.0	3.5
Strong over-consolidated	8	0.189	22	0.00018	0.46	0.2	0.008	8.0	4.5
	10	0.136	15	0.00015	0.45	0.001	0.0075	10.0	5.5

\* The parameters  $\lambda_{E_{oed}} = 0.8$ ,  $\lambda_{G_0} = 0.5$ ,  $\nu = 0.45$ , and  $E_{oed}^{ref} = 800$  kPa are valid for the respective study.

The comparative calculations are based on the assumption that the plasticity index PI and consequently also the reference shear strain  $\gamma_{0.7}$  decreases with an increased over-consolidation ratio OCR. In addition, the over-consolidation ratio has an impact on the Skempton coefficient B of the clay. For this, a decrease of the Skempton coefficient B with increasing OCR value is assumed. In the case of OCR = 10, B = 0 applies, representing a completely drained behaviour. Higher soil stiffness is taken into account for the calculations using the p-y method by appropriately reducing the strain  $\epsilon_{50}$ . In the FE calculations, higher stiffness is applied as considered by reference system. For that, the stiffness moduli  $E_{oed}$ ,  $E_{50}$  and  $E_{ur}$  are multiplied by a factor  $f_{ES}$  as well as the dynamic shear modulus  $G_0$  by a factor  $f_{G_0}$ . A lower multiplier for the dynamic shear modulus in comparison to the multiplier for the stiffness moduli is applied to obtain realistic ratio values  $E_{s,max} / E_s$  according to the recommendations of the EAD (2002).

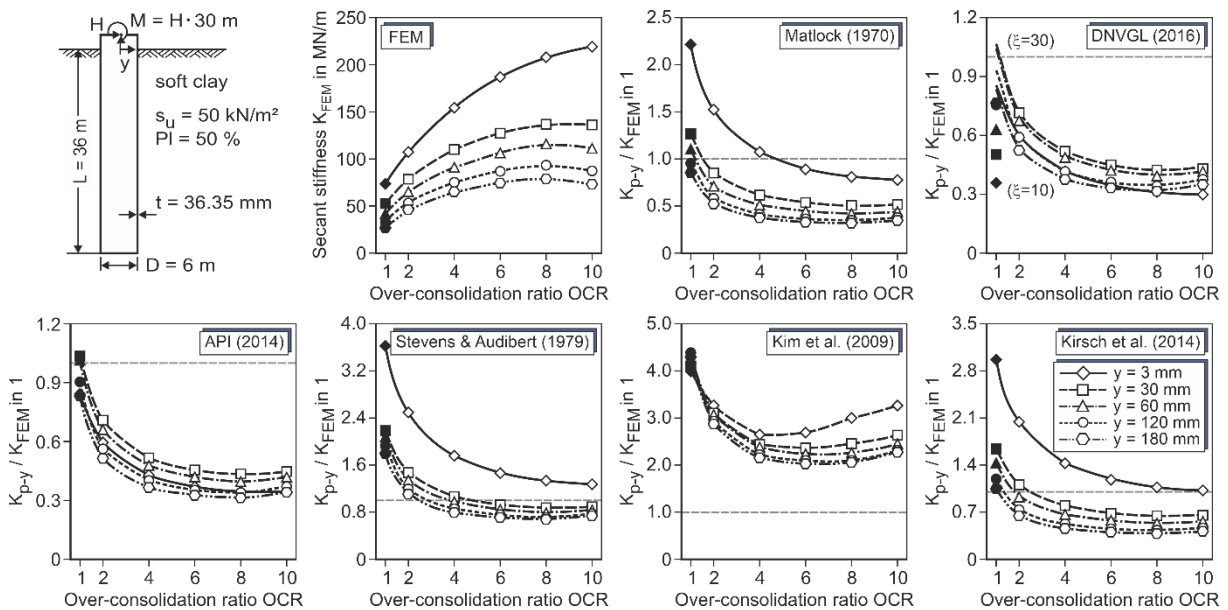


Fig. 6-13: Quotient of lateral stiffness  $K_{p-y} / K_{FEM}$  for a varied over-consolidation ratio based on the reference system of the FEM study

The results of the comparative calculations with respect to the variation of the over-consolidation ratio OCR are shown in Fig. 6-13. The FE calculations yield a strong increase of the foundation stiffness with an increasing over-consolidation ratio OCR, which is not adequately represented by any analytical approach (divergent results). An increased OCR value, has a notable effect on the secant stiffness by decreasing the ratio  $Q_K = K_{p-y} / K_{FEM}$  in most cases, as seen in Fig. 6-13. Here, the best possible fit for Matlock and API (2014) approaches could be established for an over-consolidation ratio  $OCR = 1.5$ . Apart from that, the underestimation of the foundation stiffness by DNVGL (2016) approach becomes continuously larger with an increasing over-consolidation ratio OCR. The three alternative approaches, which entail a larger foundation stiffness compared to Matlock's approach, evince the best fit to the numerical results for a large OCR. For the strongly over-consolidated North Sea conditions ( $OCR = 10$ ), the approaches introduced by Stevens & Audibert agrees comparatively well with the FEM results, except for the initial stiffness.

The results indicate that the applicability of the investigated p-y approaches on over-consolidated clay is not acceptable taken as a basis the influence of the over-consolidation ratio OCR on high increased stiffness. However, the assumptions and simplifications carried out by the present study imply that this cannot be considered absolutely certain without confirmation from further investigations.

### 6.3.7 Variation of individual soil parameters

Additional FEM calculations are carried out to identify the decisive influencing variables with regard to soil properties. The comparative calculations exhibited in Fig. 6-11 and 6-13 are distinguished from the analysis in Fig. 6-14 by selecting the variation of only one parameter instead of the variation of correlative influencing variables. Consequently, the calculations are based on the soil parameters of the so-called reference system, with the exception of the influencing variable noted in the respective axis labels. This could lead to implausible combinations in some areas due to the real dependencies of individual parameters, but the importance of individual parameters is captured for the soil resistance. Individual variations are executed for the oedometric stiffness (but with the simultaneous variation of  $f_{G0}$  according to Table 6-3), the plasticity index PI, the undrained shear strength  $s_u$ , the over-consolidation ratio OCR, and the Skempton parameter B. Fig. 6-14 depicts the effect of the variation of independent parameters on the secant stiffness  $K_{FEM}$ .



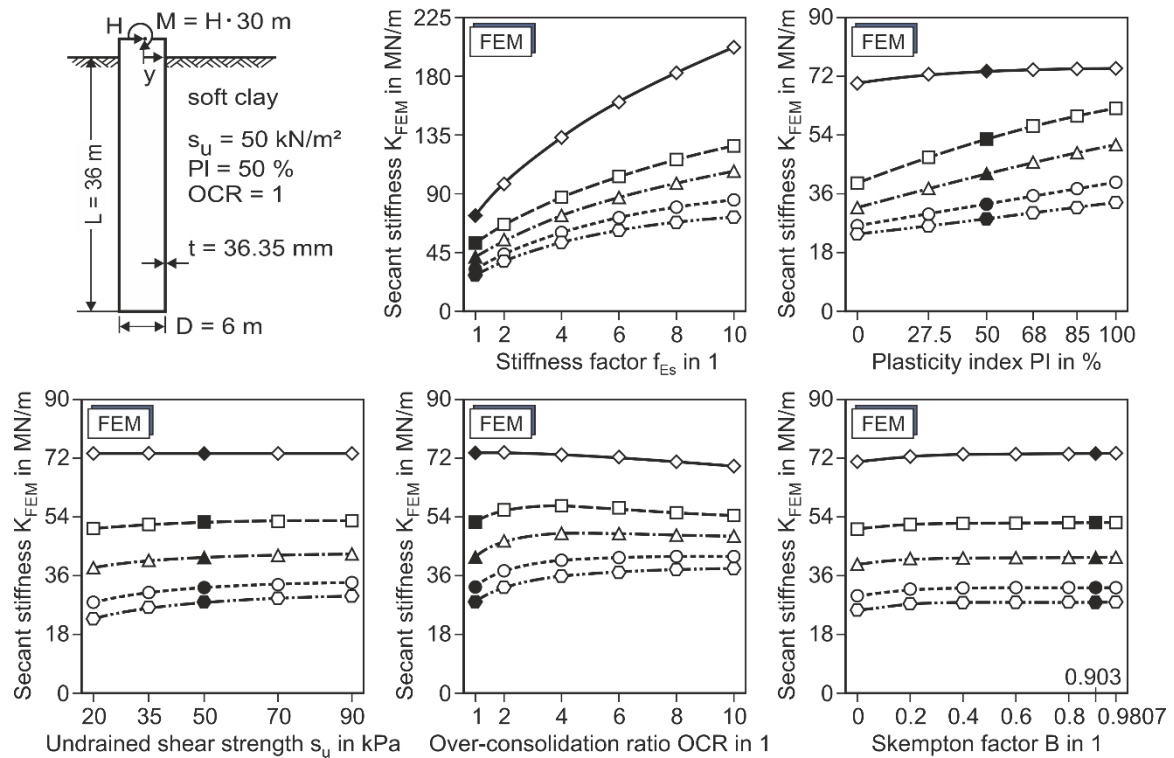


**Fig. 6-14: Secant bedding stiffness for separately varied soil parameters based on the reference system of the FEM study**

The most relevant parameters for the magnitude of the secant stiffness  $K_{FEM}$  are illustrated in Fig. 6-14 (top). It is remarkable that the foundation stiffness considerably increases by applying the stiffness factors  $f_{Es}$  and  $f_{G0}$  (cf. Table 6-3) for obtaining such an effect. The reference shear strain  $\gamma_{0.7}$  is used to define the plasticity index  $PI$ , which also shows an increment of the secant stiffness  $K_{FEM}$ . The increment of the undrained shear strength  $s_u$  yields a significant increase in secant stiffness, especially in the case of large head displacements. In contrast, considering that the system parameters remain the same, the Skempton parameter  $B$  and the over-consolidation ratio  $OCR$  only have a small, but not negligible, influence on the numerical results.

## 6.4 Parametric study with linearly increasing undrained shear strength $s_u$ over depth

The following parametric study represents an extension of the previous numerical comparative study with regard to the suitability of the original p-y approach proposed by Matlock and Matlock's linearised curve introduced by DNVGL (2016), as well as Matlock's modified curves by Stevens & Audibert for arbitrary pile dimensions embedded in over-consolidated clay. By doing so, three-dimensional FE simulations of laterally loaded piles are applied, assuming a linearly increasing undrained shear strength  $s_u$  over depth, which represented a moderately over-consolidated clay. The horizontal load-bearing behaviour of the pile is evaluated under such typical soil conditions to compare it with the results obtained from the aforementioned p-y approaches.

Table 6-4 summarises the soil parameters used for the parametric study in the present section. It has to be emphasised that the stated values are valid for the level of free soil surface whereas the values in brackets represent the increase per meter over depth.

**Table 6-4: Clay parameters used for simulations with linearly increasing parameters over depth**

Parameter	OCR	k	$\gamma'$	$s_u$	$E_{\text{Oed}}^{\text{ref}}$	e	B	$PI / \gamma_{0.7}$	$\varepsilon_{50}$	J	$f_{\text{ES}}$	$f_{G0}$
Units	1	-	kN/m <sup>3</sup>	kPa	kPa	-	-	-	-	-	1	1
Parametric study consistency	4	0.357	7.0 (2.5E-2)	30 (1.0)	700 (5.0)	1.45 (-2.5E-3)	0.5	50/3.0E-4	0.014 (-6.25E-5)	0.45 (2.5E-3)	4.0	2.5
	4	0.357	7.25 (2.5E-2)	40 (1.0)	750 (5.0)	1.425 (-2.5E-3)	0.5	50/3.0E-4	0.012 (-6.25E-5)	0.4 (2.5E-3)	4.0	2.5
	4	0.357	7.5 (2.5E-2)	50 (1.0)	800 (5.0)	1.4 (-2.5E-3)	0.5	50/3.0E-4	0.01 (-6.25E-5)	0.35 (2.5E-3)	4.0	2.5
	4	0.357	7.75 (2.5E-2)	60 (1.0)	850 (5.0)	1.375 (-2.5E-3)	0.5	50/3.0E-4	0.008 (-6.25E-5)	0.3 (2.5E-3)	4.0	2.5
	4	0.357	8.0 (2.5E-2)	70 (1.0)	900 (5.0)	1.35 (-2.5E-3)	0.5	50/3.0E-4	0.006 (-6.25E-5)	0.25 (2.5E-3)	4.0	2.5
Parametric study over-consolidation	1	0.48	7.5 (2.5E-2)	50 (1.0)	800 (5.0)	1.4 (-2.5E-3)	0.903	100/6.0E-4	0.012 (-6.25E-5)	0.35 (2.5E-3)	1.0	1.0
	2	0.447	7.5 (2.5E-2)	50 (1.0)	800 (5.0)	1.4 (-2.5E-3)	0.7	75/4.4E-4	0.011 (-6.25E-5)	0.35 (2.5E-3)	2.0	1.5
	4	0.357	7.5 (2.5E-2)	50 (1.0)	800 (5.0)	1.4 (-2.5E-3)	0.5	50/3.0E-4	0.01 (-6.25E-5)	0.35 (2.5E-3)	4.0	2.5
	6	0.305	7.5 (2.5E-2)	50 (1.0)	800 (5.0)	1.4 (-2.5E-3)	0.3	40/2.5E-4	0.009 (-6.25E-5)	0.35 (2.5E-3)	6.0	3.5
	8	0.244	7.5 (2.5E-2)	50 (1.0)	800 (5.0)	1.4 (-2.5E-3)	0.15	30/2.1E-4	0.008 (-6.25E-5)	0.35 (2.5E-3)	8.0	4.5
	10	0.174	7.5 (2.5E-2)	50 (1.0)	800 (5.0)	1.4 (-2.5E-3)	0.001	20/1.7E-4	0.007 (-6.25E-5)	0.35 (2.5E-3)	10.0	5.5

\* The parameters  $\lambda_{\text{Eoed}} = 0.8$ ,  $\lambda_{G0} = 0.5$ ,  $\nu = 0.45$  are valid for the respective study.

Table 6-4 (top) corresponds to the variation of soil consistencies. Herein, the unit weight  $\gamma'$ , the undrained shear  $s_u$ , and the parameters for the soil oedometric stiffness  $E_{\text{oed}}$  are varied while the considered over-consolidation ratio  $\text{OCR} = 4.0$  remains constant. The variation of the over-consolidation ratio  $\text{OCR}$  is given in Table 6-4 (bottom). A smaller plasticity index  $\text{PI}$  and a smaller pore pressure coefficient  $B$  are assumed as a function of the depth since the over-consolidation ratio  $\text{OCR}$  is accompanied by a larger foundation stiffness. The variation of the soil oedometric stiffness  $E_{\text{oed}}$  and the dynamic shear modulus  $G_0$  are achieved by means of individual factors for both moduli  $f_{\text{oed}}$  and  $f_{G_0}$ , respectively. A smaller multiplier for  $G_0$  is applied in accordance with the typical bandwidth  $G/G_0$  (see Benz 2007).

### 6.4.1 Results for a reference system

The reference system consists of a typical monopile foundation with a diameter  $D = 6$  m, and an embedded pile length  $L = 36$  m. The steel material properties such as the modulus of elasticity  $E_p = 210$  GPa and Poisson's ratio  $\nu = 0.27$  are also applied, but a relatively small wall thickness  $t = 35.36$  mm given by Eq. 6.1 is selected to avoid a completely stiff pile behaviour. For load eccentricity  $h$ , the monopile pipe is extended with almost steel rigid properties, approximately  $h = 30$  m from the free soil surface to apply the lateral load with its respective overturning moment. The three-dimensional numerical model of a monopile foundation system is conducted in accordance with section 5, taking into account the linear variation of soil parameters over depth, described in Table 6-4.

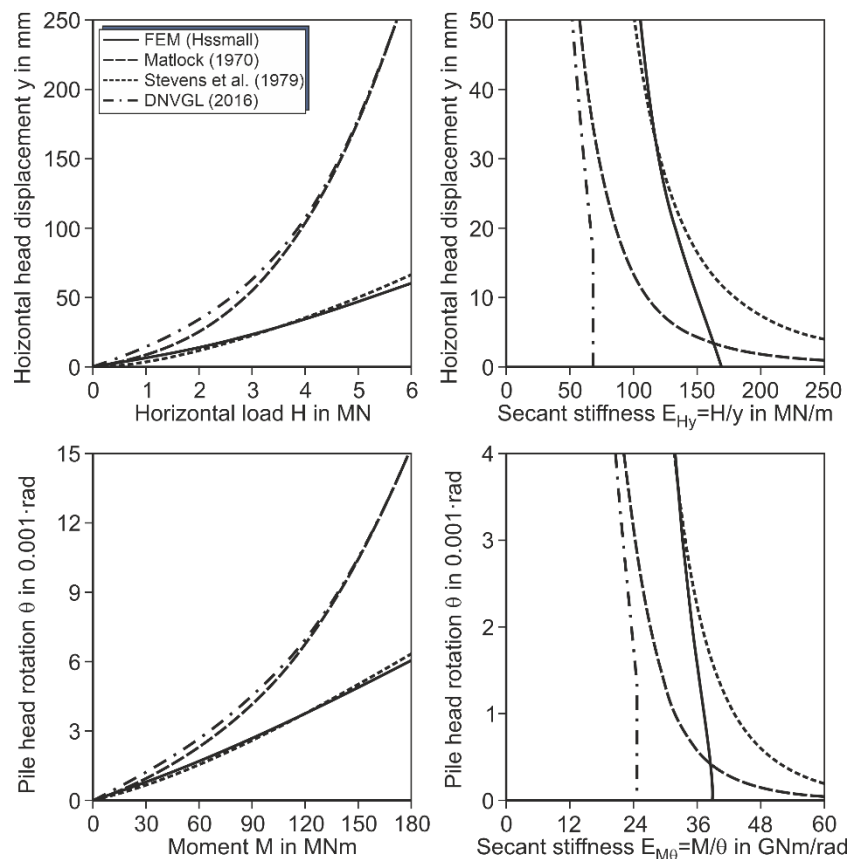


**Fig. 6-15: Load-displacement curves (top) and moment-rotation curves (bottom) for the reference system ( $D = 6$  m,  $L = 36$  m) with linearly increasing parameters over depth**

The load-displacement curves and moment-rotation curves with the corresponding secant stiffness-displacement curves, determined at the soil surface for the range of a small load are depicted in Fig. 6-15. Evidently, the p-y approaches by Matlock and Stevens & Audibert, which entail an infinite initial stiffness, significantly overestimate the foundation stiffness for the range of a very small strain, while the approach by DNVGL (2016) yields a considerable underestimation of the foundation stiffness, even though the latter approach explicitly considers the over-consolidation ratio OCR in the p-y curve formulation. For large loading conditions, the validated numerical results agree well with the approach by Stevens & Audibert whereas the approaches by Matlock and DNVGL (2016) yield an increasing underestimation of resistances.

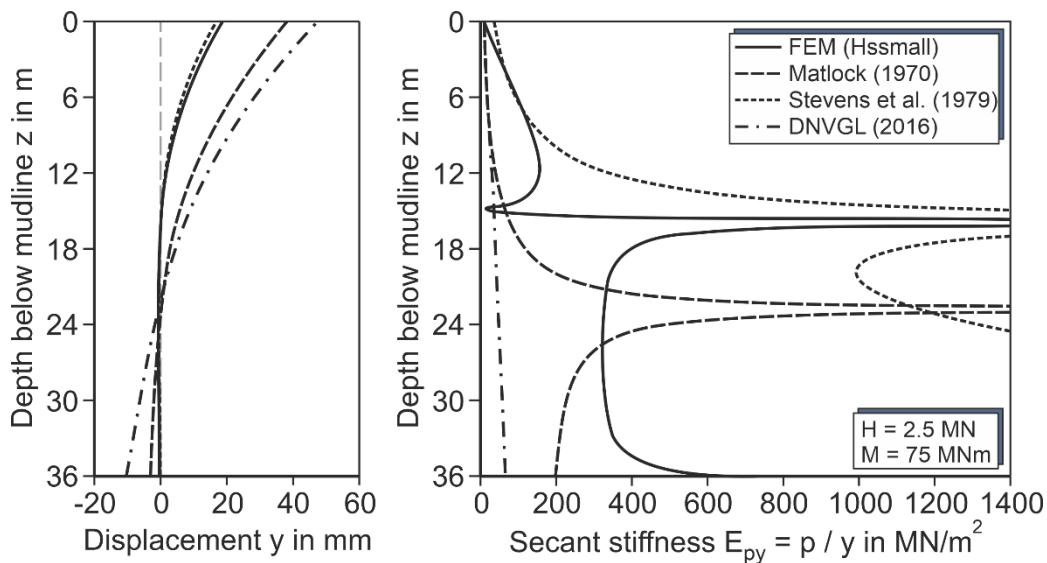


**Fig. 6-16: Pile deflection lines (left) and secant bedding stiffness (right) for the reference system ( $D = 6 \text{ m}$ ,  $L = 36 \text{ m}$ ) with linearly increasing parameters over depth**

For the load level  $H = 2.5 \text{ MN}$  and  $M = 75 \text{ MNm}$  at the pile head, the corresponding deflection lines of the pile, as well as the distribution of the secant bedding stiffness along the pile shaft are illustrated in Fig. 6-16. For the small load condition, the pile deflection line obtained from the approach according to Stevens & Audibert agrees relatively well to the numerical simulation results even though a bad agreement is evident for the secant stiffness. Due to the pile's deflection behaviour, this does not relevantly affect the head deformations. In contrast, Matlock's approach and, in particular, DNVGL (2016) underestimate the bedding stiffness along the whole pile length. Note that none of the examined p-y approaches realistically represents the distribution of the secant stiffness along the pile shaft.

Similar results were obtained from the parametric study conducted by Terceros et al. (2017). In that study, an over-consolidation ratio  $\text{OCR} = 5.0$  was taken into account as reference soil parameter and larger diameter pile. The tendencies of the load-displacement curves and pile deflection lines are quite comparable to the present study.

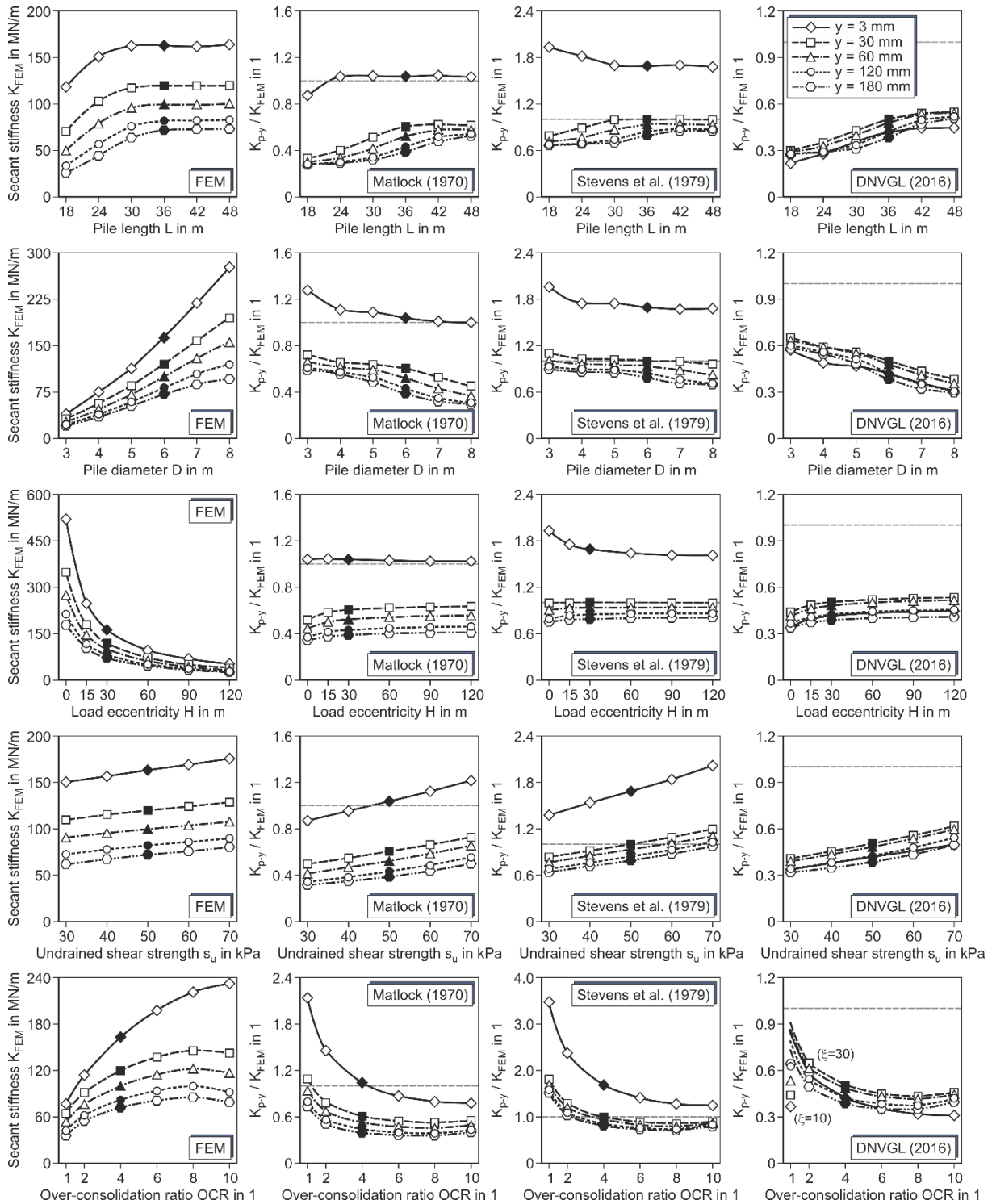


**Fig. 6-17: Quotient of lateral stiffness  $K_{p-y} / K_{FEM}$  for varied parameter with linearly increasing parameters over depth**

The results of a comprehensive parametric study for varied parameters with linearly increasing parameters over depth are depicted in Fig. 6-17. The graphs are outlined in various scales to allow a clear overview of the result discrepancies. The parameter variations such as pile length, pile diameter, load eccentricity, clay consistency, and over-consolidation ratio OCR are considered to evaluate the horizontal load-bearing behaviour of the pile. Similar to the aforementioned parametric study, the FEM results are expressed in terms of lateral secant

stiffness  $K_{FEM} = H / y$  and compared to the respective p-y approach with the quotient  $Q_K = K_{FEM} / K_{p-y}$  of the secant stiffness. Five lateral head displacements ( $y = 3, 30, 60, 120, 180$  mm) reflect the behaviour of the foundation stiffness for various depth-dependent parameters.

### ***Variation of embedded pile length L***

The first row of Fig. 6-17 refers exclusively to the variation of the embedded pile length  $L$ . Here, pile lengths between 18 and 48 meters are examined to determine the effect on lateral head displacements. Except for the smallest head deformation ( $y = 3$  mm), Matlock's approach results in a considerable underestimation of the foundation stiffness, particularly for short pile lengths. Matlock's modified approach introduced by DNVGL (2016) significantly underestimates the foundation stiffness for whole load levels, mainly due to the linearisation of the initial part of the p-y curve (cf. section 4.3.2). The revised p-y approach by Stevens & Audibert fits best, especially for large pile lengths and large load levels. However, the foundation stiffness is considerably overestimated for the smallest head displacements, again due to the application of an infinite initial stiffness of the underlying Matlock curves.

### ***Variation of Pile diameter D***

For the variation of the pile diameter  $D$ , the embedded pile length  $L$  and the load eccentricity  $h$ , as well as the wall thickness  $t$  are adapted, similar to the previous parametric study presented in section 6.3.1 (i.e. load eccentricity  $h$  set to 5 times the diameter and wall thickness  $t$  calculated by Eq. 6-1). In the second row, Fig. 6-17 shows the comparative analysis with increasing diameters from 3 to 8 m. The increase of the pile diameter  $D$  leads to a strong increment of the foundation stiffness. The almost linear trajectory of the secant stiffness  $K_{FEM}$  does not reach a threshold value. Again, the results of p-y approach proposed by Stevens & Audibert fit relatively well with the FE simulations, except for the smallest head displacement.

### ***Variation of load eccentricity h***

The third row of Fig. 6.17 shows the impact of the increment of the load eccentricity  $h$  from 0 to 120 meters on the foundation stiffness. An increasing load eccentricity leads to a significant decrease in the secant stiffness of the monopile foundation as demonstrated by the numerical simulations. This may be due to the upward motion of the zero-deflection point of the pile, resulting from the increased moment acting at the pile head. The trend of the secant stiffness  $K_{FEM}$  of the FE simulations is best captured by Stevens & Audibert's approach, except for the smallest head displacement, whereas the approaches by Matlock and DNVGL (2016) show the largest discrepancies for pure lateral load (i.e. load eccentricity  $h = 0$  m).

### *Variation of clay consistency*

The variation of clay consistency is depicted in the fourth row of Fig. 6.17. Here, the secant stiffness  $K_{FEM}$  for the respective head displacements increase almost linearly with increasing soil consistencies. The results demonstrate that none of the examined p-y approaches seem to be appropriate to accurately reproduce the effect of the soil consistency due to the consideration of the same “basic p-y curve” formulation, in this case Matlock’s curve formulation. It becomes apparent that the foundation stiffness resulting from the FE simulations is always higher than the stiffness calculated by the approach by DNVGL (2016). The results of the p-y approaches, in this case Matlock and Stevens & Audibert, lead to a better or a worse agreement with the numerical results, depending on the normalised head displacements and the soil consistency.

### *Variation of the over-consolidation ratio OCR*

Based on the numerical simulation results, a larger over-consolidation ratio OCR yields a strongly increasing foundation stiffness, which is not well-accounted for by the examined p-y approaches. It is remarkable that Matlock’s approach (despite the infinite initial stiffness) fits relatively well for normally consolidated clay  $OCR = 1$ , while the approach proposed by Stevens & Audibert best reproduces the horizontal load-bearing behaviour of the pile for over-consolidated clay  $OCR > 1$ . It can be noted that only the p-y approach introduced by DNVGL (2016) includes the coefficient  $\xi$  in the p-y curve formulation to describe the degree of clay consolidation, i.e.  $\xi = 10$  for normally and  $\xi = 30$  for over-consolidated clay. However, as seen in the last row of Fig. 6-17, the missing specification by DNVGL (2016) regarding the transition value  $\xi$  between normally and over-consolidated clays leads to a jump in the results in terms of  $Q_K$ . It becomes evident that an underestimation of the foundation stiffness is yielded in both cases, even though the deviations with respect to the results of the numerical simulation are smaller by applying  $\xi = 30$ .

## 6.5 Requirements for a new, generally applicable p-y approach

Assuming that the influences of the pile geometry and the soil parameters are tendentially correctly reproduced by the FEM model, none of the evaluated p-y methods are recommended as suitable for arbitrary pile dimensions and soil conditions as well as wide range of load magnitudes. Consequently, the development of a new, generally applicable p-y approach for soft clay is essential.

An entirely new approach has to be based on a different basic function of the p-y curve formulation developed by Matlock to overcome the questionable infinite initial stiffness associated with the requirement for linearisation and the correct description of the influence of the pile diameter.

Furthermore, the new p-y approach should predict the bedding resistances along the pile shaft with more accuracy than the examined p-y approaches. In part, this can be achieved by a better appreciation of what soil parameters are indispensable to reflect its non-linear soil behaviour. Ideally, the respective pile bending stiffness has to be taken into account as well. The innovative procedure of the p-y approach proposed by Thielen et al. (2015a) for sand could be taken as a basis for derivation of a new p-y approach for soft clay.

Consequently, based on the results of the previous parametric studies, a new p-y method shall take into account the ultimate limit bedding resistance  $p_u$  with a focus on the overburden pressure  $\sigma_v$  and the undrained shear strength  $s_u$ , but also the bedding stiffness under consideration of the oedometric soil stiffness  $E_{oed}$ , the dynamic shear modulus  $G_0$ , and the plasticity index PI decoupled from each other. The pile dimensions and stiffness must be taken into account both in the formulation of the limit bedding resistance and the bedding stiffness approach.

## 6.6 Interim conclusion

The design of monopiles used for the foundation of OWTs is carried out using the p-y method in practice. For a safe and economic design, viable p-y curve formulations are certainly required to predict the horizontal load-bearing behaviour of the pile for the entire expected deformation range with sufficient accuracy.

The scope of this thesis deals with the horizontal load-bearing behaviour of piles embedded in soft clay to increase the quality and reliability of the improved design methods. The results of more than 600 FEM calculations for different pile geometries and soil conditions, as well as diverse lateral loading conditions, are compared with the results of various static p-y methods. The FEM model was validated on the basis of a comparison of the calculation results obtained from data of field tests with pile diameters between 0.32 m and 2.4 m and diverse soil properties.



Although the FEM model cannot be considered as conclusive for larger pile diameters due to the lack of validation with respective field tests, the results indicate that none of the p-y methods investigated are suitable for all mentioned boundary conditions, being acceptable for certain conditions and load levels depending on the p-y approach applied.

Basically, the development of a new, generally applicable p-y approach for monopiles in soft clays is therefore considered indispensable with a possible extension to stiff clay. The relevant parameters of such new approach were identified in the previous section.

The mentioned comparative calculations shall be summarised in the variation of pile dimension as well as soil parameters (e.g. the consistency, the plasticity and the over-consolidation ratio of the clay) with and without depth dependence. Based on the new knowledge acquired, the requirements are defined for a new p-y method, which is valid for arbitrary soil conditions and pile dimensions.

Based on these results, a new p-y approach will be introduced which properly reproduces the results obtained from validated numerical models for arbitrary pile dimensions, soil conditions and diverse load levels.



## 7 Development of a new modelling approach

### 7.1 General

The present chapter focuses on the derivation of an innovative modelling approach, which is able to improve the prediction of the horizontal load-bearing behaviour of the pile as well as its respective local pile-soil interaction when compared to the results of the validated three-dimensional numerical model as introduced in chapter 5. Consequently, a more realistic pile behaviour is feasible than that resulting from the traditional p-y approach recommended by API (2014) and DNVGL (2016).

The new modelling approach derived from a set of validated three-dimensional numerical models considers the innovative procedure proposed by Thieken et al. (2015a) in conjunction with the application of the hyperbolic function utilised by the constitutive model HSsmall (cf. Benz 2007). By doing so, a continuous trajectory of the p-y curve's shape is obtained, characterised by the absence of supporting points or a piecewise function in the formulation up to the threshold displacement  $y_L$ , where the ultimate bedding resistance  $p_u$  occurs.

The application of the new modelling approach overcomes the usual shortcomings yielded by the conventional p-y approaches, as demonstrated in chapter 8. This is suitable for pile foundations with arbitrary dimensions embedded in cohesive soils that are subjected to short-term monotonic loading. It is remarkable that its application can also be extended for including the effect of long-term cyclic loading conditions (e.g. Albiker 2016).

### 7.2 Limitations of common p-y approaches

Traditional p-y approaches exhibit common limitations regarding the application of uncoupled spring characteristics at nodal points along the pile shaft as defined by the subgrade reaction method. Indeed, this simplified p-y model envisaged does not provide the capability to consider the treatment of the soil as a continuum, i.e. the bedding soil resistance resulting from each spring characteristic does not influence either the above or bottom adjacent spring characteristic. By doing so, they are completely independent among them, which does not realistically reflect the pile's load-bearing behaviour. It is obvious that more reliable results would be obtained by using a continuum model such as that used in sophisticated Finite-Element FE models. Besides that, the lack of the inclusion of the shear stress at the pile base in the bedding soil resistance occurs by using traditional p-y approaches. This limitation is called the "pile tip effect" and has a decisive impact, particularly on the bedding behaviour of large-diameter pile foundations typically utilised in the OWTs, i.e. for an embedded length to diameter ratio  $\leq 5$ . The effect of the pile tip should have been adjusted as a function of the distance between the head and the pile tip or also a relation to the pile diameter, i.e. through geometrical pile conditions.

To obtain a clear insight into these limitations of the analytical methods, sophisticated three-dimensional numerical models of the pile-soil system have been developed by using Finite Element Analysis for building realistic modelling of the horizontal load-bearing behaviour of a large-diameter monopile embedded in cohesive soils

Based on the reference system introduced in section 6.2, three numerical simulations are applied for carrying out a comprehensive analysis. The distinction of numerical models only concerns the variation of the wall thickness for considerably increasing the pile rigidity, i.e.  $t = 20$  mm and  $t = 200$  mm for the first and second numerical simulation, respectively. Note that the load eccentricity  $h$  used for the modelling is identical to the reference system, i.e.  $h = 30$  m.

Concerning the third pile-soil system, the pile length is extended to 100 m to avoid the so-called “pile tip effect”. Additionally, a nearly rigid behaviour of the pile ( $E_p = 1 \cdot 10^{12}$  kN/m<sup>2</sup>,  $\nu = 0.27$ ) is taken into account for a constant lateral displacement by using the prescribed surface displacements over the entire pile length.

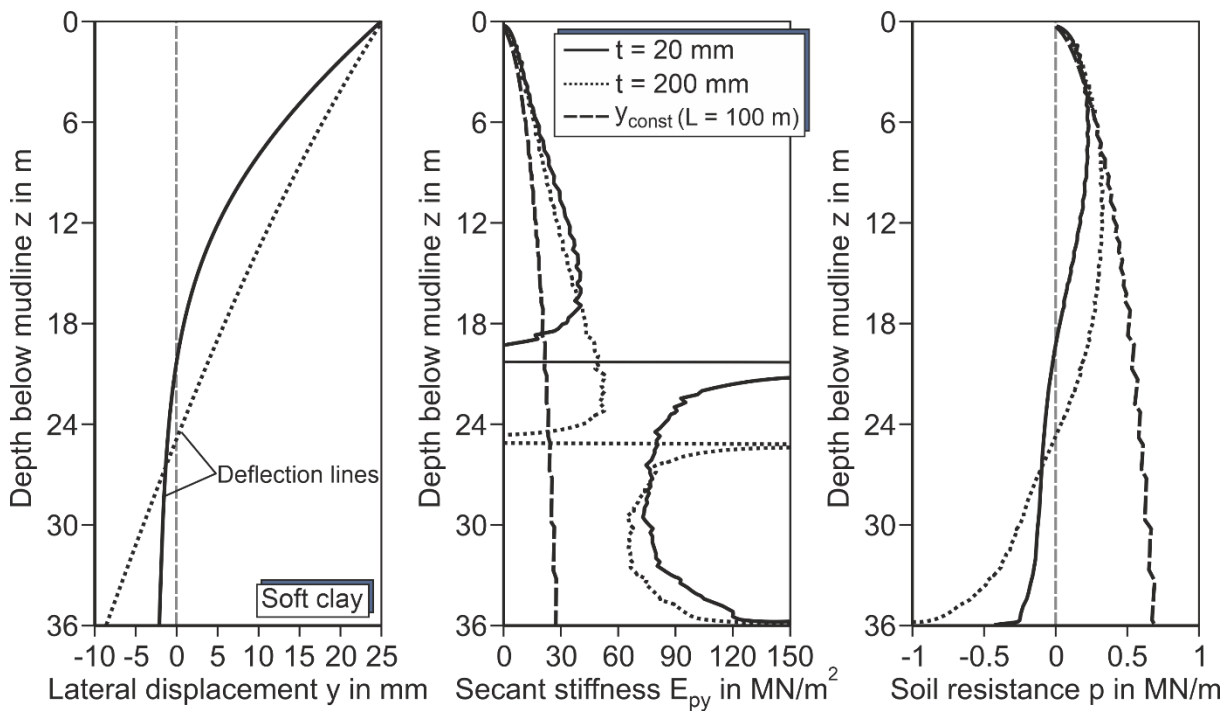


**Fig. 7-1: Impact of pile bending on bedding soil resistance ( $D = 6$  m,  $L = 36$  m, soft clay)**

To capture the limitations of the analytical  $p$ - $y$  method described above, Fig. 7-1 shows the results of three-dimensional numerical simulations in terms of deflection lines, secant bedding stiffness and bedding resistance for a prescribed pile head displacement  $y = 25$  mm in all cases. The resulting pile head displacement is defined by using displacement-controlled calculations in Plaxis 3D.

A flexible and rigid pile behaviour is treated in the first two numerical simulations through modification of the wall thickness  $t$ . Thus, it becomes evident what effect the relative pile stiffness provides on the local behaviour of the pile-soil interaction. Indeed, the depth of the zero-deflection point  $z_0$  moves downwards when the relative pile stiffness increases, resulting

in a substantial mobilisation of the soil, such as seen in the distribution of the bedding resistance over depth (see Fig. 7-1 right).

It also highlights the breaks on the distribution of secant bedding stiffness corresponding to the depth of the zero-deflection point  $z_0$ , clearly indicated by the pile deflection lines. The third pile-soil system does not appear in Fig. 7-1 (left) since the deformation is fully constant along the pile, i.e. that is a vertical line, up to the prescribed lateral deformation  $y = 25$  mm.

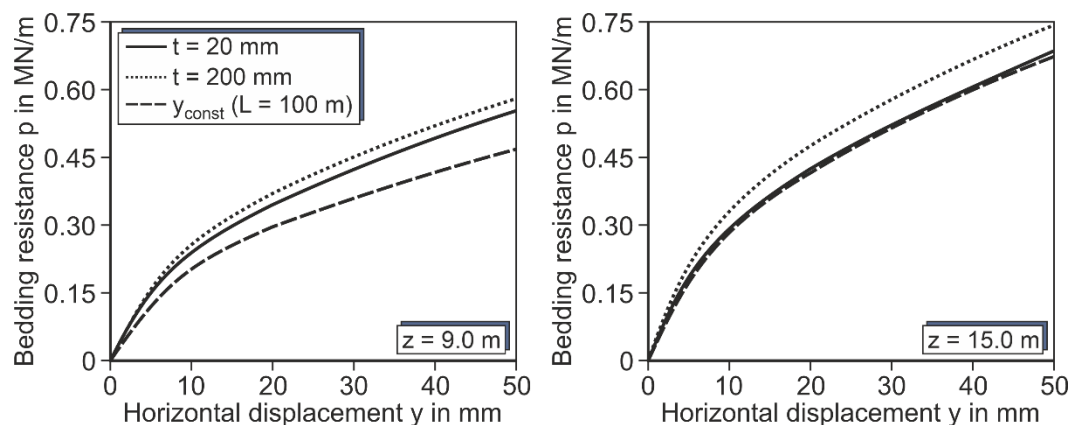


**Fig. 7-2: Influence of the pile bending on the p-y curves ( $D = 6$  m,  $L = 36$  m, soft clay)**

For completeness, the resulting p-y curves from the three aforementioned numerical simulations for two representative depths  $z = 9$  m and  $z = 15$  m that are located above the zero-deflection point  $z_0$  are depicted in Fig. 7-2. For obtaining the full path of the p-y curves, extreme loading conditions were applied to the corresponding pile-soil systems. The course of derived p-y curves highlights that the pile-soil system which is constant horizontal displacement (i.e. the third numerical system) provides a softer behaviour compared to the other two pile-soil systems laterally loaded at the pile heads.

The lack of the traditional p-y approaches lies in the fact that they were calibrated using only a specific pile stiffness obtained from the load test measurements. This leads to an unreliable extrapolation with regard to predictions of the pile's load-bearing behaviour for distinct pile-soil systems. This means that its range of application is significantly reduced to the relative pile stiffness with which they were derived. Definitely, a redistribution of shear stressing along the pile shaft occurs when changing the pile's stiffness or load level conditions that clearly affects the load-transfer behaviour for piles. To this effect, the mutual interaction of the deflection lines and the bedding resistances to overcome the relative stiffness of the pile-soil system is essential for obtaining a realistic horizontal load-bearing behaviour of the pile.

The impact of the "pile tip effect" for flexible and almost rigid pile foundations on the bedding soil resistance becomes also revealed in Fig. 7-1 (right). For the first two laterally loaded head piles used for the present analysis, a substantial increase in the bedding soil resistance near the pile tip confirms the strong interaction of the pile tip and soil, in particular for the rigid pile foundation resulting in a fully mobilised soil, thus identifying its predominantly geometrical dependence.

In contrast, the distribution of bedding soil resistance for a horizontally displaced pile (i.e. the third analysed pile-soil system) remains unaffected by the so-called pile toe shearing since the pile length was extended to  $L = 100$  m for this purpose. This means that the relevance of the “pile tip effect” that is neglected in conventional p-y approaches is decisive for describing a realistic pile’s load-bearing behaviour, as seen in Fig. 7-1.

### 7.3 Conception of the new modelling approach

A modified two-step procedure that covers most aspects to characterise the pile-soil interaction is introduced below, thus partially overcoming the aforementioned limitations of traditional p-y methods.

In the first step, the relationship between the bedding soil resistance  $p$ , acting against the pile wall, and the lateral deflection  $y$  of the pile foundation are described by p-y spring characteristics (as termed p-y curves) for infinite pile length that experiences constant horizontal displacements. The so-called “basic p-y curves” are obtained from the sophisticated three-dimensional numerical models, resulting in a completely new curve shape that depends on the relevant parameters as indicated under section 6.5. For deriving the “basic p-y curves”, piles with sufficient length had to be modelled to avoid the effect of the pile tip on the distribution of bedding soil resistance. In addition, it excludes the impact of the deflection line of the pile foundation on the “basic p-y curves” due to the constant horizontal displacement along the pile shaft. For calculating the ultimate bedding resistance  $p_u$  applied to the “basic p-y curves”, a detailed description is given in section 7.4.

The second step refers to the application of y-multipliers  $Mult_y$  on the “basic p-y curves” to achieve the interaction between the pile deflection line and the bedding resistance as well as the influence of the shearing stresses at the pile base. This means that the y-multipliers modify the stiffness of “basic p-y curves” as a function of the pile deflection line and the effect of the pile tip. To reach the equilibrium of the pile-soil system, an iterative procedure is applied until no further change of the deflection line occurs.

The y-multipliers  $Mult_y$  includes the “pile tip effect” that affects the bedding soil resistance near the pile tip. For that, the embedded length-to-diameter ratio  $L / D$  is a key characteristic when it comes to quantifying the effect of the pile tip on the bedding pile behaviour. Consequently, several  $L / D$  ratios of the pile-soil system are considered for determining the influence of the shearing stresses at the pile base.

Note that the validity range of the new modelling approach was determined by performing more than 300 three-dimensional numerical models to predict the load-bearing behaviour of the pile-soil system over a wide range of pile geometries, soil consistencies, and diverse load levels.

## 7.4 Determination of ultimate bedding resistance $p_u$

For calculating the ultimate bedding resistance  $p_u$ , the innovative procedure proposed by Thieken et al. (2015a) is adopted for cohesive soils. The sophisticated three-dimensional numerical model introduced in chapter 5 reproduces the bedding pile behaviour with constant horizontal displacement along the pile length to reach the threshold displacement  $y_L$  where the maximum bedding resistance of soil occurs. An almost rigid pile ( $E_p = 1 \cdot 10^{12}$  kN/m<sup>2</sup>,  $\nu = 0.27$ ) is laterally displaced by using the prescribed surface displacements applied to the entire pile shaft. The pile length had to be extended more than twice its original length to ensure that the pile tip does not influence the distribution of bedding soil resistance in the upper part of the pile foundation.

A large horizontal displacement of the pile foundation is required to catch the threshold displacement  $y_L$  for full mobilisation of the bedding soil resistance. This results in severe mesh distortions that lead to a slow or even non-convergence of the iteration process for solving the numerical calculation of the pile-soil system. For such reason, the soil stiffness parameters, which are not directly associated with the ultimate bedding resistance  $p_u$  were set to 20 and 30 times larger than the soil stiffness parameters specified in Table 6-1. However, identical results of the  $p_u$  are obtained when the unchanged soil stiffnesses are applied, but with higher calculation stability of the three-dimensional numerical models. It becomes evident that the large soil stiffness parameters considerably reduce the threshold displacement  $y_L$  without influencing  $p_u$  obtained from the horizontally displaced piles. The effect of the pile diameter  $D$  on the  $p_u$  was adequately captured by selecting six pile diameters distributed over a range of 0.5 to 8 meters with various soil consistencies varying from very soft clay to stiff clay.

Two failure mechanisms that are characteristic for the non-linear pile-soil behaviour became evident by applying the previously explained method for determining the ultimate bedding resistance  $p_u$ .

For shallow depths, the soil materials fail in a conical wedge mechanism that extends from the soil surface to the transition depth  $z_R$ . In contrast to Matlock's approach, a non-linear function was selected for providing a suitable description of this failure mode, as follows:

$$p_{u,s} = \frac{p_{u,d} \cdot z}{0.15 \cdot z_R + 0.85 \cdot z} \quad (7-1)$$

For calculating the transition depth  $z_R$ , Matlock's approach is applied but modifying the lateral bearing capacity factor to  $N_p = 11.3$  calibrated from the results of the validated numerical simulations. Additionally, the theoretical constant  $J$  is set at  $2 \cdot \sqrt{2} = 2.83$  adopted from the analytical solution proposed by Reese (cf. section 3.6).

$$z_R = \frac{8.3 \cdot D}{\gamma \cdot \frac{D}{s_u} + J} \quad (7-2)$$

For deep depths, the ultimate bedding resistance  $p_u$  introduced by the new modelling approach is similarly determined as Matlock's approach based on the flow-around failure mechanism.

$$p_{u,d} = N_p \cdot D \cdot s_u \quad (7-3)$$

The lateral bearing capacity factor  $N_p$  associated with the adhesion factor  $\alpha$  is re-calibrated in dependence of the roughness conditions of the pile-soil interface.

$$N_p = 2.4 \cdot \alpha + 10.1 \quad (7-4)$$

The adhesion factor  $\alpha$  related to the pile-soil interface surface lies within the range of 0 to 1 for a fully smooth and fully rough pile, respectively. In the present study, it was usually considered a semi-rough interface between pile and soil mostly, which means  $\alpha = 0.5$ , resulting in the lateral bearing capacity factor  $N_p = 11.3$ . Obviously, the ultimate lateral soil resistance  $p_u$  turns out to be the smallest value derived from both soil failure mechanisms.

$$p_u = \min[p_{u,s}, p_{u,d}] \quad (7-5)$$

A comprehensive analysis demonstrates the validity of the above formulation for calculating the ultimate bedding resistance  $p_u$  of laterally loaded piles with various dimensions and soil conditions, see Fig. 7-3.

Initially, a reasonably good agreement of the results from FE simulations and the new modelling approach concerning the lateral bearing capacity factor  $N_p$  associated with the derivation of the ultimate bedding resistance  $p_u$  are shown in Fig. 7-3. Two soil consistencies were carefully selected for exemplary presentation in this thesis, i.e. soft clay and medium soft clay, indicating a suitable adjustment by considering three representative pile diameters  $D = 1, 4, 6$  m. Appendix A provides additional diameters and soil consistencies used for supporting the proposed formula of  $p_u$ .

In addition, the results of Matlock's approach recommended by the offshore guidelines are included in all graphs. A clear underprediction of the lateral bearing capacity factor  $N_p$  exists when compared to numerical results for both considered pile diameters and soil consistencies. This mainly results from the assumption of the roughness condition imposed by Matlock as in the flow-around failure mechanism, i.e. fully smooth interface conditions (cf. section 3.6.2). Besides that, the application of a linear function to the distribution of the lateral bearing capacity factor  $N_p$  used for describing the conical wedge failure mechanism (i.e. resulting in shallow depths) is also quite inadequate when compared to the results of the validated three-dimensional numerical simulations.



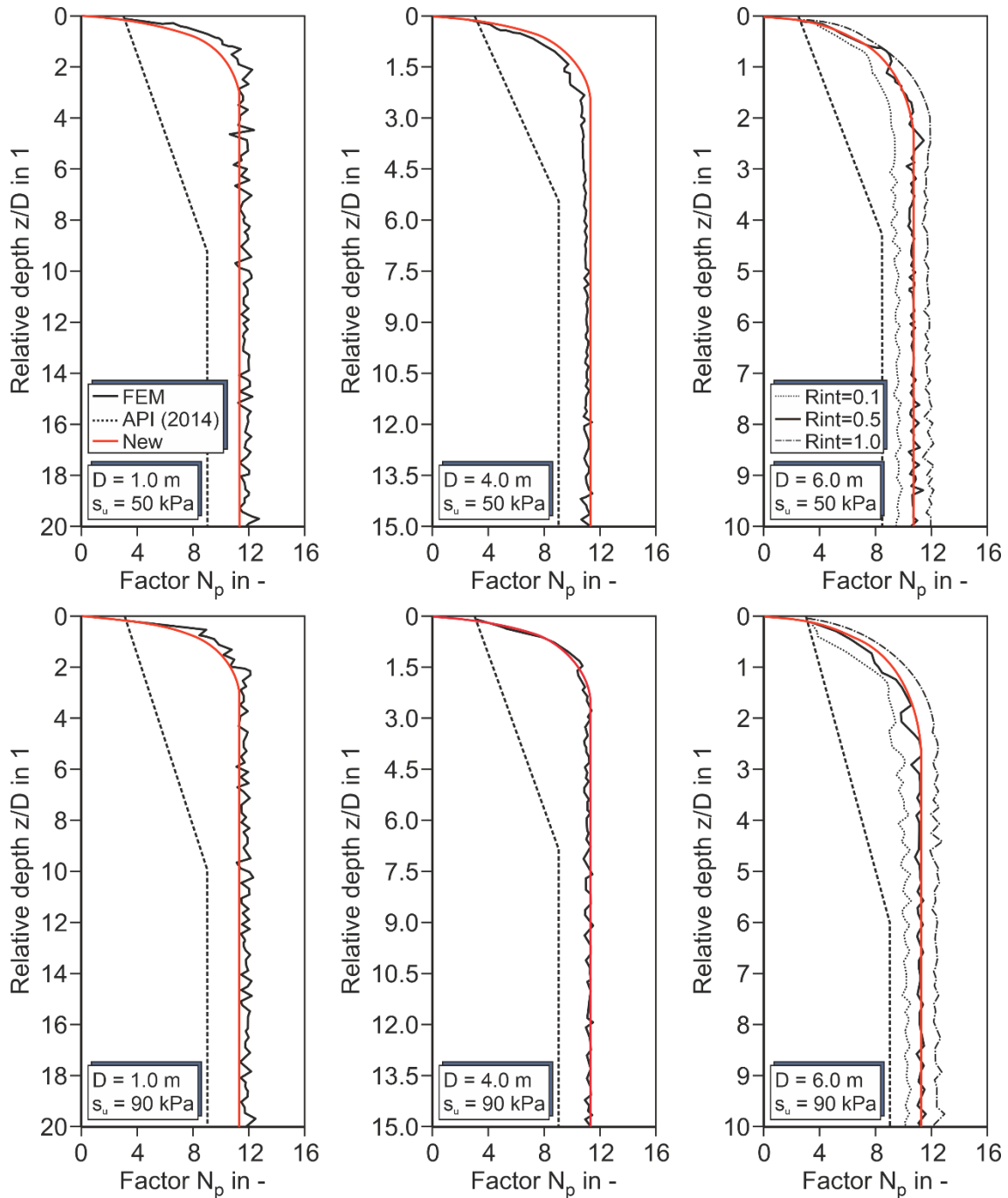


**Fig. 7-3: Course of the load-bearing capacity factor  $N_p$  resulting from the FEM analysis and p-y approach recommended by OGLs, as well as the new modelling approach**

Similarly, the effect of the roughness condition on the lateral bearing capacity factor  $N_p$  just for the pile diameter  $D = 6$  m is also depicted in Fig. 7-3 (right). This is obtained from numerical simulations by adjusting the reduction factor  $R_{int}$  applied to the elasto-plastic contact interface, i.e. for either almost fully smooth and fully rough pile-soil interface specified by  $R_{int} = 0.1$  and  $R_{int} = 1.0$ , respectively.

It must be pointed out that the fluctuation of the  $N_p$  distribution with depth provided by the numerical simulations mainly results from the numerical instability for reaching the threshold displacement  $y_L$  where the ultimate bedding resistance  $p_u$  occurs.

Finally, the validity of the lateral bearing capacity factor  $N_p$  derived from a set of three-dimensional finite element analysis is also verified by varying the undrained shear strength  $s_u$  with respect to five pile diameters for two relative depths  $z/D = 1$  and  $z/D = 6$ . Certainly, for shallow depths influenced by the soil surface, the variation of  $N_p$  depends on both the soil consistency and the pile diameter, as seen in Fig. 7-4 (top), while for the deep depths represented in Fig. 7-4 (bottom) the  $N_p$  becomes constant value for the fully examined bandwidth, mainly due to the confinement of the cohesive soil. In both cases, the lateral bearing capacity factor  $N_p$  proposed by the new modelling approach corresponds quite closely to the results obtained from the numerical simulations.

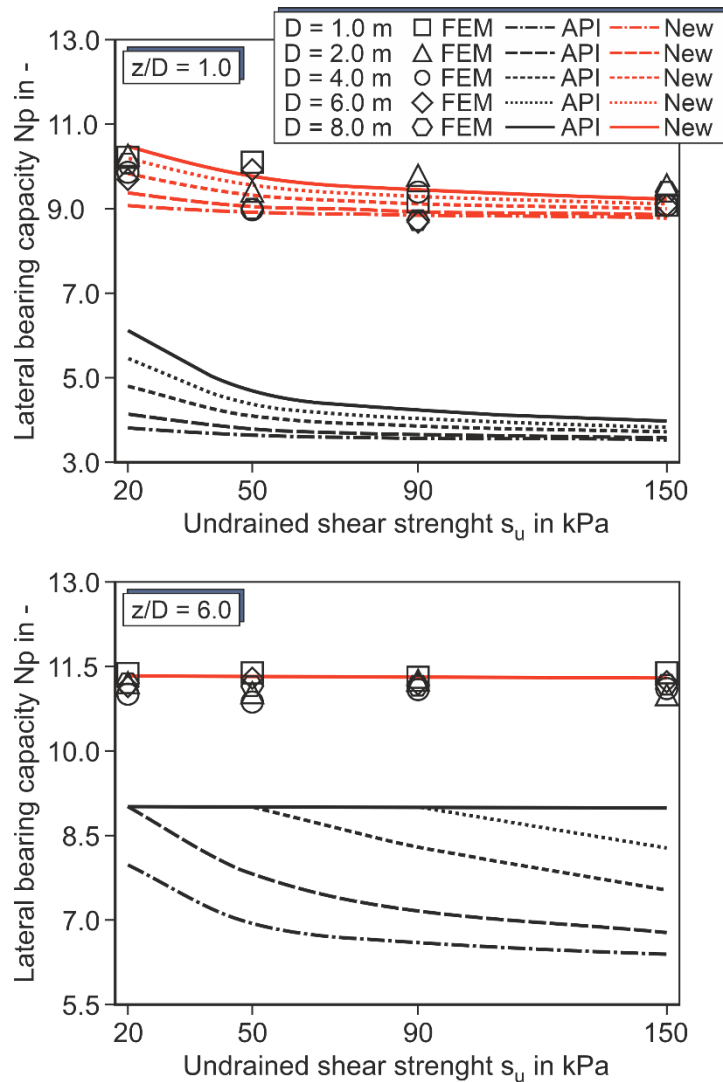


**Fig. 7-4: Comparison of the load-bearing capacity factor  $N_p$  depending on the soil consistency and pile diameters for two reference depths**

In contrast to the good suitability of new modelling approach, the p-y approach recommended in API (2014) clearly predicts a significant underestimation of the lateral bearing capacity factor  $N_p$  for both relative depths discussed in detail.

The outcome obtained from the parameter study highlight that the bearing capacity factor  $N_p$  provided by API (2014) approach does not become constant in all cases for the relative depth

$z / D = 6$  examined, whereas the transition depth  $z_R$  is significantly deeper than that obtained from the validated numerical results, Fig. 7-3 also confirms this fact. This indicates that for such reference depths the flow-around failure mechanism does not yet occur by considering the p-y approach recommended in API (2014).

## 7.5 Derivation of the initial stiffness $K_i$

Similar to the derivation of ultimate bedding resistance  $p_u$ , pile foundations embedded in different soil consistencies are horizontally displaced along the entire pile length. Very small displacements of the entire pile length resulting from a displacement-controlled calculation lead to the derivation of the initial slope of the p-y curve associated with the initial stiffness  $K_i$  of virgin loading p-y curves. To this effect, the pile lengths are considerably extended to avoid the effect of the pile tip on the determination of the initial stiffness, thus ensuring a suitable identification of this parameter in the examined depths. The distribution of the initial stiffness, which is crucial for very small strains, i.e.  $K_i = E_{py} (y \rightarrow 0)$ , can generally be described using the following relationship:

$$K_i = G_0 \cdot 1.45 \cdot (1 + \nu) \quad (7-6)$$

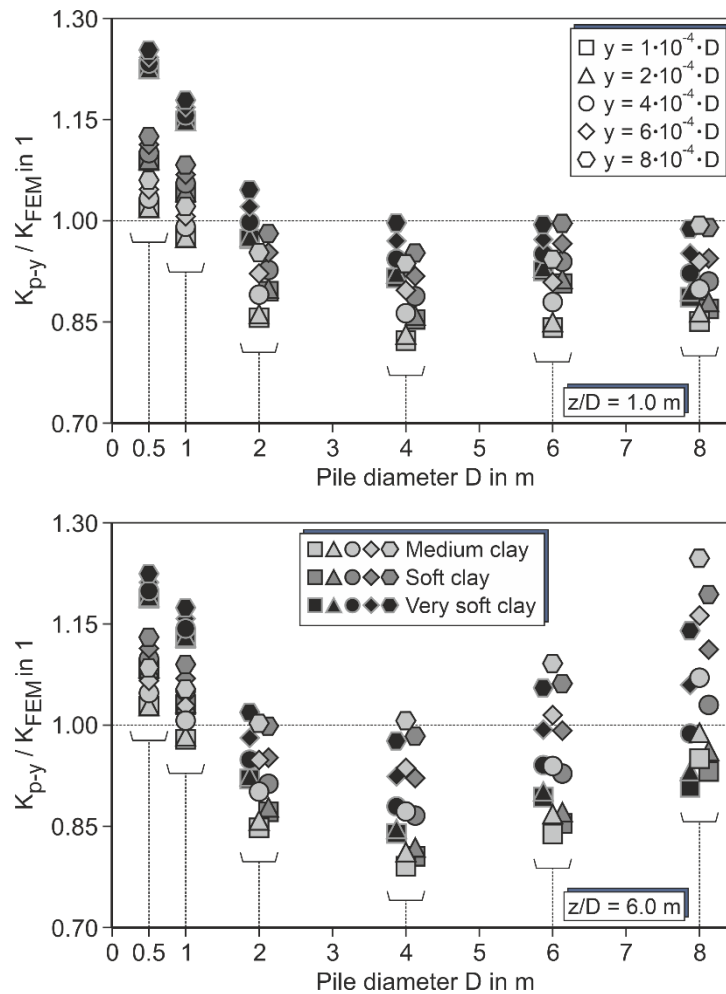
The initial stiffness  $K_i$  is a function of the dynamic shear modulus  $G_0$  and Poisson's ratio  $\nu$  as described by Hooke's law, i.e.  $E = G_0 \cdot 2 \cdot (1 + \nu)$ . The constant value 1.45 comes from the re-calibration carried out in the scope of comprehensive study for obtaining a good agreement with numerical results, as can be verified hereafter.

Fig. 7-5 depicts the results related to the initial stiffness of six pile diameters (ranging from  $D = 0.5$  to 8 m) and three soil conditions (e.g. very soft clay, soft clay and medium soft clay). For this, the quotients of the lateral stiffness  $Q_K = K_{p-y} / K_{FEM}$  are used for evaluating the initial lateral stiffness of the virgin loading p-y curves obtained from the new modelling approach and the validated numerical results. This means that the quotient  $Q_K = 1$  is a perfect match between both analysis methods.

Certainly, in the FE calculation, the initial stiffness  $K_i$  responds in a highly sensitive manner to the variation of the maximum load fraction, which significantly affects the accuracy of its estimation. It is therefore seen required to establish a bandwidth of very small lateral displacements at a range from  $y = 1 \cdot 10^{-4} \cdot D$  to  $y = 8 \cdot 10^{-4} \cdot D$  for calculating the initial lateral stiffness of the p-y curves. By doing so, the instability of such a parameter might be within this predefined range. Two relative depths  $z / D = 1$  and  $z / D = 6$  were selected to appreciate its variation.

For shallow depths represented in Fig. 7-5 (top), it is noticeable that the prediction of the new modelling approach yields an overestimation of the initial stiffness for small pile diameters, i.e.  $< 1.5$  m around. These deviations reach up to 1.25 for very soft soils, which means that the resistance from the numerical simulations is just a quarter less than the resistance predicted by the new modelling approach. Within the range of typical monopile diameters from 6 to 8 m, the differences are moderate in the bandwidth analysed, reaching at worst around 0.85 for medium

soft clay. This means that the initial stiffness obtained from the new model yields a slight underprediction of the foundation resistance compared to the numerical results.



**Fig. 7-5: Initial stiffness ratios for the pile foundations embedded in different cohesive soils with varying diameters for two reference depths**

For deep depths depicted in Fig. 7-5 (bottom), the lateral stiffness quotients  $Q_K$  are also close to 1 for the examined pile diameters. However, the bandwidth of  $Q_K$  tends to expand by increasing the pile diameters, identifying both over- and underestimation of the initial stiffness for typical monopile diameters. However, for small pile diameters  $< 1$  m, the quotient is greater than 1 for almost all soil consistencies examined.

Concluding, Eq. 7-6 is appropriate for describing the distribution of the initial stiffness over depth despite the deviations that can be considered moderate. Its main advantage is the simplicity of application, achieving that the new modelling approach becomes a robust formulation.

## 7.6 Derivation of “basic p-y curves”

For deriving “basic p-y curves”, a similar procedure to that developed in section 7.4 was conducted, but this time considering the realistic soil stiffness parameters associated with Table 6-1. The piles again exhibit constant horizontal displacements as far as possible, so that the numerical models can reach the non-linear static equilibrium solution of the pile-soil system. It was likewise assumed that the pile lengths had to be extended over twice their original length. This ensures that the effect of the pile toe on the distribution of bedding soil resistance can be overcome and thus prevent any distortion in the results. For defining an appropriate shape of “basic p-y curves”, it once again considers six pile diameters from 0.5 to 8 m over a range of soil consistencies from very soft clay to stiff clay.

The hyperbolic stress-strain relation utilised for the HSsmall constitutive model (for more details see Benz 2007) is considered for the new modelling approach as the “basic function” of the model’s formulation, which properly describes the shape of the p-y curves obtained from the sophisticated finite element FE models. The non-linear relationship between the pile displacements  $\bar{y}$  and the bedding soil resistances  $p$ , such as described by Winkler analysis, is given by the following function:

$$p = \frac{\bar{y}}{\frac{1}{E} + \frac{\bar{y}}{p_u/R_f}} \quad (7-7)$$

From the derivative of the adopted hyperbolic function  $\partial p / \partial y = 0$ , it confirms that a horizontal asymptote exists which prevents the determination of a threshold displacement  $y_L$  related to maximal bedding resistance  $p_u$ . In that case, the employment of the failure ratio  $R_f = 0.9$  similar to the applied by HSsmall is essential, thus allowing the exact calculation of both required parameters, e.g.  $y_L$  and  $p_u$  (see Fig. 7-11).

The non-linear decay of soil stiffness  $E$  with increasing lateral head displacements is suitably described using Eq. 7-8, similar to that proposed by Dos Santos & Correia (2001) in the HSsmall model, resulting in stiff and soft behaviour of the pile-soil system for very small and large displacements, respectively.

$$E = E_L + \frac{K_i - E_L}{1 + \frac{0.08 \cdot \bar{y}}{\gamma_{0.7} \cdot D}} \quad (7-8)$$

An innovative characteristic of the new analytical method lies in the consideration of soil plasticity as an input parameter for defining the non-linear response of the pile foundation, whereas the most traditional p-y approaches omitted its effect, despite being essential to a suitable description of the pile-soil interaction.

Any influence related to the soil plasticity on the pile’s load-bearing behaviour results from the threshold shear strain  $\gamma_{0.7}$ , as presented by HSsmall, that can be directly obtained from laboratory tests. Besides, according to Stokoe et al. (2004), the  $\gamma_{0.7}$  may be described as a linear

increase from 0.0001 for plasticity index  $PI = 0$  up to 0.0006 for  $PI = 100$  taken as reference values in this thesis.

The soil stiffness  $E_L$  at the threshold displacement  $y_L$  can be accurately determined using the failure ratio  $R_f = 0.9$  applied to the hyperbolic function considered. The constant value 10 in Eq. 7-9 results from the geometrical solution for calculating the required parameter.

$$E_L = 10 \cdot \frac{p_u}{y_L} \quad (7-9)$$

For determining the threshold displacement  $y_L$ , the empirical factor  $Fac$  is essential, which depends on the dynamic shear modulus  $G_0^{ref}$  and the oedometric soil modulus  $E_{oed}^{ref}$  at the reference stress  $p_{ref} = 100$  kPa.

$$y_L = Fac \cdot \frac{p_u}{E_s} \quad (7-10)$$

$$Fac = 1.7 - 0.03 \cdot \frac{G_0^{ref}}{E_{oed}^{ref}} - 8.3 \cdot \left( \frac{p_{ref}}{E_{oed}^{ref}} \right)^{1.8} \quad (7-11)$$

Effectively, a set of three-dimensional numerical simulations was also required in the calibration of the empirical factor  $Fac$  used for determining the threshold displacement  $y_L$  where the soil strength is fully mobilised. Pile foundations with six meters diameter were also horizontally displaced along the entire pile length for analysing the effect of the ratio between the dynamic shear modulus and static soil stiffness modulus  $G_0^{ref} / E_{oed}^{ref}$  on the threshold displacements  $y_L$ .

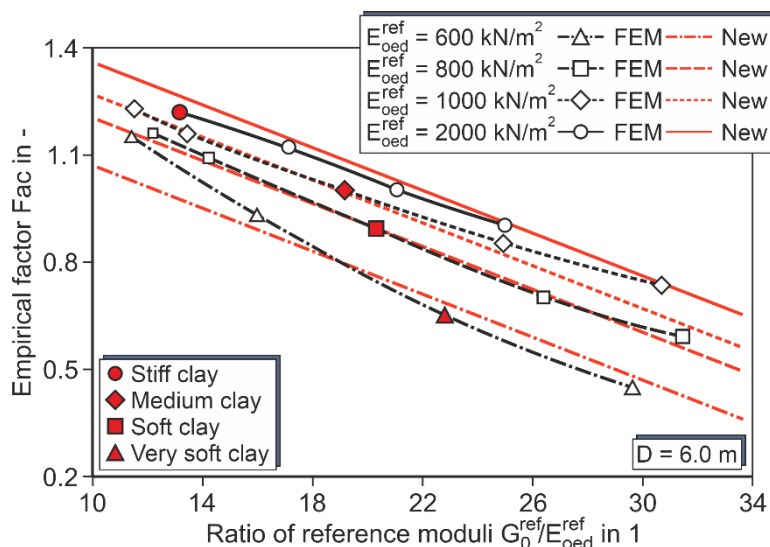


**Fig. 7-6: Derivation of the empirical factor  $F_{ac}$  by varying the ratio of the dynamic shear modulus  $G_0^{ref}$  to static soil stiffness modulus  $E_{oed}^{ref}$**

Fig. 7-6 depicts the distribution of the empirical factor  $F_{ac}$  resulted from the numerical simulations for four soil consistencies varying the ratio of the reference stiffness parameters. In addition, the analytical results derived from the Eq. 7-11 introduced in this study are included for comparing with the numerical result so that a good match between them is recognised.

The points that correspond to the reference soil consistencies used as reference soil conditions (cf. section 6.2) are also highlighted by red filling symbols. The reduction of the empirical factor  $F_{ac}$  with increasing the ratio of the reference stiffness moduli becomes evident in the figure. It should be stressed that the introduced analytical solution captures this effect well, although the agreement between the two methods of analysis is not perfect.

For demonstrating the suitability of the proposed “basic p-y curves”, two relevant reference systems from the comprehensive parameter study are exemplarily introduced in this thesis. It means that the non-linear behavioural patterns in terms of the p-y relationship for both flexible and almost rigid pile-soil systems are thoroughly analysed, as follows:

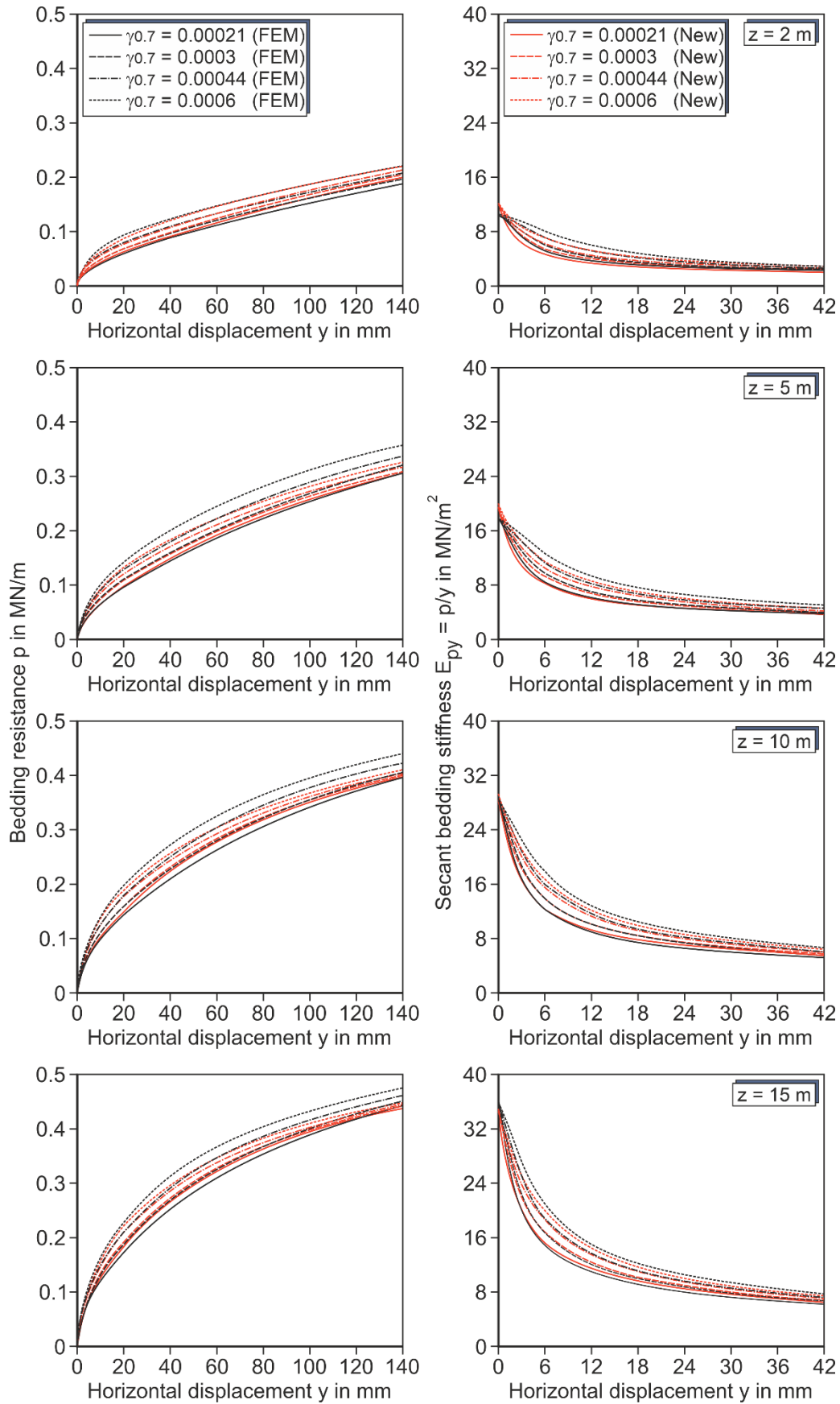


**Fig. 7-7: Comparison of the p-y curves obtained from FEM and new modelling approach for a pile with constant horizontal displacement ( $D = 1$  m, soft clay)**



Fig. 7-7 presents the “basic p-y curves” and the respective secant stiffness-displacements curves  $E_{py}$  for four representative depths, obtained from sophisticated three-dimensional numerical simulations and from the new modelling approach for comparison, related to the small pile diameter  $D = 1$  m in soft clay (i.e. used for representing flexible pile foundations). The proposed “basic p-y curves” calculated from the new modelling approach, which was calibrated using data from a set of three-dimensional numerical models, clearly exhibit a relatively good agreement with the FE simulation results.

The four “basic p-y curves” with their respective secant stiffness-displacement curves for each representative depth correspond to the variation of the plasticity index PI, which results as a function of the threshold shear strain  $\gamma_{0.7}$ . Consequently, highly plastic clays represented by  $\gamma_{0.7} = 0.0006$  lead to stiffer p-y curves than slightly plastic soil  $\gamma_{0.7} = 0.00021$ , this pattern being identical for all examined depths. Such behaviour of the pile-soil system agrees well by using the new modelling approach, as can be appreciated in the respective figures.

Based on the results of the sophisticated three-dimensional numerical simulations, the geometric characteristics of the p-y curves, such as the initial stiffness  $K_i$  and the threshold displacements  $y_L$  are not affected by changing soil plasticity, whereas the curvature is unquestionably impacted owing to its variation. Here, the secant stiffness-displacement curves confirm the non-variation of the initial stiffness  $K_i$  for the corresponding depths. It is clear that  $K_i$  increases with depth which can be attributed to the profile of the dynamic shear modulus  $G_0$  on which it is mainly dependent.

In shallow depths represented by  $z = 2$  m and  $z = 5$  m for small pile diameters  $D = 1$  m, the new modelling approach moderately overpredicts the initial slope of the p-y curves (as described in section 7.5), which can be identified in the secant stiffness-displacements curves. The reason behind that is the uncomplicated formulation adopted for determining the initial stiffness.

It is also remarkable that the new modelling approach provides a non-linear decay in soil stiffness with increasing lateral displacements quite similar to the course exhibited in the secant stiffness-displacement curves obtained from the sophisticated finite element FE models, see Fig. 7-7 and Fig. 7-8.

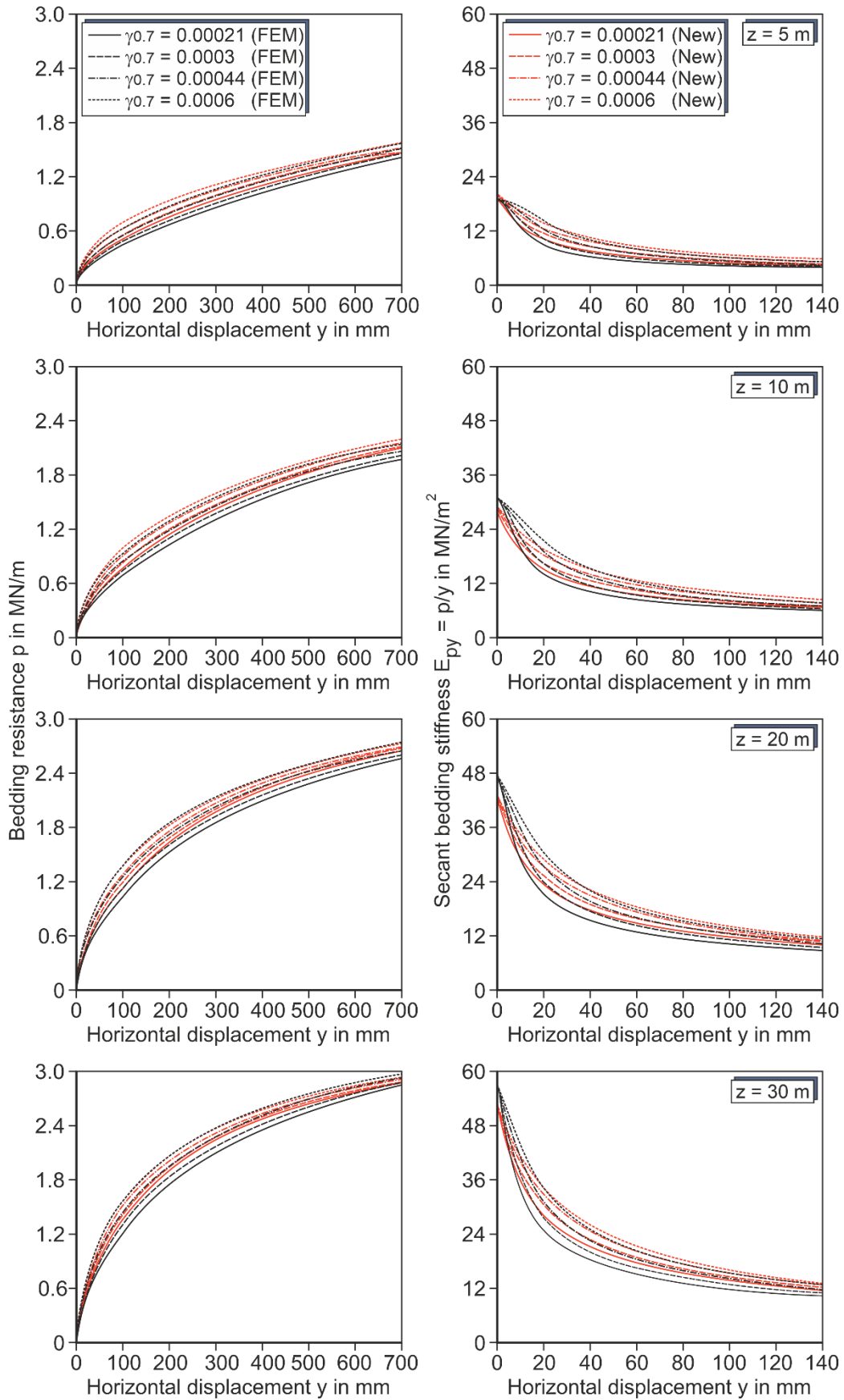


**Fig. 7-8: Comparison of the p-y curves obtained from FEM and the new modelling approach for a pile with constant horizontal displacement (D = 6 m, soft clay)**

Similarly, the resulting p-y curves from a monopile foundation with a diameter  $D = 6$  m embedded in soft clay are represented in Fig. 7-8. For four representative depths, the suitability of the introduced “basic p-y curves” is demonstrated to match the numerical results. The secant bedding stiffness-displacement curves (cf. Fig. 7-8, right) highlight the stiff behaviour of the pile-soil system for small loads, as well as its soft behaviour for large loads.

To predict the initial stiffness for the large pile diameter  $D = 6$  m, the new modelling approach moderately underpredicts the initial stiffness for deep depths, i.e.  $z = 20$  and  $z = 30$  m, with respect to the results of the numerical simulations, but such deviations which are already detected in section 7.5 can be accepted for the reasons aforementioned.

It is noted that the complete shape of the introduced “basic p-y curves” is quite similar to that obtained from numerical models, thus being optimal for analysing the laterally loaded piles embedded in cohesive soils. The small displacements related to the dynamic response of the pile foundation (FLS design proof), the middle displacements required by the usual working conditions (SLS design proof) as well as the large displacements used to prove the general stability (ULS design proof) fit quite well into the shape of “basic p-y curves” compared to the sophisticated finite element FE models.

For completeness, Fig. 7-9 depicts the effect by varying the Skempton parameter  $B$  used for controlling the excess pore pressure on the “basic p-y-curves” for pile diameters  $D = 1$  m and  $D = 6$  m corresponding to two representative depths  $z = 10$  m and  $z = 20$  m.

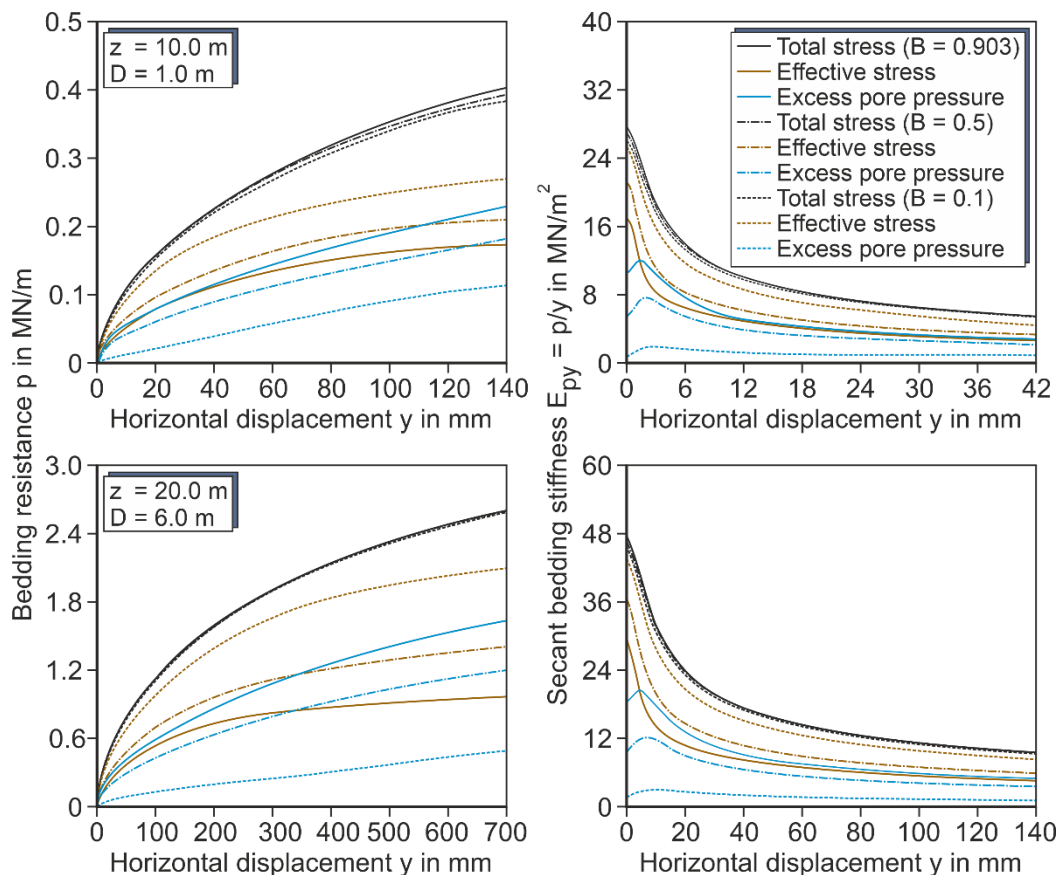


**Fig. 7-9: Influence of undrained behaviour on the p-y curves obtained from the HSsmall constitutive material model by applying the “undrained analysis B”**

The numerical results obtained from Plaxis 3D in terms of the “basic p-y curves” with the respective secant stiffness-displacement curves give an insight into the relationship between the effective stresses and the excess pore pressure  $p_{exc}$  required for calculating the total stresses exclusively used for the new modelling approach.

The insignificant variations in the total stresses results are consistent with the results presented in section 6.3.7 in which a parametric study of the secant bedding stiffness at the pile head for individually varied soil parameters is conducted. Apparently, from Fig. 7-9, it can be assumed that the sum of the different relations between excess pore pressure and effective stress resulting from the variation of the Skempton parameter B gives nearly identical total stress for the representative depths examined. Note that these results can only have a rough orientation character regarding the influence of the excess pore pressure for the reasons given in section 5.3, i.e. these results should only be of indicative use with regard to its application.

## 7.7 Consideration of the pile tip effect and pile deflection line

In the new modelling approach, the mutual interaction between the pile deflection line and the bedding resistance as well as the so-called “pile tip effect” has to be included for adequately predicting the horizontal load-bearing behaviour of the pile compared to the sophisticated FE numerical models. By doing so, y-multipliers  $Mult_y$  are applied to the stiffness of the “basic p-y curves” derived from the constant horizontal displacement along the pile length, such that similar results to the sophisticated three-dimensional numerical models become achievable by adjusting them. To derive the distribution of the y-multipliers  $Mult_y$ , more than 150 finite element FE models of the pile-soil system with various dimensions were performed under different soil conditions and various load levels.

Fig. 7-10 shows an essential analysis based on the two reference systems, introduced in section 6.2, for obtaining an appropriate distribution of the y-multipliers  $Mult_y$ . Based on the displacement-controlled calculations for reaching a lateral displacement  $y = 12.5$  mm at the pile head, a flexible and almost stiff pile behaviour is analysed with the wall thickness  $t = 20$  mm and  $t = 200$  mm, respectively. The results of both reference systems are available in terms of pile deflection lines, bedding soil resistance, and the quotient of secant bedding stiffness, which are obtained by the exclusive application of newly derived “basic p-y curves”, i.e. y-multipliers  $Mult_y = 1$ , and the results of the numerical simulation calculated subjected to monotonic loading conditions.

For both pile-soil systems, the new analytical method definitely results in a softer displacement behaviour, as revealed by the deflection lines, when compared to the numerical results. Nevertheless, the bedding resistances at the upper part of the pile are relatively similar among them. Indeed, the most discrepancies related to the bedding soil resistance are found near the pile tip since the new analytical method based on y-multipliers  $Mult_y = 1$  does not consider shearing stress resulting from the pile-soil interaction around the pile tip, yielding a sharp sub-prediction of the bedding soil resistance near the pile base. Consequently, the so-called “pile tip effect” has to be definitely included in the new modelling approach by applying it in  $Mult_y$ .

For identical loading conditions, the quotients  $E_{py}^{FEM} / E_{py}^{Mult_{py}=1}$  of the secant bedding stiffness between the new analytical method (assuming the y-multipliers  $Mult_y = 1$ ) and the numerical results are represented in Fig. 7-10 (left). The quotient of secant bedding stiffness allows a precise evaluation of the deviations of both analysis methods. Here, quotients less than 1 indicate that the “basic p-y curves” behave stiffer than those resulting from the numerical simulations. Obviously, the behaviour for quotients higher than 1 is the opposite. The distribution of the quotients along the pile length indirectly reveals the profile of the y-multipliers  $Mult_y$  when comparable results to numerical models are expected to be obtained. In this manner, the calibration of the y-multipliers  $Mult_y$  by considering pile-soil systems under various soil conditions and pile geometries is feasible.

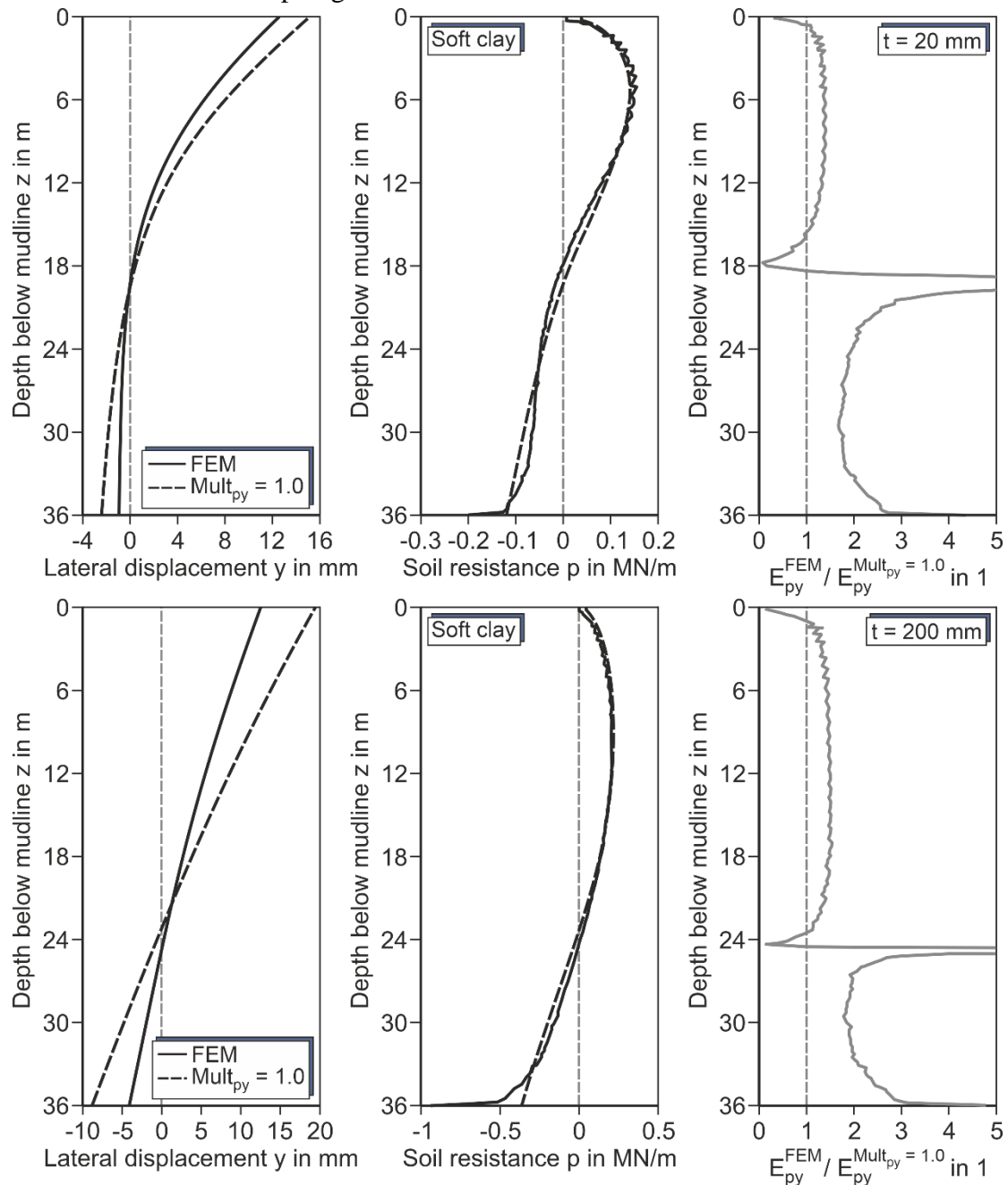


**Fig. 7-10: Comparison of secant bedding stiffness obtained from FEM and new modelling approach based on  $Mult_y = 1.0$  ( $D = 6$  m,  $L = 36$  m, soft clay)**

For both examined pile stiffnesses in Fig. 7-10, the secant bedding stiffness resulting from the new modelling approach with  $\text{Mult}_y = 1$  is clearly underpredicted along almost the entire pile length compared to the numerical results, while only above the zero-deflection point  $z_0$  and near the soil surface the secant bedding stiffness is overpredicted. The course of the deflection lines also confirms these trends.

The y-multipliers  $\text{Mult}_y$  used for adjusting the “basic p-y curves” are made up of two components  $\text{Mult}_{y,\text{bend}}$  and  $\text{Mult}_{y,\text{tip}}$ , representing the adjustment due to the influence of the deflection line as well as the shearing stress to the pile base on the bedding soil resistance, respectively.

$$\text{Mult}_y = \text{Mult}_{y,\text{bend}} + \text{Mult}_{y,\text{tip}} \quad (7-12)$$

In contrast to the p-y approach introduced by Thieken et al. (2015a) for non-cohesive soils, the new modelling approach considers a main base function meaning without the application of support points. Therefore, the y-multipliers  $\text{Mult}_y$  has to be directly applied to the hyperbolic function, as given in Eq. 7-13.

$$\bar{y} = y \cdot \text{Mult}_y \quad (7-13)$$

In other words, for calculating the soil resistance  $p$ , the lateral displacement  $y$  must be adjusted by  $\text{Mult}_y$ . By doing so, the initial stiffness  $K_i$  is also influenced by using the so-called y-multipliers.

To derive the y-multipliers  $\text{Mult}_y$ , both pile deflection line and pile geometry characteristics are considered for the correct prediction of the pile’s load-bearing behaviour. The adjustment of the bedding soil resistance mainly results from the application of  $\text{Mult}_{y,\text{bend}}$ , which consists of three segments characterised by the following equations:

$$\text{Mult}_{y,\text{bend}} = \frac{y}{y_{\text{max}}} \cdot 0.7 + 0.8 \quad \text{if } z \leq z_{y_0} \quad (7-14)$$

$$\text{Mult}_{y,\text{bend}} = \frac{y}{y_{\text{min}}} \cdot 0.7 + 0.8 \quad \text{if } z_{y_0} < z \leq z_{y_{\text{min}}} \quad (7-15)$$

$$\text{Mult}_{y,\text{bend}} = \frac{y}{y_{\text{min}}} \cdot 0.7 + 0.8 \geq 1.0 \quad \text{if } z > z_{y_{\text{min}}} \quad (7-16)$$

The distribution of the y-multipliers  $\text{Mult}_{y,\text{bend}}$  for adjusting the deflection line turns out to be a function of the pile's deformation behaviour described by the maximum deflection  $y_{\text{max}}$  at the pile head and the minimum deflections  $y_{\text{min}}$ . The inclusion of representative depths such as the zero-deflection point  $z_{y_0}$  and the minimum deflection  $z_{y_{\text{min}}}$  commonly assumed beneath  $z_{y_0}$  is also required for its implementation.

Likewise, the y-multipliers  $\text{Mult}_{y,\text{tip}}$  that consider the so-called “pile tip effect” directly depend on the pile geometry such as pile length  $L$  and pile diameter  $D$ , as follows:

$$\text{Mult}_{y,\text{tip}} = 2.5 \cdot \left( \frac{z-L}{2 \cdot D} + 1 \right)^5 \quad \text{if } z > L - 2 \cdot D \quad (7-17)$$

$$\text{Mult}_{y,\text{tip}} = 2.5 \cdot \left( \frac{z-L}{2 \cdot D} + 1 \right)^5 + 3 \quad \text{if } z > L - 0.1 \cdot D \quad (7-18)$$

Certainly, the pile geometries define the distribution of the  $\text{Mult}_{y,\text{tip}}$  fitted by two well-defined segments. The bedding soil resistance is clearly increased by applying Eq. 7-17 for describing adequately the relation of the stress-deformation near the pile tip.

## 7.8 Summarised calculation procedure

For determining the horizontal load-bearing behaviour of the pile foundation in cohesive soils subjected to short-term monotonic loading conditions, the new modelling approach is calibrated from the results of a set of validated three-dimensional numerical simulations.

For solving the one-dimensional numerical model, i.e. the beam line supported by a number of uncoupled non-linear spring characteristics (also known as p-y curves) an iterative procedure is required for finding the equilibrium of the non-linear pile-soil system. For the new modelling approach, an iterative procedure has to be carried out similarly to the usual conditions of traditional p-y approaches proposed by OGLs, but also considering that the iterative process keeps going until the pile deflection remains unchanged between iteration steps due to the application of y-multipliers  $\text{Mult}_y$  for adjusting the stiffness of “basic p-y curves”.

The iterative procedure starts by applying the unmodified “basic p-y curves”, setting the distribution of the y-multipliers  $\text{Mult}_y = 1.0$  for obtaining the respective pile deflection line, which shall be applied for determining the respective  $\text{Mult}_y$  in the next iteration step, and so on. Obviously, the y-multipliers are constantly modified in dependence of the calculated deflection lines during the iterative process, but when the convergence is achieved for the pile head displacement, they remain unchanged.

It is remarkable that the corresponding adjustment of the “basic p-y curves” during the iteration process takes place only in the pile displacements  $y$  but not in the bedding soil resistance  $p$ . Meaning that only the stiffness of the “basic p-y curves” changes. In other words, values greater than one of the y-multipliers mean that the p-y curves show a stiffer behaviour than the corresponding “basic p-y curves”, whereas the opposite occurs for values less than one.

The new modelling approach is almost identically implemented to the traditional p-y approaches in the pile design programme IGtHPile (cf. section 4.6) but including the additional condition by using the y-multipliers, which did not mean a significant increase in calculating time.

Fig. 7-11 provides a complete scheme of the calculation procedure along with the respective formulation of the innovative modelling approach using the y-multipliers  $\text{Mult}_y$  applied to the “basic p-y curves”. The formulation required for the construction of the introduced “basic

p-y curves” is depicted at the top of the figure. Similarly, the development of y-multipliers  $Mult_y$  is included at the bottom. Altogether, they describe the pile's behaviour subjected to short-term monotonic lateral loading conditions comparable to the results of the sophisticated FE numerical models introduced in chapter 5.

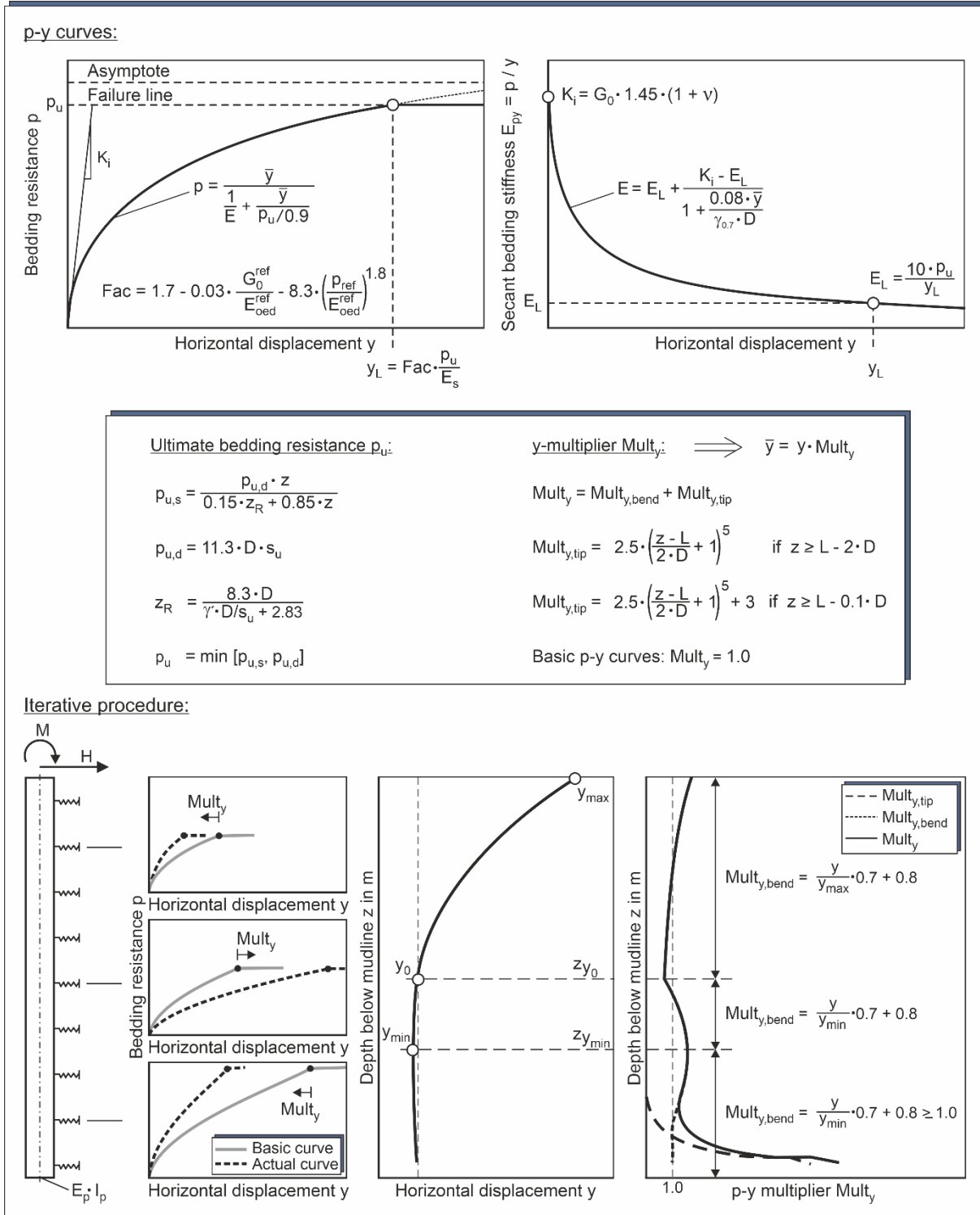


Fig. 7-11: Definition and equations for the new modelling approach



## 8 Evaluation of the new modelling approach

### 8.1 General

The following chapter deals with the evaluation of the new modelling approach used for predicting the horizontal load-bearing behaviour of pile foundations with varied geometries embedded in different cohesive soil conditions.

The comprehensive parameter study presented here provides a systematic comparison of the results obtained from the new modelling approach and the p-y approach recommended by API (2014) with the validated three-dimensional numerical simulations. The effect of varying the pile geometries and the soil conditions on the pile behaviour is analysed. By doing so, the precision level in predicting the non-linear response of the pile-soil system subjected to monotonic lateral loading conditions of the new modelling approach is thoroughly examined by comparing it to the numerical results.

Note that the Timoshenko beam theory used for analysing the laterally loaded piles is performed by the pile design programme IGtHPile, in which the new modelling approach and the conventional p-y approaches were successfully applied. Neither the self-weight of the pile nor additional vertical loads are considered since it is mainly lateral loading conditions, which are taken into account.

### 8.2 Comparison between numerical and analytical solutions

The new modelling approach derived from a set of numerical simulations is examined in terms of the distribution of deflection line, bending moment and bedding resistance along the embedded pile describing its local pile-soil interaction, as well as the load-displacement curve with the respective secant stiffness-displacement curve at the pile head, characterising the horizontal pile's load-bearing behaviour.

To this effect, two representative pile-soil systems with different pile geometries are evaluated in detail by comparing the predicted non-linear response of the pile-soil system. It can be verified that the new modelling approach can be used for either flexible pile foundations or rigid monopile foundations.

As the first pile-soil system, a typical pile foundation for a jacket substructure with a diameter  $D = 1$  m, a pile length  $L = 12$  m, a load eccentricity  $h = 5$  m, and a wall thickness  $t = 11.35$  mm embedded in medium soft clay is considered for examining the suitability of the new modelling approach with regard to the numerical results.

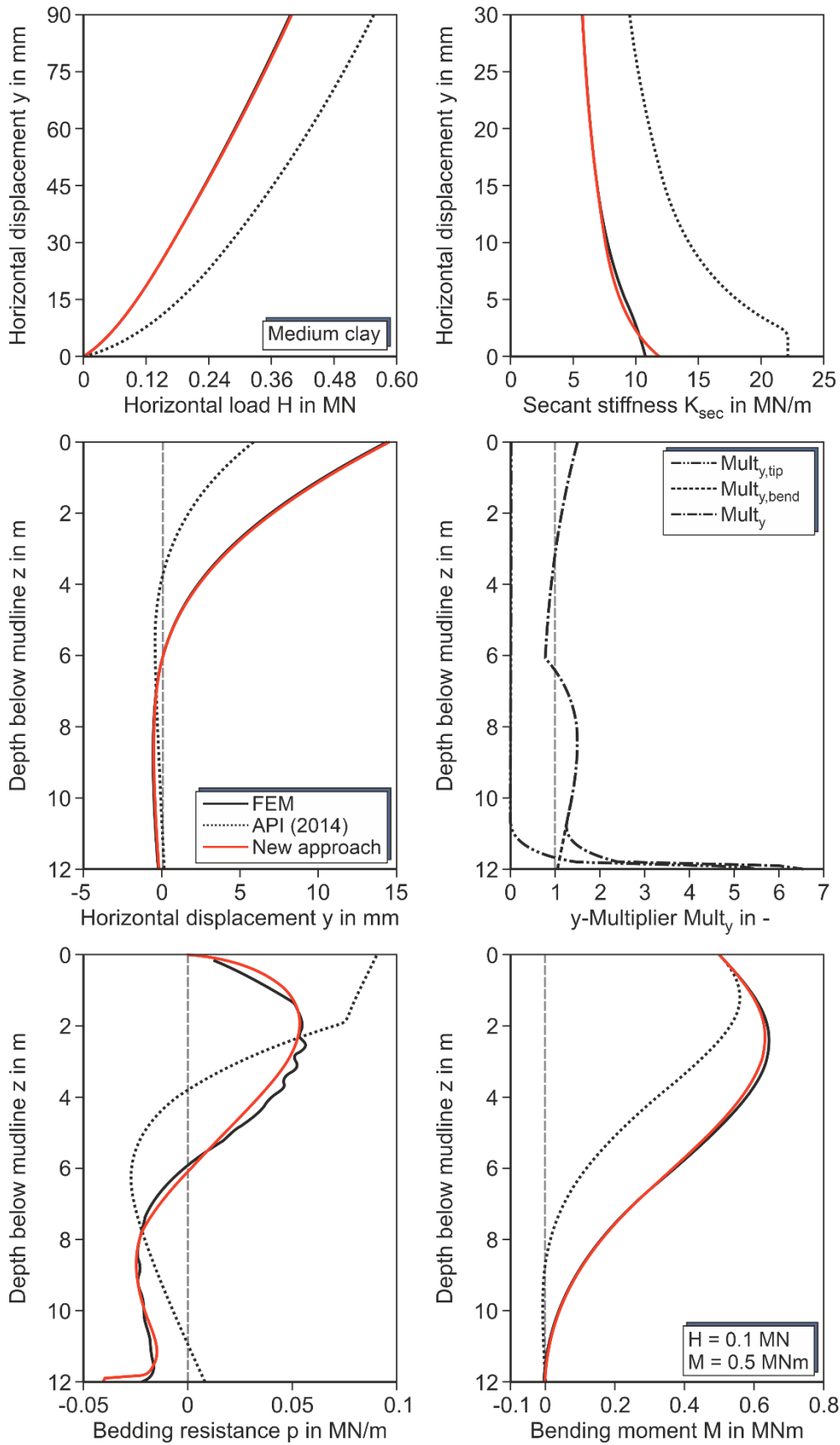


Fig. 8-1: Evaluation of the results obtained from the FEM, API (2014) and the new modelling approach for a slender pile foundation ( $D = 1$  m,  $L = 12$  m, medium soft clay)

Fig. 8-1 (see the two upper figures) shows the load-displacement curves and their respective secant stiffness-displacement curves at the pile head, directly computed by the FEM simulations and those predicted by applying the new modelling approach. This represents a direct insight into the horizontal load-bearing behaviour of the examined pile-soil system. For completeness, the results obtained from the p-y approach proposed by API (2014) are also included in the graphs with the purpose of comparison. The results of the new modelling approach match quite well with the outcomes of the numerical simulations, contrary to the p-y approach recommended by API (2014).

Similarly, the local behaviour along the embedded pile is evaluated in terms of deflection line, bedding resistance, and bending moment, as represented in Fig. 8-1 (centre, bottom). In addition, the respective y-multipliers used for reaching the equilibrium of non-linear pile-soil systems are also exhibited so that its distribution can be appreciated for the lateral loading condition  $H = 0.1$  MN. The new modelling approach reproduces the pile deflection line and the bending moment substantially better than API (2014) method when compared to the numerical results for such load level condition. The bedding resistance distribution over depth resulting from the new modelling approach exhibits slight deviations but they are marginal compared to API (2014) approach.

Based on the reference system introduced in section 6.2, the second selected pile-soil system is a monopile foundation with a diameter  $D = 6$  m, an embedded pile length  $L = 36$  m, a load eccentricity  $h = 30$  m, and a wall thickness  $t = 36.35$  mm in medium soft clay. Thus, it also examines the validity of the new modelling approach, but in this case for large diameter piles that are laterally loaded, similar to those found on wind farms.

The profile of the deflection line, the bedding resistance, and the bending moment along the pile length, obtained from the analysis methods, are depicted in Fig. 8-2 (centre, bottom). The predictions of the new modelling approach reflect the numerical results quite well for a load level  $H = 5$  MN, in opposition to that provided by the p-y method proposed by API (2014). This good agreement is directly associated with the horizontal load-bearing behaviour of the pile-soil system, which obviously also exhibits an excellent match regarding the load-displacement curves and its respective secant stiffness-displacement curves at the pile head (see upper figures).

The comparative study again confirms that, as expected, when the soil reactions determined from the three-dimensional finite element model are reproduced by the new modelling approach, the overall calculated non-linear response of the pile-soil system is similar to that obtained using the three-dimensional FE simulations. The slight discrepancies between the response of FE simulations and new modelling approach are negligible and attributed to a combination of factors such as the simplification and ease of use of the proposed formulation. Thus, it indicates that the new modelling approach turns out to be robust.

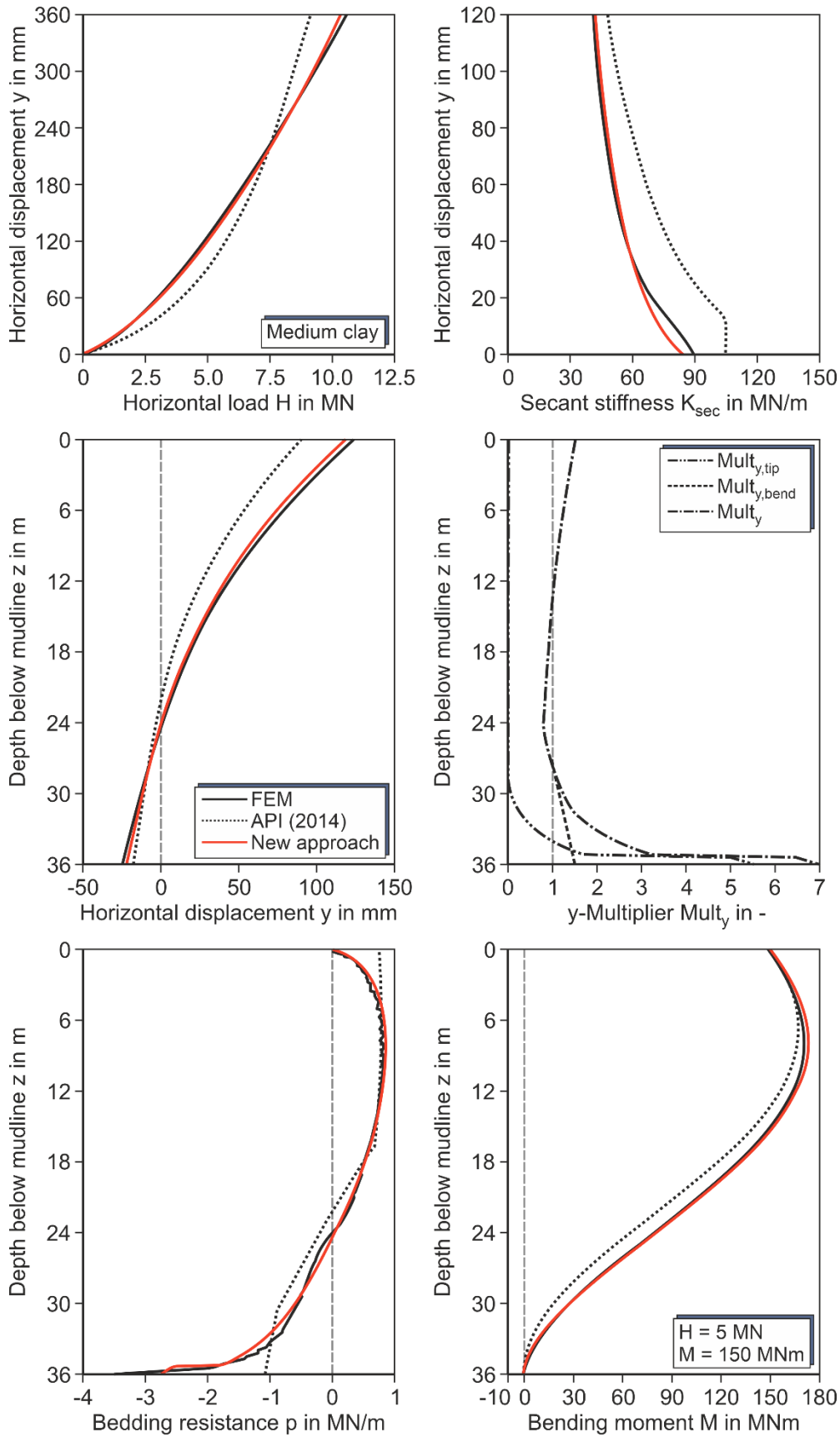


Fig. 8-2: Evaluation of the results obtained from the FEM, API (2014) and the new modelling approach for a monopile foundation ( $D = 6$  m,  $L = 36$  m, medium soft clay)

The two selected pile-soil systems clearly demonstrate that the application of the new modelling approach is quite suitable for both rigid and flexible pile foundations when it comes to the general design of laterally loaded pile foundations of OWT structures.

### 8.2.1 Parametric study for evaluating the new modelling approach

A comprehensive parametric study applying the new modelling approach for the analysis of laterally loaded piles is carried out for evaluating its validity compared to FE simulations. For this purpose, the numerical simulation was extrapolated to around 400 pile-soil systems. The variation of the pile geometries proceeds under similar boundary conditions as introduced in section 6.3.1 used for traditional p-y methods, i.e. a wide range of pile diameters  $D$  from 0.5 to 8 m and relative lengths  $L / D$  ranging from 4 to 12. Normalisation of the eccentricity of the load  $h$  and the wall thickness  $t$  as a function of the pile diameters  $D$  is also used. Three clay consistencies (i.e. very soft clay, soft clay, and medium soft clay) represent the soil characteristics that are considered by applying three normalised head displacements at the pile head (e.g.  $y = 0.0005 \cdot D$ ,  $y = 0.01 \cdot D$ , and  $y = 0.03 \cdot D$ ). Thus, an appropriate capture of the horizontal load-bearing behaviour of the pile embedded in cohesive soils becomes feasible for various load levels.

The quotients of the lateral stiffness  $Q_K = K_{p-y} / K_{FEM}$  at the pile head obtained from the new modelling approach and the FE simulations are used for comparison reasons. The quotient  $Q_K = 1$  represents a perfect match between the results obtained from both analysis methods. This implies that pile-soil systems with quotients greater than 1 behave stiffer when compared to the results of the numerical simulations. A softer behaviour obviously occurs for values less than one. The contour plots used for the present study provide a useful outcome for identifying such deviations resulting from the comparison of the analysis methods. The black dots represent the supporting points for building the contour plots, each one representing a calculation result of one pile-soil system.

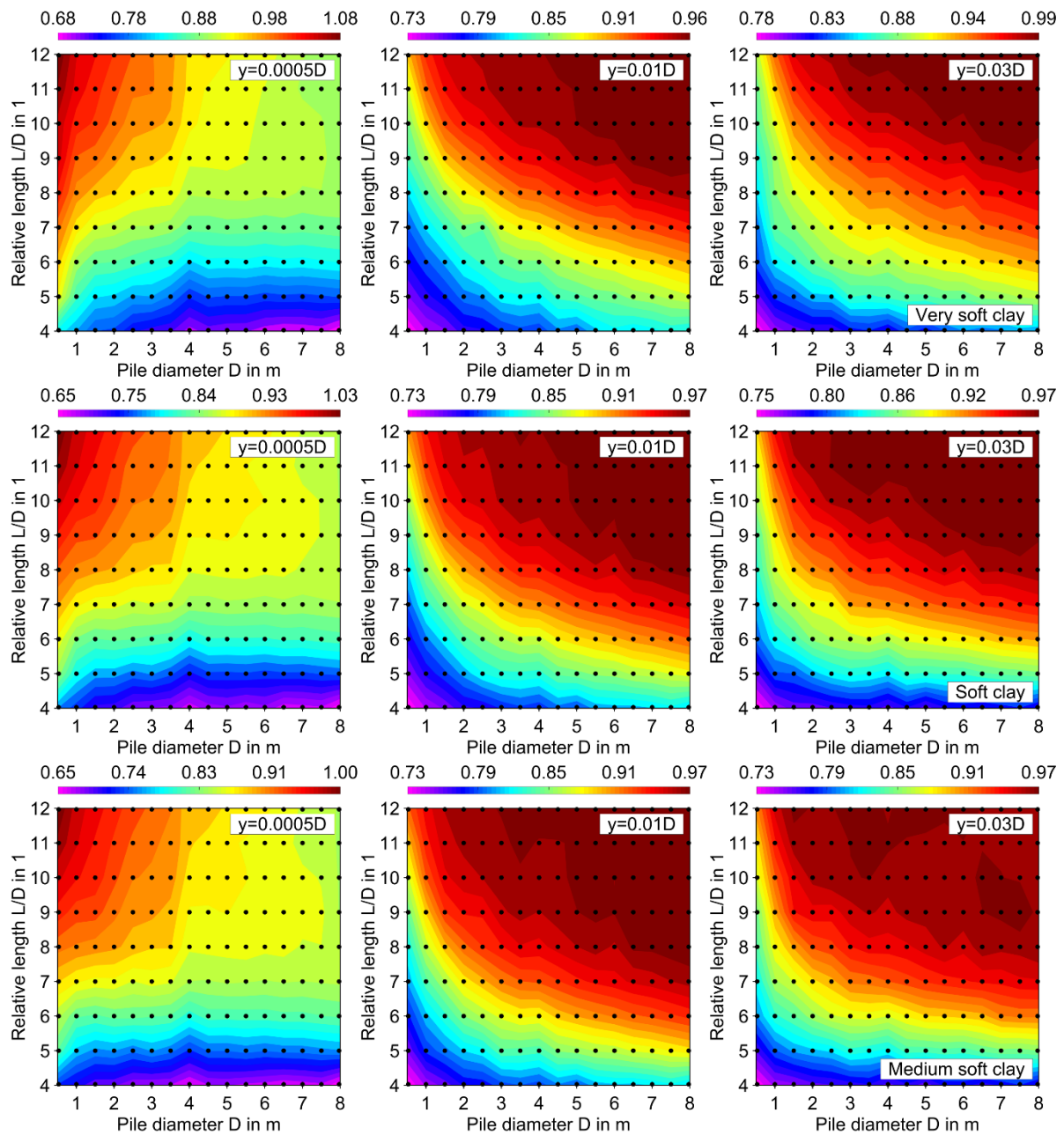
For the comprehensive parametric study presented here, it became necessary to conduct the analysis of laterally loaded piles twice, having as a unique variant the application of the  $y$ -multipliers  $Mult_y$  on the “basic p-y curves”. In other words, the first one considers that  $y$ -multipliers are set to 1.0, i.e. they do not modify the stiffness of “basic p-y curves”, while for the second one the  $Mult_y$  are normally applied in the calculation procedure. By doing so, the effect of its application can be visibly distinguished on the prediction of the horizontal pile’s load-bearing behaviour.

Fig. 8-3 shows the quantitative discrepancy distribution of the lateral secant stiffness obtained from the new modelling approach with respect to the numerical simulations at the pile head by applying  $Mult_y = 1.0$ . For the three soil consistencies (i.e. very soft clay, soft clay, and medium soft clay) examined in this study, it was found that the deviation patterns have relatively identical trends among them, varying in a range of quotients from 0.65 to 1.08.

Evidently, for the smallest normalised head displacement  $y = 0.0005 \cdot D$ , the new modelling approach leads to the most discrepancies in comparison to the results of numerical simulations

(Fig. 8-3, left). Both over- and underpredictions of the foundation stiffness result from the new modelling approach in dependence of the pile dimensions compared to the results of numerical simulations.

For larger head displacements (i.e.  $y = 0.01 \cdot D$ , and  $y = 0.03 \cdot D$ ), a relatively good agreement of foundation resistance can be found for relative pile lengths greater than 6 (cf. Fig. 8-3, centre, right). An overestimation of the pile head displacement occurs for large pile diameters and small relative lengths, which approximately corresponds to the dimensions of typical monopile foundations.



**Fig. 8-3: Quotient of lateral stiffness  $K_{p-y} / K_{FEM}$  based on the new modelling approach and FEM without applying  $y$ -multipliers**

Evidently, pile-soil systems with small relative lengths  $L/D$  are mostly affected in case of the non-application of  $Mult_y$ , when it comes to an adequate prediction of the horizontal load-bearing behaviour evaluated by the lateral stiffness at the pile head. The main reason for the resultant pile's behaviour is the consequence that it does not include the influence of the "pile tip effect" by not applying  $Mult_{y,tip}$ . The deviations derived from relatively slender pile foundations are mainly related to the non-interaction between the deflection line and the bedding soil resistance provided by  $Mult_{y,bend}$ .

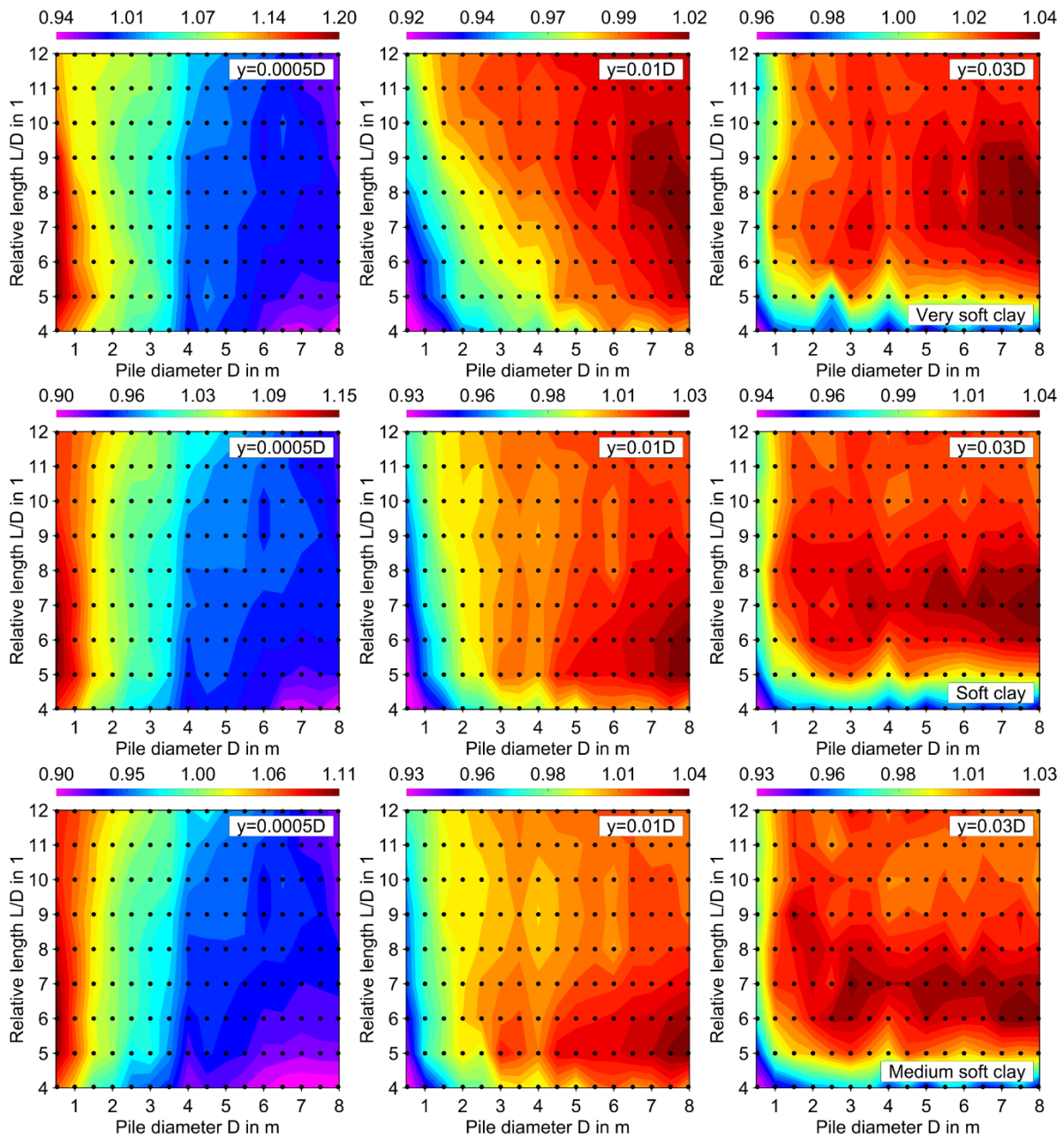


**Fig. 8-4: Quotient of lateral stiffness  $K_{p-y} / K_{FEM}$  based on the new modelling approach and FEM applying  $y$ -multipliers**

In contrast, in Fig. 8-4, the lateral stiffness at the pile head for very soft clay, soft clay, and medium soft clay match very well when employing the new modelling approach applying the "basic p-y curves" in conjunction with the respective  $y$ -multipliers  $Mult_y$ .

The prediction accuracy of the pile's load-bearing behaviour substantially improves, causing the contour plots to not present a smooth image of the discrepancies due to the small differences between the corresponding results. For large head displacements ( $y = 0.01 \cdot D$  and  $y = 0.03 \cdot D$ ), the quotient  $Q_K$  of the lateral stiffness can be found by varying over the range 0.92 to 1.04, demonstrating a great improvement compared to the  $Q_K$  range from 0.5 to 3.5 resulting from the p-y approach proposed by API (2014). For smaller head displacements ( $y = 0.0005 \cdot D$ ), an underprediction of the head displacements for pile diameters  $D < 0.5$  is evident. However, the quotient of the lateral stiffness lies in the range of 0.9 to 1.2, also resulting in a clear improvement compared to that given by the p-y methods recommended by API (2014), concretely within a  $Q_K$  range from 0.2 to 3.8, as seen in section 6.3.1.

In conclusion, despite the slight discrepancies resulting from the variation in pile geometry, the application of the new modelling approach represents a clear improvement in the prediction of pile behaviour when compared to the results obtained from traditional p-y methods.

The remaining parameters used for modelling the pile-soil system that also affect the non-linear response of the pile foundation subjected to lateral loading conditions will be evaluated in the following for obtaining a clear appreciation of the prediction capabilities of the new modelling approach. Based on the reference system parameters introduced in section 6.2, the secant bedding stiffness  $K = H / y$  resulting from the numerical and analytical methods are also determined for five predefined head pile displacements (e.g.  $y = 3, 30, 60, 120,$  and  $180$  mm) which are eventually used for evaluating all case studies. By doing so, the quotients of the lateral stiffness  $Q_K = K_{p-y} / K_{FEM}$  at the pile head are likewise applied for comparing the results of the analysed methods using one-dimensional graphs with an exclusive variation of the analysed parameters. In addition, the results obtained from the reference systems are properly indicated by filled symbols to be identified for its respective evaluation.

In addition to the variation in pile diameters and relative pile lengths, other geometric characteristics of the piles such as load eccentricity  $h$  and wall thickness  $t$  are also discussed for analysing the laterally loaded piles by using the analysis methods. The deviations of the lateral secant stiffness computed by the FE simulations and the new modelling approach are depicted in Fig. 8-5. For comparison purposes, the corresponding results obtained from the p-y approach proposed by API (2014) are also included in the graphs.



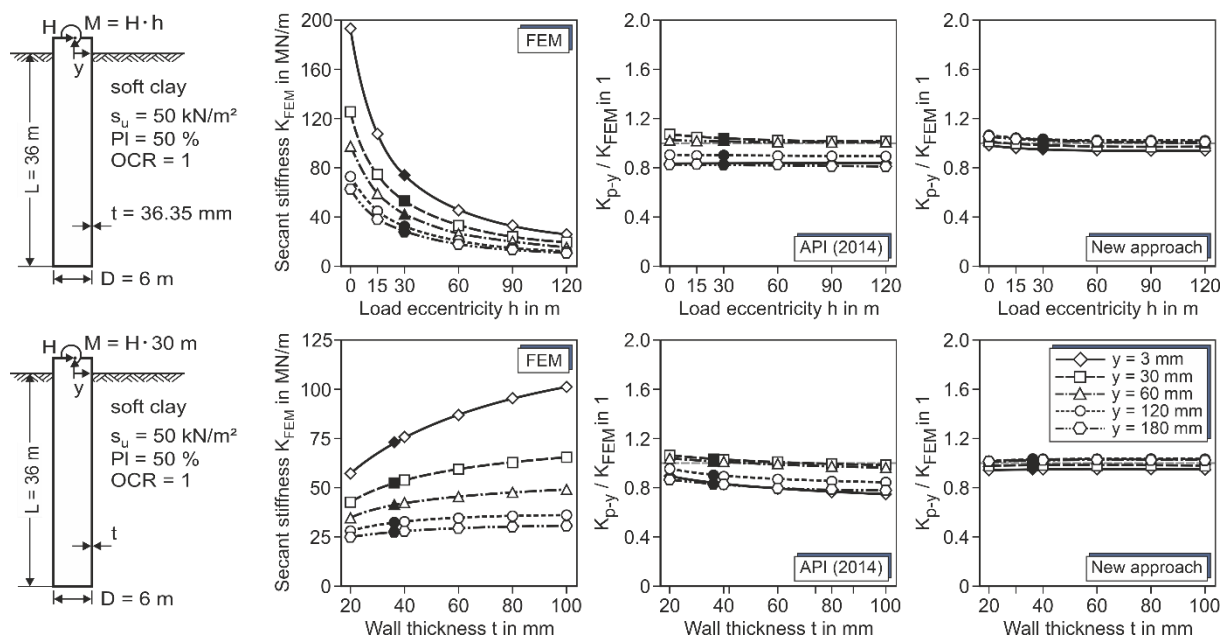


**Fig. 8-5: Parameter study for the evaluation of the new modelling approach based on the variation of the remaining geometrical pile parameters**

The first row of Fig. 8-5 depicts the variation of the load eccentricities  $h$  over a wide range from 0 m to 120 m. From the numerical results, the decay of lateral secant stiffness at the head pile is clearly recognisable with increasing load eccentricities  $h$ , which also leads to the upwards movement of the zero-deflection point  $z_0$  of the pile. The deviations of the results obtained from the p-y approach proposed by API (2014), in comparison to the numerical results, are greater than the ones obtained from the new modelling approach. The latter shows a remarkable improvement of the prediction in all lateral displacements. The quotients  $Q_K$  of the lateral bedding stiffness between the new analytical method and numerical analysis reveal deviations ranging from 0.94 to 1.06.

A further parametric study depicted in the second row of Fig. 8-5 highlights the effect of the wall thickness  $t$  on the lateral foundation stiffness. The numerical results show the increment of the bedding stiffness with increasing wall thickness  $t$ , particularly, for the smallest head displacement  $y = 3$  mm. Basically, an underestimation of the bedding soil resistance is obtained by applying the recommended OGL approach while the new modelling approach offers a good approximation to the results obtained from the numerical simulations. A small range of almost constant deviations lies within the  $Q_K$  range between 0.95 and 1.04.

Similarly, the variation of individual soil parameters such as undrained shear strength  $s_u$ , plasticity index PI, and soil stiffness factor defined by  $f_{Es}$  and  $f_{G0}$  (cf. Table 6.3) is also conducted based on the reference system parameters, thus providing an extensive evaluation for testing the suitability of a new modelling approach with regard to numerical results. It turned out that the new analytical method provides a much better fit with the FE simulation results in contrast to the conventional p-y approach recommended by API (2014), as shown in Fig. 8-6.

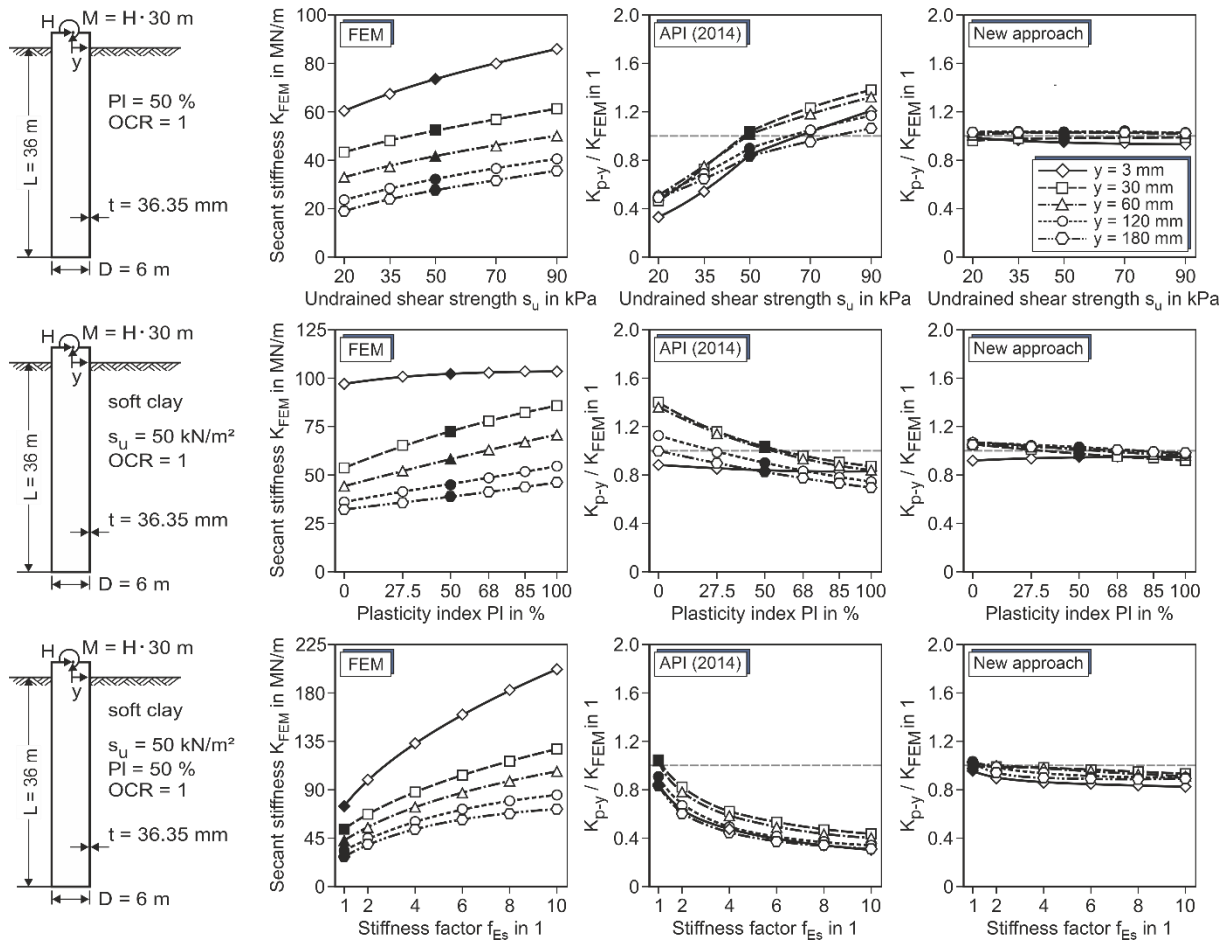


**Fig. 8-6: Parameter study for the evaluation of the new modelling approach based on the variation of the remaining soil condition parameters**

The first row of Fig. 8-6 depicts the variation of soil consistency in terms of the undrained shear strength  $s_u$  ranging from very soft clay  $s_u = 20$  kPa to medium soft clay  $s_u = 90$  kPa. The foundation stiffness resulting from the numerical simulations becomes higher with increasing the undrained shear strength  $s_u$  for all normalised head displacements. An overestimation of the pile head displacements for very soft clay but also an overestimation of the foundation stiffness for medium soft clay came out by applying API (2014) approach when compared to the numerical results. In this parametric study, it becomes clearly apparent that the new modelling approach for predicting the horizontal pile’s load-bearing behaviour is superior, producing marginal deviations of  $Q_K$  ranging from 0.93 to 1.04.

The influence for varying the plasticity index PI related to the shear strain  $\gamma_{0.7}$  according to Stokoe et al. (2004) is evaluated in the second row of Fig. 8-6. The numerical results reveal that the influence of soil plasticity on the foundation stiffness at the pile head is practically insignificant for the smallest normalised head displacements in contrast to the other displacements considered, i.e. the initial stiffness represented by the head displacement  $y = 3$  mm remains almost unaffected. In the p-y formulation proposed by API (2014), the plasticity index PI is not considered as an input parameter for describing the non-linear behaviour of the pile-soil systems. It was therefore to be expected that the respective deviations occur when compared with the numerical results. Again, the superiority of the new modelling

approach is demonstrated due to the integration of the PI parameter into the basic function, i.e. by using the hyperbolic function. The deviations represented by  $Q_K$  are certainly smaller than that resulting from API (2014) approach, ranging from 0.93 to 1.07.

In the parametric study, special focus should be laid on the changing soil stiffness, related to the oedometric stiffness modulus and the dynamic shear modulus, due to its substantial increase up to 10 times the original values, as depicted in the third row of Fig. 8-6. An overestimation of the pile head displacements resulting from p-y approach recommended by OGLs is evident, resulting in large deviations up to  $Q_K = 0.4$ . The overestimation of all lateral head displacements results from the disregard of the soil stiffness as an independent input parameter in the traditional p-y approach but is related to the strength parameters and thus remains constant when the soil stiffness factor is increased. It is noteworthy that the new analytical method offers a great advantage due to the distinction between soil stiffness and shear strength parameters. Despite the extreme increase in soil stiffness that usually occurs in over-consolidated soils, the new modelling approach delivers good compliance with respect to numerical results by varying the deviations from 0.83 to 1.03.

To conclude the aforementioned parametric study on the suitability of the new modelling approach, the effect of coupled soil parameters such as the over-consolidation ratio OCR, plasticity index PI and soil stiffness factor (e.g.  $f_{Es}$  and  $f_{G0}$ ) on the pile's load-bearing behaviour are also analysed, as depicted in Fig. 8-7. The numerical simulations executed in Plaxis 3D offer the capability to perform such combinations of soil conditions, thus allowing the reliability of the new analytical method to be demonstrated.

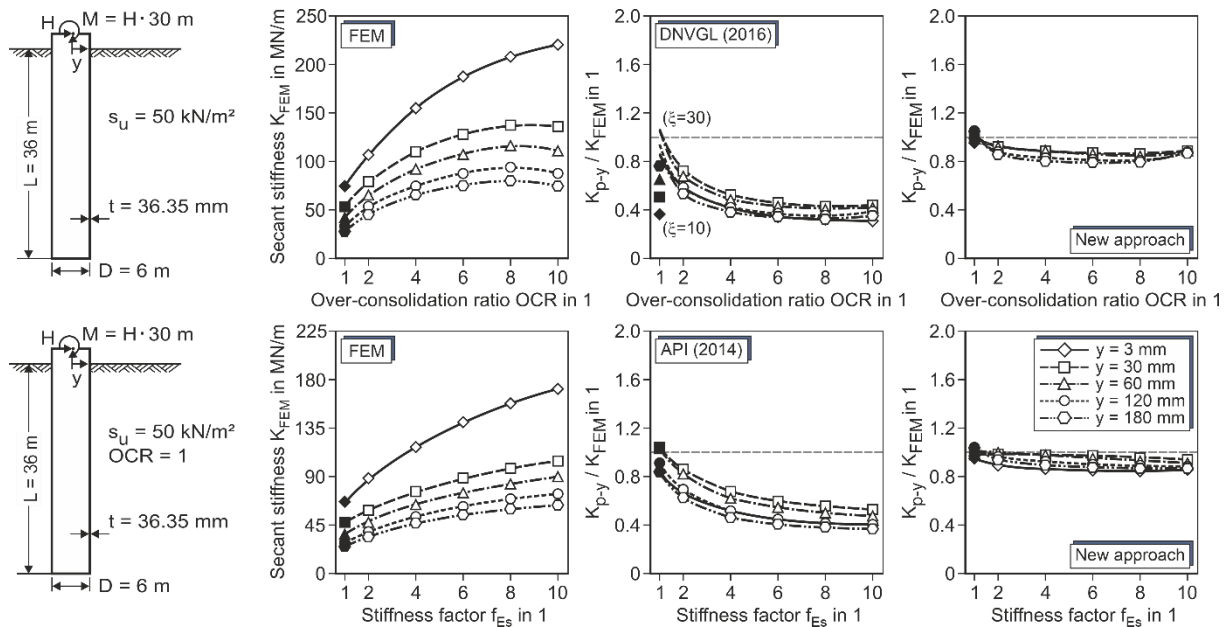


**Fig. 8-7: Parameter study for the evaluation of the new modelling approach based on the variation of coupled soil condition parameters**

To ensure that the parametric study also regards the over-consolidation ratio, coupled soil parameters described in Table 6-3 are also applied. Similar to the previous parametric study, the shear strength parameters are not depth dependent.

Even though the p-y approach recommended by DNVGL (2016) considers the over-consolidation ratio as an input parameter, a poor prediction of the bedding soil resistance results, reaching a quotient of up to 0.4 in the worst case. It becomes clear that the new modelling approach predicts the pile behaviour much better than traditional methods when compared to the numerical result. However, the deviations of  $Q_K$  reach around 0.79 due to the lack of consideration of the over-consolidation ratio OCR within its formulation. As seen in a previous study represented in Fig. 6-14, the over-consolidation ratio OCR contributes modestly to the prognosis of the lateral stiffness foundation. Therefore, the new modelling approach omitted its application to avoid a complicated p-y formulation resulting in the deviations shown in the first row of Fig. 8-7 (right).

For completeness, the parameter study represented in the second row of Fig. 8-7 is conducted, in this case, the soil condition is normally consolidated clay, i.e.  $OCR = 1$ , but the variation of the other soil parameters such as plasticity index PI and stiffness soil factors  $f_{Es}$  and  $f_{G0}$  remain for calculating the load-bearing behaviour of the pile. It becomes clear that the predictions of lateral stiffness are considerably improved by varying up to 0.87 using the new analytical method. By contrast, for the traditional p-y method, the strong overestimation of the lateral head displacements persists when compared to the numerical results.

### 8.2.2 Undrained shear strength $s_u$ linearly increasing over depth

Particularly in the offshore zones of the North Sea and Baltic Sea, where monopile foundations are commonly used for supporting the OWT structures, it is frequently found that over-consolidated clays with non-linear behaviour result in a considerable increase in stiffness and shear strength properties over depth. To test the predictive capabilities of the new analytical method, the non-linear soil response of the pile foundation is therefore also analysed by considering that the undrained shear strength parameters  $s_u$  increase linearly over depth.

Similar to the previous parametric study, the local behaviour of the pile-soil interaction and the horizontal load-bearing behaviour represented by the lateral secant stiffness at the pile head remains to be evaluated under such soil conditions. Based on the geometrical parameters of the reference system introduced in section 6.4 corresponding to a monopile foundation, a parametric study is again carried out, but taking into account the soil condition parameters listed in Table 6-4, which reflects the depth-dependent shear strength parameters relevant in this section. The non-linear soil response obtained by increasing soil stiffness and shear strength over depth that leads to realistic soil profile conditions, is captured by the respective analysis methods for the extensive comparative study of laterally loaded piles.

From a soil profile with increasing shear strength parameters, Fig. 8.8 depicts the behaviour of laterally loaded piles predicted from the numerical simulations and the new modelling approach, also including the results of the p-y approach recommended in API (2014).

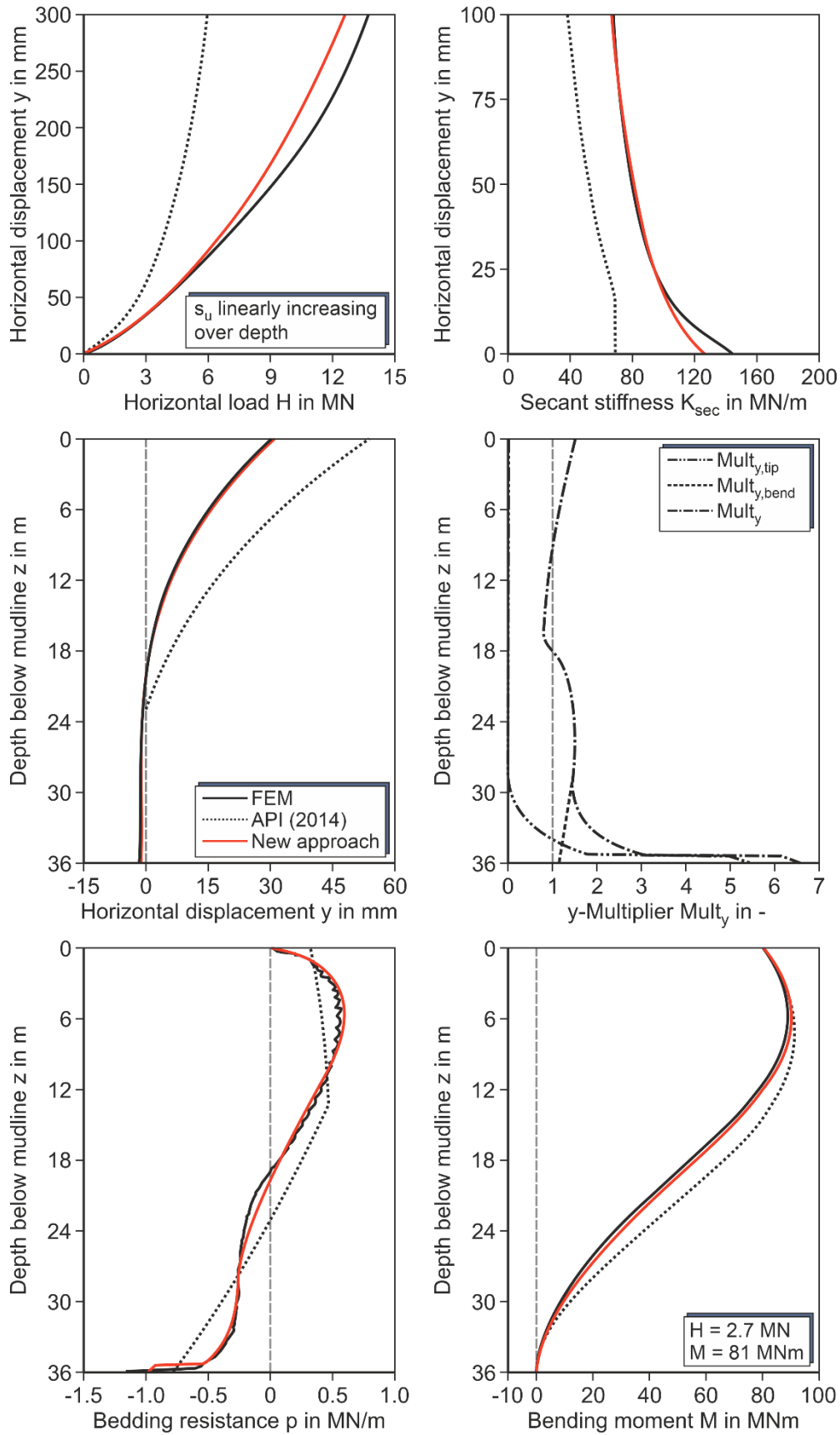


Fig. 8-8: Evaluation of the results obtained from the FEM, API (2014) and the new modelling approach for the reference system with linearly increasing undrained shear strength ( $D = 6$  m,  $L = 36$  m)

The results of the new modelling approach closely match that of the three-dimensional numerical simulations not only to be demonstrated for the local pile-soil interaction but also the horizontal load-bearing behaviour of the pile, as shown in Fig. 8-8.

Despite a moderate deviation yielded in large deformations at the pile head, the resulting pile load-displacement response demonstrates that the new analytical method is well suited to predict the response of monotonic laterally loaded monopile foundations embedded in clay that are represented by three-dimensional finite element modelling, as demonstrated in the upper figures. This is a significant improvement over the ability of the existing p-y approach proposed by API (2014) considering depth-dependent shear strength parameters.

For the lateral loading condition  $H = 2.7$  MN, the resultant internal forces confirm the ability of the calibrated new analytical approach to accurately predict the pile behaviour with linearly increasing undrained shear strength  $s_u$  over depth. Thereby, the respective y-multipliers  $Multi_y$  are also applied, leading to accurate predictions of the pile response to prescribed actions. It highlights that the resulting peak in the distribution of bedding resistance and bending moment fit quite closely, in contrast to API (2014) p-y approach.

In the following, the quotients  $Q_K$  of the lateral secant stiffness at the pile heads for the normalised head displacements are depicted in Fig. 8-9. The appropriate correlation between the new modelling approach and the numerical simulations indicates that the fundamental physics of the behaviour of the pile-soil system is well simulated for varied pile geometries and soil conditions, and also that the p-y approach proposed by API (2014) is not suitable for predicting the non-linear embedded response of monopile foundations in soft clay.

The new modelling approach appears to provide a reasonably good match with the results obtained from the three-dimensional numerical simulations. A similar pattern of deviations compared to the soil profiles without depth-dependent shear strength parameters is found for the normalised head displacement predictions, but with slightly lower than average accuracies.

The first row of Fig. 8-9 shows the effect of the variation of the embedded pile length  $L$  on the lateral secant stiffness of the monopile foundations for the normalised head displacements. Based on the numerical results, it is recognised that any additional pile length above 30 m has no additional impact on the behaviour of the pile head stiffness. The significant discrepancies between API (2014) approach and numerical simulation are quite comparable for all head displacements, reaching a considerable overestimation of lateral head displacements. In contrast, the new modelling approach yields much better results, but a moderate underprediction of the bedding soil resistance exists for short pile lengths up to  $Q_K = 0.74$ .

The lateral secant stiffness of the monopile-soil system for varied pile diameters  $D$  is depicted in the second row of Fig. 8-9. In this case, mainly the pile diameter  $D$  was modified, but also the wall thickness  $t$  and the load eccentricity  $h$  are accordingly adapted. As expected, the lateral secant stiffness increments strongly with an increasing pile diameter  $D$ , particularly for the smallest head displacement. API (2014) approach performs poorly for predicting the displacement stiffness in general, resulting in a strong overprediction of lateral head

displacements. Again, the new modelling approach demonstrates good agreement with the numerical results, resulting in a small range of quotients  $Q_K = 0.88-1.02$ .

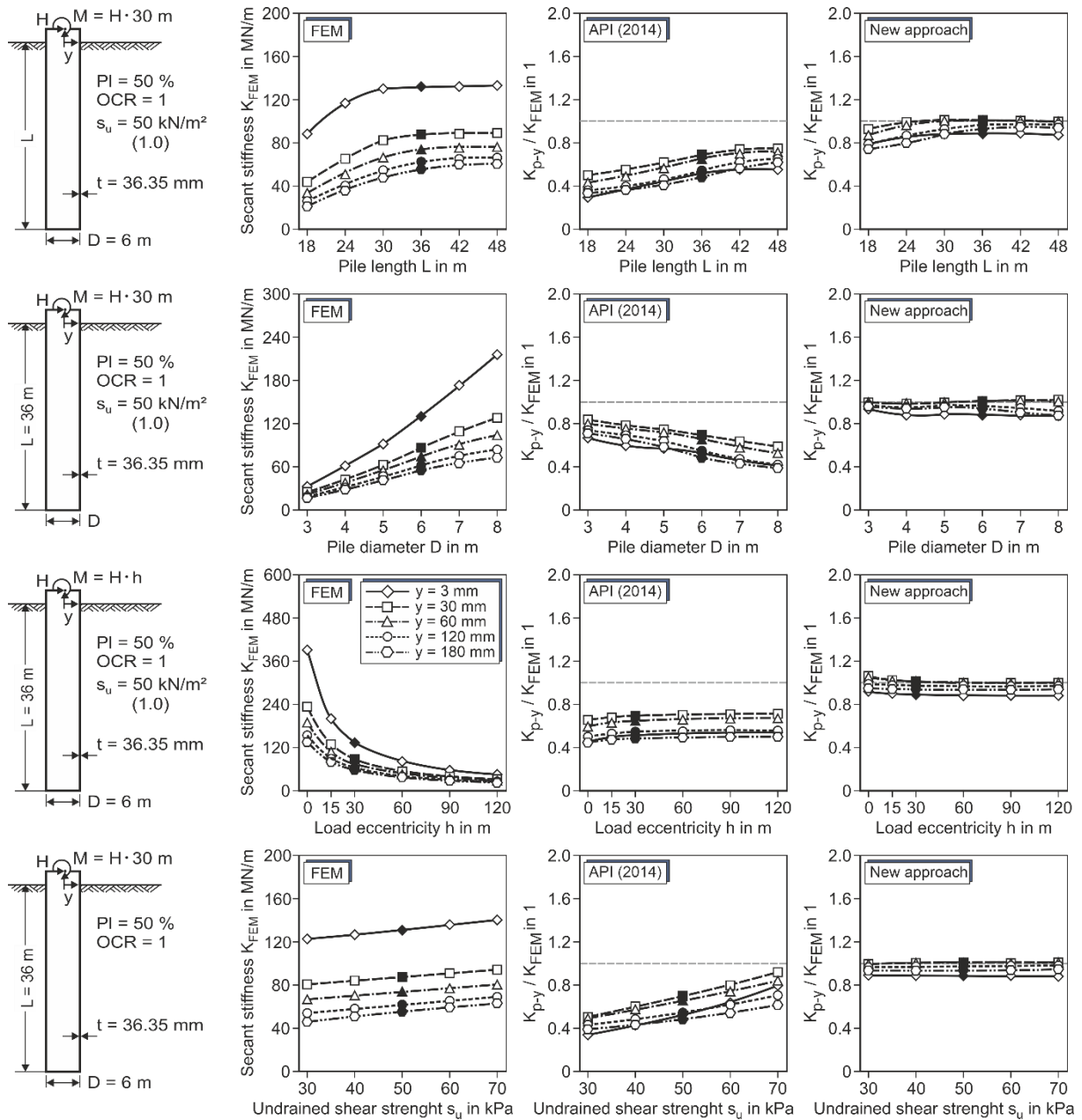


**Fig. 8-9: Quotient of lateral stiffness  $K_{p-y} / K_{FEM}$  based on the new modelling approach and FEM for varied parameters with linearly increasing undrained shear strength  $s_u$**

A parametric study concerning the effect of varying load eccentricity  $h$  on the pile behaviour is depicted in the third row in Fig. 8-9. Once again, the decay of the lateral secant stiffness with increasing load eccentricities is evident but more pronounced in comparison to the parametric study with constant shear strength parameters over depth. Both analytical methods yield regular deviations for all normalised head displacements, but the new modelling approach provides more reliable results than the ones obtained from API (2014) approach, which significantly underpredicts the bedding soil resistance represented by  $Q_K$  up to 0.42 compared to the numerical results.



The last row of Fig. 8-9 illustrates the influence of undrained shear strength  $s_u$  on the obtained response predictions of the pile behaviour for depth-dependent shear parameters. The label values represent the  $s_u$  at soil surface level, which increases over the depth as given in Table 6-4. In contrast to the results from constant shear strength parameters, an overprediction of the lateral head displacement occurs over the entire range analysed when applying the API (2014) approach. The disparity represented by the quotients of lateral stiffness is very significant. The new modelling approach again demonstrates its superiority by yielding moderate discrepancies with respect to the numerical results.

Concluding the comprehensive evaluation about the suitability of the new modelling approach, the influence of coupled soil parameters on the non-linear behaviour of the pile-soil system is again evaluated but this time also considering the depth-dependent shear strength parameters, as shown in Fig. 8-10. In fact, this parametric study should be considered as the most extreme case of variation of soil parameters.

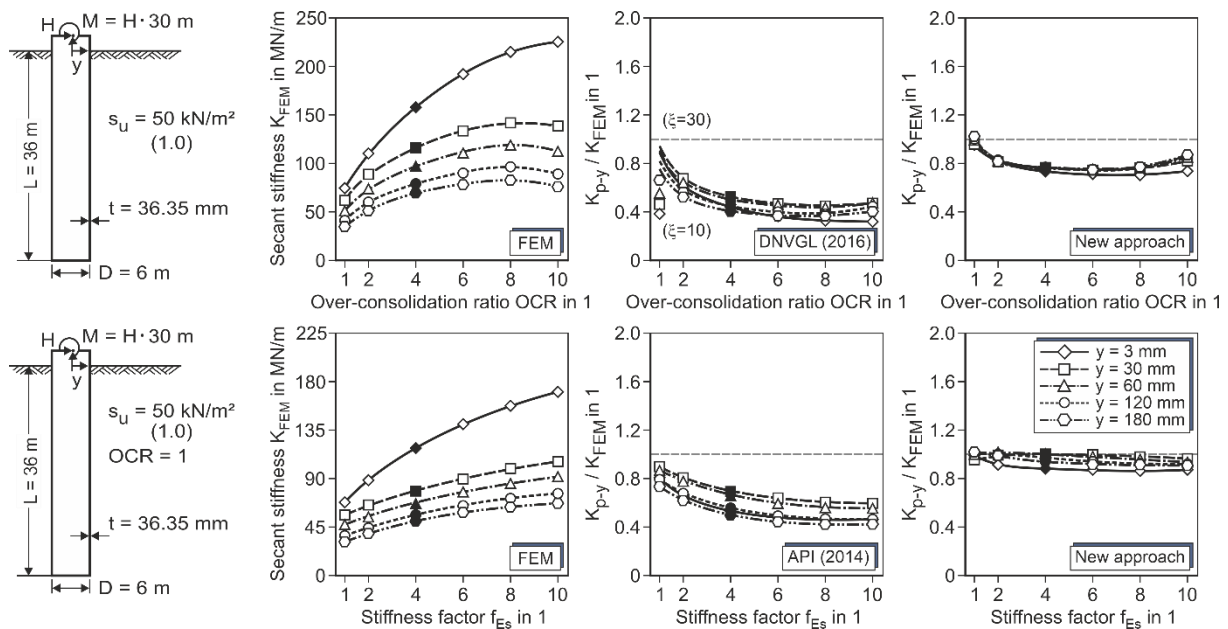


**Fig. 8-10: Parameter study for the evaluation of the new modelling approach based on the variation of coupled soil condition parameters with linearly increasing undrained shear strength  $s_u$**

In the first row of Fig. 8-10, the variation of coupled soil parameters, such as the over-consolidation ratio OCR, plasticity index PI, soil stiffness factors  $f_{Es}$  and  $f_{G0}$  is again conducted using depth-dependent parameters as introduced in Table 6-3. Based on the numerical results, the pile response at the smallest head displacement ( $y = 3$  mm) becomes stiffer with increasing OCR than the other head displacements. Both analytical methods perform identical trend patterns of discrepancies compared to the parametric study without depth dependency. The moderate deviations of  $Q_K$  up to 0.73 of the new modelling approach are attributed to the non-consideration of the over-consolidation ratio OCR in its formulation.

To enable a clear comparison, a further comparative study is carried out under almost identical soil conditions to the previous study, but without the increment of the OCR (see the second row of Fig. 8-10). In this manner, the input parameters of the three-dimensional numerical



simulations are compared to the new modelling approach, leading to an adjustment of the results with moderate deviations ranging from 0.87 to 1.03. The deviations from the p-y approach proposed by API (2014) remain considerable, suggesting that they are associated with the discrepancies obtained from constant soil parameters over depth. Strong underpredictions of the foundation stiffness can be observed in all cases.

In summary, the new modelling approach derived for cohesive soils is able to reasonably account for the variation of coupled soil parameters in conjunction with depth-dependence shear strength for accurately predicting the non-linear behaviour of the pile-system.



## 9 Discussion

To obtain an essential insight into both the capabilities and limitations of the new modelling approach introduced in this thesis, controversial topics regarding the correct prediction of the non-linear response of laterally loaded pile foundations in cohesive soils are discussed as follows:

- Typical static p-y approaches utilised in offshore design guidelines such as those proposed by Matlock (1970) for soft clay and Reese & Cox (1975) for stiff clay, as well as several modified p-y formulations presented in the literature, mainly define the undrained stiffness of p-y curves as a function of the strain  $\epsilon_{50}$  at one half the maximum principal stress obtained from the laboratory of undrained compression tests of undisturbed soil samples. Nonetheless, in practice, the strain at 50 % of maximum stress  $\epsilon_{50}$  is usually determined by using certain correlations, exclusively depending on the undrained shear strength  $s_u$ . Unquestionably, this prevents a clear distinction between soil stiffness and shear strength that defines p-y curve characteristics. In contrast, the new modelling approach assumes a soil stiffness-dependent formulation decoupled from the undrained shear strength parameters adopted by the hyperbolic relationship involved. Correspondingly, it takes into account the ultimate limit bedding resistance  $p_u$  focused on the overburden pressure  $\sigma_v$  and the undrained shear strength  $s_u$ , but also separately the bedding stiffness, considering the oedometric soil stiffness  $E_{oed}$ , the dynamic shear modulus  $G_0$ , and the plasticity index PI. Alternatively, it is also possible to convert the stiffness parameter  $E_{oed}$  used in the new modelling approach to the strain  $\epsilon_{50}$  again applying the numerical analysis. Nevertheless, in any case, the determination of realistic soil conditions as key input parameters for the correct applicability of the new modelling approach is decisive. An evaluation of the combination of field and laboratory investigations for accurately deriving the initial soil conditions is usually required. For instance, the derivation of the dynamic shear modulus  $G_0$  at very-small strains results from the laboratory triaxial and resonant column experiments, as well as in situ cross-hole and downhole shear wave dates.
- Sophisticated three-dimensional numerical models are developed to describe the undrained pile's load-bearing behaviour embedded in clay profiles for arbitrary pile foundation geometries subjected to short-term monotonic loading conditions. The numerical simulations by finite element modelling are basically an essential benchmark for a thorough evaluation of the performance of the traditional static p-y approach and the development of an innovative modelling approach, but they also highlight the limitations of the constitutive material models when it comes to modelling the undrained soil's behaviour. On the one hand, the boundary conditions of the HSsmall constitutive material model using "undrained behaviour B" (cf. section 5.3) are quite limiting when it comes to the accurate determination of the excess pore pressure  $p_{exc}$ , which is not crucial for the present work. Besides that, the necessity for modelling the undrained soil's behaviour by adopting several soil layers to obtain depth-dependent soil stiffness results is extremely laborious. On the other hand, it is quite advantageous that the HSsmall constitutive material model offers the

capability of taking into account the small-strain dependence of the soil stiffness, being crucial for catching the pile's response at very-small strains, in contrast to the remaining constitutive material models.

- The soil consistency expressed in terms of undrained shear strength  $s_u$  is a decisive influencing variable in whether the pile-soil system is susceptible to a post-peak softening response represented by the residual bedding resistance  $p_{res}$ . This means that stiff clays are more inclined to exhibit such a load-bearing pile's behaviour than soft clays, as seen in several field load tests (cf. section 5-4). Besides that, Reese & Cox (1975), concerning the derivation of static p-y curves in stiff clay, establish a residual bedding resistance  $p_{res}$  for large pile displacements, and argue for the gapping formation at the backside of the pile foundation, which would have influenced the prediction about the non-linear response of the pile-soil system. Similarly, Senanayake (2016) remarks on the relevance of the effect of gapping for determining the non-linear response of the pile. Contradictorily, for instance, the static p-y method proposed by Dunnavant & O'Neill (1989) in submerged over-consolidated stiff clay does not include a softening soil's behaviour after the peak, although in the original documents it states the existence of a gapping condition in the static field load tests used for deriving its p-y formulation. Anyhow, none of the constitutive material models available from finite element programmes can model such a post-peak softening soil response. Nevertheless, with additional soil parameters derived from laboratory tests as proposed by Gazioglu & O'Neill (1984), a more complex p-y curve characteristic could be developed that also considers the softening soil behaviour after the peak by including the residual bedding resistance  $p_{res}$ . Although, according to Pisa project (2016), this does not offer any improvement in robustness or accuracy of results, indicating that there could be a risk of an over-fitting of soil response.
- Several individual studies have dealt with the investigation of a horizontal pile's load-bearing behaviour for either sand or clay profiles. The new modelling approach offers the capacity for a general application of different soil types by including the soil plasticity as a soil input parameter in its formulation. It should be noted that almost all p-y methods examined in this thesis, except for the p-y approach introduced by Kim et al. (2009), exclude the soil plasticity to characterise the stiffness of the p-y curves. The incorporation into the new modelling approach of soil plasticity is accomplished by using the threshold shear strain  $\gamma_{0.7}$  parameter, which can be obtained from laboratory tests. By doing so, the pile's behaviour embedded in silt and silty clays, for instance, can also be predicted by using the unique basic p-y formulation, such as the hyperbolic relationship introduced in this work.

## 10 Conclusion and Perspective

The research work of this thesis mainly focuses on the investigation and development of new geotechnical methods for the design and analysis of laterally loaded pile foundations embedded in clay deposits, particularly adapted to the offshore wind sector. The proposed new modelling approach is derived from a set of three-dimensional numerical models, including the sophisticated HSsmall constitutive material model, which were validated based on small-scale field tests used for the derivation of existing p-y approaches recommended in the current OGLs (e.g. API 2014 and DNVGL 2016) as well as medium-scale field tests reported in the literature. The validated three-dimensional numerical models were applied to investigate the performance of the traditional static p-y approach, especially for large-diameter pile foundations destined for the offshore industry by using a comprehensive comparative study for laterally loaded piles embedded in either soft or stiff clays. This investigation provides the basis for developing a new modelling approach to properly counteract the usual shortcomings identified in the traditional static p-y approach. The new modelling approach introduced provides a more precise and realistic prognosis of the horizontal pile's load-bearing behaviour and the local pile-soil interaction for arbitrary pile geometries subjected to short-term monotonic loading conditions. Its application corresponds particularly to the pile foundations embedded in soft clays, but could also be extended to stiff clays.

The limitations of this thesis are the exclusive study of monotonic behaviour and the assumption of homogeneous clay profiles (i.e. layered soils have not been considered), ignoring the effects of scour and neglecting the effect of pile installation and its subsequent effects.

Results from the present research work lead to the following conclusions:

- None of p-y approaches investigated so far are adequate for predicting the numerically determined load-bearing behaviour of the pile-soil system for the relevant boundary conditions of laterally loaded piles embedded in soft and stiff clay. In this respect, the effect of varying pile geometry, loading condition, and soil consistency on the pile's load-bearing behaviour has been considered in a set of comparative studies. Neither the traditional p-y approaches recommended by API (2014) and DNVGL (2016) nor those introduced in the literature are generally suitable to be applied in the design of monopile foundations with low ratios  $L / D$  such as that employed for OWTs' substructures. It should be noted that the infinite initial stiffness of the basic p-y function introduced by Matlock's approach which most p-y approaches for soft clays assume, leads to a significant overprediction of the initial slope of static p-y curves related to low load levels. In contrast, its respective linearisations recommended by API (2014) and DNVGL (2016) for counteracting such influences are not entirely satisfactory. The identified deficiencies prevent the reliable application of typical p-y approaches for determining the pile stiffness behaviour which is required for the design of pile-soil systems.

- The calibration procedure of the new modelling approach relies on the results of sophisticated three-dimensional numerical simulations and theoretical considerations. Based on the knowledge obtained from the comprehensive parametric study, the main influencing variables used in the new modelling approach are identified, which might be valid for arbitrary soil and pile geometry conditions as well as load levels. The non-linear Winkler foundation analysis used for the conventional p-y approach to predict the horizontal pile's load-bearing behaviour is enhanced by considering the y-multipliers  $Mult_y$ , taking into account the effect of varying the pile-soil stiffness on the pile's behaviour. In addition, the shearing stress caused by the interaction of the soil resistance mobilised around the pile tip is treated quite effectively by adopting the y-multipliers  $Mult_{y,tip}$ , which are decisive in cases of pile foundations with a low embedded length-to-diameter ratio  $L / D$ . The application of deflection mode-dependent y-multipliers on the "basic p-y curves" makes possible an improved prediction of the non-linear response of arbitrary pile-soil systems compared to results of the validated numerical simulations than the ones obtained from the typical static p-y approaches recommended by API (2014) and DNVGL (2016).
- An extensive evaluation of the accuracy and reliability of the new modelling approach was carried out by varying pile geometry conditions as well as individual and coupled soil parameters in depth-dependence or constant over depth. In all cases, it has been demonstrated that the new modelling approach is significantly superior to traditional p-y approaches in predicting the horizontal pile's load-bearing behaviour and the local pile-soil interaction. A moderate discrepancy between results of the new modelling approach and numerical models was found, corresponding to the increase in the over-consolidated ratio OCR, whereas the latter is not considered as an input parameter in the new modelling approach. Nevertheless, the non-linear behaviour of over-consolidated clay could be captured by increasing the soil stiffness which is adequately reflected by the new modelling approach.
- The traditional p-y approaches recommended by offshore guideline documents and the literature as well as the new modelling approach introduced in this thesis were successfully implemented in the pile design programme IGtHPile for their application and complete analysis. It is remarkable that the computation speed for calculating the equilibrium of pile-soil systems by using an iterative process is quite similar for both types of analysing methods, but the results obtained from the new modelling approach offer comparable accuracy to the results of the validated three-dimensional numerical models with a substantially lower computational effort for solving such a complex three-dimensional geotechnical problem.

The scope of this thesis was limited to analysing only the pile's behaviour subjected to short-term monotonic lateral loading conditions in cohesive soils. Additional investigations should focus on maximising the quality and reliability of the new improved modelling approach. Further research and development are still urgently required for the following essential aspects:

- 
- Although the measurements obtained from five field load tests (cf. section 5-4) were considered to calibrate the sophisticated three-dimensional numerical models used for deriving the new modelling approach, it still requires experimental and empirical validation. Therefore, further field measurements are necessary, particularly for the calibration to the strain-softening soil response for large displacements that occasionally characterises the behaviour of stiff clay in the event of a gapping formation at the backside of the pile foundation subjected to short-term monotonic loading conditions.
  - The inclusion of the cyclic degradation of stiffness and soil strength as well as accumulated deformation in the new modelling approach can be determined from varying the essential system parameters of the pile-soil systems.
  - As previously mentioned, the new modelling approach was in principle derived by considering a fully undrained soil behaviour. Therefore, it is also recommended that further examinations be carried out for analysing the effect of the dissipation of the excess pore pressure  $p_{exc}$  on the stiffness of introduced p-y curves.
  - The application of the hyperbolic stress-strain relation, introduced by the HSsmall constitutive material model, has demonstrated that it is feasible to use a single base p-y function that correctly reflects the non-linear behaviour of the pile-soil system. A more detailed examination of other soil types should be carried out by adopting the base p-y function introduced in this thesis, which would allow the derivation of a unified p-y approach that can also enable the study of stratified soils.





## Reference

- Abdel-Rahman, K., Achmus, M. (2005): "Finite Element Modelling of Horizontally Loaded Monopile Foundations for Offshore Wind Energy Converters in Germany", Proceedings of the 1st International Symposium on Frontiers in Offshore Geotechnics (ISFOG), Perth, Australia, Francis, pp. 391-396.
- Achmus, M. (2012a): "Zum Tragfähigkeitsnachweis für horizontal belastete Pfähle für die Grenzzustände GEO-2 und GEO-3", Geotechnik, 04 June, pp. 119-129.
- Achmus, M. (2012b): "Geotechnical design of foundation structures for offshore wind energy converters in the German North Sea", ISCOG, 16-18 November, Hangzhou, china.
- Achmus, M., Thieken, K., Lemke, K. (2014): "Evaluation of p-y Approaches for Large Diameter Monopiles in Sand", Proceedings of the 24th International Ocean and Polar Engineering Conference, Busan, Korea, International Society of Offshore and Polar Engineers (ISOPE), pp. 531-539.
- Achmus, M., Terceros, M., Thieken, K. (2016): "Evaluation of p-y Approaches for Large Diameter Monopiles in Soft Clay", Proceedings of the 26th International Ocean and Polar Engineering Conference, Rhodes, Greece, International Society of Offshore and Polar Engineers (ISOPE), pp. 805-816.
- Achmus, M., Terceros, M., Thieken, K. (2017a): "Assessment of p-y Approaches for Piles in Normally and Over-Consolidated Soft Clay", Proceedings of the 27th International Ocean and Polar Engineering Conference, San Francisco, California, International Society of Offshore and Polar Engineers (ISOPE).
- Achmus, M., Thieken, K., Terceros, M., Tom Wörden, F. (2017b): "Assessment of Pile Length Criteria for Monopile Foundations", Offshore Site Investigation Geotechnics 8th International Conference, Issue 1, pp. 1140-1147.
- Achmus, M., Thieken, K., Saathoff, J-E., Terceros, M., Albiker, J. (2019): "Un- and Reloading Stiffness of Monopile Foundations in Sand", Applied Ocean Research, 01 March, Issue 84, pp. 62-73.
- Albiker, J. (2016): "Untersuchungen zum Tragverhalten zyklisch lateral belasteter Pfähle in nichtbindigen Böden", Heft 77, Hannover: Selbstverlag.
- API (2002): "Recommended Practice for Planning, Designing and Constructing Fixed Offshore Platforms – Working Stress Design", API Recommended Practice 2A-WSD, American Petroleum Institute, Twenty-First Edition, December 2000, Errata and Supplement 1, December 2002.
- API (2007): "Recommended Practice for Planning, Designing and Constructing Fixed Offshore Platforms – Working Stress Design", API Recommended Practice 2A-WSD, American Petroleum Institute, Twenty-First Edition, December 2000, Errata and Supplement 3, October 2007.

- API (2014): “Geotechnical and Foundation Design Considerations”, ANSI/API Recommended Practice 2GEO / ISO 19901-4, American Petroleum Institute and American National Standards Institute, First Edition April 2011, Addendum 1, October 2014.
- Ashour, M., Norris, G., Pilling, P. (2002): “Strain Wedge Model Capability of Analyzing Behavior of Laterally Loaded Isolated Piles”, *Drilled Shafts and Pile Groups, Journal of Bridge Engineering*, 01 July, Issue 7 (4), pp. 245-254.
- Bayton, S. M., Black, J. A. (2019): “The effect of scour on monopile lateral behaviour”, *Proceedings of the XVII ECSMGE-2019*.
- Bohne, T., Grießmann, T., Rolfes, R. (2019): “Modeling the noise mitigation of a bubble curtain”, *The Journal of the Acoustical Society of America* 146, 2212 (2019).
- Benz, T. (2007): “Small-Strain Stiffness of Soils and its Numerical Consequences”, PhD Thesis, Mitteilung 55, Stuttgart: Institut für Geotechnik Universität Stuttgart.
- BMWi (2015a): *The Energy of the Future: Fourth “Energy Transition” Monitoring Report - Summary*, Berlin: The Federal Ministry for Economic Affairs and Energy; in German.
- BMWi (2015b): “Offshore Wind Energy an Overview of Activities in Germany”, Berlin: The Federal Ministry for Economic Affairs and Energy; in German.
- Briaud, J. L., Smith, T. D., Meyer, B. J. (1984): “Using pressumeter curve to design laterally loaded piles”, In *Proc. of the 15th Annual Offshore Technology Conference*, Houston, Texas, USA, pp. 495–502.
- Brinkgreve, R. B. J., Engin, E., Swolfs, W. M. (2013): “Plaxis3D Version 2013 Manual”, Plaxis.
- Broms, B. B. (1964a): “Lateral Resistance of Piles in Cohesionless Soils. *Journal of the Soil Mechanics and Foundations Division*”, Issue 90 (3), pp. 123-156.
- Broms, B. B. (1964b): “Lateral Resistance of Piles in Cohesive Soils”, *ASCE - Proceedings - Journal of the Soil Mechanics and Foundations Division*, Issue 90 (2), pp. 27-63.
- BSH (2014): “Standard Ground Investigations”, Minimum requirements for geotechnical surveys and investigations into offshore wind energy structures, offshore stations and power cables, Second update from 5.2.2014.
- BSH (2015): “Minimum Requirements Concerning the Constructive Design of Offshore Structures within the Exclusive Economic Zone (EEZ)”, Hamburg and Rostock: Federal Maritime and Hydrographic Agency (BSH), in German.
- Burland, J. (1990): “On the Compressibility and Shear Strength of Natural Clays”, *Géotechnique*, September, Issue 40 (2), pp. 329-378.
- Byrne, B. W., Burd, H. J., Zdravković, L., McAdam, R. A., Taborda, D. M.G., Houlsby, G. T., Jardine, R. J., Martin, C. M., Potts, D. M., Gavin, K. G. (2017): “PISA: New Design Methods for Offshore Wind Turbine Monopiles”, *Proceedings of the 8th International Conference for Offshore Site Investigation and Geotechnics*, London, UK, PISA Projekt.

- Byrne, B. W., McAdam, R. A., Burd, H. J., Beuckelaers, W., Gavin, K. G., Houlsby, G. T., Igoe, D., Jardine, R. J., Martin, C. M., Muir Wood, A., Potts, D. M., Skov Gretlund, J., Taborda, D., Zdravkovic, L. (2020): "Monotonic laterally loaded pile testing in a stiff glacial clay till at Cowden", *Géotechnique*, November, pp. 970-985.
- DIN 1054:2010-12: "Baugrund - Sicherheitsnachweise im Erd- und Grundbau - Ergänzende Regelungen zur DIN EN 1997-1", Deutsches Institut für Normung e.V., Beuth Verlag GmbH, Berlin, Februar 2010.
- DIN 4085:2011-05: "Baugrund - Berechnung des Erddrucks", Deutsches Institut für Normung e.V., Beuth Verlag GmbH, Berlin, May 2011.
- DIN EN 1997-1/NA:2010-12: "Nationaler Anhang zum Eurocode 7: Entwurf, Berechnung und Bemessung in der Geotechnik", Deutsches Institut für Normung e.V., Beuth Verlag GmbH, Berlin, Dezember 2012.
- DIN EN 1997-1:2009-09: "Eurocode 7: Entwurf, Berechnung und Bemessung in der Geotechnik - Teil 1: Allgemeine Regeln", Deutsches Institut für Normung e.V., Beuth Verlag GmbH, Berlin, September 2009.
- DNVGL (2016): "Support Structures for Wind Turbines", Standard, DNVGL-ST-0126, Det Norske Veritas and Germanischer Lloyd, Edition April 2016.
- DNVGL (2018): "Support Structures for Wind Turbines", Standard, DNVGL-ST-0126, Det Norske Veritas and Germanischer Lloyd, Edition July 2018.
- Dos Santos, J. A., Correia, A. G. (2001): "Reference Threshold Shear Strain of Soil. Its Application to Obtain an Unique Strain-Dependent Shear Modulus Curve for Soil", *Proceedings of the 15th International Conference on Soil Mechanics and Geotechnical Engineering*, Istanbul, Turkey, Balkema, pp. 267-270.
- Dunavant, D. A. (1985): "High degree efficient symmetrical Gaussian quadrature rules for the triangle". *International Journal of Numerical Methods in Engineering*, No. 21, pp. 1129-1148.
- Dunavant, T. W., O'Neill, M. W. (1989): "Experimental p-y Model for Submerged Stiff Clay", *Journal of Geotechnical Engineering*, January, Issue 115 (1), pp. 95-114.
- EAD (2002): "Empfehlungen des Arbeitskreises Baugrunderdynamik", Berlin, Eigenverlag Grundbauinstitut der Technischen Universität Berlin.
- EA-Pfähle (2012): "Empfehlungen des Arbeitskreises Pfähle (EA-Pfähle) ", German Society for Geotechnics e.V., 2nd Edition, Ernst & Sohn, Berlin, January 2012.
- EAU (2012): "Empfehlungen des Arbeitsausschusses Ufereinfassungen, Häfen und Wasserstraßen", German Society for Geotechnics e.V., 11th Edition, Ernst & Sohn, Berlin, Januar 2012.
- EEG (2017): "Renewable Energy Sources Act 2017", Berlin: Federal Ministry for Economic Affairs and Energy (BMWi) in German.

- Gazioglu, S. M. & O'Neill, M. W. (1984): "Evaluation of p-y Relationships in Cohesive Soils", Analysis and Design of Pile Foundations, pp. 192-213.
- Georgiadis, M. (1983): "Development of p-y Curves for Layered Soils, Proceedings of the Conference on Geotechnical Practice in Offshore Engineering", Austin, Texas, American Society of Civil Engineers, pp. 536-545.
- Haiderali, A. E., Madabhushi, G. S. (2013): "Evaluation of the p-y Method in the Design of Monopiles for Offshore Wind Turbines, Proceedings of the Offshore Technology Conference", Houston, Texas, Offshore Technology Conference, pp. 1824-1844.
- Hetenyi, M. (1946): "Beams on Elastic Foundation: Theory with Applications in the Fields of Civil and Mechanical Engineering", Baltimore, The University of Michigan Press.
- Isenhower, W. M., Wang, S.-T. (2015): "User's Manual for LPile 2015", Version 8, Ensoft, INC.
- Jeanjean, P., Zhang, Y., Zakeri, A., Andersen, K., Gilbert, R., Senanayake, A. I. M. J. (2017): "A Framework for Monotonic p-y Curves in Clays", Offshore Site Investigation Geotechnics 8th International Conference Proceeding, 12 September, Issue 1, pp. 108-141.
- Jeanjean, P. (2009): "Re-assessment of p-y Curves for Soft Clays from Centrifuge Testing and Finite Element Modeling", Proceedings of the Offshore Technology Conference, Houston, Texas, Offshore Technology Conference.
- Kiekbusch, M. (1999): "Beziehung zwischen Konsistenzzahl und Undranierter Scherfestigkeit", Bautechnik, Issue 76 (9), pp. 775-784.
- Kim, T. C., Novak, M. (1981): "Dynamic Properties of Some Cohesive Soils of Ontario", Canadian Geotechnical Journal, Issue 18 (3), pp. 371-389.
- Kim, Y., Jeong, S., Won, J. (2009): "Effect of Lateral Rigidity of Offshore Piles Using Proposed p-y Curves in Marine Clay", Marine Georesources & Geotechnology, 05 February, Issue 27 (1), pp. 53-77.
- Kirsch, F., Richter, T., Coronel, M. (2014): "Geotechnische Aspekte bei der Grundungsbemessung von Offshore-Windenergieanlagen auf Monopfahlen mit sehr groen Durchmessern", Stahlbau, 01 Marz, Issue 83 (S2), pp. 61-67.
- Lesny, K. (2010): "Foundations for Offshore Wind Turbines: Tools for Planning and Design", First edition, Essen: VGE Verlag GmbH.
- Malhotra, S. (2011): "Selection, Design and Construction of Offshore Wind Turbine Foundations", In: Wind Turbines. United States of America: In Tech, pp. 231-264.
- Martin, C. M., Randolph, M. F. (2006): "Upper-bound Analysis of Lateral Pile Capacity in Cohesive Soil", Geotechnique, 01 March, Issue 56 (2), pp. 141-145.
- Matlock, H. (1962): "Correlations for design of laterally loaded piles in soft clays", Report to Shell Development Company.

- Matlock, H. (1970): "Correlation for Design of Laterally Loaded Piles in Soft Clay", Proceedings of the 2nd Offshore Technology Conference, Houston, Texas, Offshore Technology Conference, pp. 577-594.
- McClelland, B., Focht, J. (1958): "Soil modulus for laterally loaded piles", Transaction, ASCE, Volume 123, pp. 1049-1063.
- Murff, J. D., Hamilton, J. M. (1994): "P-ultimate for Undrained Analysis of Laterally Loaded Piles. Journal of Geotechnical Engineering", Issue 120 (8), pp. 1462 - 1465.
- Nielsen, S. D., Ibsen, L. B., Nielsen, B. N. (2017): "Transiently Loaded Bucket Foundations in Saturated Dense Sand – Demonstration of the Boot Effect", Geotechnical Testing Journal, 01 November, Issue 40 (6), pp. 1101-1114.
- Norris, G. M. (1986): "Theoretically based BEF laterally loaded pile analysis", Proc., 3rd Int. Conf. on Numerical Methods in Offshore Piling, pp. 361-386.
- O'Neill, M. W., Dunnavant, T. W. (1984): "A Study of the Effects of Scale, Velocity, and Cyclic Degradability on Laterally Loaded Single Piles in Over-consolidated Clay", Department of Civil Engineering, University of Houston, October.
- Ohde, J. (1939): "Zur Theorie der Druckverteilung im Baugrund", Bauingenieur, 25 August, Issue 20 (33/34), pp. 451-459.
- PISA Project (2016): "Final Report", Report Produced by Members of the PISA Academic Work Group (University of Oxford, Imperial College London, University College Dublin) and the PISA Representatives of Dong Energy, UK: PISA.
- Poulos, H. G., Davis, E. H. (1980): "Pile Foundation Analysis and Design", Chichester, England: Wiley (John) & Sons, Limited.
- RAB & DTI (2007): "Study of the Costs of Offshore Wind Generation: A Report to the Renewables Advisory Board (RAB) and Department of Trade and Industry (DTI)", London (United Kingdom): Department for Business Enterprise and Regulatory Reform; Offshore Design Engineering.
- Randolph, M. F. (1981): "The Response of Flexible Piles to Lateral Loading", Geotechnique, Vol. 31, No 2, pp. 247-259.
- Randolph, M. F., Gourvenec, S. (2011): "Offshore Geotechnical Engineering", 1st edition, Abingdon, UK: Spon Press.
- Randolph, M. F., Houlsby, G. T. (1984): "The Limiting Pressure on a Circular Pile Loaded Laterally in Cohesive Soil", Géotechnique, 4 December, Issue 34 (4), pp. 613-623.
- Reese, L. (1958): Discussion of "Soil modulus for laterally loaded piles" by McClelland and Focht, Transactions ASCE, Vol.123, pp. 1071-1074.
- Reese, L. C., Cox, W. R., Koop, F. D. (1974): "Analysis of Laterally Loaded Piles in Sand", Proceedings of the 6th Annual Offshore Technology Conference, Houston, Texas, Offshore Technology Conference, pp. 473-484.

- Reese, L. C., Cox, W. R., Koop, F. D. (1975): "Field Testing and Analysis of Laterally Loaded Piles in Stiff Clay", Proceedings of the Offshore Technology Conference, Houston, Texas, Offshore Technology Conference.
- Reese, L. C., Van Impe, W. F. (2001): "Single Piles and Pile Groups Under Lateral Loading", 1st edition Rotterdam (and Amsterdam), Balkema.
- Reese, L. C., Van Impe, W. F. (2011): "Single Piles and Pile Groups under Lateral Loading", 2nd edition, CRC Press/Balkema.
- Schanz, T. (1998): "Zur Modellierung des Mechanischen Verhaltens von Reibungsmaterialien", Mitteilung 45, Stuttgart: Institut für Geotechnik Stuttgart.
- Senanayake, A. I. M. J. (2016): "Design of Large Diameter Monopiles for Offshore Wind Turbines in Clay"; PhD Thesis, Austin, Texas: The University of Texas at Austin.
- Skempton, A. W. (1954): "The Pore-Pressure Coefficients A and B", Géotechnique, 4 December, Issue 4 (4), pp. 143-147.
- Sørensen, S. P. H. (2012): "Soil-Structure Interaction for Non-Slender, Large-Diameter Offshore Monopiles", PhD Thesis, Volume 1, Aalborg, Denmark: The Faculty of Engineering and Science, Aalborg University.
- Stevens, J., Audibert, J. (1979): "Re-Examination of p-y Curve Formulations, Proceedings of the Offshore Technology Conference", Houston, Texas, Offshore Technology Conference.
- Stokoe, K. H., Darendeli, M. B., Menq, F. Y., Choi, W. K., Gilbert, R. B. (2004): "Development of a New Family of Normalized Modulus Reduction and Material Damping Curves", UC, Berkeley: International Whorkshop on Uncertain in Nonlinear Soil Properties and their Impact on Modeling Dynamic Soil Response.
- Sullivan, W. R., Reese, L. C., Fenske, C. W. (1980): "Unified method for Analysis of Laterally Loaded Piles in Clay", Numerical Methods in Offshore Piling, 07 July, pp. 135-146.
- Terceros, M., Achmus, M., Thieken, K. (2017): "Evaluation of p-y Approaches for Piles in Soft Clay", Offshore Site Investigation Geotechnics 8th International Conference Proceeding, Issue 1, pp. 724-731.
- Terceros, M., Schmoor, K. A., Thieken, K. (2015): "IGtHPile Version 4 Software and Reference Manual", Hannover, Germany: Leibniz University of Hannover, Institute for Geotechnical Engineering.
- Terceros, M., Thieken, K., Achmus, M. (2019): "Bewertung Statischer p-y Ansätze für Lateral Belastete Pfähle in Weichem Ton", Bautechnik, Februar, Issue 96 (2), pp. 195-211.
- Terzaghi, K. (1925): "Principles of Soil Mechanics: I-Phenomena of Cohesion of Clays", Engineering News-Record, Vol. 95, No. 19, pp. 742-746.
- Terzaghi, K. (1955): "Evaluation of Coefficients of Subgrade Reaction", Géotechnique, December, Issue 5 (4), pp. 297-326.

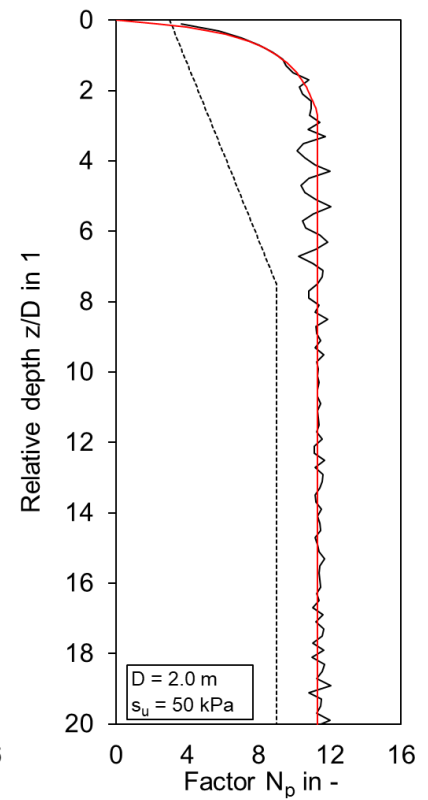
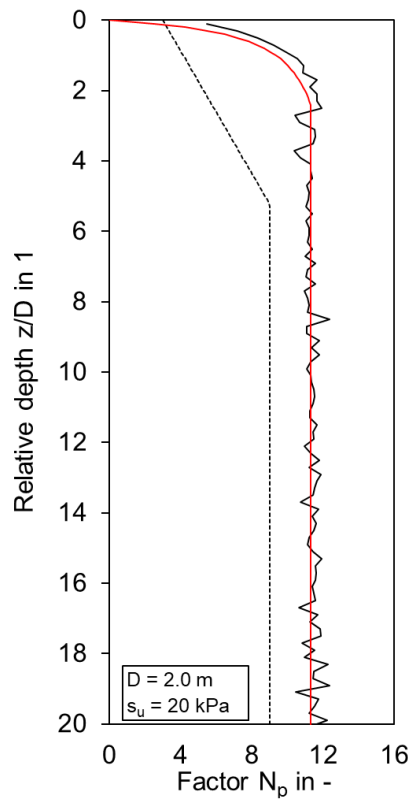
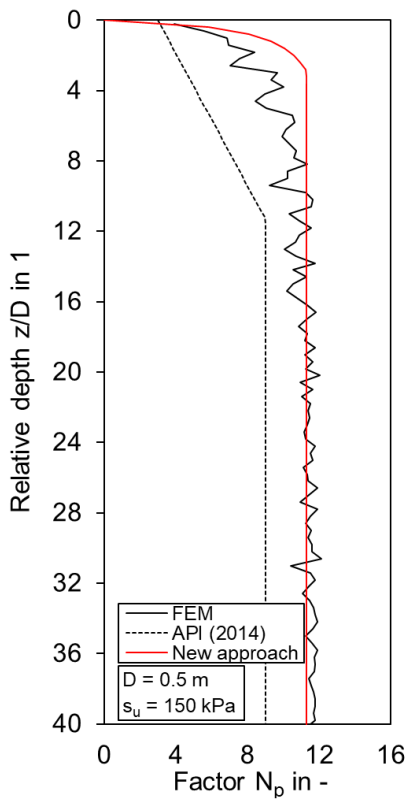
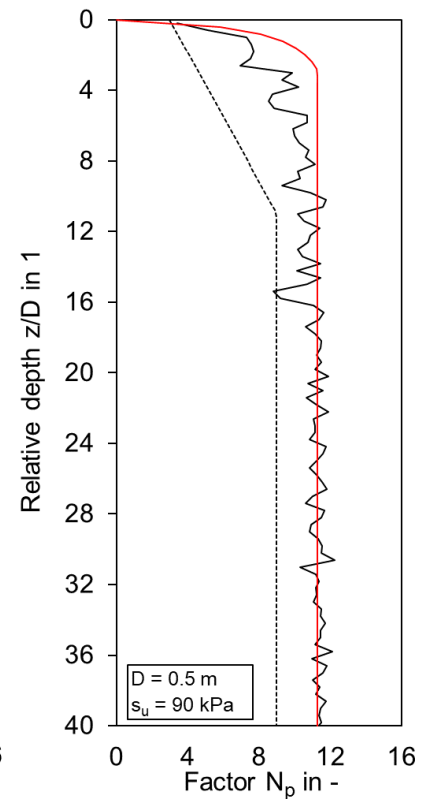
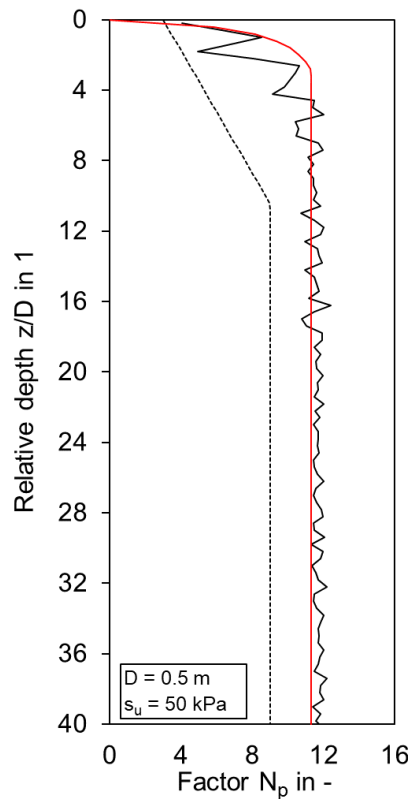
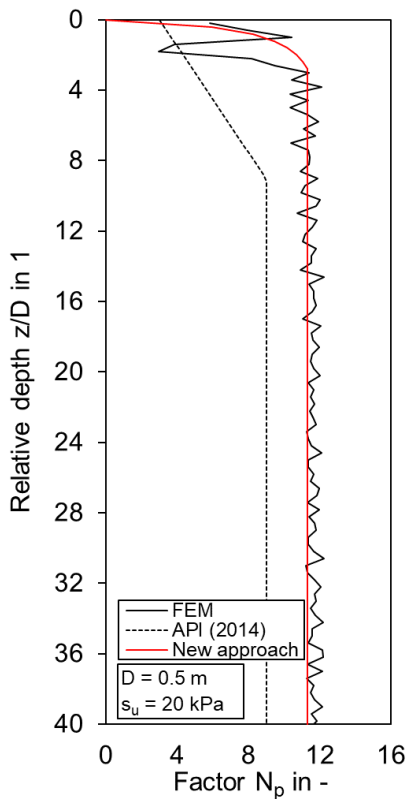
- Thieken, K., Achmus, M., Schmoor, K. A. (2013): "On the ultimate limit state design proof for laterally loaded piles", *Geotechnik* 37(1), pp. 19-31
- Thieken, K., Achmus, M. (2012): "Untersuchung der Interaktionsbeziehungen Kombiniert Belasteter Pfähle in Bindigen und Nichtbindigen Böden", *Geotechnik*, 11 December, Issue 35 (4), pp. 217-228.
- Thieken, K., Achmus, M., Lemke, K. (2015a): "A New Static p-y Approach for Piles with Arbitrary Dimensions in Sand", *Geotechnik*, 02 December, Issue 38 (4), pp. 267-288.
- Thieken, K., Achmus, M., Lemke, K. (2015b): "Bewertung Statistischer p-y Ansätze für Horizontal Belastete Pfähle Beliebiger Durchmesser in Nichtbindigem Boden", Braunschweig, Institut für Grundbau und Bodenmechanik Technische Universität Braunschweig, pp. 467-486.
- Thieken, K., Achmus, M., Terceros, M., Lemke, K. (2015c): "Evaluation of p-y Approaches for Large-Diameter Piles in Sand", *International Journal of Offshore and Polar Engineering*, Juni, Issue 25 (2), pp. 134-144.
- Thieken, K., Achmus, M., Terceros, M., Lemke, K. (2018a): "Evaluation of p-y Approaches for Large Diameter Piles in Layered Sand", *International Journal of Offshore and Polar Engineering (IJOPE)*, 01 September, Issue 28 (3), pp. 318-327.
- Thieken, K., Achmus, M., Saathoff, J-E., Albiker, J., Terceros, M., (2018b): "Stiffness of Monopile Foundations under Un- and Reloading Conditions", In: *Numerical Methods in Geotechnical Engineering IX*, 2 (1), Porto, Portugal: CRC Press, pp. 1469-1476.
- Vogt, S. R. K. (2017): "Zeitabhängiger Verformungswiderstand weicher Böden und seine Berücksichtigung bei der Tragfähigkeitsprognose stabilitätsgefährdeter Pfähle", München: Technische Universität München - Zentrum Geotechnik.
- Vucetic, M. & Dobry, R. (1991): "Effect of Soil Plasticity on Cyclic Response", *Journal of Geotechnical and Geoenvironmental Engineering*, January, Issue 117 (1), pp. 89-107.
- Wehnert, M. (2006): "Ein Beitrag zur Drainierten und Undrainierten Analyse in der Geotechnik", Mitteilung 53, Stuttgart: Institut für Geotechnik Stuttgart.
- Welch, R. C., Reese, L. C. (1972): "Lateral Load Behavior of Drilled Shafts", Austin, Texas: Center of Highway Research the University of Texas at Austin.
- Winkler, E., (1867): "Die Lehre von der Elastizität und Festigkeit", Prag.: Dominicus.
- Yu, J., Huang, M., Zhang, C. (2015): "Three-dimensional Upper-bound Analysis for Ultimate Bearing Capacity of Laterally Loaded Rigid Pile in Undrained Clay", *Canadian Geotechnical Journal*, Issue 52, pp. 1775-1790.

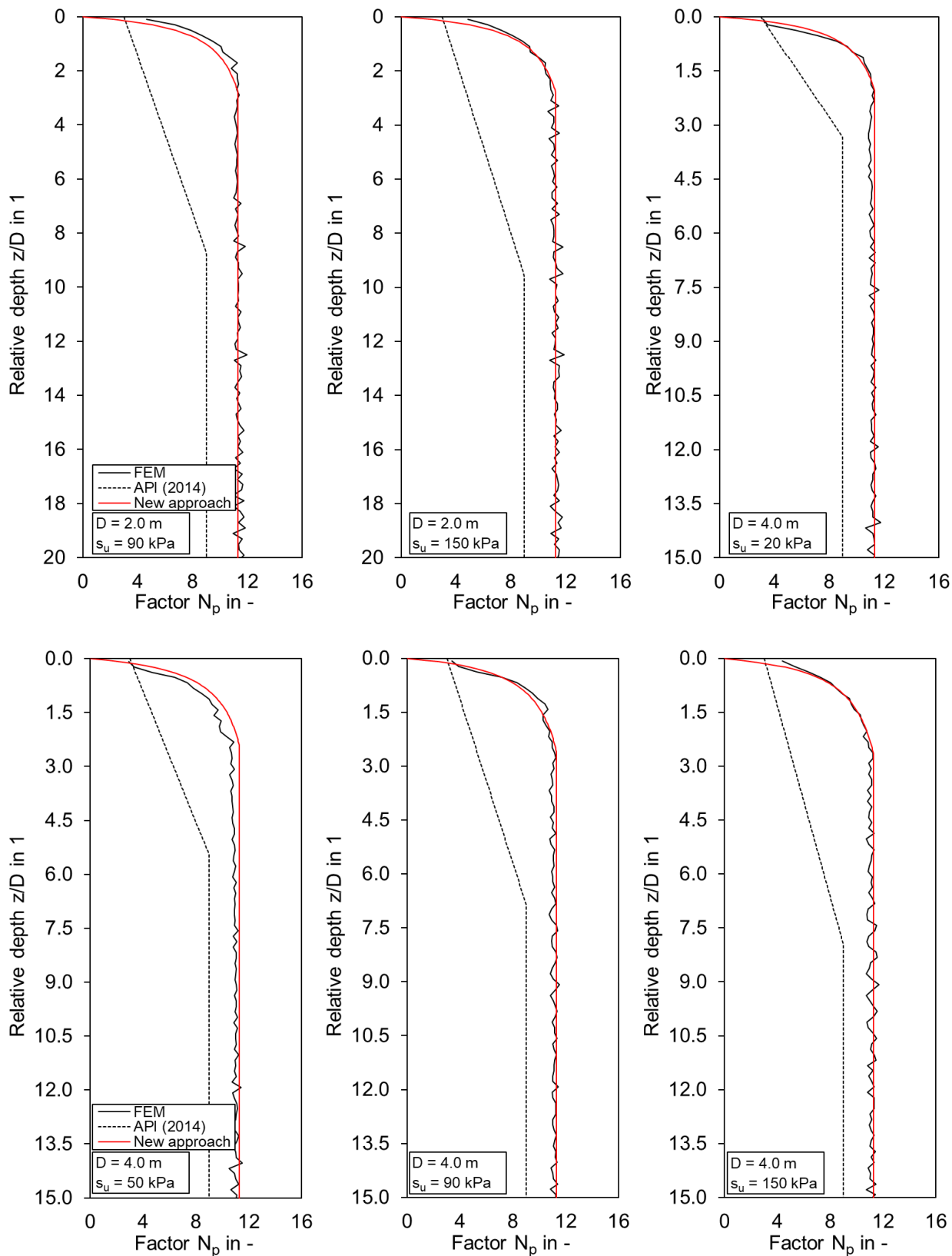


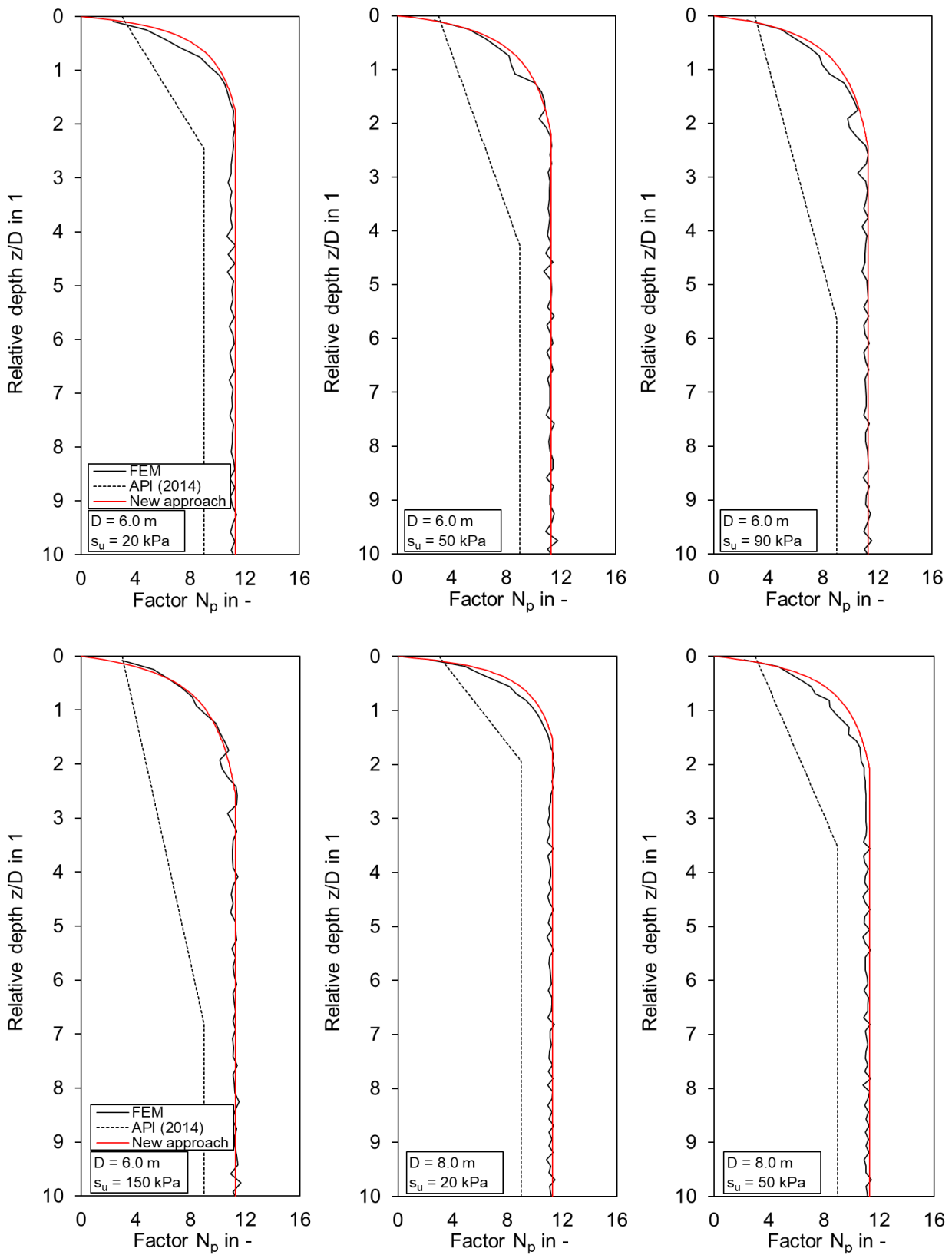


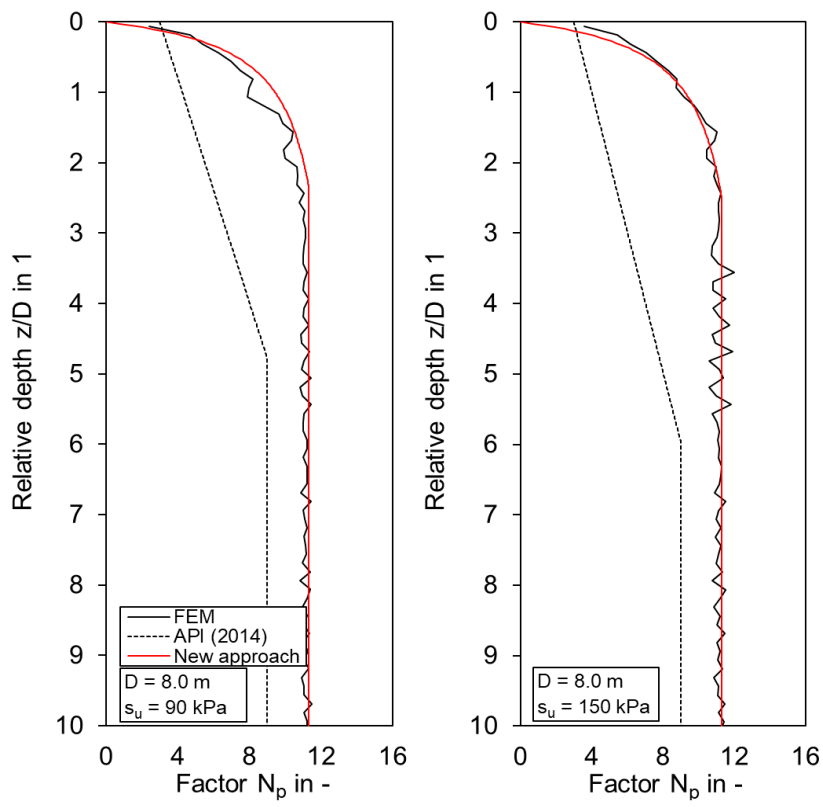
# Appendix A

Load-bearing capacity factor  $N_p$  associated with ultimate bedding resistance  $p_u$  resulting from the FEM analysis and the p-y approach recommended by API (2014) as well as the innovative modelling approach





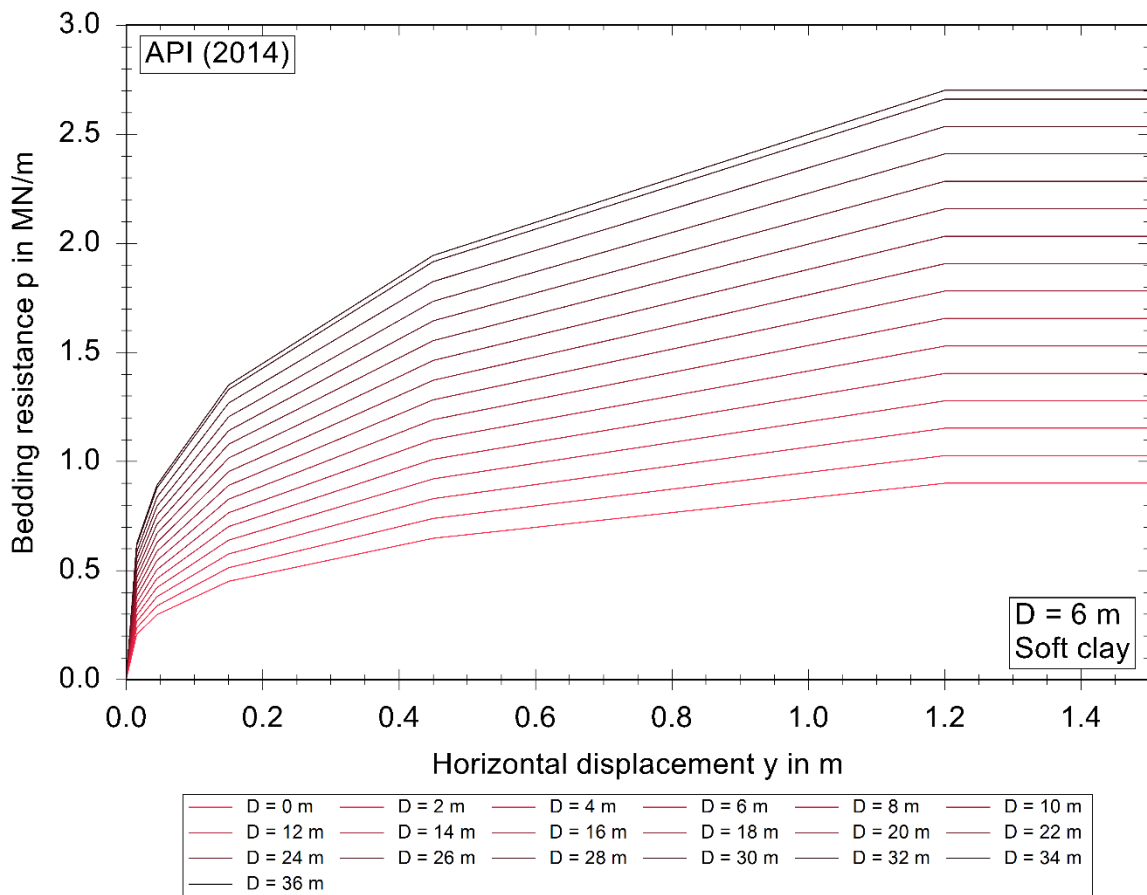
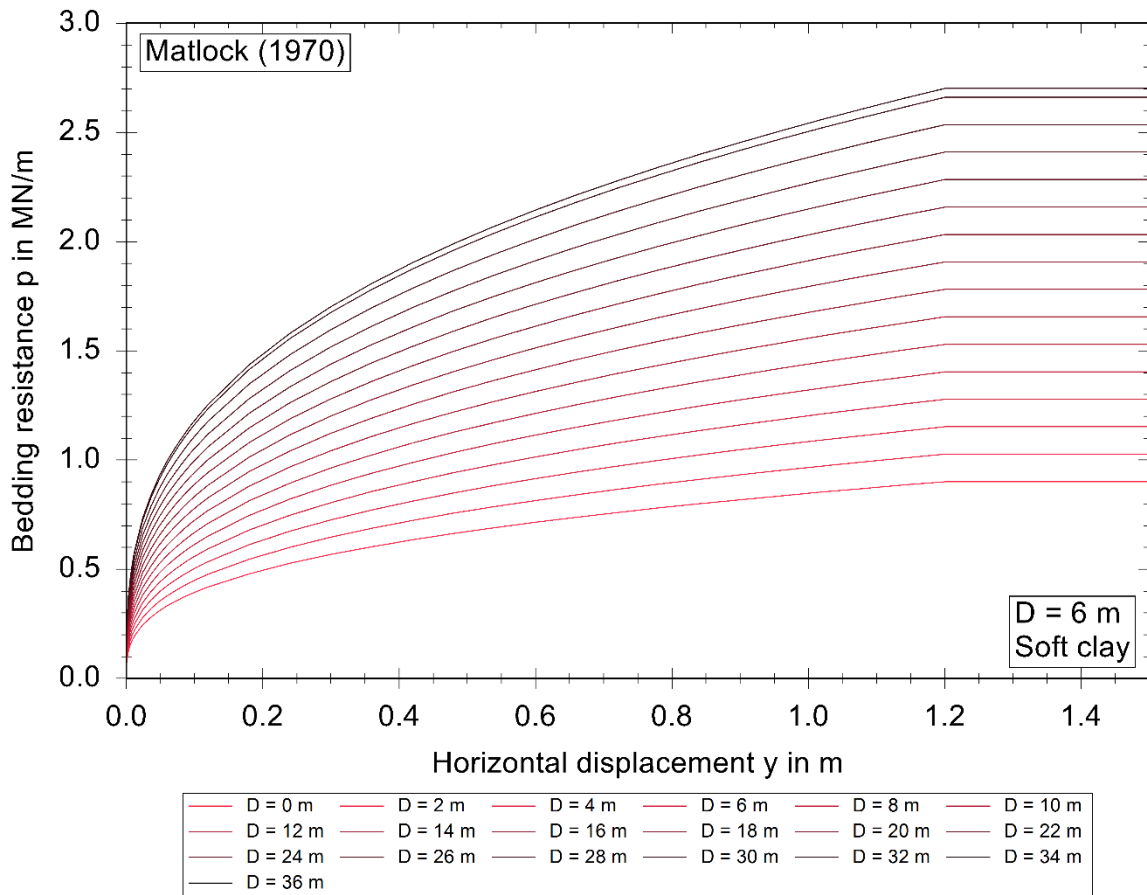




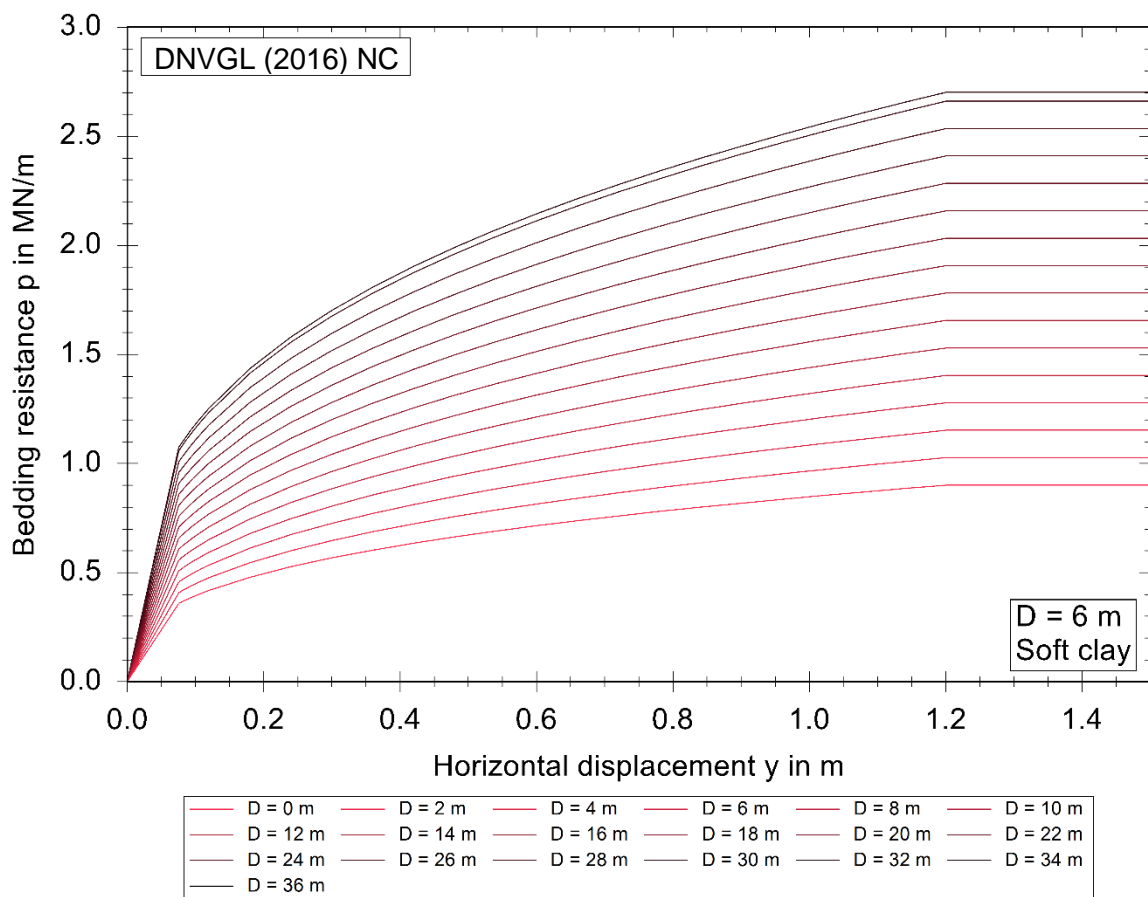
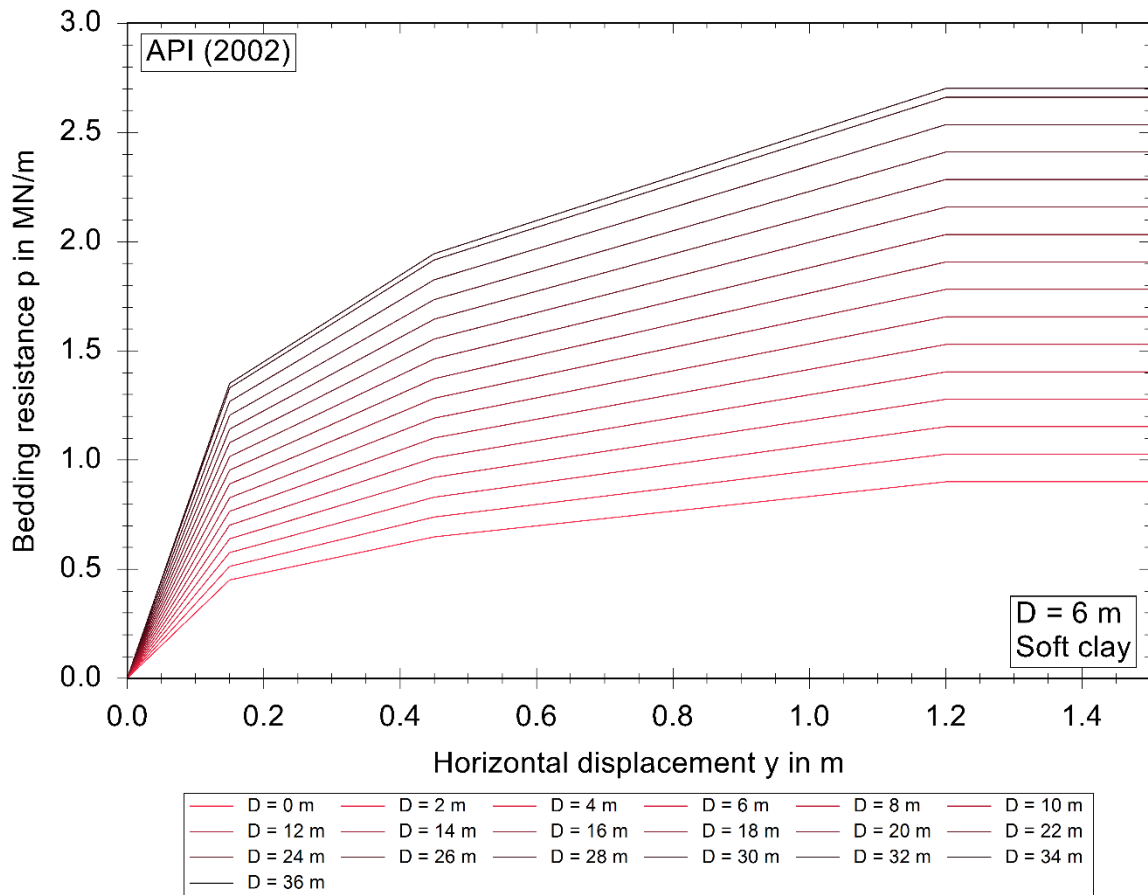


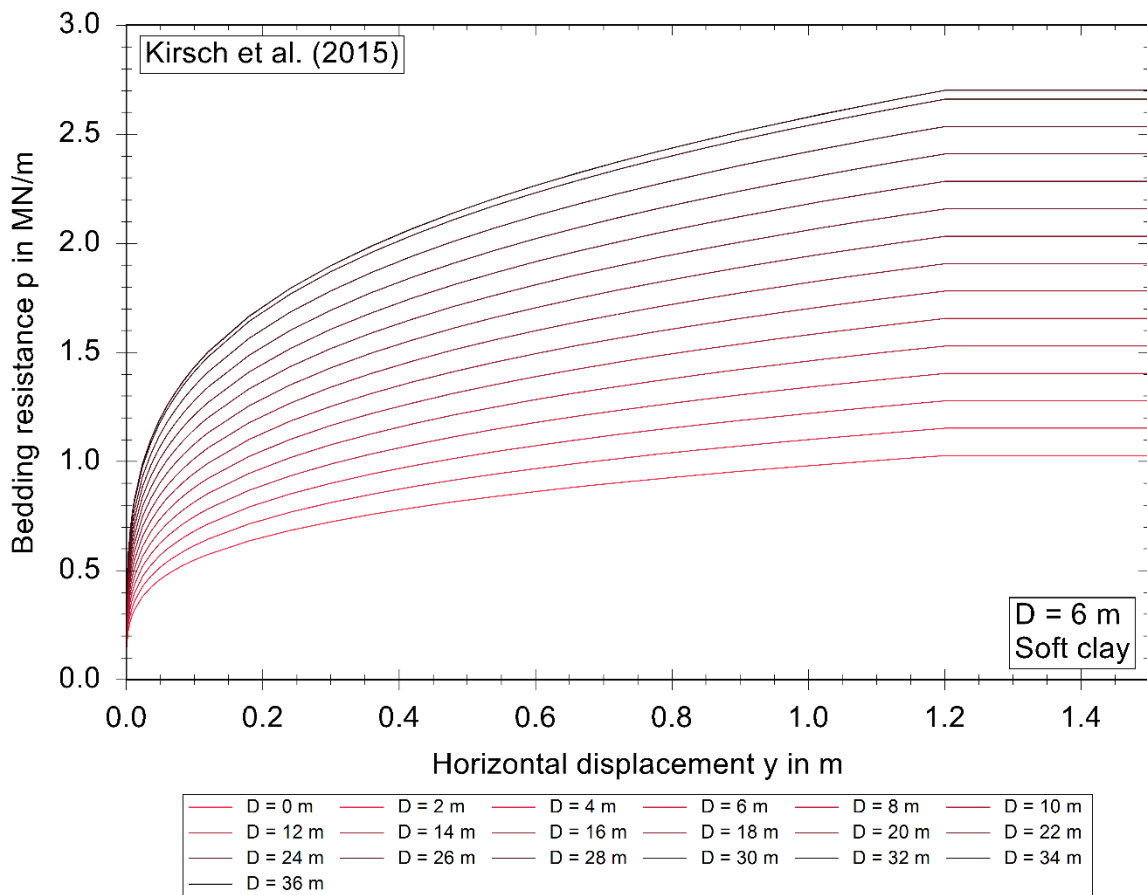
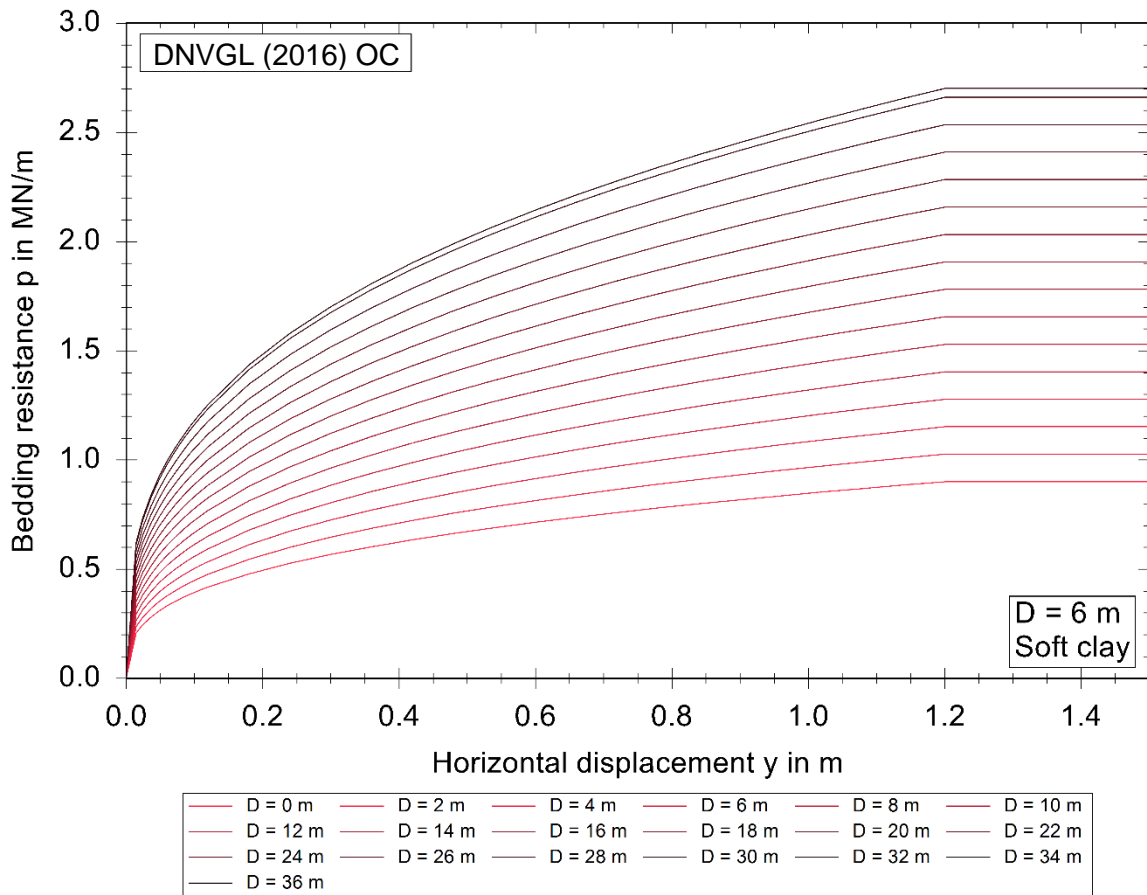
# Appendix B

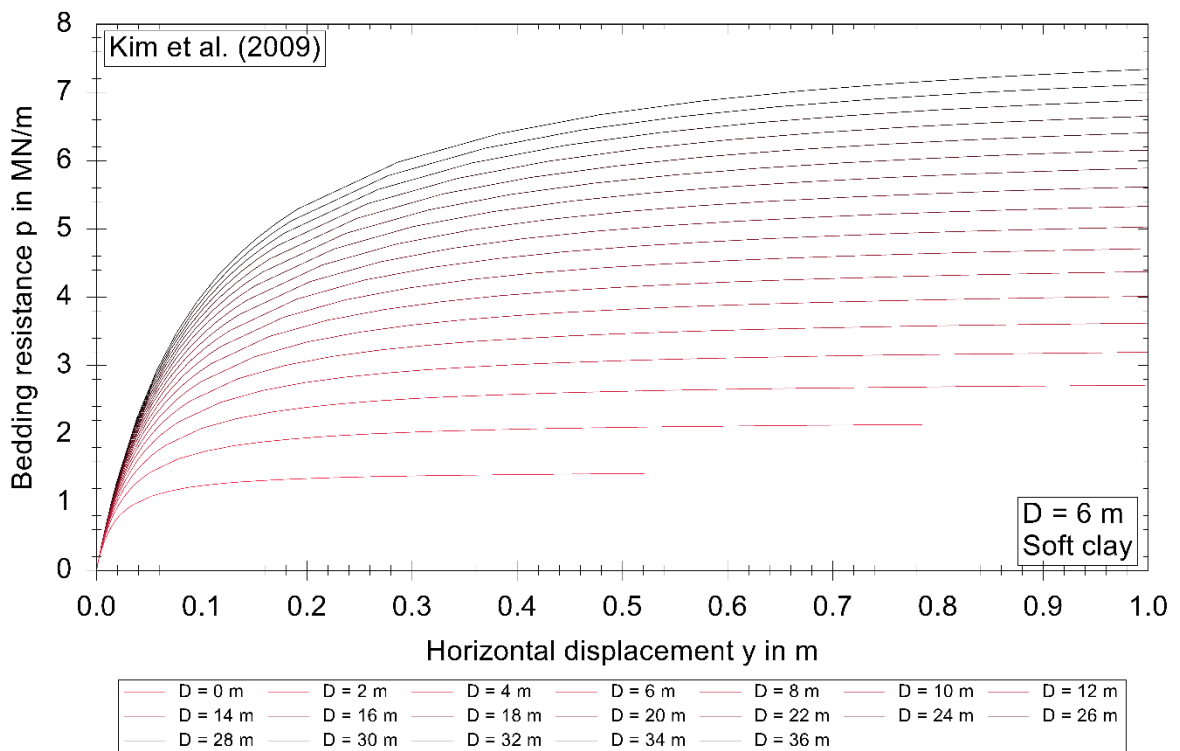
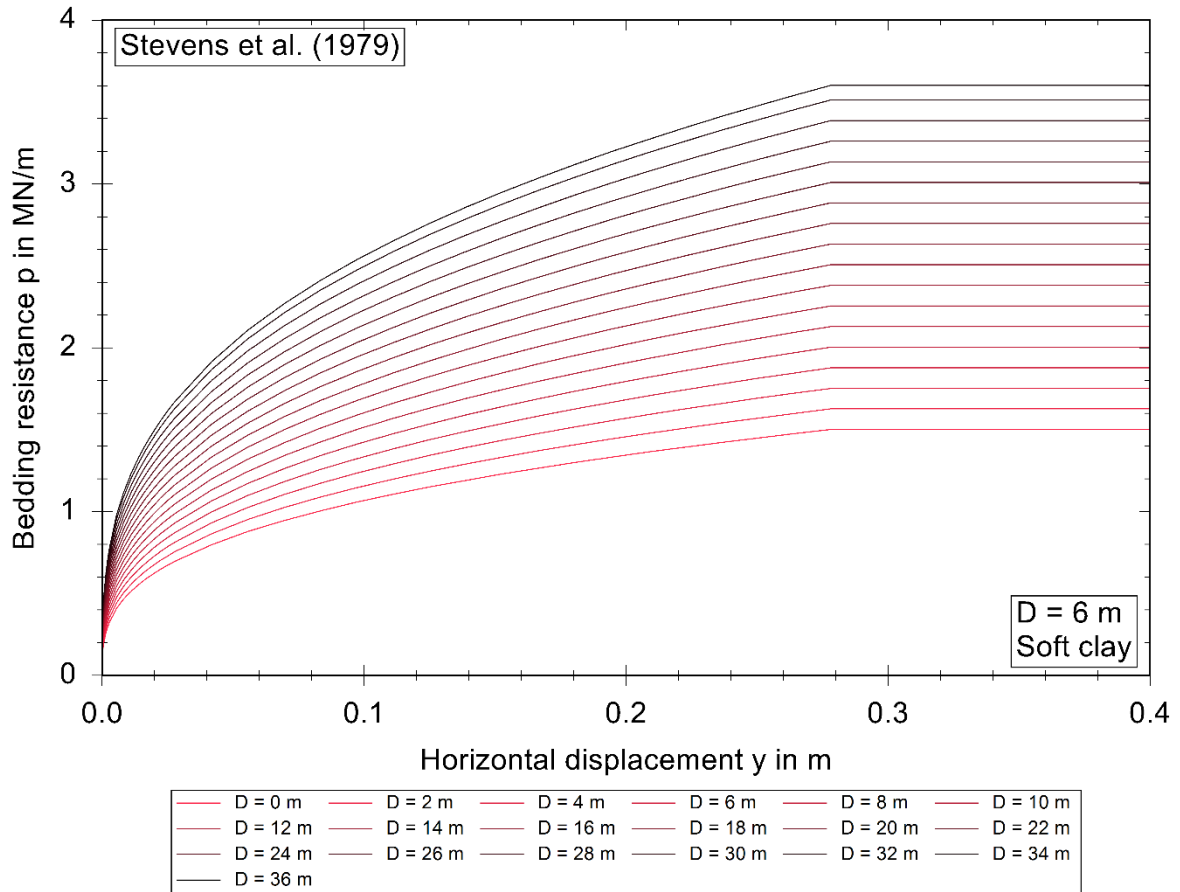
Non-linear, soil- and depth-dependent characteristics of soil springs (also termed p-y curves) acting orthogonally to the pile axis

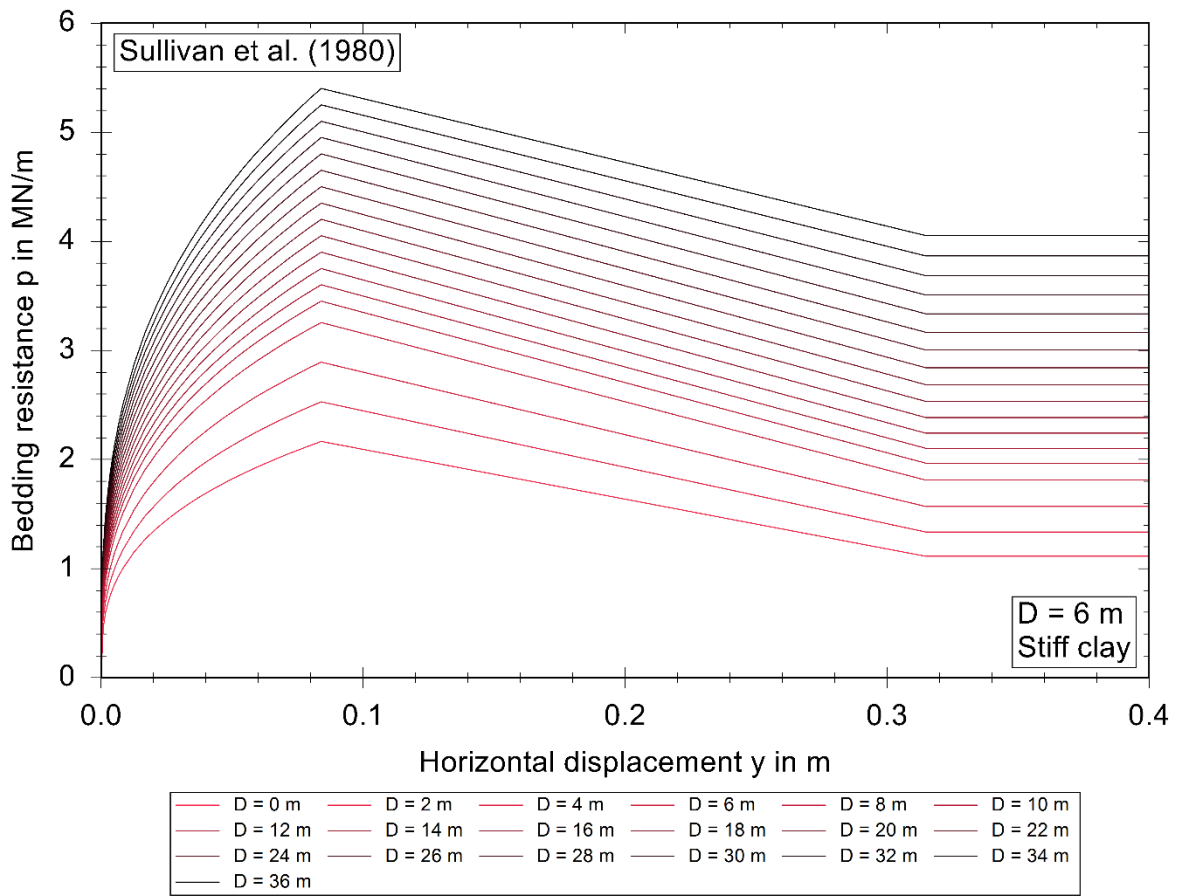
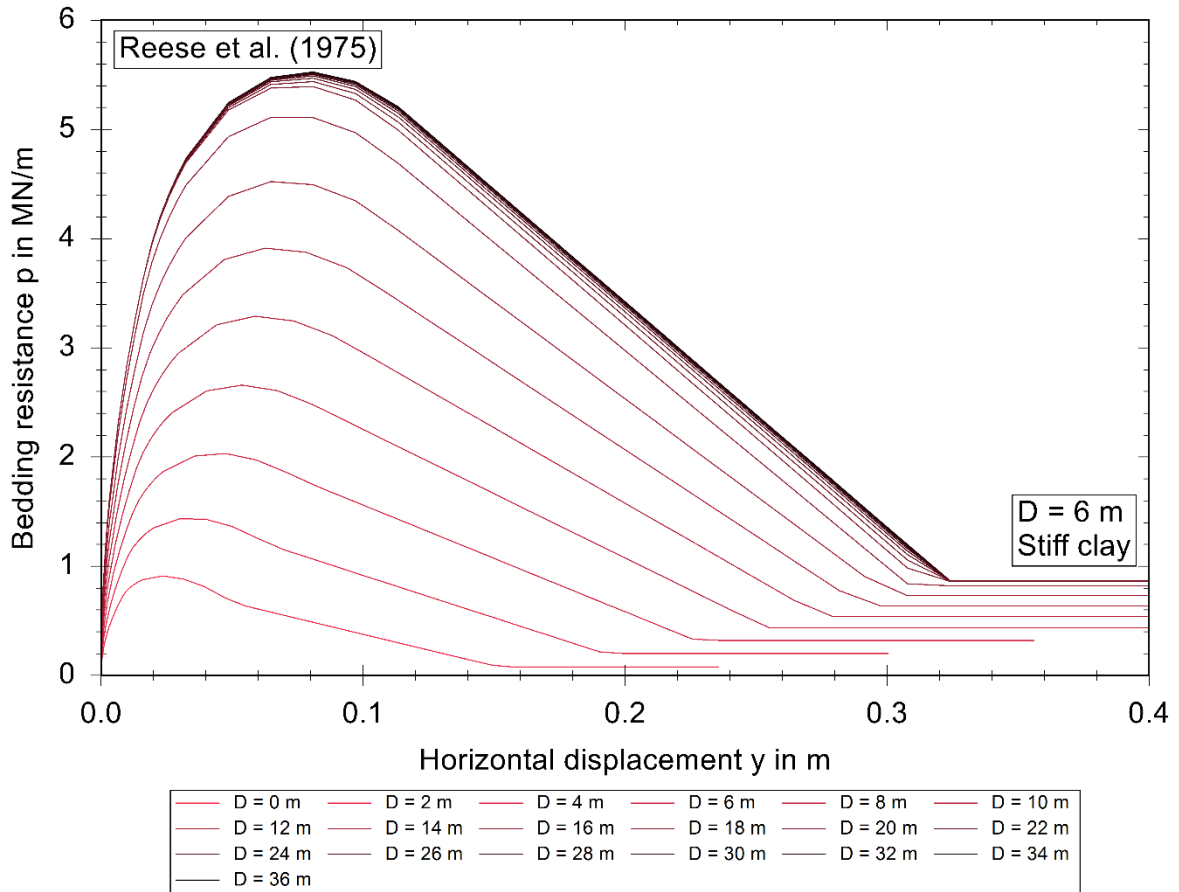












# Appendix C

Contour plots of the quotients  $Q_K = K_{p-y} / K_{FEM}$  between the lateral stiffness resulting from the conventional p-y approaches and the FEM analysis

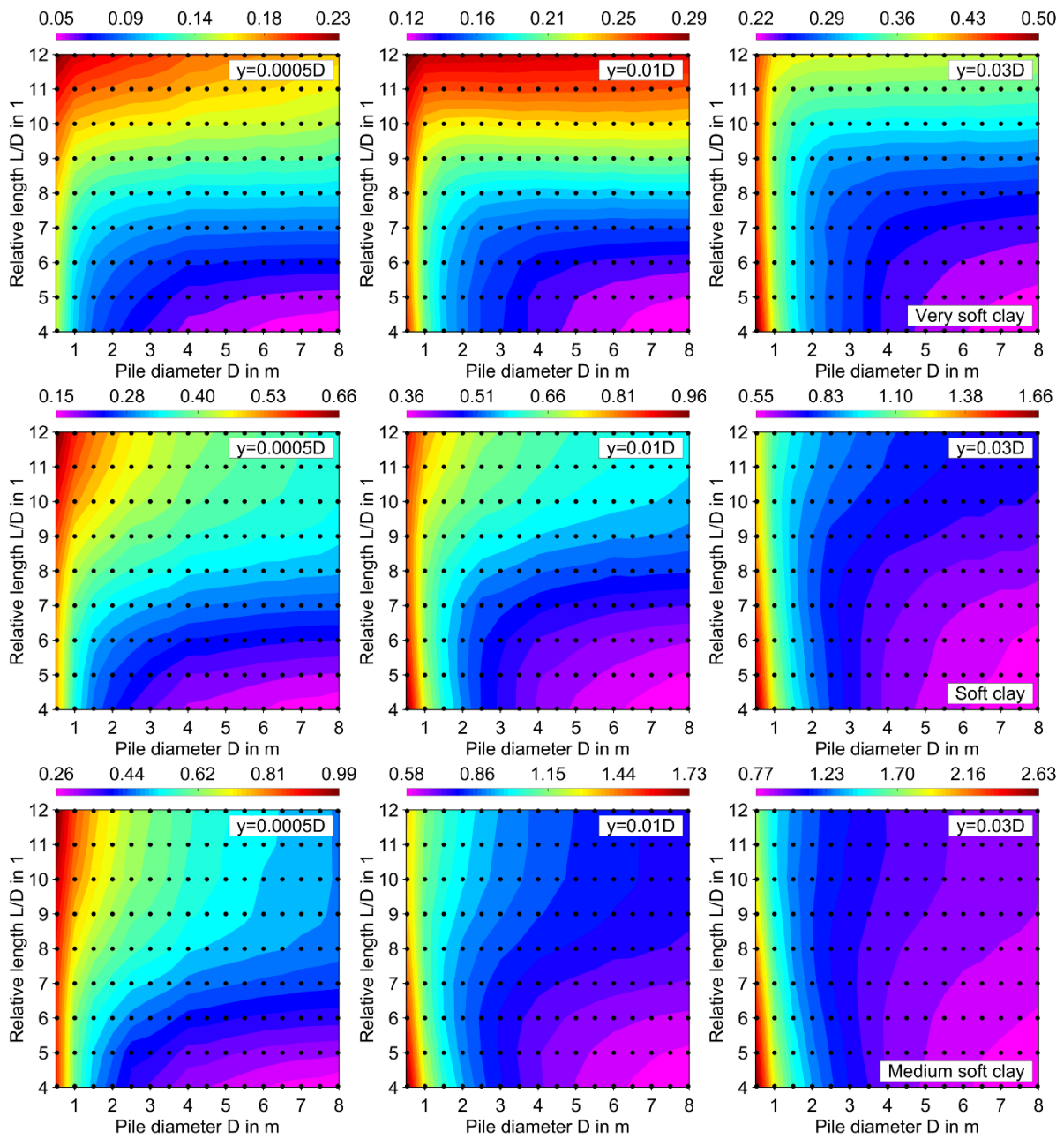


Figure C-1: Quotient of lateral stiffness  $K_{p-y} / K_{FEM}$  based on the approaches by API (2002) and FEM

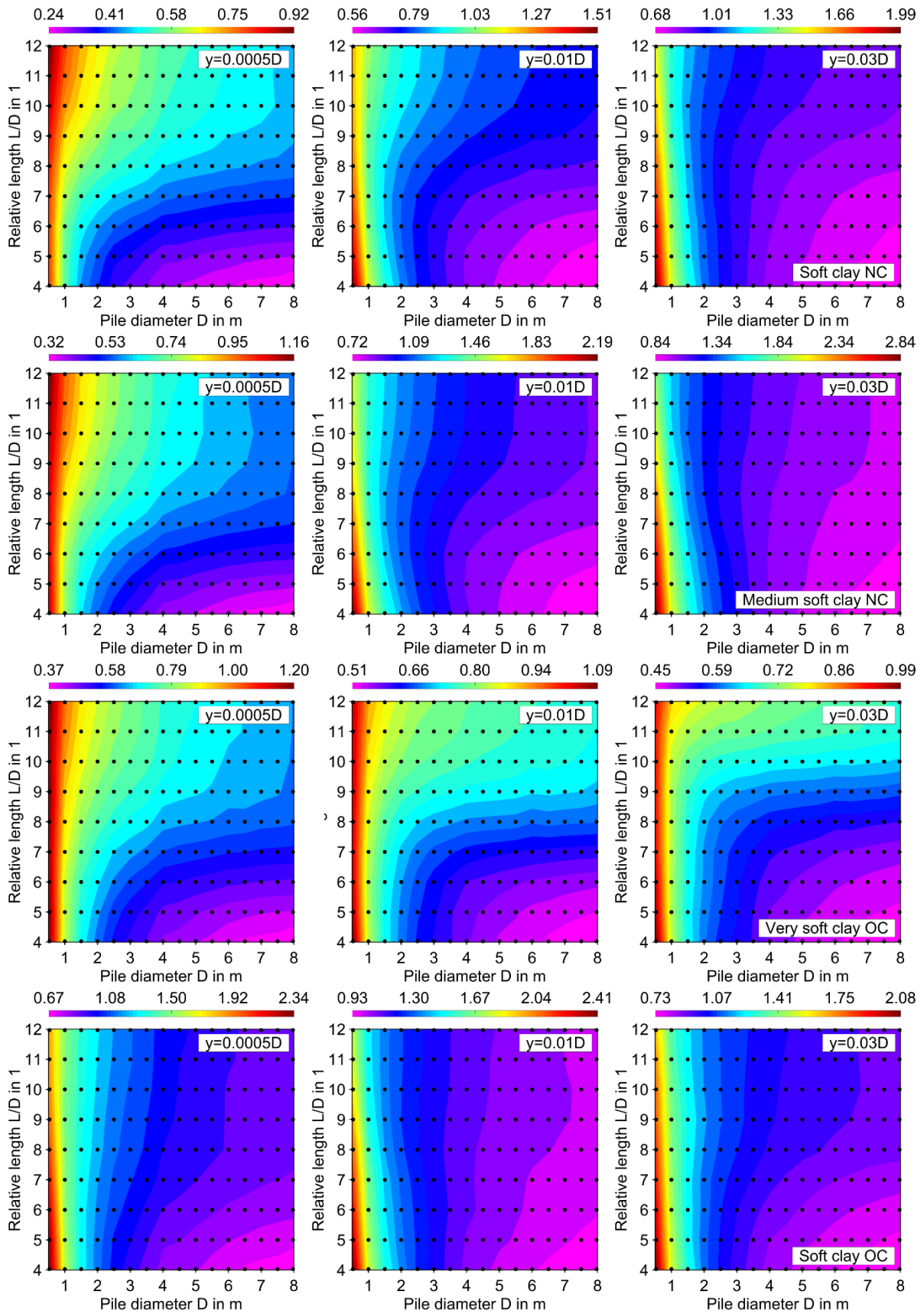


Figure C-2: Quotient of lateral stiffness  $K_{p-y} / K_{FEM}$  based on the approaches by DNVGL (2016) and FEM

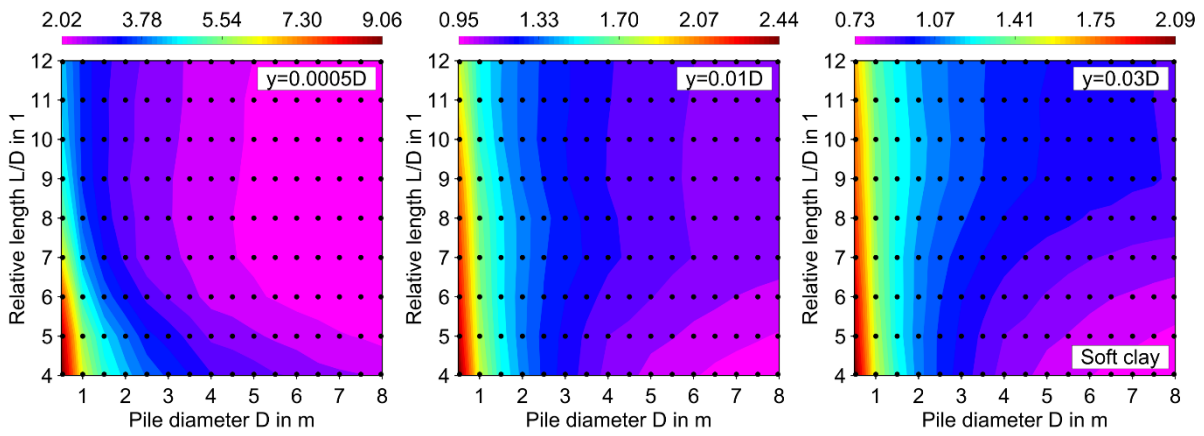


Figure C-3: Quotient of lateral stiffness  $K_{p-y} / K_{FEM}$  based on the approaches by Matlock (1970) and FEM

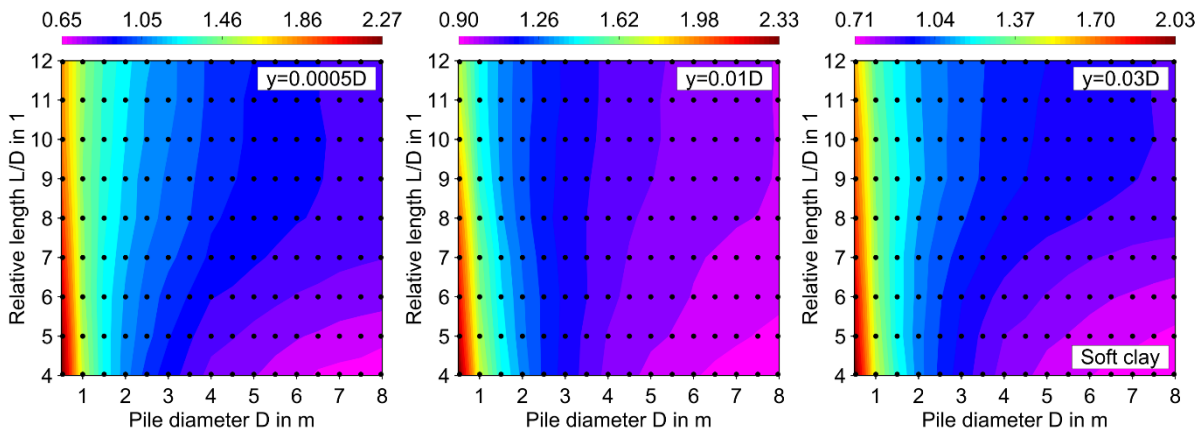


Figure C-4: Quotient of lateral stiffness  $K_{p-y} / K_{FEM}$  based on the approaches by API (2014) and FEM

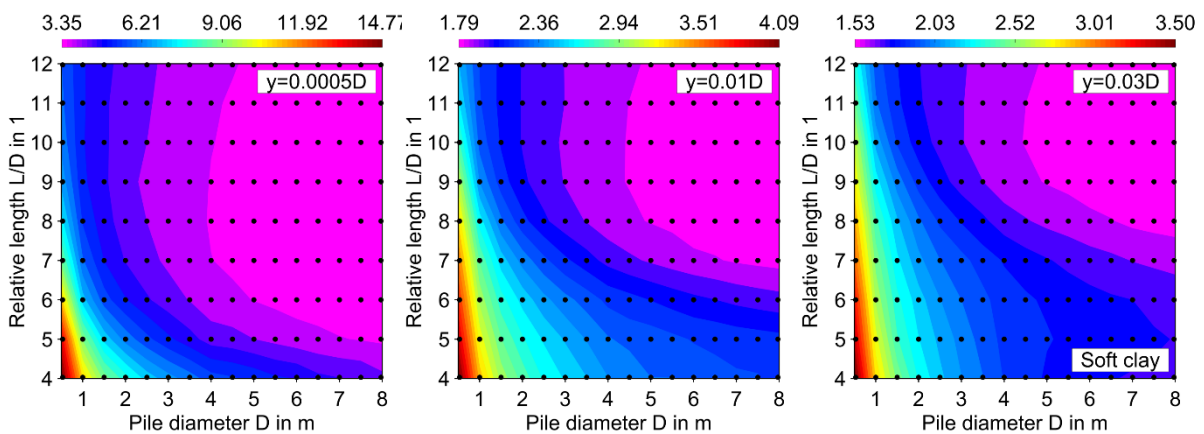


Figure C-5: Quotient of lateral stiffness  $K_{p-y} / K_{FEM}$  based on the approaches by Stevens et al. (1979) and FEM



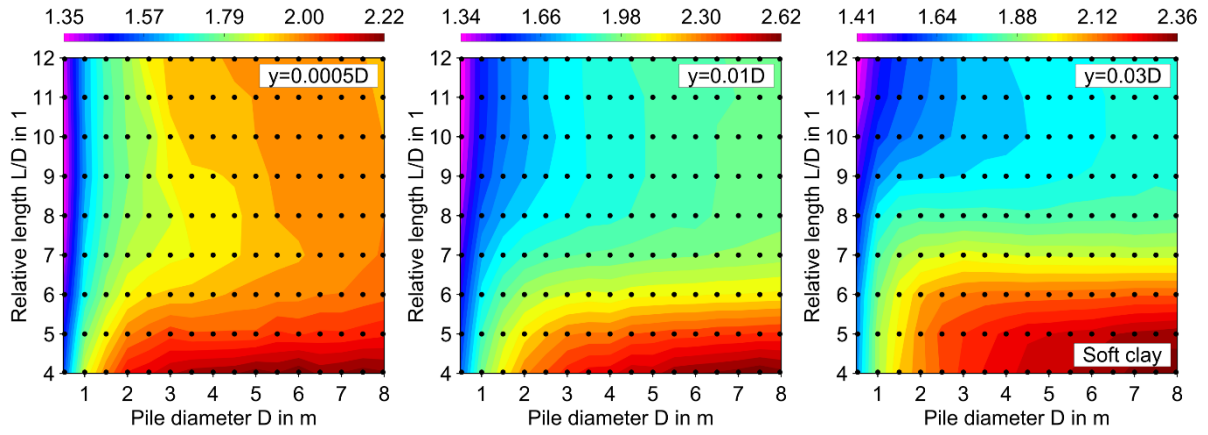


Figure C-6: Quotient of lateral stiffness  $K_{p-y} / K_{FEM}$  based on the approaches by Kim et al. (2009) and FEM

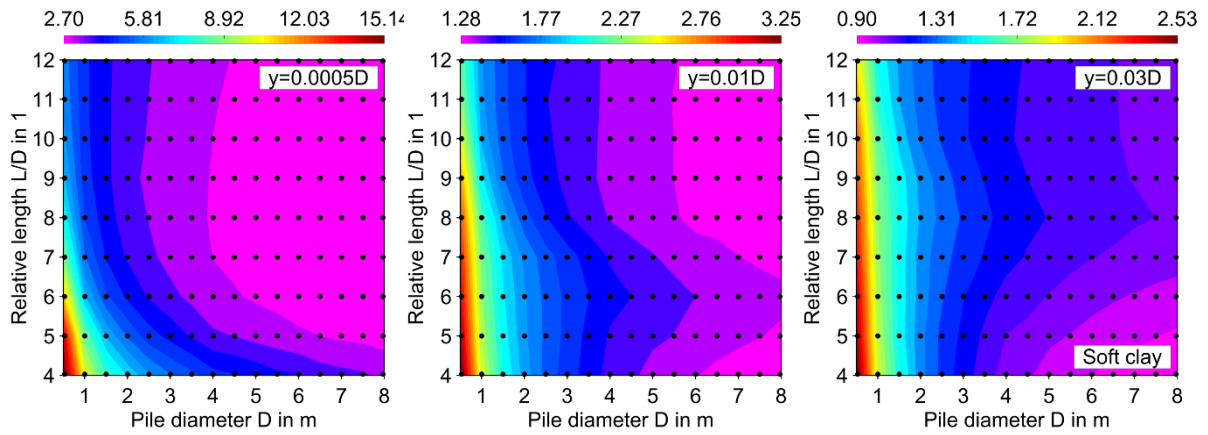


Figure C-7: Quotient of lateral stiffness  $K_{p-y} / K_{FEM}$  based on the approaches by Kirsch et al. (2014) and FEM



## CURRICULUM VITAE

Name: Mauricio Marcelo Terceros Almanza

Nationality: Bolivian / German

Personal status: Married

Born: 20.04.1980 in Oruro, Bolivia

Parents: Matilde Almanza Lizarazu  
Luis Rafael Terceros Vergara

School education: 1985-1993 Primary school, Deutsche Schule, Oruro, Bolivia  
1994-1997 High school, English Catholic School, La Paz, Bolivia

Study: 1998-2003 Diploma in civil engineering, EMI “Mcal. Antonio José de Sucre”, La Paz, Bolivia  
2010-2012 Master of Science for Geotechnique and Infrastructure, Leibniz Universität Hannover, Germany

Work experience: since 2021 Consultant/ Geotechnical Engineer  
ACP Geotechnik GmbH  
Hannover, Germany  
2013-2020 Research Assistant,  
Institute for Geotechnical Engineering (IGtH),  
Leibniz University Hannover  
2016-2020 Occasional Freelancer,  
ACP Geotechnik GmbH  
Hannover, Germany  
2003-2010 Construction Manager,  
Prosec Ingenieros SRL, La Paz, Bolivia

Hannover, September 2021